UNIVERSITY OF LIVERPOOL

Syndecan-3-Mediated Signalling in the Regulation of Myogenesis

Thesis submitted in accordance with the requirements of the University of Liverpool for the degree of Doctor of Philosophy

Fiona Kate Jones

September 2017

Acknowledgements

There are many people I would like to thank for their professional and personal help over the last three years. Without them I wouldn't have had such an enjoyable time carrying out my PhD, nor would I be writing these acknowledgements right now!

First of all, I would like to thank the BBSRC and the University of Liverpool for funding this project as it would have been impossible without them. Secondly, I would like to thank Dr Dada Pisconti and Prof Jerry Turnbull for giving me the opportunity to train towards my PhD and learn about the fascinating world of muscle regeneration and proteoglycans. An extra huge thank you to Dada for helping me with all aspects of my project, providing incredible amounts of support (with my project and life in general), and giving me the chance to take part in several conferences and training events which has allowed me continually to develop as a person. The passion and commitment Dada has shown towards science has always inspired me to the achieve the best I could. Without her in the lab I imagine the days would have been very dull indeed!

Thank you to everyone who contributed to discussion of these results. Special thanks Prof Andy Jones whose contribution to the phosphoproteomics analysis was invaluable and to Mr Al Philips, Mr Simon Perkins and Miss Suzan Ozkan who helped progress this analysis. A big thank you to Prof Claire Eyers, Dr Philip Brownridge, Miss Sam Ferries and Dr Deb Simpson and for continuous helpful discussion regarding phosphoproteomics. Thanks to Dr Max Degano who advised on methods for recombinant protein purification.

A huge thankyou to past and present members of Lab B: Ed, Scott, Chris, Sarah, Han, Rach and Becky for providing discussion and many brain storms when things were looking pear shaped- you kept me going. Extra thanks to Sarah, Han and Rach for all the laughs, (much needed) coffee runs and friendship, we made it!

Finally, thanks to all of my friends and family who have supported me over the years, not only during my PhD but always. Thanks to: Amy G (Yes, you can sing that song now), to 'da babez'- Holly, Katie, Emma and Jenna and to members of Man Squad for always cheering me on and keeping my morale high, even if they didn't have a clue what was going on other than "muscle stuff". I can't thank Ian enough for always giving me encouragement especially when I stressed about anything PhD-related, or otherwise, and somehow not hating me (maybe just a bit) - you're the best! Lastly, thanks to my Mum and Dad who have always provided help and advice whilst supporting all my decisions; I would not be where I am without you.

Pass me the gin!

Abstract

Long-term maintenance of skeletal muscle is important for tissue health and function. Muscle stem cells, also termed satellite cells, are quiescent muscle progenitors residing within the muscle tissue and are indispensable for postnatal muscle growth and regeneration. Once activated by injury, satellite cells convert to proliferating myoblasts, which eventually differentiate and fuse to generate muscle fibres. Heparan sulphate proteoglycans, such as the syndecans, are expressed in satellite cells and contribute to regulation of several growth factor signalling pathways in addition to regulating cell-cell and cell-matrix adhesion. Previous studies have shown that genetic ablation of syndecan-3, a transmembrane heparan sulphate proteoglycan expressed in satellite cells and myoblasts, dramatically improves muscle regenerative potential in ageing and in pathological conditions such as muscular dystrophy. However, the molecular mechanisms underlying syndecan-3 function in muscle regeneration are poorly understood. In this project, I used an unbiased approach based on proteomics and bioinformatics to identify syndecan-3-regulated signalling pathways in myoblasts. I then validated the proteomics and bioinformatics results using traditional biochemistry and cell biology techniques. Interesting results were obtained from a global phosphoproteomic analysis of a control myoblast cell line compared to a syndecan-3 knockdown myoblast cell line. A general trend was observed in syndecan-3 knockdown myoblasts where the insulin/PI3K/mTOR signalling pathway was over-activated in serum-starved syndecan-3 knockdown myoblasts compared to control myoblasts. However, the same insulin/PI3K/mTOR signalling pathway showed a reduced response to serum stimulation in syndecan-3 knockdown myoblasts compared to control myoblasts. Therefore, I investigated the role of syndecan-3 in the regulation of insulin signalling in myoblasts. Results from insulin stimulation experiments in C2C12 and primary satellite cell-derived myoblasts revealed that syndecan-3 regulates the insulin signalling pathway likely by inhibiting AKT activation and consequently regulates the balance between myoblast proliferation and differentiation. These results indicate a novel role for syndecan-3 in the regulation of insulin signalling during myogenesis.

Table of contents

List of Figures

List of Tables

List of abbreviations

4E-BP1	Eukaryotic translation initiation factor 4E-binding protein 1
4E-BP2	Eukaryotic translation initiation factor 4E-binding protein 2
ADAM17	A-disintegrin and metalloproteinase 17
BMP	Bone morphogenetic protein
C1	Conserved 1 region
C2	Conserved 2 region
CAMKII	Ca2+/calmodulin-dependent protein kinase II
cDNA	Complementary DNA
CK2	Casein kinase 2
DAPI	4,6-diamidino-2-phenylindole
ECM	Extracellular matrix
EGF	Epidermal growth factor
ERK1/2	Extracellular signal–regulated kinase 1/2
FAK	Focal adhesion kinase
FAP	Fibro-adipocyte progenitors
FBS	Foetal bovine serum
FGF	Fibroblast growth factor
GAG	Glycosaminoglycan
GAP	GTPase-activating protein
GAPDH	Glyceraldehyde-3-phosphate dehydrogenase
GDNF	Glial cell line-derived neurotrophic factor
GO	Gene ontology
GST	Glutathione S-transferase
HGF	Hepatocyte growth factor
HSPG	Heparan sulphate proteoglycans
IGF	Insulin-like growth factor
IPA	Ingenuity Pathway Analysis
IRS1	Insulin receptor substrate 1
IRS2	Insulin receptor substrate 2
Larp1	La-related protein 1
LC-MS/MS	Liquid chromatography- tandem mass spectrometry
MAPK	Mitogen-activated protein kinase
MMP	Matrix metalloproteinase
MRFs	Myogenic regulatory factors
mTOR	Mammalian target of rapamycin
mTORC1	Mammalian target of rapamycin complex1
MyHC	Myosin heavy chain
NFATc2	Nuclear factor of activated T-cells c2
NGF	Nerve growth factor
NICD	Notch intracellular domain
PAX3	Paired box 3
PAX7	Paired box 7
PBS	Phosphate-buffered saline

PDGF	Platelet-derived growth factor
PI3K	Phosphoinoside 3-kinase
PKA	Protein kinase A
PKC	Protein kinase C
PMA	Phorbol 12-Myristate 13-Acetate
pNPP	p-Nitrophenyl Phosphate
pSer	Phosphorylated serine
pThr	Phosphorylated threonine
PTP	Protein tyrosine phosphatase
pTyr	Phosphorylated tyrosine
qPCR	Quantitative polymerase chain reaction
RPS6	Ribosomal protein S6
RTK	Receptor tyrosine kinase
RT-PCR	Reverse transcription polymerase chain reaction
S3ED	SDC3-ectodomain
S3KD	Syndecan-3 knockdown
S6K	S6 kinase
SCA-1	Stem cells antigen-1
SDC1	Syndecan-1
SDC2	Syndecan-2
SDC3	Syndecan-3
SDC4	Syndecan-4
SEM	Standard error of the mean
shRNA	Short hairpin RNA
Spry1	Sprouty homolog 1
SQSTM1	Seqestosome-1
TACE	Tumor necrosis factor-alpha converting enzyme
TGF-β	Transforming growth factor-β
TNF	Tumor necrosis factor
ULK1	Unc-51 like kinase 1
V	Variable region
VCAM1	Vascular cell adhesion protein-1
VEGF	Vascular endothelial growth factor

Chapter 1

General Introduction

1.1 Outline

This introduction is presented in four parts to give an overview of the current literature related to the topics presented in this thesis, including: muscle biology, muscle regeneration and proteoglycan biochemistry. More specifically, I will cover:

1. Skeletal muscle biology and muscle regeneration, focussing on the extrinsic and intrinsic factors regulating muscle stem cell function.
2. An overview of the structure and function of heparan sulphate proteoglycans with a focus on syndecans.
3. The role of syndecans, and in particular syndecan-3, in myogenesis.
4. General thesis aims and objectives of each preceding results chapter.

1.2 Skeletal muscle anatomy

Skeletal muscle is one of three types of contractile tissue found in the body, in addition to cardiac and smooth muscle, and contributes to a large proportion (~40%) of body weight. Skeletal muscle is under voluntary control and is important for many physiological functions of vertebrates. Including mechanical purposes such as: movement, maintaining posture, strength and breathing, as well as contributing to metabolic functions such as: regulating blood glucose levels, generating heat and amino acid storage. Skeletal muscle develops *in utero*, rapidly increasing in muscle mass postnatally until puberty, where muscle mass and strength peak in early adulthood. From around the age of 30 years onwards muscle mass, predominantly in the lower limbs, begins to decline in an age-related manner (Lexell, 1995). Age-related loss of skeletal muscle mass, strength and function is termed sarcopenia and leads to impaired voluntary movement, increased fragility and a poorer quality of life in the elderly population. Muscle mass is also lost as a consequence of pathological conditions such as amyotrophic lateral sclerosis, which is a neurological disease leading to the death of motor neurons and causes progressive loss and weakness of muscle. Lastly, muscle mass and strength are often lost in many types of inherited muscular dystrophies such as Duchenne muscular dystrophy. In order to develop new therapies to target age-related muscle loss and the various types of myopathies, an in-depth understanding of the musculoskeletal system is essential.

Skeletal muscle is a complex heterogenous tissue which is attached to the skeleton via tendons and appears striated under the microscope (Fig. 1.1). Each muscle is composed of bundles of multinucleated cells that appear elongated and cylindrical in shape and are called myofibres. The muscle is surrounded by connective tissue called the epimysium. Bundles of myofibres are contained by connective tissue called the perimysium, which separates the muscle into compartments. An individual myofibre, or muscle cell is surrounded by the endomysium. The endomysium is composed of the basal lamina which is in direct contact with the myofibre plasma membrane (sarcolemma) and the reticular lamina.

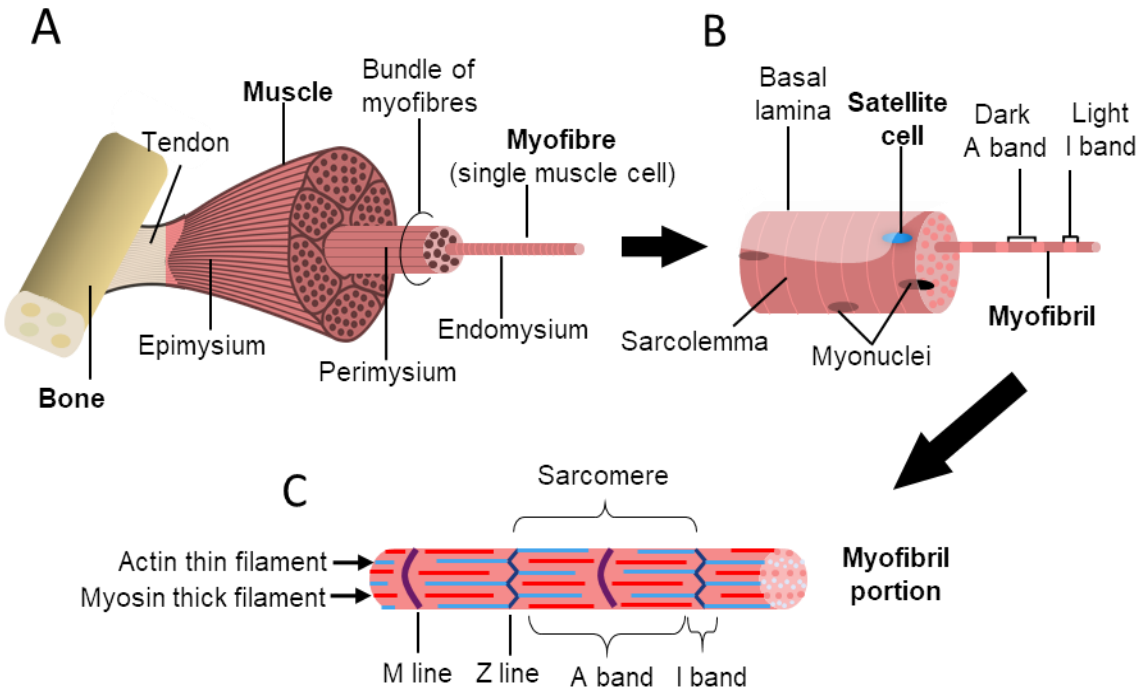

Figure 1.1: Structure of skeletal muscle. **(A)** Skeletal muscle is anchored to the bone by tendons. The muscle is composed of bundles of myofibres which are surrounded by connective tissue called the perimysium. **(B)** A single myofibre contains many myonuclei at the periphery of the cylindrical cell contained within the sarcolemma. The myofibre consists of many myofibrils which are composed of repeating dark and light bands giving rise to the striations observed under microscopy. **(C)** Myofibrils contain mostly actin and myosin proteins that overlap to form cross bridges that slide against each other to generate the force required for muscle contraction.

The myofibre contains thousands of myofibrils, which are the supramolecular protein complexes generating the forces that produce myofibre contraction. Due to these forces, the myofibre nuclei (myonuclei) are pushed to the outer edges of the cell under the plasma membrane. Myofibrils are formed from billions of myofilaments. Thick and thin filaments primarily consist of myosin and actin protein respectively, and in combination form the sarcomeres, which are the minimal contractile units of skeletal muscle. Repeating sections of sarcomeres give rise to the visual dark (A) and light (I) bands of the myofibre (Fig. 1.1).

The sarcomeres are the functional components of the muscle cell and muscle contraction occurs when the thick and thin filaments slide past one another, a process that requires ATP and Ca^{2+} ions.

The heterogeneity of skeletal muscle originates from the various types of myofibres found in different muscles. Nearly all muscles are composed of a mixture of fast-twitch (Type II) and slow-twitch (Type I) myofibres that are distributed in an organised manner to achieve specific muscle function. There are four myofibre types in the human body: Type I, Type IIa, Type IIb and Type IIx and are classified based on which myosin heavy chain isoform is expressed in the myofibre (Pette and Staron, 2000). The overall type of a muscle depends on the ratio of slow to fast myofibres. Each myofibre type also has varying physiological and metabolic properties such as oxidative capacity, power production and resistance to fatigue. For example, Type IIb myofibres are the fastest and produce the greatest force production but have a very low oxidative capacity and fatigue quickly therefore suited for short-bursts of use like sprinting.

1.3 Developmental myogenesis

Skeletal muscle is composed of multi-nucleated myofibres and arise from the fusion of muscle progenitor cells during early development. Vertebrate skeletal muscle develops early in the embryo, mostly arising from the paraxial mesoderm which then segments into the somites (Christ and Ordahl, 1995). As the somites mature the dermomyotome is formed and is the source of muscle progenitor cells expressing the transcription factors Paired box 3 (PAX3) and Paired box 7 (PAX7); these are important for formation of the skeletal musculature (Relaix *et al.*, 2005, Buckingham, 2007). PAX3-expressing muscle progenitors are essential for delamination and migration of muscle progenitors from the dermomyotome to the limb buds (Goulding *et al.*, 1994). The muscle progenitor cells begin to rapidly proliferate becoming myoblasts, which eventually terminally differentiate into myocytes and fuse together to form the myotome. Development of the skeletal musculature is a multistep process; it begins with the formation of small primary myofibres that provide a scaffold for secondary myofibres to form as the muscle grows. During late muscle development, a subset of muscle progenitor cells, termed satellite cells, are kept from differentiating to form a reserve pool of muscle progenitor cells which are essential for postnatal muscle growth and regeneration (Zammit *et al.*, 2004, Relaix and Zammit, 2012).

1.4 Satellite cells and postnatal myogenesis

Postnatal skeletal muscle has a remarkable ability to regenerate following repeated injury, extreme exercise or disease. Regeneration is attributed to the action of muscle stem cells, which are also termed satellite cells due to their anatomical position along the myofibre

under the basal lamina (Mauro, 1961). Satellite cells are considered the adult muscle stem cells as they can form myofibres but also self-renew. The ability of satellite cells to self-renew has been demonstrated through serial transplantation experiments (Cousins *et al.*, 2004, Hall *et al.*, 2010, Rocheteau *et al.*, 2012). Satellite cells are termed adult *muscle* stem cells because only muscle can be formed from the satellite cells *in vivo,* although there is some evidence that satellite cells can undergo multilineage differentiation into osteocytes or adipocytes *in vitro* (Asakura *et al.*, 2001, Shefer *et al.*, 2004). The number of satellite cells per myofibre varies across species, muscles and fibre types but generally they comprise around 5% of the sublaminal nuclei on myofibres in healthy adult muscle. This is a decline from early postnatal muscle where the number of satellite cells is around 30% (Schultz, 1974). The location of the satellite cells has been examined and they appear well organised within the muscle, for example, there is a higher proportion of satellite cells at the growing ends of the myofibre, at perisynaptic regions and in close proximity to the blood vessels (Gibson and Schultz, 1982, Christov *et al.*, 2007, Allouh *et al.*, 2008).

In healthy undamaged muscle, satellite cells are kept mitotically quiescent (in G0 of the cell cycle) and are virtually transcriptionally inactive except for cell homeostasis. In response to injury satellite cells become activated, migrate out of the basal lamina and begin to proliferate as myoblasts. Currently it is thought that during the early proliferative stages a subset of myoblasts exit the cell cycle and return to a quiescent state to replenish the quiescent satellite cell pool, this is essential to retain efficient regeneration of skeletal muscle throughout life (Kuang *et al.*, 2007, Olguin and Pisconti, 2012). The remaining myoblasts continue proliferating then terminally differentiate into myocytes and either fuse to one another to generate new myofibres, called myotubes, or to existing myofibres to repair them (Fig. 1.2). The process of myoblast fusion is complex and well-orchestrated; involving cell migration, recognition and adhesion, eventually followed by plasma membrane fusion. The fusion process can be divided into two parts. The first is the formation of nascent myotubes, which contain few nuclei. The second is further maturation of the nascent myotube, which increases in size due to incorporation of additional differentiated myocytes (Fig. 1.2B) (Abmayr and Pavlath, 2012). Although seemingly similar processes, evidence suggests that fusion of myocytes with one another utilises different proteins to when myotubes fuse with nascent myotubes (Rochlin *et al.,* 2010). For example β1 integrin and calveolin-3 play a role in myocyte adhesion to one another whereas the NFATc2 (Nuclear factor of activated T-cells c2) signalling pathway is critical for myotube maturation (Horsley et al., 2001, Schwander *et al.*, 2003). More recently a muscle-specific protein named myomaker was identified as a critical component of myoblast fusion following acute and chronic adult muscle injury (Millay et al., 2014). Interestingly, when myomaker was ectopically expressed in fibroblasts this allowed them to fuse with

myoblasts, but not other myomaker-expressing fibroblasts. This indicated that another protein was required for fusion, later discovered as a membrane protein exclusively expressed in skeletal muscle named myomerger, (Quinn *et al.,* 2017).

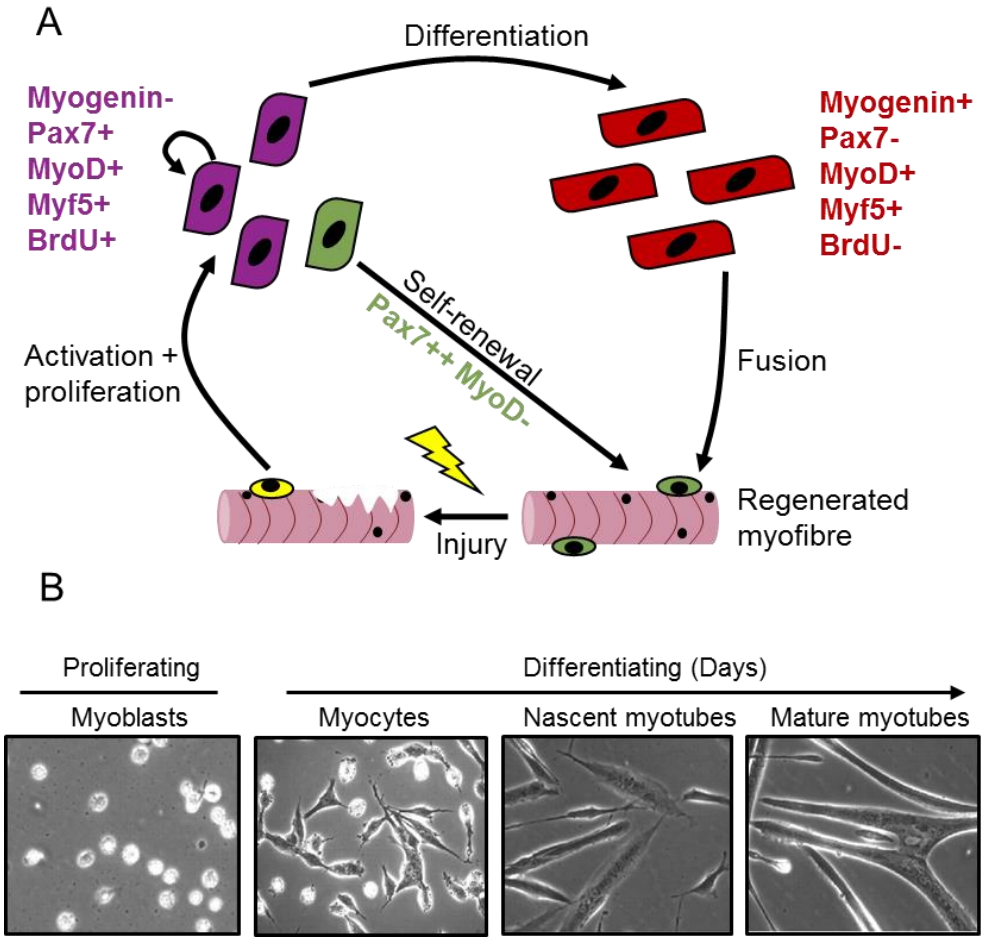

Figure 1.2: Satellite cell function in myogenesis. (A) Mechanisms of skeletal muscle regeneration. Upon injury to the myofibre (yellow bolt) quiescent satellite cells (green) become activated and migrate away from the niche to begin proliferating (purple cells). Some of the proliferating myoblasts will upregulate PAX7 and return quiescent to the satellite cell niche to renew the satellite cell pool (green cells). Other myoblasts will terminally differentiate (red cells) and fuse to the damaged myofibre to regenerate it. **(B)** Phase contrast images of proliferating and differentiating myogenic cells ex vivo depicting the morphology of fused myoblasts. Images adapted from Kim et al. (2015).

Satellite cells express several markers distinguishing them from other mononucleated cells in the muscle. Of importance is PAX7, which was the first marker to uniquely identify quiescent and proliferative satellite cells in muscle. PAX7 is essential for satellite cell specification during development and for satellite cell survival and function during muscle regeneration (Seale *et al.*, 2000, Kuang *et al.*, 2006, Gunther *et al.*, 2013, von Maltzahn *et al.*, 2013). Other key transcription factors include the myogenic regulatory factors (MRFs), which are members of the basic helix-loop-helix transcription factor family: MyoD1, Myf5, MRF4 and myogenin. The MRFs are dynamically regulated throughout myogenesis and

are essential for myogenic specification and commitment to differentiation (Fig. 1.2A) (Tapscott, 2005). MyoD1 is known as the master regulator of myogenesis as its ectopic expression in non-myogenic cells, such as fibroblasts, is sufficient to activate the entire myogenic programme (Weintraub *et al.*, 1989). Quiescent satellite cells express PAX7 and a sub-population co-express Myf5 (Seale *et al.*, 2000, Gayraud-Morel *et al.*, 2012). In response to injury satellite cells become activated, express MyoD1 and Myf5, and begin proliferating whilst maintaining expression of PAX7 (Cooper *et al.*, 1999). Proliferating cells eventually downregulate PAX7 and upregulate MyoD1, activating the myogenic programme (Zammit *et al.*, 2006). After one or more rounds of division, myoblasts withdraw from the cell cycle to terminally differentiate, as marked by expression of myogenin (Edmondson and Olson, 1990, Zammit *et al.*, 2006). Alternatively, satellite cells can self-renew and return to quiescence via two possible mechanisms: either via asymmetric cell division at the moment of the first division (Kuang *et al.*, 2007, Rocheteau *et al.*, 2012, Troy *et al.*, 2012) or via stochastic upregulation of PAX7 and downregulation of MyoD1 in a subset of proliferating myoblasts, which promote return to quiescence (Olguin and Olwin, 2004, Olguin *et al.*, 2007). In combination with PAX7, membrane proteins including syndecan-3, syndecan-4, SCA-1 (Stem cells antigen-1), CD34, calcitonin receptor, VCAM1 (Vascular cell adhesion protein-1), M-cadherin, integrin alpha 7, integrin beta 1 and c-Met are used to identify satellite cells (Olguin and Pisconti, 2012).

1.5 The satellite cell niche

Stem cells reside in a specific anatomical position within the tissue which helps maintain their stem cell attributes by allowing association with other supporting cells (Scadden, 2006). Quiescent satellite cells are located in a specialised microenvironment between the basal lamina and the myofibre sarcolemma, commonly termed the satellite cell niche (Fig. 1.3) (Mauro, 1961). Increasing evidence suggests that the components of the niche are critical for maintaining quiescence and transmitting external signals to the satellite cells to regulate activation, proliferation and differentiation (Cornelison *et al.*, 2004, Kuang *et al.*, 2008, Yin *et al.*, 2013, Pisconti *et al.*, 2016, Quarta *et al.*, 2016, Ghadiali *et al.*, 2017). The satellite cell niche is rich in collagens, laminins, fibronectin and proteoglycans. In particular collagen IV and laminin-211, (composed by α2, β1 and γ1 chains) to which satellite cells adhere, mainly via α7β1 integrin (Rapraeger *et al.*, 1991, Chakravarthy *et al.*, 2000, Shea *et al.*, 2010, Brandan and Gutierrez, 2013). The membrane proteins CD34 and M-cadherin mediate satellite cell adhesion to the myofibre plasma membrane (Florini *et al.*, 1996, Stewart *et al.*, 1996). Linkage to laminin and collagen IV allows satellite cells to associate with proteoglycans such as decorin, perlecan and biglycan. Proteoglycans are important components of the satellite cell niche involved in growth factor sequestration, cell signalling

and cell adhesion (Rapraeger, *et al.*, 1991, Cornelison, *et al.*, 2004, Pisconti, *et al.*, 2016, Ghadiali, *et al.*, 2017)

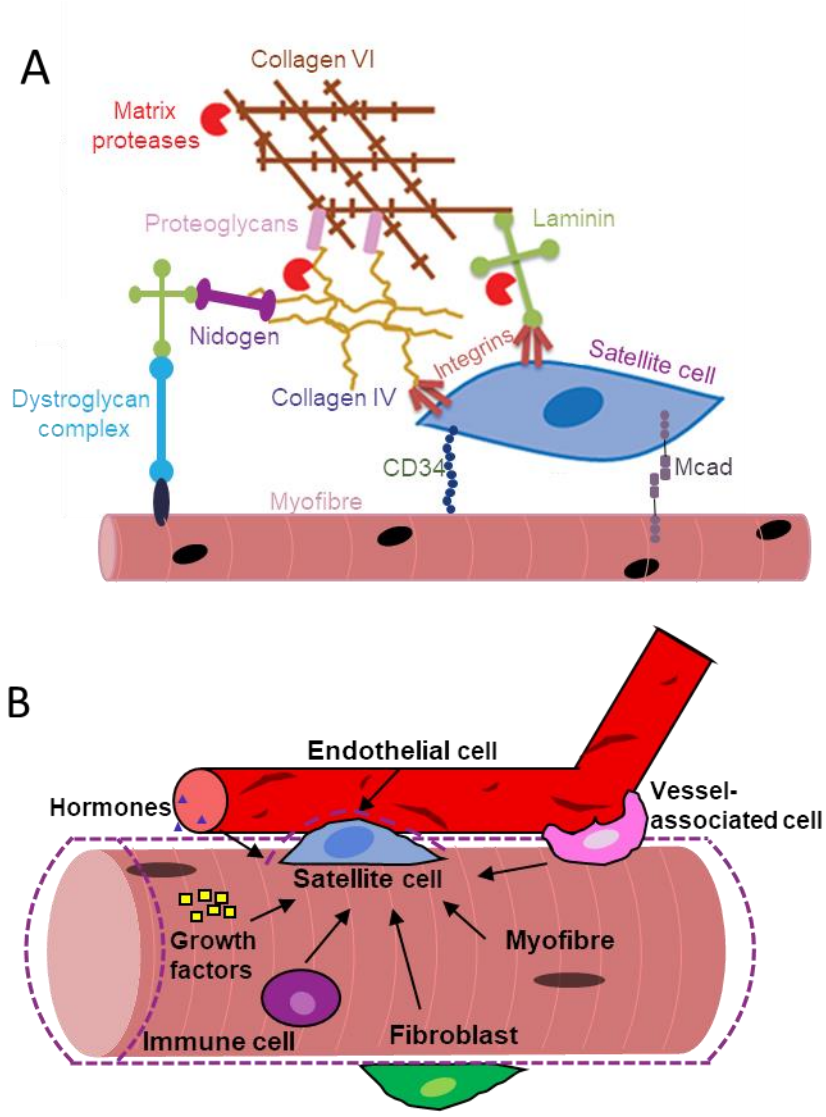

Figure 1.3: Schematic representation of the satellite cell niche. The top part of the figure represents the immediate satellite cell niche and the cross-linking of major extracellular matrix proteins to the satellite cells and the myofibre. The bottom half of the figure depicts the role of supporting cells such as fibroblasts, endothelial cells and immune cells and how these all work together to regulate satellite cell fate.

In skeletal muscle the satellite cell niche is extensively remodelled in response to injury (Bentzinger *et al.*, 2013, Thomas *et al.*, 2015). Much of the remodelling occurs by matrix metalloproteinases (MMPs) which degrade the extracellular matrix (ECM) and release growth factors from the niche leading to changes in cell signalling. Roles for MMP-2, -9, -10 and -14 have been identified in skeletal muscle (Yamaguchi *et al.*, 2015). For example, MMP-9 and MMP-2 gene expression is upregulated after muscle injury and their expression appears to be localised around activated satellite cells. This suggests that the satellite cells themselves break down the ECM which allows them to migrate to the site of injury (Kherif

et al., 1999). Additionally, neutrophil proteases are released in the early stages of muscle regeneration and play important roles by degrading the ECM, and either activating or inactivating several growth factors and cytokines (Arecco *et al.*, 2016). Deposition of ECM components such as laminin, fibronectin, collagens and proteoglycans by fibroblasts and satellite cells change the structural composition of the niche during regeneration (Urciuolo *et al.*, 2013, Lukjanenko *et al.*, 2016). Loss of fibronectin from the niche impairs satellite cell function by dysregulation of cell adhesion via integrin-FAK signalling (Fukada *et al.*, 2011, Lukjanenko *et al.*, 2016). Satellite cell adhesion appears to be important for maintaining function, as loss of the proteoglycan SDC3 causes spontaneous activation of satellite cells and reduced adhesion to the myofibre *ex vivo* (Pisconti *et al.*, 2016).

Several mononuclear cells are resident within the stem cell niche and actively support satellite cell function such as fibro-adipocyte progenitors (FAPs), immune cells, fibroblasts and vascular cells. FAPs are mesenchymal stem cells that can differentiate into fibroblasts or adipocytes and reside in the interstitial space in skeletal muscle, supporting satellite cells in response to injury. FAPs and fibroblasts heavily contribute to deposition of ECM proteins, such as collagen and fibronectin, and secrete pro-myogenic cytokines which regulate satellite cells and influences myogenesis (Chang *et al.*, 2002, Joe *et al.*, 2010, Judson *et al.*, 2013). Upon injury to the muscle, FAPs and fibroblasts become activated and quickly proliferate within the interstitial space (Joe *et al.*, 2010). When isolated from regenerating muscles FAPs promote satellite cell proliferation and differentiation in co-culture (Joe *et al.*, 2010). Fibroblasts also promote myoblast proliferation but are not pro-differentiative, instead they promote self-renewal (Joe *et al.*, 2010, Murphy *et al.*, 2011).

Immune cells such as mast cells, macrophages, monocytes and neutrophils are resident in small numbers within the satellite cell niche and become activated in response to muscle injury orchestrating the inflammatory response which attracts infiltration of further immune cells. The first immune cells to infiltrate the injured muscle are neutrophils, which are responsible for clearing the tissue debris and triggering the macrophage-dominated inflammatory response (Arecco *et al.*, 2016, Tidball, 2017). Macrophages differentiate from monocytes and exist as a heterogenous population during regeneration but can be simply divided into M1 and M2 populations which are pro-inflammatory and anti-inflammatory, respectively (Saclier *et al.*, 2013). M1 macrophages secrete pro-inflammatory cytokines such as tumor necrosis factor (TNF)-α and Interleukin-1β, which promote myoblast proliferation (Arnold *et al.*, 2007). As regeneration progresses a second wave of macrophages, named M2, become active and secrete anti-inflammatory signals, which change the dynamics of the satellite cell niche and promotes myoblast differentiation (Arnold *et al.*, 2007, Tidball, 2017).

Satellite cells are found in close proximity to capillaries, regardless of their activation state, suggesting an important role for endothelial cells and the vasculature in the regulation of satellite cell function (Gibson and Schultz, 1982, Christov *et al.*, 2007). After muscle injury the number of capillaries increase before returning to normal after 3-4 weeks (Luque *et al.*, 1995). Endothelial cells promote myoblast proliferation *in vitro* and, interestingly, myogenic cells undergoing differentiation secrete vascular endothelial growth factor (VEGF) promoting angiogenesis, suggesting mutually beneficial interactions between endothelial cells and satellite cells (Chazaud *et al.*, 2003, Christov *et al.*, 2007),. VEGF and other mitogenic factors such as fibroblast growth factors (FGFs), Insulin-like growth factor-1 (IGF1) and hepatocyte growth factor (HGF) are secreted by endothelial cells and influence satellite cell growth (Hawke and Garry, 2001, Christov *et al.*, 2007).

1.6 Intrinsic and extrinsic regulation of satellite cell function

Regulation of satellite cell function during adult myogenesis is believed to be controlled by a mixture of pre-programmed intrinsic factors and extrinsic signals governed by the satellite cell niche. Whilst many regulators of satellite cell fate have been discovered there is still much to be understood about how the different molecular mechanisms cross-talk and interact. Many of the intrinsic factors affecting myoblast fate are affected by extrinsic signals and vice-versa, therefore the following discussion will combine both intrinsic and extrinsic factors.

1.6.1 Satellite cells are a heterogeneous population

Although all satellite cells express PAX7, evidence now suggests that they are a heterogenous population governed by specific gene expression signatures which are associated with different cell functions and/or fates (Ono *et al.*, 2010). Moreover, gene expression profiling experiments have concluded that satellite cells derived from different areas of the body have differing genetic and functional characteristics, increasing the complexity of satellite cell studies (Harel *et al.*, 2009, Ono *et al.*, 2010). For example small stem cell-like subpopulations identified by different markers have been discovered which can undergo asymmetric cell division, generating an identical sub-population via self-renewal, and a different sub-population that is capable of sustained muscle regeneration (Sherwood *et al.*, 2004, Kuang *et al.*, 2007, Tanaka *et al.*, 2009).

Variations in the proliferation rate of different subsets of satellite cells have also been reported. Fast-dividing satellite cells undergo fewer rounds of division and rapidly differentiate, but also give rise to larger numbers of proliferating and self-renewing cells. However, these self-renewing cells quickly differentiate without further replenishing the satellite cell pool, which ultimately leads to exhaustion of the satellite cell pool. In contrast,

slow-dividing satellite cells produce fewer myogenic cells in total, but the long-term potential of satellite cell self-renewal is increased as indicated by a higher number of PAX7+ undifferentiated cells after serial passages (Ono *et al.*, 2012). Furthermore, engraftment experiments using satellite cells isolated from different muscles in the body has proven that the potential for proliferation and self-renewal differs depending on which muscle the engrafted satellite cells originated from, further suggesting that the satellite cell pool is functionally heterogenous (Collins *et al.*, 2005, Sacco *et al.*, 2008).

1.6.2 Chromatin remodelling and telomeres

Epigenetic marks such as methylation and acetylation of histones are important for regulation of gene transcription. Genome wide approaches suggest that the progression of myogenesis is underpinned by epigenetic changes which allow coordinated regulation of myogenic gene expression (Penn *et al.*, 2004, Blais *et al.*, 2005, Guasconi and Puri, 2009). The repressive histone methylation mark (H3K27me3) is found in high abundance surrounding genes associated with commitment to non-muscle lineages, permanently silencing them. However, genes involved in promoting differentiation, including *myog,* are less highly enriched for H3K27me3 and are induced during differentiation (Asp *et al.*, 2011). Suv4-20H1, a histone H4 lysine 20 methyltransferase, regulates the chromatin structure in satellite cells by repressing MyoD1 which prevents satellite cell activation and further supports the notion that satellite cell quiescence is an actively maintained state. (Boonsanay *et al.*, 2016). A recent study investigated the chromatin environment of myogenic precursors using an inducible PAX7 embryonic stem cell system and discovered PAX7 expression in embryonic stem cells dramatically remodels chromatin and allows access to myogenic genes (Lilja *et al.*, 2017).

Telomeres are non-coding repeating units of DNA that are located at the end of chromosomes and become shorter with each successive round of cell division. Since telomeres help maintain chromosome integrity once telomeres are lost after several rounds of division, cells enter senescence. Therefore, the proliferative potential of cells can be determined by their telomere length and by their capacity to synthesise telomeres at each cell division (Allsopp *et al.*, 1992). Telomere length is not static and can be increased by enzymes known as telomerases. Most somatic cells lack telomerase activity but stem cells and progenitor cells express low levels of telomerase which likely contributes to an increased proliferative capacity in these cells (Gunes and Rudolph, 2013). Indeed, when telomerase is expressed in satellite cells their proliferative ability is increased, however, induction of telomerase activity alone is not sufficient to immortalise satellite cells (Di Donna *et al.*, 2003). Furthermore, on examination of telomerase activity and telomere length in satellite cells associated with myofibres, it was determined that upon activation and

differentiation of satellite cells telomerase activity declined, suggesting interactions with the myofibre are important to maintain telomerase activity in satellite cells (O'Connor *et al.*, 2009).

1.6.3 Notch and Wnt signalling

Notch signalling regulates multiple functions of satellite cells during adult myogenesis such as quiescence, proliferation and differentiation (Kopan *et al.*, 1994, Kuroda *et al.*, 1999, Conboy and Rando, 2002). Notch was identified as a satellite cell quiescence regulator as Notch activity is high in quiescent satellite cells. Interruption of Notch signalling by genetic ablation of RBPJ, a Notch target, promotes spontaneous cell differentiation and loss of the quiescent satellite cell pool resulting in a failure of muscle regeneration after muscle injury (Kitzmann *et al.*, 2006, Mourikis *et al.*, 2012). Loss of other Notch downstream targets such as HEY1, HEYL and numb also promotes spontaneous activation of satellite cells and impairs self-renewal (Conboy and Rando, 2002, Bjornson *et al.*, 2012). Overexpression of NOTCH1 intracellular domain (NICD), in satellite cells inhibits myogenic differentiation but increases the number of PAX7+ cells and promotes satellite cell self-renewal (Wen *et al.*, 2012). Genetic ablation of syndecan-3 (SDC3), a NOTCH1 co-receptor, causes loss of NOTCH1-mediated signalling consequently resulting in an increase in the number of activated satellite cells and a reduction in the quiescent satellite cell pool (Pisconti *et al.*, 2010).

Wnt proteins are a large diverse family of signalling glycoproteins which bind to Frizzled receptors located on the plasma membrane of cells and can signal via canonical and non-canonical pathways. Both the canonical and non-canonical Wnt signalling pathways are important for satellite cell function. There are 19 Wnt proteins and although they share homology they appear to have distinct signalling functions (Nusse, 2008). Wnt signalling is involved in all aspects of muscle regeneration by regulating proliferation, self-renewal and differentiation of satellite cells. Several Wnt proteins are expressed in satellite cells such as: Wnt1, Wnt3a, Wnt4, Wnt6, Wnt5a, Wnt5b, Wnt7a and Wnt7b, indicating a complex role for Wnt signalling in myogenesis (von Maltzahn *et al.*, 2012). Wnt7a stimulates symmetric cell division of satellite cells via activation of the non-canonical Wnt signalling pathway. Overexpression of Wnt7a dramatically improves muscle regeneration in response to injury (Le Grand *et al.*, 2009). Additionally, Wnt7a treated myotubes become hypertrophic via activation of the AKT/mTOR signalling pathway (von Maltzahn *et al.*, 2011). Wnt1, Wnt3a and Wnt5a, but not Wnt4 and Wnt6, stimulate satellite cell expansion via the canonical Wnt signalling pathway (Otto *et al.*, 2008). Wnt signalling also appears to regulate myogenic differentiation by antagonising Notch signalling (Brack *et al.*, 2008), which normally promotes proliferation and self-renewal (Conboy and Rando, 2002, Pisconti *et al.*, 2010).

1.6.4 Hormone effects on satellite cell function

Several endogenous hormones including insulin, calcitonin and anabolic steroids such as oestrogen, androgen and testosterone are known to regulate proliferation and differentiation of satellite cells (Kahlert *et al.*, 1997, Deane *et al.*, 2013). Following gene expression analysis Fukada *et al.* (2007) discovered that the calcitonin receptor is downregulated during satellite cell activation, allowing myogenic cells to proliferate by induction of MyoD1 expression. Additionally, incubation of single myofibres with calcitonin prolonged satellite cell quiescence and attachment to the myofibre (Fukada *et al.*, 2007). More recently the calcitonin receptor was found to be critical for maintaining satellite cell quiescence via the cAMP/PKA (protein kinase A) and cAMP/Epac pathways and to maintain satellite cells in their sublaminar position within the niche (Yamaguchi *et al.*, 2015).

Insulin shares high homology with IGF, as does the catalytic domain of the insulin receptor and the catalytic domain of the IGF receptor (Nakae *et al.*, 2001), suggesting similar pathways may be activated by insulin in myoblasts. Investigation into insulin-mediated cell signalling in myogenesis is scarce compared to IGF signalling. However, the data collected so far about insulin signalling and myogenesis have proven that similar effects are obtained with insulin stimulation as with IGF stimulation. For example, insulin stimulation of myoblasts *in vitro* accelerates differentiation by activation of the PI3K/AKT/S6K (S6 kinase) pathway (Jiang *et al.*, 1999). Chronic insulin stimulation of pre-confluent myoblasts inhibits the MAPK pathway, and enhanced differentiation (Conejo *et al.*, 2001). On the other hand, insulin stimulation promotes proliferation in C2C12 myoblasts and is associated with increased cyclin A and cyclin D1 production (Grabiec *et al.*, 2014).

1.6.5 Growth factor regulation of myogenesis

Growth factors and cytokines play important roles in activation, proliferation and differentiation of myogenic cells and are released from the satellite cell niche (Yin *et al.*, 2013). The most studied growth factors involved in the regulation of myogenesis include: HGF, FGFs, transforming growth factor-β (TGF-β) and IGFs.

FGF signalling in myogenic cells is one of the best characterised and most studied cell signalling events and is known to promote proliferation and repress differentiation via mitogen-activated protein kinase (MAPK) signalling pathways (Clegg *et al.*, 1987, Rapraeger *et al.*, 1991, Fuentealba *et al.*, 1999). In particular, FGF2 is highly expressed in regenerating muscle and ERK1/2 activation is essential for transition of satellite cells from G1 to S phase (Jones *et al.*, 2001). Furthermore, addition of FGF2 enhances satellite-cell proliferation in a dose-dependent manner (Jones *et al.*, 2001). Regulation of FGF2

signalling during myogenesis occurs at multiple levels, such as downstream of the FGF receptors by sprouty homolog 1 (Spry1) which inhibits the ERK1/2 signalling pathway (Shea *et al.*, 2010), or extracellularly via heparan sulphate proteoglycans (Olwin and Rapraeger, 1992, Cornelison *et al.*, 2004, Brandan and Gutierrez, 2013).

IGFs are other important growth factors regulating satellite cell function. IGFs are released from the satellite cell niche and are capable of stimulating both proliferation and differentiation of myogenic cells (Florini *et al.*, 1996, Chakravarthy *et al.*, 2000, Yu *et al.*, 2015). This is counter-intuitive, since proliferation and differentiation are mutually exclusive events. This may be explained by temporal differences in IGF signal transduction (Engert *et al.*, 1996). Initially, IGFs promote proliferation via activation of the ERK1/2 pathway but then subsequently decreases phosphorylation, and therefore activity, of ERK1/2 in myoblasts (Adi *et al.*, 2002). Moreover, addition of IGF1, under pro-differentiative conditions, further promotes differentiation via the PI3K/AKT signalling pathway (Coolican *et al.*, 1997, Xu and Wu, 2000). Further downstream of AKT is mTOR which is also involved in muscle differentiation and hypertrophy when activated (Park *et al.*, 2005). More often IGFs are associated with differentiation because *ex vivo* they are potent stimulators of differentiation and muscle hypertrophy, in particular IGF is upregulated during differentiation in a MyoD1-dependant manner and induces expression of myogenin (Florini *et al.*, 1991, Montarras *et al.*, 1996, Stewart *et al.*, 1996, Semsarian *et al.*, 1999). Additionally IGF-induced muscle hypertrophy is observed in mice overexpressing IGF1 in skeletal muscle (Coleman *et al.*, 1995).

Interestingly, the IGF/PI3K/AKT signalling pathway has also been linked to promotion of proliferation. The downstream mechanisms of IGF/AKT-induced proliferation are not fully understood, however evidence supports that specific isoforms of AKT may be involved during different stages of myogenesis, with AKT1 being involved in proliferation and AKT2 being involved in differentiation. Although how these different kinases are activated by the same set of receptors and ligands is unknown (Gonzalez *et al.*, 2004, Heron-Milhavet *et al.*, 2006).

Mechanical stimuli such as myofibre stretching causes synthesis of nitric oxide and subsequent release of HGF, mediated by metalloproteinases, from the extracellular matrix, (Yamada *et al.*, 2006, Wozniak and Anderson, 2007). HGF levels spike during early muscle regeneration and signal via the c-Met receptor on the satellite cell causing activation and promoting proliferation (Tatsumi *et al.*, 2001). More recently a new satellite cell status was identified, termed G-alert, in satellite cells isolated from muscle contralateral to an initial site of muscle injury, suggesting long-distance extracellular stimuli can affect satellite cells

poising them in a state closer to activation (Rodgers *et al.*, 2014). G-alert cells re-enter the cell cycle faster than G0 satellite cells which is important for rapid satellite cell activation and muscle regeneration in response to injury. Furthermore, this altered state of quiescence appears dependant on mTORC1 (Mammalian target of rapamycin complex 1) signalling and this may arise from systemic release of HGF from the site of injury (Rodgers *et al.*, 2014).

1.6.6 The TGF-β superfamily

The TGF-β superfamily includes the TGF-β-like family, BMP (bone morphogenetic protein)-like family and the GDNF (glial cell line-derived neurotrophic factor)-like family. TGF-β potently inhibits myogenic differentiation mainly by repressing MyoD1 and myogenin activity (Martin *et al.*, 1992, Liu *et al.*, 2001, Liu *et al.*, 2004). Myostatin belongs to the BMP-like family and is a major signalling pathway that controls skeletal muscle growth. Genetic ablation of myostatin results in significantly larger animals compared to their wild type counterparts and a widespread increase in skeletal muscle mass (McPherron *et al.*, 1997). Additionally, muscle atrophy was induced in mice who were administrated myostatin, suggesting that myostatin is a negative regulator of muscle growth *in vivo* (Lee, 2004). *In vitro* experiments show that myostatin blocks myoblast proliferation, inhibits protein synthesis and reduces the myotube size of differentiating myogenic cells by downregulating MyoD1 (Taylor *et al.*, 2001, Langley *et al.*, 2002).

Follistatin is a secreted protein that acts as an antagonist for members of the TGF-β superfamily including myostatin and activin-A, which promotes muscle fibre growth (Michel *et al.*, 1993, Hemmati-Brivanlou *et al.*, 1994, Lee, 2004). Overexpression of follistatin results in a dramatic increase in muscle mass, a phenotype that is even greater than when myostatin is genetically ablated (Lee and McPherron, 2001, Lee, 2007). Muscle hypertrophy induced by follistatin overexpression is partly mediated by an increased activation and proliferation of satellite cells (Gilson *et al.*, 2009).

Heparan sulphate proteoglycans are resident within the satellite cell niche and are important regulators of myogenesis as they are involved in nearly all of the above-mentioned signalling pathways. Therefore, the next section will focus on heparan sulphate proteoglycans and, in particular, the syndecan family.

1.7 Heparan sulphate proteoglycans

Heparan sulphate proteoglycans (HSPGs) are complex macromolecules that consist of a core protein plus one or more covalently attached heparan sulphate glycosaminoglycan chains (Esko *et al.*, 2009). There are several types of HSPGs which are categorised by their location: membrane bound HSPGs such as the syndecan family and the glypican family, ECM HSPGs such as perlecan and agrin, and the secretory vesicle proteoglycan serglycin. HSPGs are ubiquitously present throughout mammalian tissues and are involved in several physiological and pathological processes such as: cell adhesion, ECM organisation, inflammation, tissue repair, cancer and differentiation amongst many others as reviewed extensively elsewhere (Park *et al.*, 2000, Whitelock and Iozzo, 2005, Esko *et al.*, 2009, Knelson *et al.*, 2014). With accumulating evidence it is clear that HSPGs are important regulators of cell functions and as a result are attracting an interest in a variety of fields.

1.7.1 Heparan sulphate

Glycosaminoglycans (GAGs) are complex linear polysaccharides composed of repeating disaccharides units of N-acetylglucosamine or N-acetylgalactosamine followed by glucuronic acid, iduronic acid or galactose**.** Members of the GAG family include heparan sulphate, chondroitin sulphate, dermatan sulphate, keratan sulphate and hyaluronic acid. The GAGs vary in their disaccharide composition, chain length and degree of modification such as sulphation and acetylation pattern. The composition of GAGs varies depending on the origin and expression of enzymatic GAG modifiers. Heparan sulphates are the most variable GAGs, due to extensive structural modifications throughout synthesis and are often considered as a heterogenous family. The structural diversity of heparan sulphate leads to the possibility of binding a plethora of molecules (Turnbull *et al.*, 2001, Handel *et al.*, 2005). Furthermore, increasing evidence suggests that specific structures of heparan sulphate are required for protein interaction and modulation of signalling pathways (Bernfield *et al.*, 1999, Guimond and Turnbull, 1999, Gao *et al.*, 2016, Ghadiali *et al.*, 2017).

1.7.1.1 Biosynthetic pathway and post-synthetic modification

HSPGs primarily contain heparan sulphate chains, however, some also harbour chondroitin sulphate chains. Heparan and chondroitin sulphate are assembled on the core protein in the Golgi through a series of enzymatic steps, as shown in Figure 1.4. Briefly, a tetrasaccharide linker region is formed on the serine residue of the core protein consisting of xylose-galactose-galactose-glucuronic acid. Here the biosynthetic pathway diverges depending on whether chondroitin or heparan sulphate is formed. In heparan sulphate, disaccharides consisting of glucuronic acid and N-acetylglucosamine are added whereas in chondroitin sulphate, glucuronic acid and N-acetylgalactosamine are added (Esko *et al.*,

2009). The elongation of the GAG chains by addition of repeating disaccharide units is catalysed by the exostosin glycosyltransferases 1 and 2 (EXT1 and EXT2), for heparan sulphate and chondroitin synthases 1, 2 and 3 (CHSY-1, -2, -3) for chondroitin sulphate. During the synthesis of GAG chains further structural modifications can occur in the form of sulphation and epimerisation. Chondroitin sulphate tends to have long stretches of fully modified disaccharides whereas heparan sulphate may have clusters of modifications giving rise to segments with high levels of sulphation, termed S-domains, alternating with areas of low or no sulphation, termed NA-domains.

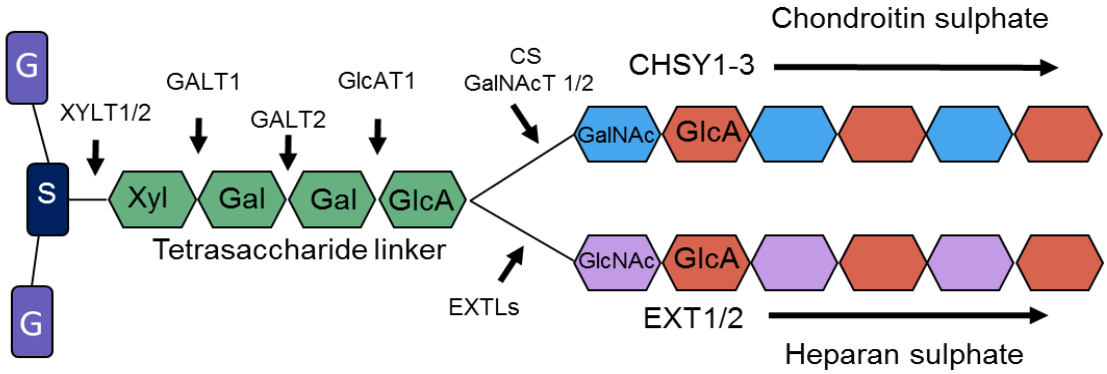

Figure 1.4 Biosynthesis pathway of heparan and chonroitin sulphate. A tetrasaccharide linker is covelantly attached to a serine residue within the core protein by a series of enzymatic reactions as indicated. At this point the biosynthetic pathway diverges and either a GalNAc (N-Acetylgalactosamine) followed by GlcA (glucuronic acid) is added to begin elongation of the chondroitin sulphate chain or a GlcNAc (N-Acetylglucosamine) followed by GlcA to begin elongation of the heparan sulphate chain. Key: Gal = galactose, Xyl = Xylose, S = serine, G = glycine.

After the HSPG translocates to its final subcellular compartment the heparan sulphate chains can be further modified by proteins resident on the cell surface or within the extracellular matrix. Heparanase is an endo-β glucuronidase that cleaves heparan sulphate into smaller fragments thus altering the heparan sulphate biological activity (Patel *et al.*, 2007, Hammond *et al.*, 2014). The 6-O-endosulfatases, SULF1 and SULF2, are plasma membrane proteins which can remove a sulphate group from glucosamine at the 6-O position, further resulting in modulation of growth factor-mediated cell signalling (Pye *et al.*, 1998, Esko and Selleck, 2002, Langsdorf *et al.*, 2007, Ghadiali *et al.*, 2017).

1.8 The syndecan family

The syndecan family are type-I transmembrane HSPGs that are ubiquitously expressed on the cell surface of adherent cells. The syndecans were first discovered in 1989 whilst investigating heparan sulphate- and chondroitin sulphate- containing cell-surface proteins (Saunders *et al.*, 1989). The name syndecans is derived from the Greek term *syndein* meaning 'to bind together', as it was thought that these proteins were important for cell adhesion to the ECM. In the non-mammalian vertebrates studied so far only one syndecan is present, whereas mammals have four distinct genes: Syndecan-1, -2, -3 and -4 (Fig. 1.5) (Bernfield *et al.*, 1999, Couchman, 2003). Since they were first discovered, the syndecans have had alternative names: SDC1 is also known as simply syndecan and CD138, SDC2 is also known as fibroglycan and CD362, SDC3 is also known as N-syndecan, SDC4 is also known as ryudocan and amphiglycan. Although they are less often mentioned by these names much of the older literature refers to them by those names. The expression pattern of each of the mammalian syndecans varies by tissue and by stage of development: SDC1 is primarily found in epithelial and mesenchymal tissues; SDC2 in mesenchymal, liver and neuronal tissues; SDC3 is mostly neuronal but is expressed in some musculoskeletal tissue, in macrophages, and blood vessels; and lastly, SDC4 is present in several different tissue types, which makes SDC4's expression unique compared with SDC1, -2 and -3 (Marynen *et al.*, 1989, Saunders *et al.*, 1989, Carey *et al.*, 1992, David *et al.*, 1992, Couchman, 2003, De Rossi and Whiteford, 2013).

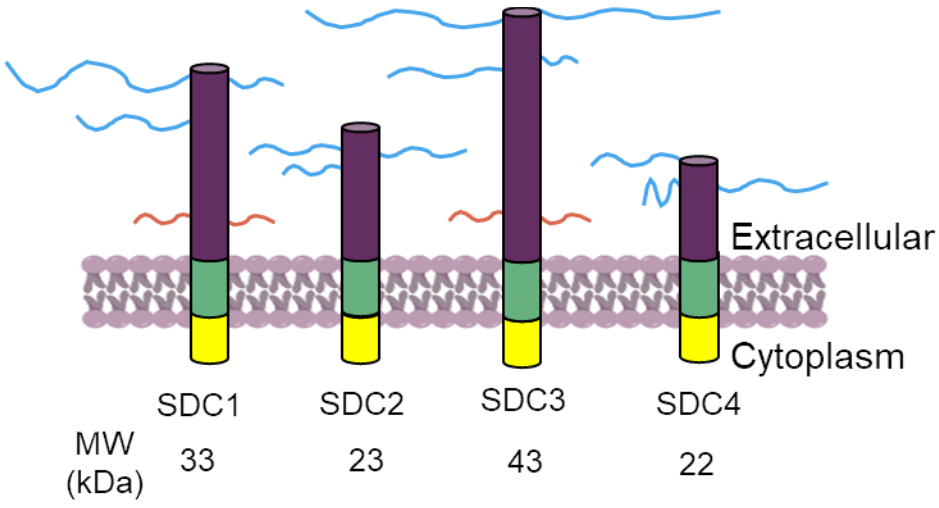

Figure 1.5: The mammalian syndecan family. There are four members belonging to the mammalian syndecan family (SDC1, -2,-3,-4). They consist of an extracellular domain (purple), transmembrane domain (green) and intracellualr domain (yellow). The syndecans can be decorated with glycosaminoglycan chains such as heparan sulphate (blue) or chondrotin sulphate (red). MW = predicted molecular weight.

1.8.1 Syndecan structure

The syndecans share a common structure consisting of a larger ectodomain where GAG chains attach, a transmembrane domain and a short intracellular domain (Fig. 1.6). The cytoplasmic and transmembrane domains are highly conserved whereas the ectodomains are highly variable across the syndecans. However, between vertebrate species the syndecan ectodomain and variable regions are highly conserved, suggestive of important specific functions in these domains. Based on sequence homology SDC1 and SDC3 form a subfamily and SDC2 and SDC4 form another. Additionally, SDC1 and SDC3 can bear both heparan sulphate and chondroitin sulphate chains as opposed to SDC2 and SDC4, which only have heparan sulphate chains (Bernfield *et al.*, 1999). Very limited structural information is available on the syndecans, particularly for the ectodomains as these are predicted to be intrinsically disordered (Leonova and Galzitskaya, 2015). Only the structure of the SDC4 cytoplasmic domain, in complex with syntenin, is known which adopts a symmetrical twisted clamp dimer (Shin *et al.*, 2001, Choi *et al.*, 2016).

The syndecans are fairly small proteoglycans with their core proteins predicted to be between 20 and 45 kDa, although in reality they appear almost two and a half times more than their predicted molecular weight by SDS-PAGE. This is likely due to their strong SDS-resistant dimerization which is mediated by the transmembrane domain plus a small amino acid sequence contained within the ectodomain (Asundi and Carey, 1995, Couchman, 2003). A highly conserved GxxxG motif is critical for syndecan homodimerization and for syndecans to transduce their signals across the plasma membrane (Choi *et al.*, 2005). Syndecan heterodimers have not been observed *in vivo* despite the similarity between their transmembrane domains and cytoplasmic domains. However, SDC2 and SDC4 have been shown to dimerize *in vitro* leading to an impairment in the activity of both syndecans (Choi *et al.*, 2015, Kwon *et al.*, 2016).

The conserved syndecan cytoplasmic domain is less than 40 amino acids long and contains no intrinsic kinase activity. The cytoplasmic domain is divided into three parts: two conserved regions (C1 and C2) which are highly conserved between the syndecans and flank a variable region (V) which is unique to each syndecan but highly conserved between species (Fig. 1.6). The function of the variable region in the cytoplasmic domain is largely unknown amongst each syndecan and little investigation into the protein interactors has been completed, with the exception of SDC4 (Couchman, 2003). A thorough study of the SDC4's variable region revealed that it includes a phosphatidylinositol-4,5-bisphosphate (PIP2) binding site which is important for SDC4 cytoplasmic dimerization and a binding site for protein kinase C-alpha (PKCα) (Oh *et al.*, 1997, Oh *et al.*, 1998). The C1 and C2 regions are much more studied and have revealed common functions between the syndecans (Fig.

1.6). The C1 region is involved in endocytosis, syndecan dimerization and interaction with actin-binding proteins such as ezrin and cortactin (Kinnunen *et al.*, 1998, Granes *et al.*, 2000). Whilst the C2 region binds to PDZ-containing proteins such as syntenin which modulates syndecan trafficking and recycling (Grootjans *et al.*, 1997, Zimmermann *et al.*, 2005) (Fig. 1.6). More in depth discussion regarding syndecan cytoplasmic signalling will occur later.

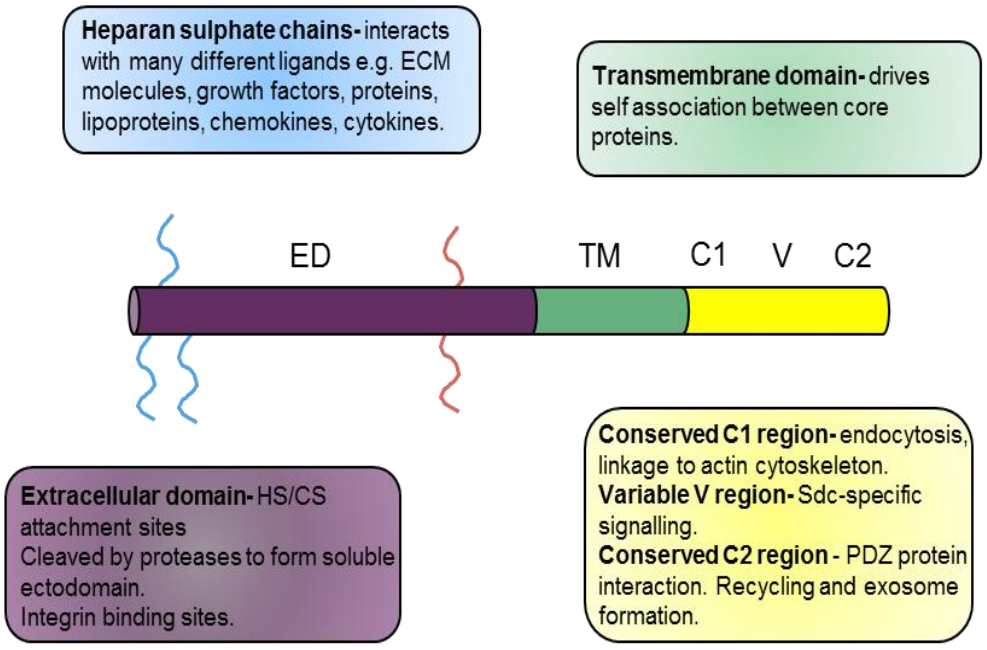

Figure 1.6: Basic structure and function of the syndecans. Key: ED = extracellular domain, TM = transmembrane domain, C1 = Conserved C1 region, V = Variable region, C2 = Conserved C2 region, HS/CS = heparan/chondroitin sulphate, ECM = extracellular matrix.

1.9 Syndecan function in cell signalling

The syndecans are involved in regulating a vast number of biological processes due to the high variability of the GAG chains in addition to their core proteins (Turnbull *et al.*, 2001). Syndecans can bind to ECM components, growth factors, cell adhesion molecules, lipases, chemokines and pathogens. As a result the syndecans act as receptors and co-receptors to modulate biological functions such as: cell proliferation, differentiation, myogenesis, cell adhesion, cell migration, cytoskeleton rearrangement, vesicular trafficking, inflammation, angiogenesis amongst many others (Tkachenko *et al.*, 2005, Morgan *et al.*, 2007, Choi *et al.*, 2011). The characteristics of the syndecans and how their structure translates to syndecan-mediated signalling is shown in Figure 1.7.

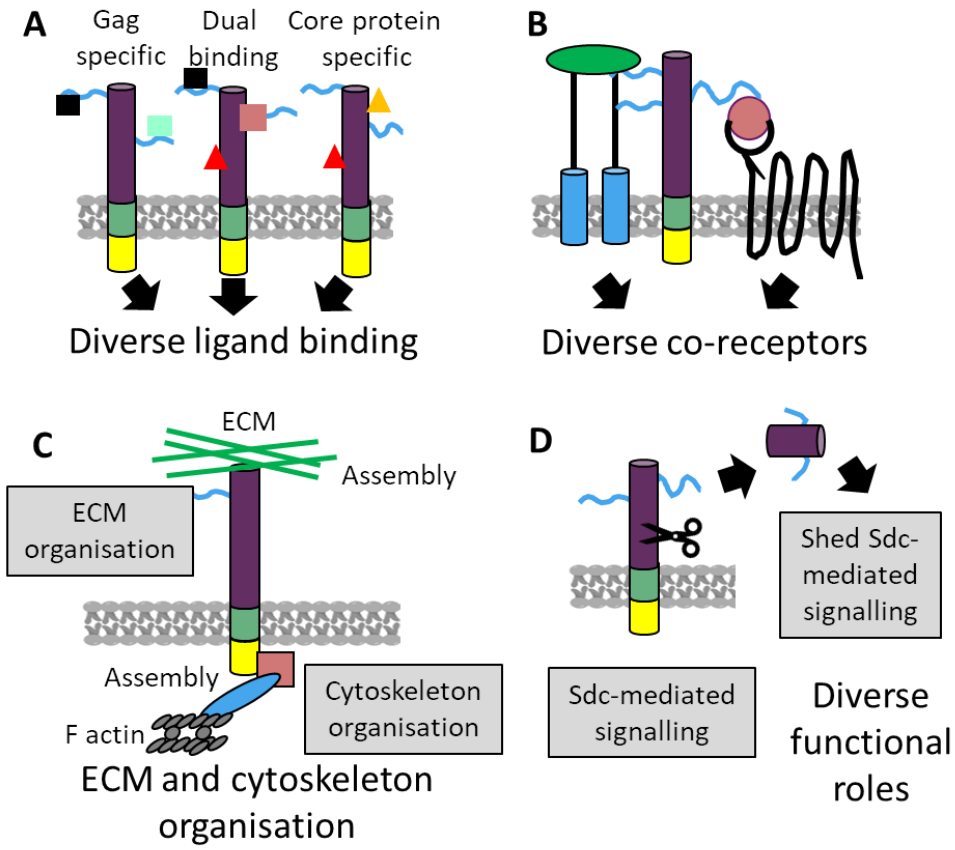

Figure 1.7: The various syndecan structural features which give rise to their diverse signalling capabilities. (A) Syndecans can bind to a diverse number of ligands. Some syndecan ligands are GAG or core protein specific, whilst some require cooperation. **(B)** Syndecans can act as co-receptors. **(C)** Syndecans regulate cell-ECM binding and cytoskeletal organisation. **(D)** Syndecans can shed their ectodoamins and signal in a paracine or autocrine manner. Figure from (Choi, *et al.*, 2011)

Both the core syndecan protein and the heparan sulphate chains are important for syndecan-mediated signalling. For example, heparan sulphate is required for FGF2 signalling and inhibition of binding between heparan sulphate and FGF2 resulted in a significantly reduced response to FGF2 stimulation and reduced FGF2-meduated inhibition of myoblast differentiation (Rapraeger *et al.*, 1991, Chu *et al.*, 2004). Similarly, removal of heparan sulphate or inhibition of sulphation prevented the proliferative response of cells to FGF2 (Clayton *et al.*, 2001). Sulphation clearly plays an important role in heparan sulphate-mediated signalling as inhibition of sulphation also disrupts BMP2/noggin signalling, (O'Connell *et al.*, 2007), and different sulphation patterns are observed between proliferating and differentiating myoblasts (Ghadiali *et al.*, 2017). Heparan sulphate is also essential for syndecan-mediated binding of the hepatitis E virus and subsequent infection of liver cells (Kalia *et al.*, 2009).

The requirement of heparan sulphate in various syndecan-mediated biological processes led scientists to believe that the syndecan core proteins primarily acted as

scaffold proteins for the GAG chains. However, more recently this attitude has changed as all the core syndecan proteins have shown biological activity, independent of heparan sulphate. All four mammalian core syndecan ectodomains have shown cell adhesion/migration regulatory properties (Beauvais and Rapraeger, 2003, Whiteford and Couchman, 2006, Whiteford *et al.*, 2007, De Rossi and Whiteford, 2013). Furthermore, the addition of a deglycosylated SDC2 ectodomain to cultured colon cancer cells inhibits epidermal growth factor (EGF)-mediated MAPK activation, promotes cell cycle arrest and inhibits tumour cell adhesion to the ECM (Park *et al.*, 2002).

The study of heparan sulphate and the core syndecan proteins have provided important information on syndecan-mediated signalling and suggests that both parts of the molecule are important. Cooperation of the core protein and GAG chains also appears important for modulation of signalling pathways, as cell-surface SDC3 has a higher affinity for thrombospondin-1 compared to free heparan sulphate (Herndon *et al.*, 1999). This was also observed for syndecan/fibronectin interactions (Tumova *et al.*, 2000). Pleiotrophin and Midkine can bind to both the core syndecan protein and heparan sulphate (Deepa *et al.*, 2004, Muramatsu *et al.*, 2006). Synstatin binds to SDC1's core protein to disrupt SDC1/αvβ3/IGFR interactions and inactivate signalling (Beauvais and Rapraeger, 2010). These data suggest that the syndecan core protein and GAG chains may work together to bind ligands increasing the complexity of the syndecan interactome (Choi *et al.*, 2011).

1.9.1 Syndecans as receptors and co-receptors

The syndecans have been implicated in direct interactions with components of the ECM and are thought to be involved in reorganisation of the ECM and actin cytoskeleton (Morgan *et al.*, 2007, Xian *et al.*, 2010). Many ECM components such as fibronectin, collagen type I, collagen type IV and laminins contain heparin binding motifs, which allow for heparan sulphate binding and therefore syndecan interactions (Kouzi-Koliakos *et al.*, 1989, San Antonio *et al.*, 1994, Lin *et al.*, 2000, Yamashita *et al.*, 2004, Cavalheiro *et al.*, 2017). Often the syndecans act as co-receptors for integrins which are key receptors involved in anchoring the actin cytoskeleton to the ECM and mediating cell adhesion. SDC1, SDC2 and SDC4 have been fairly well characterised in terms of ECM-integrin interactions in various cell types. For example, SDC1 forms a complex with α6β4 integrin in cancer cells plated on laminin 332 and is required for downstream signalling through the PI3K/AKT signalling pathway leading to cell spreading and protection from apoptosis (Wang *et al.*, 2010). SDC1 also supports integrin α2β1-mediated adhesion to collagen in a heparan sulphate-dependent manner; this mechanism is specific to SDC1 as genetic manipulation of SDC2 or SDC4 does not affect binding to collagen, suggesting a degree of specificity for syndecan ligand interactions (Ishikawa and Kramer, 2010). SDC1 has been associated with

dramatically altered ECM fibre architecture mediated by stromal fibroblasts and integrin αvβ3 is requires SDC1-dependent ECM fibre alignment (Yang and Friedl, 2016). SDC4/fibronectin/integrin signalling has been extensively studied and it is now known that SDC4 binds to fibronectin and cooperates with integrin α5β1 to activate Rac signalling and regulates cell migration (Yoo *et al.*, 2005, Bass *et al.*, 2007, Mahoney *et al.*, 2009). SDC4 in complex with Frizzled-7 binds to fibronectin to stimulate symmetric expansion of satellite cells (Fukada *et al.*, 2011). Additionally SDC4 can activate PKCα upon binding to fibronectin to modulate Rho GTPases (Lim *et al.*, 2003, Mahoney*, et al.*, 2009). SDC2 can also interact with ECM components such as fibronectin in cooperation with α5β1 to regulate actin stress fibre formation in Lewis lung carcinoma-derived P29 cells (Kusano *et al.*, 2000). In normal rat epithelial cells, overexpression of SDC2 enhanced collagen adhesion and cell migration in an integrin α2β1-dependent manner (Choi *et al.*, 2009). Currently there are no reported studies involving SDC3/integrin interactions.

FGF2, TGFβ, IGF, VEGF and Platelet-derived growth factor (PDGF) are all well known to cooperate with syndecans to mediate growth factor signalling (Choi *et al.*, 2011). Heparan sulphate bound to SDC4 interacts with both FGF2 and the FGF2 receptor forming a ternary complex, resulting in downstream signalling and activation of PKCα (Pellegrini *et al.*, 2000, Simons and Horowitz, 2001). The other mammalian syndecans have also been shown to interact with FGFs to modulate downstream signalling (Steinfeld *et al.*, 1996, Fuentealba *et al.*, 1999). The IGF receptor is activated by clustering of SDC1 in complex with integrins and is independent of IGF stimulation (Beauvais and Rapraeger, 2010). SDC2 can bind to VEGF and its role in angiogenesis has been investigated revealing that SDC2 inhibits angiogenic sprout formation *in vitro* (De Rossi *et al.*, 2014). Additionally the SDC3 ectodomain also appears to inhibit angiogenesis in cell culture (Chen *et al.*, 2004, De Rossi and Whiteford, 2013). SDC1 mediates HGF signalling and promotes the activation of PI3K signalling (Derksen *et al.*, 2002). More recent studies indicate that SDC2 and SDC4 can both bind HGF to activate signalling (Do *et al.*, 2015). SDC1 can also bind EGF to promote clustering and activation of the EGF receptor (Mahtouk *et al.*, 2006). Lastly, SDC1, SDC2 and SDC4 have been implicated in regulating Wnt signalling and together with syntenin, another syndecan binding protein, may function as a direct intracellular link between Frizzled receptors (Fukada *et al.*, 2011, Pataki *et al.*, 2015).

1.9.2 Intracellular domain interactions

The short cytoplasmic domain of the syndecans has no intrinsic kinase activity, however, they support roles for interaction with the actin cytoskeleton and downstream kinases, and functions in endocytosis (Lambaerts *et al.*, 2009). All of the syndecans have been shown to interact with the cytoskeleton. In the case of SDC3 the C1 region binds to Src kinase and

cortactin, whereas SDC2 binds to ezrin which signals to the actin cytoskeleton and is involved in endocytosis (Kinnunen *et al.*, 1998, Granes *et al.*, 2003). More mechanistic detail has been shown for SDC1 where activation of ERK signalling interrupts the SDC1, and α-tubulin binding. Src kinases can then phosphorylate tyrosine resides in the C region of SDC1 allowing recruitment of cortactin and actin-mediated endocytosis (Chen and Williams, 2013). The universally conserved C2 region is important for PDZ binding proteins. Four proteins have been identified so far that bind to the syndecans by this domain: syntenin, synectin, synbindin, and calcium/calmodulin dependent serine protein kinase (CASK) (Tkachenko *et al.*, 2005). Little is known about how these proteins and the syndecans interacts to regulate function. However, work on syntenin suggests a role for syndecan in trafficking and recycling (Zimmermann *et al.*, 2005, Lambaerts *et al.*, 2009). Additionally, syntenin can crosslink the Frizzled7 receptor and SDC2 or SDC4, via its PDZ1 and PDZ2 domains (Luyten *et al.*, 2008). SDC2 and SDC4 in complex with synectin appear to regulate adhesion and migration (Gao *et al.*, 2000). Furthermore, phosphorylation of SDC4^{Y180} by c-Src, controls recycling of α5β1 and αVβ3 integrins to the plasma membrane in an Arf6-dependent manner (Morgan *et al.*, 2013). In contrast to what is known about C1 and C2 interactors in syndecans, almost nothing is known about what proteins interact with the variable regions. The exception being SDC4, where it is known that PKCδ, PKCα, syndesmos and α-actinin bind the variable region, and many of these interactions are involved in formation of focal adhesions (Denhez *et al.*, 2002, Bass *et al.*, 2008, Okina *et al.*, 2012, Couchman *et al.*, 2015).

1.9.3 Syndecan shedding

The extracellular domain of the syndecans can be proteolytically cleaved at a juxtamembrane site, releasing the ectodomain from the cell surface in a highly-regulated process called shedding (Hooper *et al.*, 1997). The syndecans are cleaved by various membrane-bound and soluble matrix metalloproteinases (MMPs) such as MMP-2, MMP-3, MMP-7, MMP-9, MMP-14 or A-disintegrin and metalloproteinase 17 (ADAM17) (Endo *et al.*, 2003, Pruessmeyer *et al.*, 2010, Manon-Jensen *et al.*, 2013). When the ectodomains are shed they become soluble HSPGs that can act in a paracrine or autocrine manner, behaving as negative or positive regulators of several biological processes. Shedding reduces the number of syndecan proteins on the cell surface, which may limit cell signalling or remove syndecan-mediated inhibition of cell signalling. Additionally the soluble ectodomain may compete with the cell surface bound syndecans for ligands (Steinfeld *et al.*, 1996).

Syndecan shedding occurs constitutively in some cultured cells, as part of normal syndecan turnover, but can also be accelerated in response to various stimuli or during

pathophysiological events (Yanagishita and Hascall, 1984, Manon-Jensen *et al.*, 2010). External stimuli affecting syndecan shedding include: Phorbol 12-Myristate 13-Acetate (PMA), FGF2, EGF, VEGF, bacterial virulence factors and various cytokines (Subramanian *et al.*, 1997, Su *et al.*, 2007). The precise mechanisms which cause activation of shedding are unknown as different agonists appear to activate different intracellular pathways. The intracellular domains appear to play a role in the regulation of syndecan shedding as phosphorylation of tyrosine residues on the SDC1 intracellular domain promote its shedding (Reiland *et al.,* 1996). However, it seems unlikely that this is the only mechanism involved in syndecan shedding as Rab5 is able bind to SDC1 and stimulate shedding independently from tyrosine phosphorylation (Hayashida *et al.*, 2008). Syndecan shedding has been found in various biological functions such inflammatory responses, cell migration, tumour progression and angiogenesis (Li *et al.*, 2002, Seidel *et al.*, 2003, Fears *et al.*, 2006, Manon-Jensen *et al.*, 2010). Syndecan shedding is a significant aspect of syndecan biology, although not well mechanistically characterised, it is clear that the soluble ectodomains are important for regulation of several biological functions and tight control of shedding is necessary for physiological syndecan function.

1.10 Syndecans and the regulation of myogenesis

Syndecans are important regulators of myogenesis and are expressed dynamically during activation, proliferation and differentiation of satellite cells (Pisconti *et al.*, 2012). During mouse muscle development SDC1, SDC3 and SDC4 are present in both myoblasts and myofibres and peak around embryonic day (E) 12.5, E14.5 and E13.5 respectively. SDC1 expression rapidly declines after this point until absent in postnatal muscle. In contrast, SDC3 and SDC4 expression declines much more slowly and is still present in postnatal muscle tissue, however, they are restricted to satellite cells (Cornelison *et al.*, 2001, Olguin and Brandan, 2001). SDC2 is undetectable in muscle cells during mouse embryonic development (David *et al.*, 1993).

In adult skeletal muscle, the expression pattern of the syndecans is well described for SDC3 and SDC4, which are the only syndecans observable in quiescent satellite cells by immunostaining (Cornelison *et al.*, 2001). Additionally SDC3 and SDC4 protein levels are significantly up and down regulated during injury-induced muscle regeneration suggesting that these syndecans are important regulators of satellite cell function (Cornelison *et al.*, 2001, Casar *et al.*, 2004). However it has also been reported that upon activation, the mRNA for all syndecans can be detected in myoblasts isolated from injured muscle (Pisconti*, et al.*, 2012). This apparent inconsistency with previously published literature might be due to the different techniques employed to detect the four syndecans in postnatal satellite cells; Cornelison *et al.* (2001) used immunofluorescence whereas Pisconti *et al.*

(2012) used microarray analysis. Therefore it is possible that either the genes are not expressed at the protein level or that the antibodies to SDC1 and SDC2 used in immunofluorescence were not sensitive enough to detect low protein levels. In a C2C12 myoblast cell line SDC1 and SDC3 are downregulated upon differentiation of myoblasts suggesting that SDC1 and SDC3 may promote proliferation or prevent differentiation (Larrain *et al.*, 1997, Fuentealba *et al.*, 1999). On the other hand SDC2 expression dramatically increases between proliferating and differentiating C2C12 cells (Moran *et al.*, 2002). More recent studies have shown that SDC2 and SDC4 are more abundantly expressed compared to SDC1 and SDC3 in early differentiated primary satellite cells, consistent with the reduced expression of SDC1 and SDC3 during differentiation of myoblasts previously observed (Do *et al.*, 2015).

The discovery that SDC3 and SDC4 are expressed in quiescent satellite cells and their expression is maintained for at least 96 hours post injury suggested that SDC3 and SDC4 are important regulators of adult myogenesis (Cornelison *et al.*, 2001). Indeed, distinctive roles for SDC3 and SDC4 in muscle regeneration were discovered in mice when SDC3 and SDC4 were genetically ablated (Cornelison *et al.*, 2004). *Sdc3*$^{-/-}$ tibialis anterior muscles showed more than a 15-fold increase in the number of centrally located myonuclei compared to wild type mice, suggesting that a number of myofibres were undergoing regeneration in the absence of induced injury (Cornelison *et al.*, 2004). In contrast, *Sdc4*$^{-/-}$ mice did not display the same phenotype. Multiple rounds of muscle injury in *Sdc3*$^{-/-}$ mice progressively increased the median myofibre size of the muscle whereas the median myofibre size in wild type mice decreased (Pisconti *et al.*, 2010, Pisconti *et al.*, 2016). In a dystrophic mouse model, where the muscle undergoes repeated cycles of degeneration and regeneration, loss of SDC3 appears to be protective, reducing the amount of fibrosis and increasing myofibre area *in vivo* (Pisconti et al., 2016). Functionally, *Sdc3*$^{-/-}$ dystrophic mice run further and for longer than their dystrophic counter parts and the diaphragm muscles of *Sdc3*$^{-/-}$ dystrophic mice are dramatically improved as observed by less fibrosis and more muscle mass (Pisconti *et al.*, 2016).

Upon closer inspection of explanted myofibres and satellite cell-derived myoblasts in culture, further differences between *Sdc3*$^{-/-}$ and *Sdc4*$^{-/-}$ mice were observed. The number *Sdc3*$^{-/-}$ satellite cells per myofibre, identified as SDC4+ myofibre-associated cells, exceeded that of wild type satellite cells by five-fold (Cornelison *et al.*, 2004), which was not accompanied by an equal increase when PAX7 was used as a satellite cell marker (Pisconti *et al.*, 2016). It was later shown that SDC3 loss somehow impairs PAX7 expression and acquisition or maintenance of quiescence (Pisconti *et al.*, 2016). Consistently *Sdc3*$^{-/-}$ satellite cells, cultured in low serum-conditions to induce differentiation, show increased

differentiation and larger myotubes compared with wild type satellite cells (Pisconti *et al.*, 2010). Furthermore, when myofibres are explanted from *Sdc3*$^{-/-}$ mice, left in suspension for 2.5 days then moved to gelatin-coated plates to allow satellite migration from the myofibre to the plate, the number of *Sdc3*$^{-/-}$ satellite cells that had migrated away from explanted myofibres and adhered to gelatin-coated plates *in vitro* was two-fold more than that observed in wild type myofibre cultures (Pisconti *et al.*, 2016). This adhesion/migration phenotype, along with the impairment in PAX7 expression, and the greater numbers of SDC4+ satellite cells and centrally-nucleated myofibres in uninjured muscle, all support a model whereby SDC3 controls the balance between satellite cell differentiation and self-renewal. The *Sdc4*$^{-/-}$ satellite cell phenotypes are different from the *Sdc3*$^{-/-}$ phenotypes. The number of *Sdc4*$^{-/-}$ satellite cells per myofibre in uninjured muscle is no different to wild type satellite cells, (Cornelison *et al.*, 2004). However, *Sdc4*$^{-/-}$ satellite cells show impaired activation, proliferation and differentiation of satellite cells in response to injury and a failure to regenerate muscle (Cornelison *et al.*, 2004, Farina *et al.*, 2012).

Although some of the functional details of SDC3 and SDC4 have been revealed for muscle regeneration, there is far less known about the mechanistic details. It was hypothesised that SDC3 and SDC4 could mediate myoblast cell signalling through interactions with receptors known to bind to heparan sulphate, as disruption of heparan sulphate in cultured primary satellite cells resulted in impaired myogenesis (Cornelison *et al.*, 2001). FGF signalling is dependent on heparan sulphate to transduce signals and is important for proliferation and activation of satellite cells (Rapraeger *et al.*, 1991, Olwin and Rapraeger, 1992). Additionally, the sulphation pattern of heparan sulphate is important for FGF2-mediated myoblast proliferation and differentiation (Ghadiali *et al.*, 2017). *Sdc4*$^{-/-}$ satellite cells fail to activate FGF2 signalling as measured by ERK1/2 phosphorylation, whereas *SDC3*$^{-/-}$ satellite cells are hypersensitive to FGF2 stimulation (Fuentealba *et al.*, 1999, Cornelison *et al.*, 2004). More detailed mechanistic information was identified by Pisconti *et al.* (2010) when SDC3 was found in complex with NOTCH1 and this interaction facilitated NOTCH1 cleavage by TACE (tumor necrosis factor-alpha converting enzyme), which promoted NOTCH1 signalling in satellite cells. Loss of SDC3 dramatically reduced NOTCH1 cleavage and subsequently reduced activation of NOTCH1 target genes, likely leading to the impaired self-renewal observed in *Sdc3*$^{-/-}$ satellite cells (Pisconti *et al.*, 2010). Intriguingly, *Sdc3*$^{-/-}$ satellite cells cultured in growth medium had observably higher levels of global tyrosine phosphorylation compared to wild type satellite cells, suggesting that activation of receptor tyrosine kinase pathways were increased when SDC3 was lost (Cornelison *et al.*, 2004). This effect was not observed in *Sdc4*$^{-/-}$ myoblasts, indicating that this phenotype was SDC3 specific (Cornelison *et al.*, 2004).

1.11 Hypothesis and project aims

There is strong evidence from the literature that SDC3 is an important regulator of satellite cell homeostasis and is important for interactions with the satellite cell niche. However, little is known about the SDC3-mediated cell signalling mechanisms leading to these phenotypes. Since *Sdc3*$^{-/-}$ myoblasts show a general upregulation of tyrosine phosphorylation, I hypothesised that SDC3 regulates myogenesis by modulating several signalling pathways simultaneously. Therefore, the overall aims of my project were to:

1) Identify SDC3-regulated signalling pathways during myogenesis by using a top-down, unbiased approach.
2) Validate these signalling pathways by using cell biology/biochemistry-based approaches.

Chapter 2

2 Materials and methods

2.1 Routine culture of C2C12 myoblasts

C2C12 myoblast growth medium: Dulbecco's Modified Eagle's Medium – high glucose (DMEM, D6429 Sigma-Aldrich), 10% foetal bovine serum (FBS, Gibco), 1% penicillin/ streptomycin (Invitrogen).

C2C12 myoblast differentiation medium: Dulbecco's Modified Eagle's Medium – high glucose (DMEM, D6429 Sigma-Aldrich), 2% horse serum (HyClone), 1% penicillin/ streptomycin, 2 mM glutamine.

The same batches of FBS and horse serum were used throughout the study. The parental C2C12 myoblast cell line was obtained from ATCC. For routine culture C2C12 myoblasts were cultured in growth medium between 40 and 70% confluence at 37°C under a humidified atmosphere of 5% CO_2 and atmospheric O_2. C2C12 myoblasts were cultured on uncoated plastic dishes. Cells were detached for passaging using 0.5% trypsin-EDTA (Ethylenediaminetetraacetic acid) solution obtained from Sigma (T3924). For differentiation of C2C12 myoblasts, 90% confluent cultures were washed twice with DMEM before being cultured in differentiation medium for various time points between 1 and 7 days.

2.2 Expression and purification of GST-S3ED in C2C12 cells

The N-terminal plasma membrane signal sequence of SDC3 and syndecan-3-ectodomain (S3ED) cDNA (amino acids A_1-R_{338}) were cloned into the OG1238 vector backbone following manufacturers' recommendation (Oxford Genetics). The OG1238 vector fused a glutathione S-transferase (GST) tag to the C-terminus of S3ED upon translation and conferred cellular resistance to puromycin. Purified OG1238-S3ED was transfected into myoblasts using Lipofectamine 2000 (ThermoFisher) according to manufacturer instructions. Twenty-four hours after transfection, the culture medium was replaced with selective medium (growth medium + 2 µg/µl puromycin) and sub-cultured for additional 4-5 passages. After a stably transfected cell line was established, the conditioned medium from myoblasts cultured in growth medium, was collected and frozen if not used immediately.

S3ED-GST protein expressed by mammalian myoblasts was designed to be secreted into the cell culture medium for easy purification. 50 µl of glutathione-coated sepharose 4B beads (GE Healthcare) were added to the conditioned medium to bind GST-proteins according to the manufacturers protocol. Beads were boiled in 5 x laemmli buffer before proteins resolved on an 8% SDS-PAGE and subjected to western blotting.

2.3 Western Blotting

Cells were lysed in modified RIPA buffer (50 mM Tris-HCl, pH 7.4, 1% NP-40, 0.25% sodium-deoxycholate, 150 mM NaCl, and 1 mM EDTA) supplemented with a protease inhibitor cocktail (Complete, Roche) and phosphatase inhibitors (2 mM Na_3VO_4, 2 mM NaF and 1 x PhosSTOP (Roche)). Lysates were rotated end-over-end for 30 minutes at 4°C, then lysates were clarified by centrifugation at 13,000 *x g* for 10 minutes at 4 °C. Clarified lysates were snap frozen in liquid nitrogen for long term storage. Total protein content was quantified using the bicinchoninic acid assay kit from Pierce (BCA, Thermo Scientific) according to manufacturer's instructions. For non-HSPG western blotting total protein (10-20 µg) was separated on 8% or 10% SDS-PAGE and then transferred onto a nitrocellulose membrane (Hybond, GE Healthcare) for 2 hours at 250 mA on ice.

For detection of HSPGs, cell lysates were precipitated with methanol overnight at -20 °C. Lysates were centrifuged to collect precipitates at 13,000 *x g* then washed once with ice cold acetone and centrifuged again to collect precipitates. Pellets were left to air dry until glassy in appearance. Pellets were then re-suspended in heparinase buffer (100 mM sodium acetate, 0.1 mM calcium acetate and 1 mM magnesium chloride) and digested with 0.25 mU heparinase III (Ibex) and 0.5 mU chondroitinase-ABC (Sigma-Aldrich) for 2 hours at 37 °C, before addition of a second aliquot of heparinase III for an additional 2 hours at 37 °C. Treatment with heparinise III and chondroitinase-ABC removed heparan sulphate and chondroitin sulphate chains respectively. Following digestion, samples (50 µg) were transferred to a nitrocellulose membrane as described for non-HSPG western blotting.

Membranes were then blocked with either 5% milk or 5% bovine serum albumin (BSA) in 0.1% TBST (Tris buffered saline + Tween20, pH 7.5) for 1 hour at room temperature. Primary antibodies were incubated overnight at 4 °C in the recommended blocking solution (Table 2.1). Secondary antibodies (HRP-conjugated, Santa Cruz) were diluted at 1: 10,000, in the same blocking buffer as used for primary antibodies and incubated with membranes for 1 hour at room temperature. Western blots were visualised using chemiluminescence (Clarity™ ECL, Biorad) and imaged on an ImageQuant-Las4000 (GE healthcare) gel doc system. Band intensity was analysed using the 'Analyze Gel' function in ImageJ.

Table 2.1: Primary antibodies used for western blotting. BSA = bovine serum albumin, p = phosphorylated, CST = Cell Signaling Technology, HRP = Horseradish peroxidase

Target	Dilution	Blocking solution	Secondary antibody	Manufacturer, product code
AKT	1:3000	5% BSA	α-Rabbit-HRP	CST, 9272
pAkt^{S473}	1:3000	5% BSA	α-Rabbit-HRP	CST, 4060
ERK1/2	1:3000	5% BSA	α-Rabbit-HRP	CST, 9102
pERK1/2$^{T202/Y204}$	1:3000	5% BSA	α-Rabbit-HRP	CST, 9101
GAPDH	1:8000	5% milk	α-Mouse-HRP	Sigma, G8795
GST	1:1000	5% milk	α-Mouse-HRP	Thermo, MA4-004
IR/IGFR	1:1000	5% BSA	α-Rabbit-HRP	CST, 3025
pIR/IGFR	1:1000	5% BSA	α-Rabbit-HRP	CST, 3024
IRS1	1:3000	5% BSA	α-Rabbit-HRP	CST, 3407
pIRS1^{S302}	1:2000	5% BSA	α-Rabbit-HRP	CST, 2384
pIRS1^{S307}	1:2000	5% BSA	α-Rabbit-HRP	CST, 2381
pIRS1^{Y608}	1:3000	5% BSA	α-Rabbit-HRP	Millipore, 09432
RPS6	1:3000	5% BSA	α-Rabbit-HRP	CST, 2217
pRPS6$^{S236/S236}$	1:3000	5% BSA	α-Rabbit-HRP	CST, 4858
pRPS6$^{S240/S244}$	1:3000	5% BSA	α-Rabbit-HRP	CST, 5364
SDC3	1:1000	5% milk	α-Goat-HRP	R&D systems, AF2734
SDC3	1:4000	5% milk	α-Rabbit-HRP	Donated by Prof Alan Rapraeger, University of Wisconsin
pTyrosine	1:2000	5% BSA	α-Rabbit-HRP	CST, 8954

2.4 Expression and extraction of GST-S3ED in *Escherichia coli*

A pGEX-2T plasmid containing S3ED cDNA (amino acids A45-R338) was kindly donated by Prof Alan Rapraeger (University of Wisconsin at Madison, USA). When expressed in *Escherichia coli* this plasmid produces S3ED fused to a N-terminal glutathione S-transferase (GST) tag. Plasmids were transformed into the *E. coli* strain BL21 (#C2530H, New England Biolabs), then a single colony was picked for culture in Luria broth (LB) medium with 100 µg/mL ampicillin. Protein expression was induced by addition of 1 mM Isopropyl β-D-1-thiogalactopyranoside (IPTG) when cells reached an OD_{600} of 0.5. Cells were cultured for 8 hours at 28 °C, then cultures were centrifuged at 4 °C and 6,000 *x g* for 10 minutes. LB medium was removed and pellets were snap frozen and kept at -80°C if not lysed immediately.

E. coli cell pellets containing S3ED-GST were resuspended in lysis buffer (50 mM Tris-HCl pH 7.5, 150 mM NaCl, 5% glycerol, 0.2% deoxycholate, 1 mM phenylmethylsulfonyl fluoride (PMSF), 1 mM EDTA and 200 µg lysozyme). DNA was digested in the lysates by adding 5 mM $MgCl_2$ and 1 µg/ml of Dnase I (Sigma Aldrich) for 30 minutes at 4°C. Lysates were centrifuged at 13,000 x g for 20 minutes to separate soluble and insoluble fractions. Glutathione-coated sepharose 4B beads (GE healthcare) were used to purify GST-S3ED fusion protein from bacterial cell lysates as per manufacturer's instructions. Purified GST-S3ED protein was aliquoted and snap frozen in liquid nitrogen then stored at -80°C.

2.4.1 Separation of bacterially expressed GST-S3ED by size exclusion

Size exclusion chromatography was performed on an AKTA purifier (GE Healthcare) using a Superdex 200 10/300, 24 mL column (GE Healthcare). The column was equilibrated with 50 mL of 50 mM Tris-HCl and 500 mM NaCl, pH 8.0. After equilibration, a 0.5 ml aliquot of GST-S3ED (4 mg/ml) was injected and separated on an isocratic path (24 mL) at a flow rate of 0.5 mL/min. The absorbance was measured at 280 nm. After 5 mL had passed through the column, 0.5 mL fractions were collected.

2.4.2 Separation by anion exchange

To further purify the recombinant S3ED anion exchange chromatography was performed on an AKTA purifier (GE Healthcare). A 1 mL HiTrap Q-HP column (GE Healthcare) was equilibrated with binding buffer (50 mM Tris, pH 7.5) with a flow rate of 0.5 mL/min. 500 µg of recombinant GST-S3ED were passed through the column and allowed to bind, followed by 5 column volumes of binding buffer to remove non-bound protein. A step gradient of increasing salt concentration (0 – 500 mM) was employed to elute the bound protein.

2.5 Pull-down of GST-S3ED proteins

The recombinant SDC3-ectodomain-GST (S3ED-GST) and GST proteins were purified from *E. coli* according to the following two methods:

Method A: Equal amounts of recombinant S3ED and GST (50 µg) were bound to glutathione-coated sepharose beads for 6 hours at 4 °C. Beads were washed twice with 1x PBS to remove unbound protein. C2C12 cells were lysed with either modified RIPA buffer or HSPG buffer (1 X PBS, 1% Triton X100, 0.1% SDS), then insoluble cell debris removed by centrifugation. Equal amounts of cell lysate were added to the beads, which had been pre-bound with either GST-S3ED or GST. 1x PBS plus protein inhibitors (Complete, Roche) were added to bring the bead-protein slurry up to 600 µl. The bead-protein mixture was

purified as per manufacturers' instructions. Soluble extracts were run on an 8% SDS-PAGE and proteins visualised by Coomassie or Silver staining.

Method B: Equal amounts of recombinant S3ED or GST (50 µg) were added to C2C12 myoblasts cultured in growth medium, for 20 minutes before culture medium was removed and myoblasts lysed in either RIPA buffer or HSPG buffer. Equal amounts of cell lysate were then added to the pre-prepared glutathione-coated beads and GST proteins purified as per manufacturers' instructions. Soluble extracts were run on an 8% SDS-PAGE and proteins visualised by Coomassie or Silver staining.

2.5.1 Coomassie and Silver staining

SDS-PAGE gels were stained with Coomassie stain (0.1% Coomassie Brilliant Blue R250 (Sigma Aldrich), 50% MeOH (v/v), 10% Glacial acetic acid (v/v) 40% H_2O) overnight at room temperature with agitation. To destain and visualise protein bands a destaining buffer (50% MeOH (v/v), 10% Glacial acetic acid (v/v) 40% H_2O) was added to the gels until sufficient Coomassie background stain removed.

For Silver staining an online protocol was followed (Chevallet *et al.*, 2006). Silver Nitrate, Sodium thiosulfate, sodium carbonate and formaldehyde were obtained from Sigma Aldrich.

2.6 SDC3 knockdown in C2C12 myoblasts

Two different SDC3 knockdown (S3KD) cell lines and a related control cell line were previously established in the lab (S3KD90 and S3KD91). Briefly, C2C12 myoblasts were transfected with plasmids containing anti-SDC3 shRNAs (S3KD90: Sigma Mission # TRCN0000071990 or S3KD91: Sigma Mission # TRCN0000071991) or the empty vector (pLKO-1, Sigma), sequences available online at www.sial.com. The pLKO-1 plasmid confers resistance to puromycin therefore S3KD myoblasts and empty vector control (Vector) myoblasts were cultured with 2 µg/mL puromycin to select for positively transfected cells. No clonal selection was employed because C2C12 myoblasts are a heterogenous population: sub-cloning would have inevitably randomly selected for clones with different proliferative and differentiative properties and therefore it would have been impossible to discriminate whether the phenotypes observed were due to sub-cloning or to SDC3 knockdown.

2.7 Reverse Transcription- polymerase chain reaction (PCR)

2.7.1 RNA extraction and cDNA synthesis

C2C12 Myoblasts were washed once with sterile 1 x PBS then lysed on plate with RNA extraction buffer (RNA easy-mini kit, Qiagen). RNA was extracted as described in the manufacturers' protocol. RNA was quantified using Nanodrop2000 (Thermo Scientific). Equal amounts of RNA were converted into cDNA using tetroreverse cDNA kit (Bioline).

2.7.2 PCR to confirm SDC3-knodwon in C2C12 myoblasts

SDC3 cDNA was amplified using Phusion High-Fidelity DNA Polymerase (New England Biolabs) and specific primers for SDC3 (**F:** GGTGGTGGCTGTGGAAGGAG, **R:** GGAGGGAATGGGACCAAAGAA). β-actin was amplified as an internal loading control (β-actin primers were **F:** CCCTAGGCACCAGATCATG **R:** TGGTACCACCAGACAGCAC). A total of 50 ng cDNA was used in each reaction. Polymerase chain reaction (PCR) buffer was supplemented with GC-rich buffer as recommended for GC-rich templates by the manufacturer. Equal amounts of PCR products were loaded onto a 0.8% agarose gel and run at 90 volts for 30 minutes. Gels were visualised by ultraviolet light.

2.7.3 Real-time quantitative PCR (qPCR)

Primers for qPCR were designed using the NCBI Primer-BLAST software to have a melting temperature of 60 °C and an amplicon size between 60-150 base pairs (Table 2.2). Primers were optimized to form one PCR product and with an efficiency of above 0.8. Primers were purchased from Eurofins Genomics. Relative gene expression was quantified from cDNA of proliferating and 5-day differentiating C2C12 cells by Real-time quantitative PCR (qPCR) using the LightCycler 480 SYBR Green I Master mix kit (Roche) following manufacturers' instructions. 0.3 µM of primers were used for each PCR reaction and equal amount of cDNA was used for each syndecan primer pair, while a smaller amount was used to detect GAPDH as indicated in Table 2.2. Reactions were completed in triplicate. The qPCR programme used was as follows: *Pre-incubation*: 1 cycle of 95°C for 5 minutes, *amplification*: 45 cycles of 95°C for 20 seconds, 60°C for 15 seconds, 72°C for 10 seconds and *melting curve*: 1 cycle of 95°C for 5 seconds, 70 °C for 1 minute, 95°C continuous. Results were analysed with the LightCycler480 software (Roche) using the second derivative maximum method to set the threshold cycle (CT). The relative quantification of Syndecan1-4 expression was calculated using the delta-delta-CT method using GAPDH as reference gene and "Vector proliferating" as reference condition.

Table 2.2: Primers used for real-time PCR.

Gene	Forward primer	Reverse primer	Amplicon size (bp)	cDNA used (ng)
SDC1	TCTGGGGATGACTCTGACAAC	TGCCGTGACAAAGTATCTGG	60	200
SDC2	GTTCTAGCAGCCGTCATTGCT	GCGTTCTCCAAGGTCGTAGC	120	100
SDC3	AGCCTGATGTTGCTGAGAGGA	TTACTGGCACCTCTGGCTCAT	129	200
SDC4	CTTGGCAGCTCTGATCGTGG	GGGTTTCTTGCCCAAGTCGT	121	100
GAPDH	CCCCTTCATTGACCTCAACTAC	TCCACGACATACTCAGCACC	182	5

2.8 C2C12 myoblast stimulation with FGF2 or FBS

S3KD and Vector C2C12 myoblasts were plated at a density of 45,000 cells per 10 cm plate and cultured for two days. Cells were serum-starved for 5 hours by washing twice with warm DMEM and then left in 9 mL of DMEM + 2 µg/mL puromycin. After serum-starvation myoblasts were treated with either 1 mL 100% FBS or 2 nM FGF2 (donated by Prof David Fernig; see section 2.14 for further details). Myoblasts were lysed after the indicated times with RIPA buffer and centrifuged to remove insoluble cell extracts. Soluble lysates were snap frozen ready for western blotting.

2.9 Immunostaining of cells

To fix cells, medium was aspirated, then a 4% paraformaldehyde (PFA, Sigma) solution (prepared in 1 x PBS, pH 7.4) was added to cover the cells. Cells were incubated with PFA at room temperature for 10 minutes, then PFA was aspirated. Cells were washed three times with 1 x PBS for five minutes each, then stored at 4 °C covered in PBS, until immunostaining. For detection of DNA and therefore the nucleus, DAPI (Life Technologies) was added to the cells at a concentration of 2 µg/mL in PBS and incubated at room temperature for 5 minutes. Cells were washed 3 times with 1 x PBS and stored at 4°C until imaging.

For detection of myosin heavy chain (MyHC), cells were permeabilised with PBS + 0.2% TritonX100 for 10 minutes at room temperature. Cells were incubated with blocking solution (PBS + 10% horse serum) for 40 minutes. The primary anti-MyHC antibody (Developmental Studies Hybridoma Bank at Iowa University, MF20 clone) was diluted at 1:150 in PBS + 1% horse serum before being incubated with the cells overnight at 4°C. The next day cells were washed once with PBS + 0.2% TritonX100 then twice more with PBS before blocking for

30 minutes in blocking solution. The blocking solution was removed and the secondary antibody (anti-mouse conjugated to AlexaFluor 488) was diluted at 1:500 in PBS + 5% horse serum and incubated with cells for 1 hour. Cells were then washed once with PBS + 0.2% TritonX100 then twice more with PBS then stored in the dark at 4°C.

2.10 Microscopy, image processing and quantification

Images were taken using an epifluorescence microscope (EVOS-FL, Life Technologies. A 10X magnification was used unless otherwise stated. Images were adjusted using the 'Subtract Background' function in ImageJ (Version 1.48) for visualization purposes only.

2.10.1 Quantification

Quantification of immunostaining was performed by taking at least 10 random images per well, with three technical replicates and three biological replicates unless otherwise stated. A bespoke script written for Fiji (available at [http://fiji.sc]) was used to count DAPI+ nuclei and myotube area as described previously (Ghadiali *et al.*, 2017). For differentiation and fusion index immunofluorescence was manually counted as described below:

a) The Differentiation Index

$$\left(\frac{\text{MyHC positive nuclei}}{\text{Total nuclei}}\right)*100$$

b) The Fusion Index:

$$\left(\frac{\text{MyHC positive cells with at least two nuclei}}{\text{Total number of nuclei in all MyHC positive cells}}\right)*100$$

2.11 C2C12 myoblast adhesion assay

Vector and S3KD myoblasts were trypsinised, collected then centrifuged at 360 *x g* for 5 minutes. Myoblasts were re-suspended in C2C12 growth medium and counted using a haemocytometer. An equal number of cells were collected and centrifuged to remove growth medium, myoblasts were then washed twice with either growth medium or serum-free medium (DMEM + 1% penicillin/streptomycin), centrifuged and re-suspended at 7,000 cells/mL. For each condition, 1 mL/well of the cell suspension was then plated in triplicate in a 12-well plate. Cells were left for 1 hour in a cell incubator (humidified 37 °C, 5% CO_2 and atmospheric O_2). Cells were washed once with 1x PBS to remove non-adherent cells then fixed in 4% PFA for 10 minutes at room temperature and stained with DAPI to visualise cell nuclei.

2.12 Phosphatase activity assay

Cells were lysed in HSPG buffer without phosphatase inhibitors. Equal amounts of lysate were incubated with 50 mM pNPP (p-Nitrophenyl Phosphate, New England Biolabs) in a 96-well plate over a 5-hour time period. Colorimetric change was measured at 405 nm every 10 minutes with 5 seconds shaking before each measurement using a Polarstar Optima (BMG Labtech) plate reader.

2.13 Phosphoproteomics

2.13.1 Sample preparation

Vector and S3KD myoblasts were cultured in growth medium in 15 cm^2 plates as described in section 2.1 for two days. For each condition, four biological replicates were produced. Myoblasts were serum-starved for 5 hours in DMEM + 2 µg/mL puromycin then lysed in a mass spectrometry compatible buffer (50 mM ammonium bicarbonate, 0.25% RapiGest™ (Waters, UK), 2 mM NaF, 2 mM Na_3VO_4 and 1x PhosSTOP) or stimulated with 10% FBS for 10 minutes before lysis. Lysates were rotated end-over-end for 30 minutes at 4°C, then sonicated with a Vibracell ultrasonic processor (Sonics, Newtown, USA) on ice for 10 seconds with a tapered microtip. Lysates were then snap-frozen in liquid nitrogen and submitted to the Centre for Proteome Research (CPR), University of Liverpool, for LC-MS/MS analysis. Briefly, 200 µg of protein sample were digested with 0.2 µg/µL trypsin overnight at 37 °C. RapiGest™ was hydrolysed by the addition of trifluoroacetic acid (TFA), for 2 hours at 60 °C, followed by centrifugation at 17,000 x g for 30 minutes at 4 °C. Supernatants were concentrated using a speedvac (Univapo-150 ECH) at a fixed speed of 1,250 rpm, 30 °C for 40 minutes and resuspended in 150 µL of 1% TFA, then desalted on macro spin columns (Harvard Macro Spin Columns). Samples were enriched for phosphopeptides using Titansphere PhosTiO columns (200 µL 5010-21312, Hichrom) prior to being solubilised in 20 µL 1% TFA, and centrifuged at 17,000 *x g* for 15 minutes. 10 µL of supernatant were transferred to total recovery vials for LC-MS/MS analysis.

2.13.2 LC-MS/MS

LC-MS/MS was performed by Dr Deborah Simpson (CPR). Briefly, 4 µL of the phospho-enriched sample were analysed using an Ultimate 3000 RSLC™ nano system (Thermo Scientific, Hemel Hempstead) coupled to a QExactive™ mass spectrometer (Thermo Scientific). The sample was loaded onto the trapping column (Thermo Scientific, PepMap100, C18, 300 µm x 5 mm), for 7 minutes at a flow rate of 9 µL/min with 0.1% TFA and 2% acetonitrile. The sample was resolved on the analytical column (Easy-Spray C18 75 µm x 500 mm 2µm column) using a gradient of 97% buffer A (0.1% formic acid in water) and 3% buffer B (99.9% acetonitrile, 0.1% formic acid) to 60% buffer A and 40% buffer B

(all v/v) over 90 minutes at a flow rate of 300 nL/min. The data-dependent program used for data acquisition consisted of a 70,000 resolution full-scan MS scan (automatic gain control (AGC) set to 1 x10^6 ions with a maximum fill time of 250 ms) and the 10 most abundant peaks were selected for MS/MS using a 35,000 resolution scan (AGC set to 1 x 10^5 ions with a maximum fill time of 100 ms) with an ion selection window of 2 m/z. To avoid repeated selection of peptides for MS/MS, the program used a 20 second dynamic exclusion window.

2.13.3 Peptide identification

Peptide identification, phosphosite localisation and quantification were performed in collaboration with Prof Andy Jones (University of Liverpool). Briefly, peptides were identified using PEAKS Studio 8 searched against the Uniprot *Mus musculus* proteome database (Database version: October 2016). A fixed carbamidomethyl modification for cysteine and variable modifications of oxidation for methionine were specified. A variable modification for phosphorylation of serine, threonine and tyrosine were specified. A precursor mass tolerance of 10 ppm and a fragment ion mass tolerance of 0.05 Da were applied. The results were then filtered to obtain a peptide false discovery rate of 1%. The localisation probability of all putative phosphorylation sites were determined using PEAKS PTM and reported as Ascore. An Ascore of 13 or more is equivalent to $p < 0.05$ and this value or even higher ($p < 0.25$) has been used in previous phosphoproteomic analyses (Beausoleil *et al.*, 2006, Sarhan *et al.*, 2017). Where localisation score was considered important, mainly for motif analysis, an Ascore of >13 was used.

2.13.4 Peptide quantification

Label free quantification of phosphopeptide abundance was performed using Progenesis QI (Version 2.0). Alignment of the chromatograms was automatically processed using Progenesis QI. This method compared all of the given sample chromatograms, deduced which chromatogram was the most similar between all the chromatograms and designated it as reference sample. Once a reference had been established, each peak identified at a specific m/z value (and therefore each peptide) in each chromatogram was quantified by measuring the area underneath the peak, which was reported as a numerical value. These data from Progenesis QI showed that although many of the samples aligned well with the reference sample, the alignment became progressively worse as the samples were run through the LC column, which may have indicated a progressive drift in retention time between sample runs (Table 2.3 and Appendix 1). However, this was not a major issue as tandem mass spectrometry allows for highly confident identification of peptides by amino acid sequence, which was carried out for each peak identified, and the corresponding abundance value reported. This resulted in the same peptide being reported, with different

abundance values, multiple times and allowed for the abundances of individual occurrences of the same peptide to be concatenated (summed, using Microsoft Excel) to give a "final" abundance value for each unique peptide identified (Table 2.4).

Table 2.3 Chromatogram alignment scores from Progenesis QI™. S3KD = SDC3 knockdown, T0 = Time 0, T10 = Time 10. Samples are listed in the same randomised order in which they were run for LC-MS/MS analysis

Sample #	Alignment score (%)	Corresponding sample
16	Reference	S3KD T10
18	94.5	Vector T10
9	94.2	Vector T0
11	92.5	S3KD T0
12	92	S3KD T10
13	91.8	Vector T0
5	91.3	Vector T0
17	91.2	Vector T0
20	89.3	S3KD T10
6	87.1	Vector T10
10	86.2	Vector T10
19	53.9	S3KD T0
14	48.2	Vector T10
7	40.1	S3KD T0
8	40.1	S3KD T10
15	37.5	S3KD T0

Table 2.4: Method used to concatenate phosphopeptide abundances. When the same phosphopeptide was reported across multiple rows, the corresponding abundances were summed to generate one single entry for each unique phosphopeptide.

		Time 0				Time 10			
Unique peptide ID	Uniprot	5	9	13	17	6	10	14	18
ASLSPMDEPVPDSESPVEK[4] S(+79.97)	P14873	7939.538	15482.44	82039.91	16205.55	0	8296.824	552890.9	553647.9
ASLSPMDEPVPDSESPVEK[4] S(+79.97)	P14873	0	0	0	0	1447413	0	647.5676	461534.4
ASLSPMDEPVPDSESPVEK[4] S(+79.97)	P14873	470687.8	927576.8	712719	859589.7	47753.39	1359748	328496.8	271397.5
ASLSPMDEPVPDSESPVEK[4] S(+79.97)	P14873	5003294	6452394	4833481	7501234	3942437	7698564	2721470	637333.7

Data combined

		Time 0				Time 10			
Unique peptide ID	Uniprot	5	9	13	17	6	10	14	18
ASLSPMDEPVPDSESPVEK[4] S(+79.97)	P14873	5481921	7395453	5628240	8377029	5437603	9066609	3603505	1923913

2.13.5 Phosphoproteomics statistical analysis

After all peptides were quantified, we encountered another problem; many peptides were missing one or more abundance values. This is a common problem in label-free phosphoproteomics and many groups have attempted to counter this problem by 'gap-filling' with either generic very low values, such as 0.1, or by using the lowest value identified within a data set or within each specific replicate of the dataset, as it is assumed that when LC-MS/MS reports a zero value, it is because the actual level of peptide abundance is so low to be undetectable (Stead *et al.*, 2008, Grimes *et al.*, 2013, Trentini *et al.*, 2016). However, this method of 'gap-filling' is often inappropriate and results in many false positives (Grimes *et al.*, 2013). The missing values in our dataset posed a problem as they rendered normal parametric tests inappropriate for identification of statistically significant changes in phosphopeptide abundance. In order to solve this problem we collaborated with Prof Andy Jones and Mr. Alexander Phillips (University of Liverpool) to develop a Bayesian inference model which would confidently identify whether there was a significant difference between phosphopeptide abundances with at least a ± 1.5 fold change between conditions. Bayesian inference is a strong statistical method which, in this case, assigned to each set of replicates a range of values, rather than a fixed average ± error, and used these ranges of values to calculate significance between conditions at a given threshold (in this case ±1.5 fold change) and a given FDR (in this case less than 5%). This method is much more robust at calculating significant differences when there are missing values in a data set, however may also result in fewer true positives being identified compared to other methods. We decided to be more cautious and generate comparative datasets with highly confident phosphopeptide changes, rather than risk to take further many false positives.

2.13.6 Motif-x

Phosphopeptide sequences were centred on the phosphorylation site and extended to 15-amino acids (± 7 residues either side of phosphosite) using the whole mouse proteome by Mr Simon Perkins (Computational Biology Facility, University of Liverpool). Where the phosphosite was close to the N or C terminus of the amino acid sequence I manually inputted 'X's to fill in the 15-amino acid sequence and used the software tool Motif-x (Schwartz and Gygi, 2005, Chou and Schwartz, 2011) to extract over-represented phosphorylation motifs from significantly regulated phosphopeptides that had an Ascore > 13. Once phosphopeptides were aligned, they were submitted to Motif-x. The complete mouse International Protein Index database was used as background. The significance threshold was left as recommended and the occurrence threshold was set to 5 as recommended for smaller datasets (Chou and Schwartz, 2011). To compare the obtained over-represented motifs to known substrate motifs the resources PhosphoMotifFinder (Amanchy *et al.*, 2007) and RegPhos 2.0 (Lee *et al.*, 2011) were used.

2.13.7 Gene Ontology enrichment analysis

Phosphopeptides, with no restriction on localisation score, were converted to their respective Uniprot protein identifier. DAVID 6.8 (Huang da *et al.*, 2009, 2009) (updated October 2016) was used for Gene Ontology enrichment analysis of significantly regulated phosphoproteins. The background dataset consisted of all the phosphoproteins identified in the phosphoproteomics experiment (refer to *Chapter 5*, section 5.2.3.2 for further details on why this dataset was used as background). Enriched terms with a p-value of less than 0.05 were considered statistically significant.

2.13.8 Ingenuity Pathway Analysis

Significantly regulated phosphopeptides, with no restriction on their localisation score, and their corresponding Uniprot protein ID and natural log fold change were submitted to Ingenuity Pathway Analysis (IPA, Qiagen) for canonical pathway enrichment and upstream regulator analysis, using the phosphoproteome analysis tool. For canonical pathway enrichment analysis, pathways were restricted to Receptor Tyrosine Kinase (RTK) pathways (Table 2.5) and for a positive or negative Z-score. Pathways with an enrichment score of $p < 0.05$ were considered statistically significant. IPA was also used to identify predicted upstream regulators of phosphoproteins identified in these data sets. Predicted upstream regulators with a $p < 0.05$ were used to automatically create networks for visualisation purposes.

Table 2.5: List of canonical signalling pathways filtered for IPA analysis

Canonical Receptor Tyrosine Kinase pathways				
EGF	ErbB2-ErbB3	FGF	mTOR	p70S6K
Eph receptor	ErbB4	HGF	Neurotrophin/TRK	PDGF
Ephrin A	ERK/MAPK	IGF	NFKβ	Pi3K/AKT
Ephrin B	ERK5	Insulin receptor	NGF	STAT3
ErbB	FAK	JAK/STAT	P38	VEGF

2.14 Isolation and culture of primary mouse myoblasts

Primary myoblast growth medium: F12 + 0.4 mM $CaCl_2$ (F12C), 15% horse serum, 1% penicillin/streptomycin, 2 mM GlutaMax, 2 nM FGF2.

Primary myoblast differentiation medium: F12C, 3% horse serum, 2 mM GlutaMax, 1% penicillin/streptomycin.

Primary myoblasts were isolated from mouse hindlimbs in collaboration with Dr Dada Pisconti or Dr Rachel Ghadiali (University of Liverpool) as described previously (Pisconti *et al.*, 2010, Ghadiali *et al.*, 2017). Briefly, mice hindlimb muscles were dissected then minced with scissors before digestion with 400 units/mL collagenase type I (Worthington Biochemical Corporation) in F12C for 1.5 hours at 37 °C with agitation every 15 minutes. The homogenate was centrifuged at 30 *x g* for 5 minutes and the supernatant collected and diluted in primary growth medium. The suspension was centrifuged for 10 minutes at 500 *x g* to collect cells in a pellet. The pellet was re-suspended in primary myoblast growth medium then filtered through a 40 µm cell strainer. Filtered cells were collected in a pellet again and re-suspended in primary myoblast growth medium before being plated onto gelatin-coated plates (pre-plating 1) under a humidified atmosphere of 5% CO_2 and atmospheric O_2 for two hours. Plates were gently washed with primary myoblast growth medium and cells in suspension collected for re-plating onto a fresh gelatin-coated plate (pre-plating 2) for one hour. For the final plating plates cell suspensions were collected, centrifuged, re-suspended in fresh primary myoblast growth at the desired concentration and plated onto fresh gelatin-coated plates for routine culturing.

Isolated primary myoblasts were expanded in primary myoblast growth medium under a humidified atmosphere of 5% CO_2 and atmospheric O_2 at 37°C for two days then split for experiments using 40 units/mL of collagenase I in PBS and re-seeded at the density of 3,000 cells/well in 12-multiwell plates for proliferation experiments and 7,000 cells/well in 12-multiwell plates for differentiation (induced and spontaneous) experiments. Primary myoblasts were only split once after isolation and always used at passage 1. For induced differentiation myoblasts were gently washed with F12C then the medium replaced with primary myoblast differentiation medium.

Recombinant human FGF2 was generously donated by Prof David Fernig, University of Liverpool. It is extremely well established that FGFs are highly conserved (Oulion *et al.*, 2012). Such conservation enables each FGF in mammals to be functionally identical, with the small number of amino acid changes being outside the surfaces that engage with the HS co-receptor and the FGFR. Recombinant human FGF2 is the standard and has allowed

the elucidation of the key functional properties of the FGF receptor-ligand system in many cell types, including myoblasts (Rapraeger *et al.*, 1991). The same batches of collagenase, gelatin and horse serum were used throughout the study.

2.15 Insulin stimulation of myoblasts

For proliferation experiments, C2C12 myoblasts were seeded at a density of 4,000 cells/well in 12-multiwell plates and cultured in growth medium for 24 hours with or without insulin (I0516, Sigma Aldrich). Similarly, primary myoblasts were cultured in primary growth medium with or without insulin for 24 hours. Myoblasts were then fixed and stained for DAPI to visualise nuclei before imaging.

For induced differentiation experiments myoblasts were grown to 90% confluence then induced to differentiate for three days as described in section 2.1. Insulin was added to differentiation medium for the entire course of the experiment (three days). Cells were then fixed and stained with DAPI and an anti-MyHC antibody (DSHB, MF20 clone) to visualise nuclei and late stage differentiation, respectively. Imaging and image analysis were carried out as specified in section 2.10.

For spontaneous differentiation experiments, C2C12 myoblasts were seeded at a density of 20,000 cells/well in 12-multiwell plates and cultured in growth medium. Insulin and an AKT inhibitor (AZD5363, SelleckChem) were added to the myoblasts two hours after plating for a total of five days. Cells were then fixed and stained with DAPI and an anti-MyHC antibody (DSHB, MF20 clone) to visualise nuclei and late stage differentiation respectively. Imaging and image analysis were carried out as specified in section 2.10. A volume of DMSO equal to the volume of AKT inhibitor, was added to the wells that did not receive AKT inhibitor to produce a vehicle control.

For spontaneous differentiation of primary satellite cell-derived myoblasts, myoblasts were seeded at a density of 7,000 cells/well in 12-multiwell plates. Myoblasts were cultured in primary growth medium for 2-3 days until confluent then FGF2 was removed from the medium and myoblasts were cultured for a further two days in primary myoblast growth medium (without FGF2) supplemented with either insulin and/or AKT inhibitor or an equal volume of DMSO.

In the alternative method for studying spontaneous differentiation, myoblasts were seeded at a density of 7,000 cells/well in 12-multiwell plates. Myoblasts were cultured in growth medium and allowed 4-5 hours to adhere to the gelatin-coated plates before beginning treatment with insulin and/or AKT inhibitor. Myoblasts were cultured in primary

growth medium for 2-3 days until confluent then FGF2 was removed from the medium and myoblasts were cultured for a further two days in primary myoblast growth medium (without FGF2) still in the presence of insulin and/or AKT inhibitor. A volume of DMSO equal to the volume of AKT inhibitor, was added to the wells that did not receive AKT inhibitor to produce a vehicle control.

2.16 Immunoprecipitation

Parental C2C12 myoblasts were cultured in growth medium then lysed in HSPG buffer. Lysates were precleared for 1 hour at 4°C using 30 µl of Pierce™ Protein A/G Magnetic Beads. 1 mg of pre-cleared lysate was used for each immunoprecipitation and respective controls. Immunoprecipitations were performed as per the manufacturers' instructions in the presence of equal amounts of antibody: anti-SDC3 (donated by Prof Alan Rapraeger, see Table 2.1), anti-IRβ (Rabbit mAb #3025, Cell Signalling Technology) or Normal rabbit IgG (Cell Signalling Technology) were used. Pre-cleared lysates and antibodies were incubated overnight at 4°C. For bead-only controls, 25 µl of beads were incubated with 1 mg of precleared lysate over night at 4°C.

2.17 Statistical analysis (not applicable to Proteomics analysis)

All statistical analysis for biochemical and immunofluorescence experiments were performed in GraphPad Prism 6 or Microsoft Excel. Each experiment contained three technical replicates, and was repeated at least three independent times (at least three biological replicates) unless otherwise stated. Data were checked for normal distributions and statistical significance was calculated using the Student's t-test or one-way ANOVA. Data were considered significant if $p < 0.05$. Data were plotted as average ± SEM (standard error of the mean).

Chapter 3

3 Pull-down of SDC3 interactors using recombinant proteins

3.1 Introduction

Studying syndecans is particularly difficult because of their negatively charged large glycosaminoglycan (GAG) chains which are differentially modified in different cell types and under different physiological conditions, adding a high degree of complexity to the study of structure-function relationships (Turnbull *et al.*, 2001, Sarrazin *et al.*, 2011, Ghadiali *et al.*, 2017). Syndecans are difficult to express and to purify, do not resolve as a clear band, even under denaturing conditions, following SDS-PAGE electrophoresis. Instead they resolve as a high molecular weight smear, unless the GAGs are removed via enzymatic digestion by heparinases. However, this method is costly and adds extra steps to experimental design. After removal of the GAGs the syndecans still do not resolve to their predicted molecular weights; they appear to be more than twice their predicted size and this is likely due to some GAGs that are heparinase digest resistant and/or intrinsic properties of the core syndecan protein (Asundi and Carey, 1995).

There is no information on the effect of GAGs on the structural stability of the core syndecan proteins or whether they influence the secondary and tertiary structure at all. The structure and sequence of heparan sulphate and chondroitin sulphate chains attached to the syndecans varies depending on the type of cell they are produced by and the physiological context in which the cell exists (Kato *et al.*, 1994). Although some degree of structural analysis of the heparan sulphate complement of a cell type or tissue is achievable and has been done (Guimond and Turnbull, 1999, Turnbull *et al.*, 2001, Ghadiali *et al.*, 2017), sequencing of native heparan sulphate chains, especially if isolated from specific core proteins, is technically challenging and virtually impossible with the technology currently available (Turnbull *et al.*, 2010). Therefore, currently there is no complete sequence data available for syndecan GAG chains, which limits our understanding of how syndecan GAGs affect cell signalling. However, it is well documented that the sulphation pattern, disaccharide composition and domain structure of heparan sulphate is important for modulating cell signalling (Guimond *et al.*, 2001, Lamanna *et al.*, 2007, Ghadiali *et al.*, 2017).

As work progressed by scientists in the field, became clear that the syndecans were directly involved in the regulation of growth factor signalling, cell-matrix interactions, cytoskeleton rearrangement and endocytosis amongst other biological processes (Choi *et al.*, 2011, Couchman *et al.*, 2015). When the syndecans were first discovered little attention was given to the core proteins, as they were considered scaffold proteins for heparan sulphate chains and thought to primarily signal via their attached GAG chains. However, more recent evidence suggests that the core syndecan proteins contain biological activity (McFall and Rapraeger, 1997, Park *et al.*, 2002, Beauvais *et al.*, 2004, De Rossi and Whiteford, 2013). However, whilst much evidence has accumulated in the last two decades on the role of syndecan core proteins and heparan sulphate chains in signalling regulation, much remains to be understood of the precise mechanistic details of syndecan interactions with their binding partners.

Protein studies of the syndecans are particularly difficult due to their large GAG chains and because the syndecans exist in an SDS-resistant homodimer, mediated mainly via their transmembrane domains and partly by their ectodomains (Asundi and Carey, 1995). Structural information regarding the syndecans is very limited except for the cytoplasmic domain of SDC4, which has been studied by nuclear magnetic resonance (NMR) and appears to adopt a twisted clamp conformation (Shin *et al.*, 2001, Choi *et al.*, 2016). Syndecan ectodomains are predicted to be intrinsically disordered therefore likely able to change structure depending on the ligand bound; it is thought that this high degree of flexibility is what allows the syndecans to bind to numerous interactors (Leonova and Galzitskaya, 2015, Wright and Dyson, 2015).

SDC3 is the least studied syndecan, closely followed by SDC2, and as a result few anti-SDC3 antibodies are commercially available which show high specificity in immuno-precipitation or immunofluorescence assays. This has led to limited information on SDC3 interactors although a few signalling pathways are known to be regulated by SDC3 such as: NOTCH1, FGF2, BMP2 and pleiotrophin, mainly via heparan sulphate and not the core SDC3 protein (Chernousov and Carey, 1993, Raulo *et al.*, 1994, Pisconti *et al.*, 2010). A commonly used method to identify a protein interactors in a tissue or cell type is to use that protein as a bait on a column that is flushed with the tissue's or cell type's homogenate to capture interacting protein complexes (Berggard *et al.*, 2007). Usually the bait protein is fused to a tag, which allows high affinity purification of the bait protein plus its protein interactors. There a several tags available, such as glutathione-S-transferase (GST), $Histidine_6$-tag, maltose-binding protein or streptavidin, which can be fused to the protein of interest and each have their advantages and disadvantages. For example GST is a 26 kDa protein than can be easily expressed in *Escherichia coli* typically yielding ~10 mg/L. The

high expression of GST can lead to accumulation of aggregated protein in inclusion bodies, which results in misfolded protein that must be then refolded before being used in a pull-down experiment. Refolding a protein is a complex task and the success depends on the intrinsic properties of the protein of interest. However, fusing GST to another protein can aid its translation and solubility if these are issues. Furthermore, GST can be easily purified on a glutathione-coated resin and then cleaved from the fusion protein whilst still bound to its glutathione-coated resin to release the protein bait and its interactors (Smith 2000, Kimple *et al.*, 2013). The maltose binding protein can also promote protein solubility but also suffers from the same aggregation problems as GST, additionally, the large size of maltose binding protein (~45 kDa) can cause problems with protein folding of its fused partner and is a particularly poor tag for larger proteins. (Kimple *et al.*, 2013). Pull-down experiments allow for confirmation of protein-protein interactions or for discovery of new interactions and might be exploited for identifying novel SDC3-binding proteins.

3.1.1 Chapter hypothesis, aims and objectives

SDC3 regulates satellite cell function however the mechanistic details are unclear. I hypothesised that the molecular mechanisms underlying SDC3 function in satellite cells could be inferred if the identity of SDC3 binding proteins was known. Therefore, the aims of this chapter were:

1) To identify proteins that interact with fully glycosylated SDC3 or with the core SDC3 proteins.
2) To infer SDC3-mediated signalling pathways in myogenesis based on the identity of SDC3-interacting proteins.

To achieve these aims we set the following objectives:

1) Use plasmids containing SDC3 cDNA fused to a tag to express recombinant SDC3 proteins in mammalian and bacterial cells. Since bacterial cells lack the machinery to synthesise complex sugar molecules like GAG chains we could obtain the core SDC3 protein from bacterial cells and the GAG-decorated SDC3 proteins from mammalian cells.
2) Purify recombinantly expressed SDC3 proteins, with or without GAGs, and use them as baits to pull-down SDC3 and its interactors from proliferating and differentiating myoblasts.
3) Carry out pull-downs and identify the protein-protein complexes using mass spectrometry.
4) Use bioinformatics tools to infer signalling pathways regulated by SDC3.

This chapter covers the attempts to express and purify SDC3 from different types of cells and use these recombinant SDC3 proteins to pull-down SDC3-binding partners from myoblasts.

3.2 Results

3.2.1 Expression of SDC3 ectodomain

Previously in the Pisconti lab, full-length SDC3 was expressed in C2C12 myoblasts and *E. coli*, which yielded unsuccessful results. Therefore, a second generation of plasmids were designed containing only the SDC3 ectodomain (S3ED), since I was specifically interested in characterising the extracellular SDC3 interactors that modulate myoblast function. Two plasmids were used to express S3ED in mammalian and bacterial cells to obtain glycosylated and non-glycosylated S3ED, respectively (Fig. 3.1). These plasmids contained S3ED cDNA fused to cDNA for a GST tag, creating a GST-S3ED recombinant protein upon translation. A GST tag was chosen to aid solubility of S3ED. For mammalian expression of S3ED, the S3ED and secretory N-terminal signal sequence was ligated into a vector containing a C-terminal GST-tag (Fig. 3.1A). This plasmid was designed so that the SDC3 secretory signal sequence would not be interrupted by the GST tag, as it is placed at the end of S3ED, and the S3ED-GST protein could be secreted into the culture medium for easy purification of GST-tagged protein. The mammalian expression vector also contained resistance to puromycin so that myoblasts transfected with the GST-S3ED plasmid could be selected for. For expression in bacterial cells the S3ED, without the secretory signal sequence, was ligated into a vector containing an N-terminal GST-tag (Fig. 3.1B). A C-terminal GST-tag was not used because previous work in the Pisconti lab showed no expression of S3ED with a C-terminal tag in *E. coli*. Moreover, previous work showed successful expression of S3ED with an N-terminal GST tag (De Rossi and Whiteford, 2013). The vectors used for bacterial expression contained resistance to ampicillin, which allowed selection of bacteria containing the GST-S3ED plasmid.

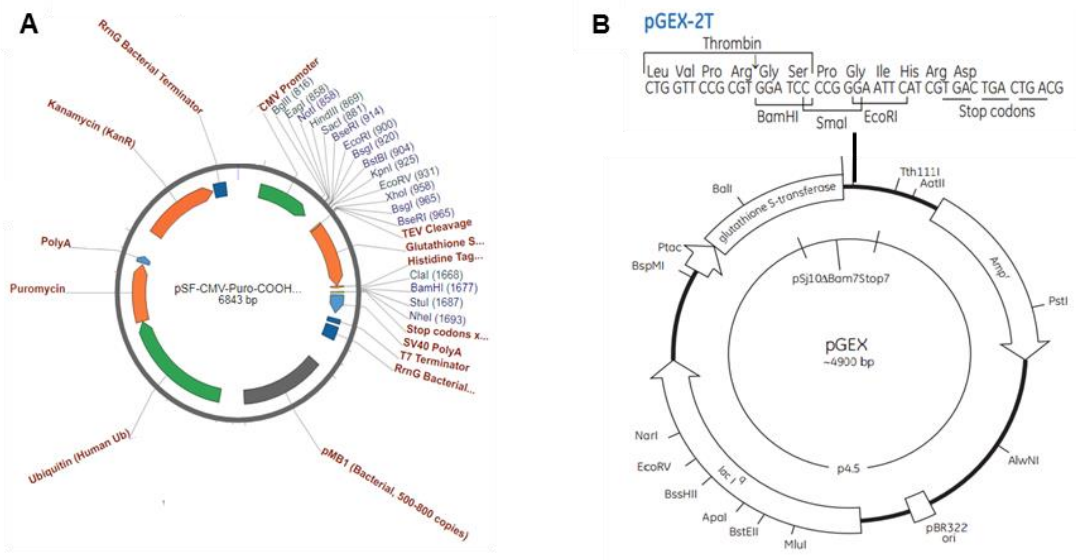

Figure 3.1: Protein expression plasmids to express S3ED. (A) Plasmid used for mammalian cell expression. **(B)** Plasmid used for bacteria cell expression.

3.2.2 Expression and purification of S3ED in mammalian cells

Stable expression of S3ED was performed in a C2C12 myoblast cell line to generate recombinant S3ED with myoblast-specific GAG chains, as different heparan sulphate structures confer different binding properties. Overexpression of GST-S3ED in C2C12 myoblasts showed a cell adhesion/morphology phenotype compared to non-transfected myoblasts: myoblasts transfected with GST-S3ED appeared less spread out (Fig. 3.2). Additionally, GST-S3ED appeared to proliferate more slowly compared to control cells (Fig. 3.2).

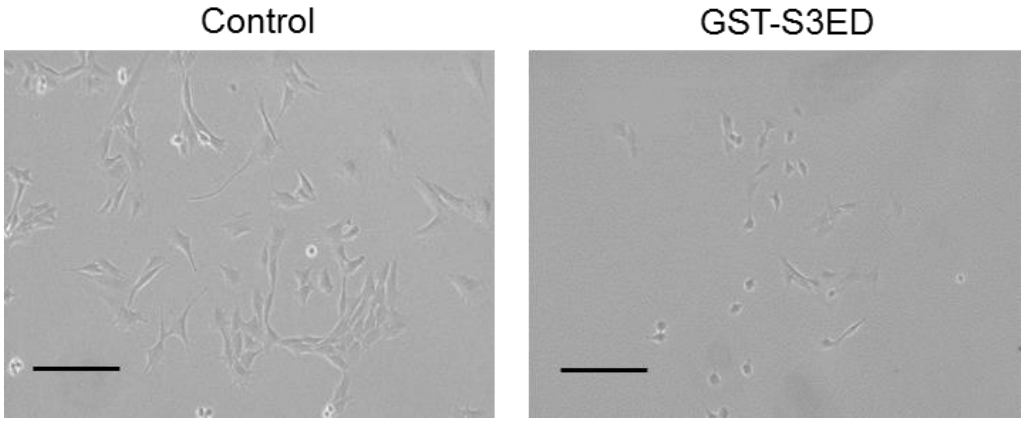

Figure 3.2: Phase contrast images of C2C12 myoblasts before and after transfection with GST-S3ED. C2C12 myoblasts were stably transfected with a plasmid containing S3ED cDNA and a C-terminal GST tag (GST-S3ED). Non-transfected control C2C12 myoblasts were grown simultaneously (Control). SDC3-ectodomain myoblasts grew more slowly compared to control cells and appeared smaller and less spread out. Scale bar represents 400 µm.

To purify glycosylated GST-S3ED from control and GST-S3ED myoblasts, the conditioned medium was incubated with glutathione-coated resin, which binds to GST, and an aliquot of the captured proteins was processed for western blotting to test whether the purification was successful (Fig. 3.3). When an anti-GST antibody was used to probe the western blot, a faint band (~80 kDa) was observed in the non-transfected and the GST-S3ED protein samples, which suggested that this was a non-specific band as GST should not be present in the control cells (Fig. 3.3). Furthermore, using an anti-SDC3 antibody two bands were observed (~55 to 70 kDa) which did not correspond to any previously observed SDC3 species and did not correspond to the bands observed by the anti-GST antibody. There was no difference in the molecular weight of the bands observed by the anti-SDC3 antibody between the control and GST-S3ED cells which indicated that a GST tag was not present in the GST-S3ED sample otherwise there would have been a ~26 kDa shift upwards of the bands observed in the GST-S3ED sample.

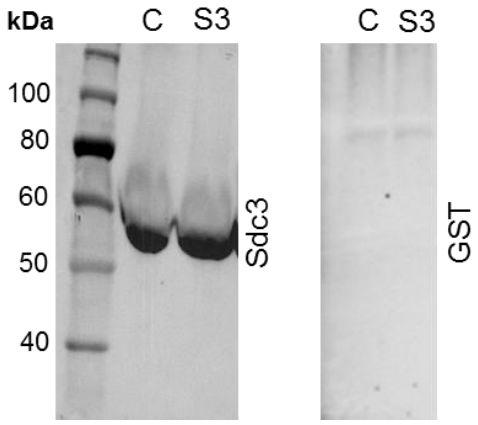

Figure 3.3: Western blotting shows that expression and/or secretion of GST-S3ED was not successful in C2C12 myoblasts. Non-transfected myoblasts (C) and GST-S3ED-transfected myoblasts (S3) were cultured in growth medium. Conditioned medium was incubated with glutathione-coated resin to purify GST-containing proteins. Proteins were digested with heparinase III to remove GAG chains then processed for western blotting. Antibodies were used to detect GST or SDC3.

Together these data suggested that S3ED was not successfully purified from C2C12 myoblasts. Additionally, after communication with experts in the syndecan field it was suggested that overexpression of the syndecans using a strong promoter will cause a shift from heparan sulphate production to chondroitin sulphate production, which would then cause changes to the SDC3 interactors (Shworak *et al.*, 1994, Longley *et al.*, 1999, Sarrazin *et al.*, 2010). Therefore because S3ED expression appeared problematic I decided to continue only with the bacterially expressed S3ED, which should not contain GAG chains.

3.2.3 Expression and purification of SDC3-ectodomain in bacterial cells

Previously in the Pisconti lab the expression and purification of GST-S3ED was optimised which involved enzymatic cell lysis, followed by purification using glutathione-coated beads then size exclusion chromatography and finally validation using western blotting. For use in pull-down experiments batches of recombinant GST and GST-S3ED were purified and snap frozen in aliquots after confirming purification efficiency by gel electrophoresis followed by Coomassie stain (Fig. 3.4).

A clear purification of the GST tag was achieved from expression of pGEX-GST (Fig. 3.4A, GST eluate lane, ~27 kDa) while a prominent band at ~90 kDa was observed from the expression of GST-S3ED (Fig. 3.4A, S3ED eluate lane) amongst a few extra bands of lower molecular weight. Western blotting with an anti-GST antibody confirmed that these lower molecular weight bands contained GST (Fig. 3.4B), suggesting that translation of GST-S3ED was terminated early after GST was translated. Interestingly, the immunoreactivity of the GST antibody against the ~90 kDa band was minimal, suggesting that the GST epitope recognised by the anti-GST antibody might be masked in the full GST-S3ED fusion protein (Fig. 3.4B, S3ED eluate lane).

To further purify GST-S3ED, the fraction obtained from the glutathione-coated resin was subjected to size exclusion chromatography to separate the lower molecular weight

bands from the main ~90 kDa band. Separation on a size-exclusion column was partially successful, however a high proportion of the lower molecular weight proteins still eluted with the main ~90 kDa protein (Fig. 3.4C). Moreover, an additional high molecular weight species had appeared which was not identified before. We thought that this new high molecular weight species was possibly aggregated protein. Nonetheless, after size exclusion chromatography fractions 2 and 3 (Fig. 3.4C) appeared fairly pure and were therefore collected to be used for pull-down experiments.

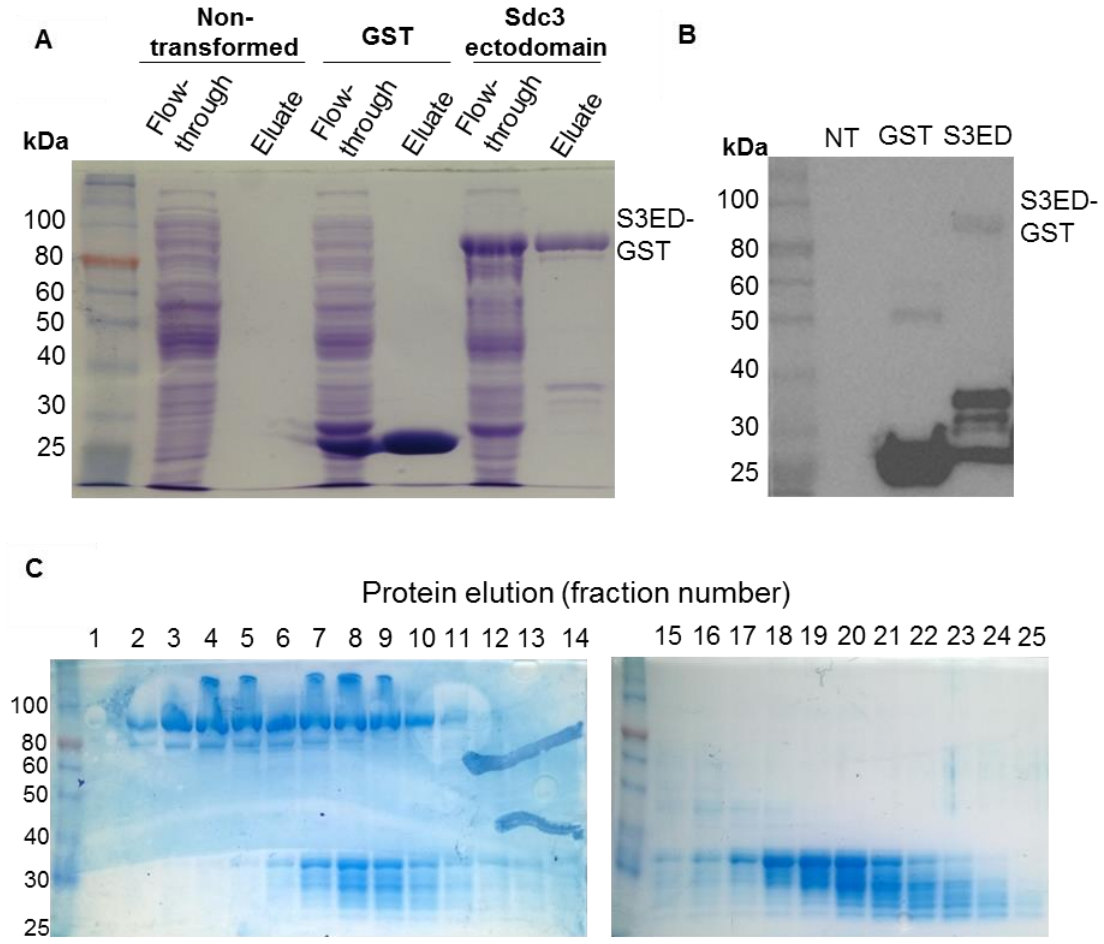

Figure 3.4: (A) Purification of bacterially expressed SDC3-ectodomain with an N-terminal GST tag. Escherichia coli that had been transformed with either pGEX-GST or S3ED-GST were enzymatically lysed and soluble cell lysates were purified using glutathione-coated beads to capture the GST-tag. The GST-tag alone was purified successfully but GST-S3ED contained several additional low molecular weight proteins. **(B)** Western blots were probed with an anti-GST antibody which confirmed the low molecular weight bands purified from the S3ED-GST containing cell lysate were GST rich and not a non-specifically bound protein. **(C)** Size exclusion chromatography of bacterially expressed GST-S3ED. A pre-packed Superdex 200 10/300 column was used to separate the low molecular weight GST fusion proteins from the ~90 kDa band. Fractions 1-25 were collected and analysed on an SDS-PAGE.

3.2.4 Pull-down assays using recombinant GST-S3ED

GST-S3ED and GST recombinant proteins were used as bait to pull-down SDC3 interactors from lysates of proliferating C2C12 cells. Two different buffers (RIPA and HSPG lysis buffer, see *Methods* section 2.5 for details) and two different methods (A and B) were tested for the pull-down experiments (Fig. 3.5 and 3.6). In method A the cell lysate was added to glutathione-coated beads pre-bound with recombinant proteins (GST and GST-S3ED); in method B, GST or GST-S3ED were added to the culture medium of proliferating C2C12 myoblasts then lysed. I hypothesised that method A would yield many non-specific proteins whereas method B would yield more membrane-bound or ECM SDC3-interactors. Both methods were followed by purification of the protein complexes on glutathione-coated beads.

When pull-down samples were prepared with method A, and resolved by SDS-PAGE followed by Coomassie stain, no significant differences were identified in the bands obtained from bead-control and GST-control pull-downs versus the bands obtained from GST-S3ED pull-downs (Fig. 3.5A). Indeed, only the bands corresponding to the recombinant proteins were visible by Coomassie stain (Fig. 3.5A). When the same experiment was repeated with method B, no bands were detected by Coomassie stain, not even the GST-S3ED and the GST bands (Fig. 3.5A). Therefore, I hypothesised that Coomassie stain was not sensitive enough to detect low abundance proteins, and decided to resolve the same protein samples by SDS-PAGE followed by Silver staining (Fig. 3.5B). In the lanes loaded with pull-downs obtained with method A there were many bands visible in the bead-control and GST-control that were also present in the GST-S3ED pull-down (Fig. 3.5B). Other bands were visible in the GST-S3ED pull down but not in the GST or bead control but these corresponded to bands observed in the recombinant GST-S3ED protein input (Fig. 3.5B). In the lanes loaded with pull-downs obtained with method B there were fewer bands but, similarly, no bands were exclusively present in the GST-S3ED pull-down lane and absent in the control lanes (Fig. 3.5B). Furthermore, the protein bands corresponding to the recombinant input proteins (GST and GST-S3ED) were completely absent from the lanes loaded with pull-downs obtained using method B, suggesting that the recombinant proteins had not bound to any cellular proteins during cell culture and were washed away when the medium was removed before cell lysis. Further analysis revealed that the recombinant proteins were indeed present in the myoblast-conditioned medium, further supporting the idea that no binding had occurred between the cell surface or extracellular matrix proteins and GST or S3ED-GST proteins (Fig. 3.5C).

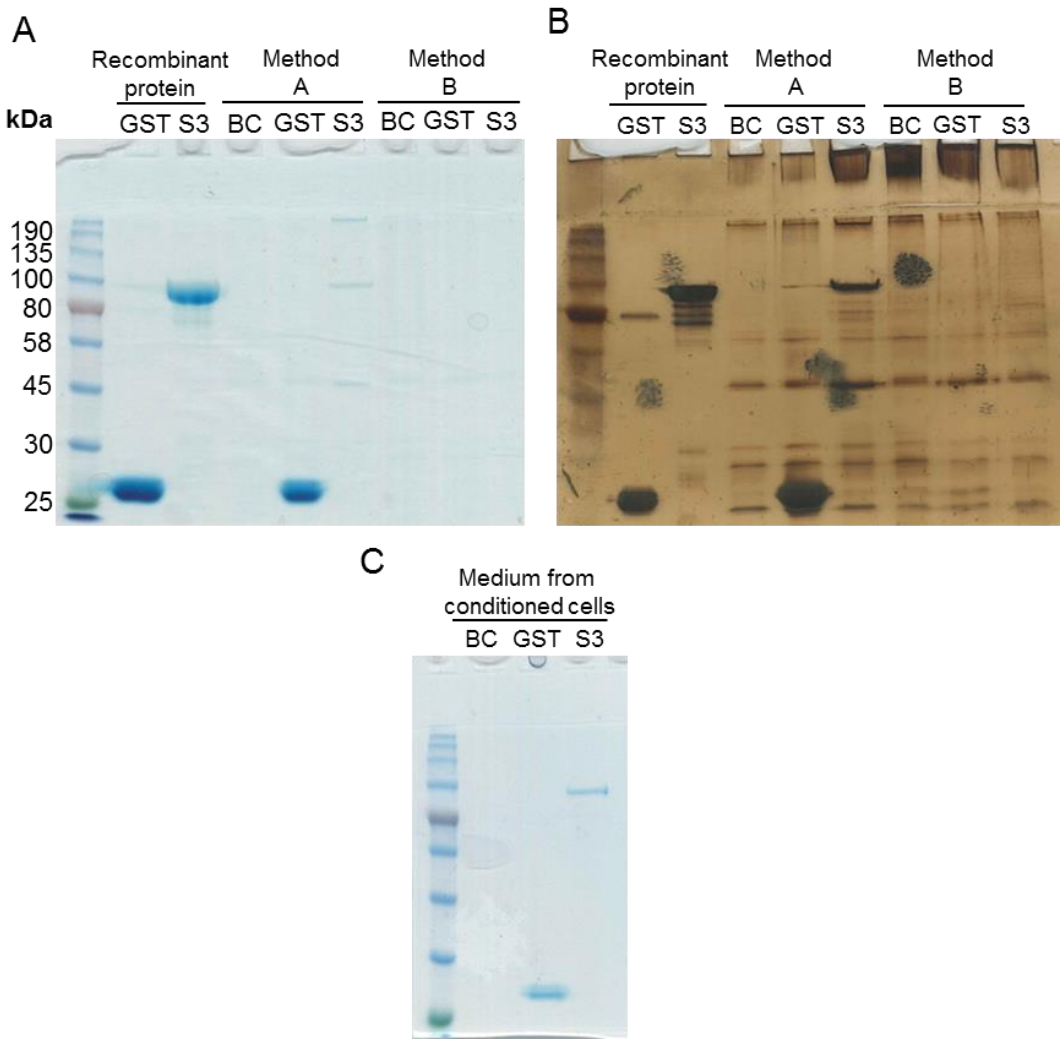

Figure 3.5: Proteins from pull-downs using recombinant syndecan-3 ectodomain (S3) or glutathione-S-transferase (GST) as baits for C2C12 myoblast lysates were resolved via SDS-PAGE and visualised using Coomassie or Silver staining. (A) Protein complexes from a pull-down with cells lysed in RIPA buffer using method A (cell lysate added to glutathione-coated beads pre-bound with recombinant GST or S3ED) or method B (recombinant protein added to cultured myoblasts, lysed then protein complexes purified on glutathione-coated beads). Key: BC = bead only control; GST = GST only used as bait; S3 = GST-S3ED used as bait **(B)** The same protein samples as in (A) now visualised via Silver staining. **(C)** Coomassie staining of an SDS-PAGE resolving the conditioned media from C2C12 cells after being incubated with recombinant proteins as indicated.

RIPA buffer contains significantly high concentrations of detergents and might have been too harsh for pull-down experiments, as the high detergent concentrations might have disrupted protein-protein interactions. Therefore I repeated the pull-down experiments with the two methods presented above, but this time using a more gentle lysis buffer which contains smaller amounts of detergent (HSPG lysis buffer, Fig. 3.6) and has been used to pull-down HSPGs and/or profile them by western blotting previously (Pisconti *et al.*, 2010).

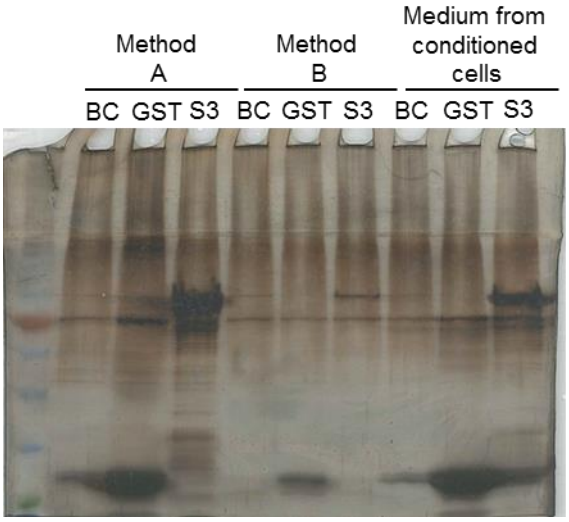

Figure 3.6: GST-fused recombinant syndecan-3 ectodomain (S3) or glutathione-S-transferase (GST) were used as bait for C2C12 cell lysates. Protein complexes from a pull-down with cells lysed in HSPG lysis buffer using method A (cell lysate added to glutathione-coated beads pre-bound with recombinant GST or S3ED) or method B (recombinant protein added to cultured myoblasts, lysed then protein complexes purified on glutathione-coated beads). BC = bead control.

The HSPG lysis buffer provided a more promising result as the lanes loaded with bead-control pull-downs following method A showed fewer non-specific bands (Fig. 3.6) compared to the samples obtained when method A and RIPA buffer were employed (Fig. 3.5B). Unfortunately when using HSPG lysis buffer there were still no obvious differences in the protein bands obtained from pull-downs of GST only compared to pull-downs of GST-S3ED, other than the recombinant protein inputs (Fig. 3.6). The only major difference between using RIPA versus HSPG lysis buffer was that with the HSPG lysis buffer GST-S3ED input was detected in the pull-downs obtained with method B. However, the amount of input GST-S3ED detected from method B pull-downs was still much less than that detected when method A was used (Fig. 3.6), further suggesting that in method B the recombinant protein added to the medium did not strongly bound to any proteins on the cell surface and subsequently was lost in the conditioned medium as previously observed in Figure 3.5.

Upon myoblast lysis, insoluble proteins were removed via centrifugation, therefore I tested whether it would be beneficial to omit centrifugation before performing a pull-down. Since I hypothesised that S3ED-interactor complexes might be present in the insoluble fraction of the cell lysate. At this point I decided to continue only with method A because in method B the vast majority of recombinant protein input remained unbound in the medium (Fig. 3.5B and C, Fig. 3.6). Additionally HSPG lysis buffer appeared to generate fewer non-specific bands therefore I opted to use HSPG lysis buffer over RIPA lysis buffer. Figure 3.7 shows a test between clarified and non-clarified cell lysates obtained using HSPG lysis

buffer. Although the bead- and GST- controls were relatively free from excess bands, there appeared to be numerous visible bands in the lane loaded with GST-S3ED pull-down, all of which, unfortunately, appeared to correspond to the recombinant GST-S3ED protein input (Fig. 3.7). Moreover, there was no difference in the number of protein bands between clarified and non-clarified cell lysate.

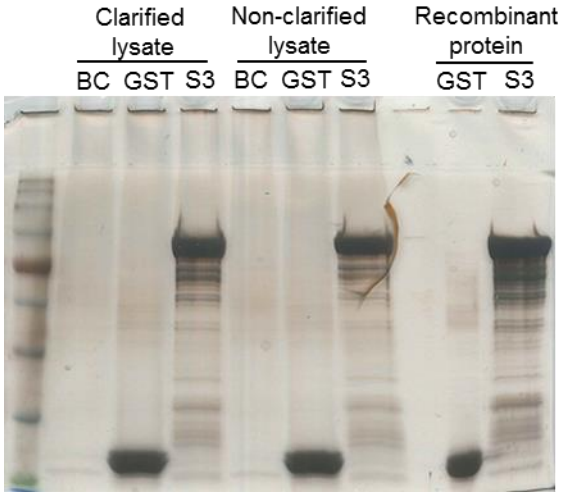

Figure 3.7: Clarification of myoblast lysate does not affect the number of proteins pulled-down. Myoblasts were lysed in HSPG buffer then either clarified by centrifugation or not to test whether this impacted the number of SDC3-ectodomain-interactors obtained using pull-down method A (lysates added to resin pre-bound with GST or GST-S3ED (S3). Protein complexes obtained were resolved by SDS-PAGE then visualised by Silver staining. BC = bead control.

Many bands that were visualised in the GST-S3ED pull-downs seemed to correspond to the recombinant protein input (Fig. 3.5B, Fig. 3.6, Fig. 3.7). However, Silver staining is a very sensitive method for visualising protein bands and I hypothesised that by using large amounts of bait protein the relatively low-abundance contaminants were still being detected by Silver staining and subsequently masked S3ED-protein interactors. Therefore I performed a pull-down using less bait protein with method A and HSPG lysis buffer (Fig. 3.8). From this experiment it was concluded that the majority of unique bands found in the GST-S3ED pull-down lanes originated from the recombinant GST-S3ED input and were most likely not SDC3 interactors.

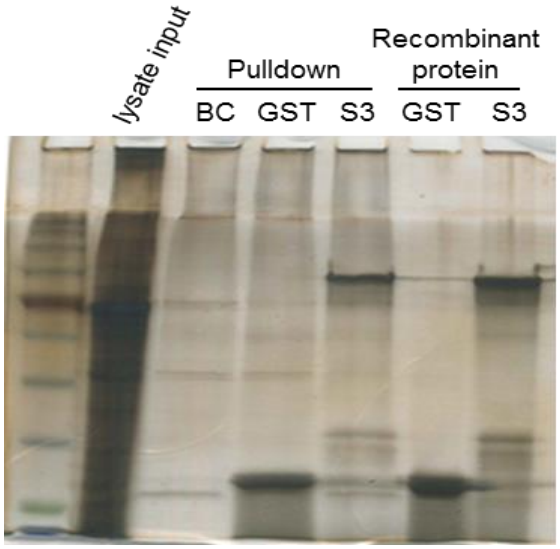

Figure 3.8: Optimisation of syndecan-3-ectodomain (S3) pull-downs. Myoblasts were lysed in HSPG buffer then lysates were added to resin containing 10 µg of pre-bound GST or GST-S3ED (S3). Protein complexes were purified, resolved by SDS-PAGE and visualised by Silver stain. No obvious difference was observed between S3 pull-down and S3 input. BC = bead control, GST = GST control, S3 = GST-S3ED control.

The results shown so far indicated that further purification of the GST-S3ED protein was necessary if continuing to use this protein as bait for SDC3 interactors, otherwise in-gel digestion for mass spectrometry analysis would be difficult as SDC3-interactor bands could not be identified to excise. SDC3 is predicted to have a low isoelectric point (4.61, http://web.expasy.org/compute_pi/) therefore I hypothesised that anion exchange chromatography could be used to separate GST-S3ED protein from the other GST-containing protein species, as the negatively charged SDC3 would bind tightly to the column and the other proteins would elute with a low salt concentration. An increasing salt gradient was used to elute the proteins from the column and two major peaks were observed (Fig. 3.9) corresponding to GST-S3ED at ~90 kDa and another protein at ~32 kDa. The majority of the GST-S3ED protein eluted at a lower salt concentrations (Fig. 3.9, fractions 1-7), which was unexpected because of SDC3's predicted low isoelectric point. However when all fractions collected from the anion exchange column were resolved on a SDS-PAGE and stained with Coomassie, it appeared that the purification had dramatically improved (Fig. 3.9A). To further confirm that the purification was improved fractions 3 through to 11 were resolved by SDS-PAGE and protein bands were visualised by silver stain (Fig. 3.9B). The prominent band observed at ~32 kDa was successfully separated from the major ~90 kDa band. However, there were still other bands visible at lower molecular weight. This would not have been a problem if the GST-S3ED were to be used for applications other than a pull-down because the relative abundance of these extra bands is extremely low as they are only visible upon overloading of the wells followed by Silver staining. However, as the

aim of this project was to use the recombinant GST-S3ED protein in pull-down experiments, the extra protein bands observed via Silver staining would mask potential S3ED interactors. This would cause identification of interactors by SDS-PAGE, and therefore in-gel digestion followed by mass spectrometry, difficult. Furthermore, the buffers used in these pull-down experiments were not compatible with mass spectrometry meaning further optimisation would be required.

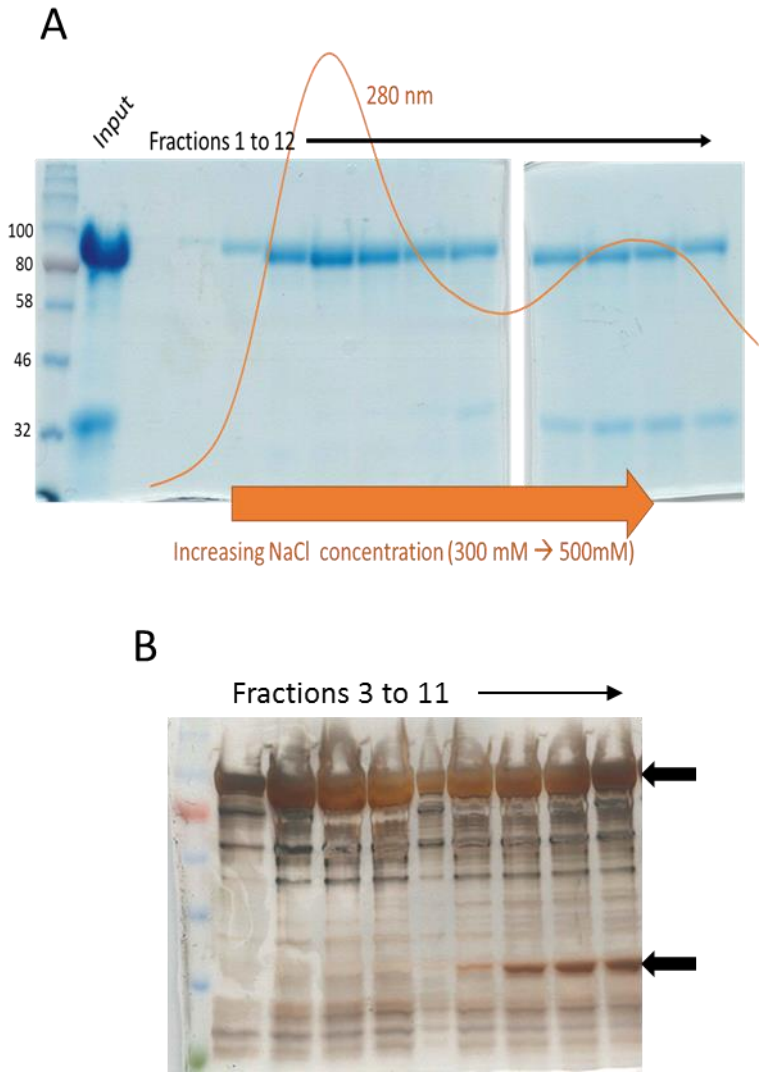

Figure 3.9: Purification of recombinant GST-SDC3-ectodomain (GST-S3ED) using anion exchange chromotography. **(A)** GST-S3ED protein was passed through a 1 mL HiTrap Q-HP column at a flow rate of 0.5 mL/min. Proteins were eluted using an increasing salt gradient and collected in 0.5 mL fractions. Proteins were then resolved on an 8% SDS-PAGE and stained with Coomassie. Corresponding chromatogram peaks obtained from Unicorn (GE healthcare) were overlayed to the SDS-PAGE images to help identify protein fractions. The purest fraction of protein eluted first at ~350 mM NaCl. **(B)** The same samples (fractions 3-11) were resolved by SDS-PAGE and visualised using Silver staining to determine the purity. Arrow indicate the two prominent bands observed with Coomassie staining (~90 kDa and ~32 kDa).

3.2.5 Structural analysis of S3ED

Whilst the GST-S3ED pull-downs were being optimised a collaboration with Dr Massimo Degano (San Raffaele Scientific institute, Milan, Italy) was organised to gain structural information about the SDC3 ectodomain. Unfortunately, it was during this stage that we were advised the GST-S3ED protein degraded in solution upon cleavage of the GST tag, and therefore not enough recombinant S3ED could be obtained for crystallography experiments. As previously mentioned, the syndecans are predicted to be largely unstructured which is thought to dramatically reduce protein stability in solution (Leonova and Galzitskaya, 2015, Deller *et al.*, 2016).

3.3 Discussion

The objectives of this chapter were to use recombinantly expressed SDC3 as a bait to pull down SDC3 interactors from myoblasts. Unfortunately, from the very beginning there were problems with this approach. Expression of full length SDC3 caused death in mammalian cells and only partially translated in bacterial cells. Furthermore, over-expression of syndecans in mammalian cells potentially causes alterations to GAG chain synthesis (Shworak *et al.*, 1994, Longley *et al.*, 1999, Sarrazin *et al.*, 2010), which meant that we could not be confident that the glycosylated recombinant SDC3 produced would represent endogenous SDC3 found in myoblasts and may then lead to identification of false SDC3 interactors. Instead I decided to focus on the core SDC3 ectodomain, which appeared to be expressed well in bacterial cells.

Initially the expression and purification of GST-S3ED seemed successful, as a good yield of GST-S3ED protein was obtained. The biggest challenge was obtaining a pure enough recombinant protein to be able to identify, by Silver stain, bands that were unique to S3ED-GST pulldown compared to control pull-downs, as the GST-S3ED protein formed multiple bands spanning the entire lane of the SDS-PAGE. The purity of the recombinant protein was not improved even after using sequential different techniques to purify it. Furthermore, I was made aware that the GST-S3ED produced had a tendency to degrade when the GST tag was removed, which meant that the use of this recombinant SDC3 protein for further structural studies by NMR or X-ray crystallography would be challenging.

The recombinant GST-S3ED protein had other characteristics which were unexpected and may have hinted that the protein was incorrectly translated. For example the predicted molecular weight of GST (26 kDa) and S3ED (35 kDa) adds up to 61 kDa and none of the abundant protein bands observed in the GST-S3ED purification matched that molecular weight. The syndecans tend to run on SDS-PAGE at a higher molecular weight than predicted and the SDC3 ectodomain contains a mucin-like domain, which may contain

further glycosylations in addition to the O-linked GAG chains(Carey*, et al.*, 1992). These mucin-type O-glycosylations, which would be added in a bacterial cells, could contribute to the higher than predicted molecular weight observed in the GST-S3ED (Zhou and Wu, 2009, Nothaft and Szymanski, 2010). Additionally, when the recombinant GST-S3ED did not separate well by size exclusion chromatography, or as expected with anion exchange chromatography, I hypothesised that this was another feature of the unusual SDC3 biochemical properties. The low isoelectric point of SDC3 may affect the migration of the protein in an SDS-PAGE by limiting interaction with SDS. With these pieces of information in mind I was not initially concerned that the recombinant S3ED resolved higher than expected via SDS-PAGE. However, the presence of low molecular weight bands containing GST suggested that after translation of the GST tag the translation of the S3ED was terminated prematurely.

One possibility is that the GST-S3ED protein became aggregated upon translation and/or purification. SDC3 is predicted to be intrinsically disordered and the transmembrane and extracellular domains are known to form dimers (Asundi and Carey, 1995, Leonova and Galzitskaya, 2015). Additionally, GST forms a dimer in solution, a combination of these factors may have contributed to the possible aggregation of GST-S3ED (Fabrini *et al.*, 2009). Furthermore, some proteins tend to aggregate when in high concentrations and the expression of GST-S3ED protein was robust leading to high concentrations of protein in the cells and subsequently in solution after purification. Whether GST-S3ED aggregated is unknown and would require further investigation to confirm. Previous reports suggest that expression of GST-S3ED is possible however, the purity of that GST-S3ED protein was not shown (De Rossi and Whiteford, 2013). It is possible that using a different vector with a weaker promoter, lower plasmid copy number, or a different protein tag may aid future attempts to purify S3ED. Alternatively, expression of the SDC3 cytoplasmic domain may be more fruitful and would provide us with information regarding the intracellular signalling events mediated by SDC3.

As this part of the project progressed it became apparent that there were several issues with this approach. Therefore we decided to try a different approach to identify SDC3-mediated cell signalling in myogenesis.

Chapter 4

Characterisation of SDC3 knockdown in C2C12 myoblasts

4.1 Introduction

Isolation and *ex vivo* culture of satellite cell-derived myoblasts, from skeletal muscle, is a commonly used method to study molecular mechanisms involved in the regulation of myogenesis. To further understand myogenesis, most studies have used mouse-derived myoblasts because of the difficulties in obtaining human muscle biopsies and thus large numbers of satellite cells (Boldrin *et al.*, 2010). Satellite cells are isolated from the myofibres by mincing the muscle followed by enzymatic digestion, which disrupts the satellite cell niche leading to satellite cell activation and conversion to myoblasts. Cultured primary myoblasts can be further expanded over several rounds of division and a limited number of passages before inevitably undergoing differentiation. However, satellite cells are not the only mono-nucleated cells present in muscle, also resident are FAPs, fibroblasts, blood vessel cells and macrophages, which must be removed before experimentation.

Currently, there are several methods available to isolate satellite cell-derived myoblasts from whole skeletal muscle such as differential plating, Percoll density centrifugation or fluorescence-activated cell sorting (FACS) (Richler and Yaffe, 1970, Morgan, 1988, Yablonka-Reuveni, 1988, Rando and Blau, 1994, Sacco *et al.*, 2008, Tanaka *et al.*, 2009). Differential plating is a common, simple, and rapid method to isolate satellite cells. The principle relies on the different adhesive properties of the cells in the mixture. Satellite cells adhere more slowly to culture dishes than fibroblasts, FAPs, blood vessel cells and macrophages. Therefore, a short pre-plating yields a cell suspension that contains poorly adhesive cells, mostly satellite cells, which can be removed and plated onto a fresh culture plate. Although differential plating yields higher numbers of myogenic cells than Percoll density centrifugation or FACS, differential plating rarely yields a 100% pure myogenic cell population, some myogenic cells adhere early and are subsequently lost during plating. Moreover, a small percentage of non-myogenic cells remains in suspension during the first hours post-isolation and throughout serial pre-plating. Often the purity of the final myoblast preparation is normally no greater than 95%. A balance between the number of plating rounds and myogenic cell purity is important because primary myoblasts have an increased

propensity to differentiate, once removed from the satellite cell niche, making studies during proliferation more difficult. Additionally, primary satellite cells must be plated on a matrix, which can interfere with downstream analysis by mass spectrometry, making the use of primary myoblasts for proteomic experiments challenging for proteomics studies.

Myogenic cell lines are frequently used as an alternative to primary myoblasts when studying molecular mechanisms of myogenesis *ex vivo*. There are several reasons to use myogenic cell lines such as their robustness, relative ease of culture and ability to generate large numbers of myoblasts or myotubes for large scale experiments. There are several murine myoblast cell lines available, including C2C12 (Yaffe and Saxel, 1977, Blau *et al.*, 1983), MM14 (Linkhart *et al.*, 1980) and H2K-2B4, which were derived from satellite cells and whose behaviour corresponds to that of a muscle progenitor lineage. C2C12 myoblasts are most commonly used due to their robustness, extensive characterisation and simple culture requirements (Burattini *et al.*, 2004), unlike MM14 myoblasts which depend on the additional supplement of FGF2 for their proliferative maintenance (Linkhart *et al.*, 1980, Clegg *et al.*, 1987).

There are many biochemical and morphological differences between C2C12 myoblasts and primary adult myoblast. For example, C2C12 myoblasts are flat and spread whereas primary myoblasts tend to be smaller and more rounded. However, these morphological differences depend on which substrates the cells are plated on. Similarly, there are differences in the gene expression profiles between primary and C2C12 myoblasts (Cornelison, 1998, Lamon *et al.*, 2014). On the other hand, there are many similarities between C2C12 myoblasts and primary adult myoblasts, for example, both form multinucleated myotubes when cultured in low serum and the overall myogenic programme is regulated by similar molecular mechanisms (Cornelison, 2008, Grabowska *et al.*, 2011, Fukada *et al.*, 2013, Kawesa *et al.*, 2015). The numerous advantages of myoblast cell lines have led many scientists to use them for detailed mechanistic studies and/or preliminary hypothesis generation studies, prior to further validation of experimental conclusions in primary myoblasts, which are still considered a better model of myogenesis than myoblast cell lines.

As previously discussed in *Chapter 1*, genetic ablation of SDC3 in mice leads to several abnormalities in adult myogenesis. After muscle injury *SDC3*$^{-/-}$ mice show impaired satellite cell self-renewal, leading to an increased population of activated and proliferating myoblasts in the regenerated muscle, eventually leading to myofibre hypertrophy (Cornelison *et al.*, 2004, Pisconti *et al.*, 2010). Moreover, SDC3 loss impairs adhesion of satellite cells to the myofibre *ex vivo* (Pisconti *et al., 2016)*. Explanted *SDC3*$^{-/-}$ satellite cell-

derived myoblasts cultured *ex vivo* show enhanced fusion, leading to increased myotube size, and a reduction in $PAX7^{+}$ reserve cell generation (Pisconti *et al.*, 2010). All these observations together suggest that SDC3 plays an important role in both satellite cell adhesion and fate determination, and that the effects of SDC3 loss *in vivo* are cell autonomous, as they are reproduced *ex vivo*.

Experimental work has been carried out to try and elucidate the mechanistic details of SDC3's role in myogenesis and this led to the discovery of several differences in cell signalling pathways of cultured *SDC3*$^{-/-}$ myoblasts. Major work describing the role of SDC3 and NOTCH1 in satellite cells led us understand that SDC3 interacts with NOTCH1, which is required for NOTCH1 cleavage by ADAM17 and downstream signalling, and that the loss of SDC3 impairs satellite cell homeostasis and muscle regeneration (Pisconti *et al.*, 2010). Additionally, *SDC3*$^{-/-}$ myoblasts are more sensitive to HGF and FGF2 signalling as measured by ERK1/2 phosphorylation, which was also observed in C2C12 myoblasts (Fuentealba *et al.*, 1999, Cornelison *et al.*, 2004). Lastly, a global increase in tyrosine phosphorylation was observed in *SDC3*$^{-/-}$ myoblasts cultured under standard growing conditions compared with wild type myoblasts, suggesting that SDC3 regulates several signalling pathways other than NOTCH, FGF2 and HGF (Cornelison *et al.*, 2004). Exactly how loss of SDC3 causes such dramatic changes to the phosphoproteome is unknown, nor is it known which other signalling pathways are regulated by SDC3 during myogenesis.

4.1.1 Hypothesis and Aims

Based on previous work showing that the adhesion and cell fate phenotypes of SDC3 loss *in vivo* were reproduced *ex vivo* in cultures of explanted primary *SDC3*$^{-/-}$ myoblasts (Pisconti *et al.*, 2010, Pisconti *et al.*, 2016) we hypothesised that:

1) SDC3 regulates myoblast proliferation, differentiation, growth factor sensitivity and cell adhesion in a cell-autonomous manner.
2) Loss or dramatic reduction of SDC3 in a myoblast cell line would reproduce the same phenotypes observed in primary *SDC3*$^{-/-}$ myoblasts.
3) A myoblast cell line where SDC3 has been stably knocked-down could be a useful tool to study how SDC3 regulates the myoblast phosphoproteome.

Therefore, the overall aim of this chapter was to test whether shRNA-mediated SDC3 knockdown in C2C12 myoblasts led to the same myogenic phenotypes, differences in growth factor sensitivity and increased tyrosine phosphorylation as previously observed in *SDC3*$^{-/-}$ primary myoblasts.

4.2 Results

4.2.1 Syndecan-3 is stably knocked down in C2C12 myoblasts

To explore how a reduction in SDC3 levels affects myogenesis, the Pisconti lab previously produced two C2C12 cell lines in which SDC3 was stably knocked-down using shRNAs. A third myoblast cell line was established, as a comparative control for SDC3 knockdown effects by stably expressing an empty shRNA vector (Fig. 4.1). Briefly, all cell lines were transfected with a plasmid vector conferring resistance to puromycin and this vector was flanked by Long Terminal Repeat (LTR) sequences for insertion into the genome and stable expression of a puromycin resistance gene and shRNAs. Two different shRNAs targeting SDC3 were used, we termed cells transfected with these plasmids: SDC3-knockdown-90 (S3KD90) and SDC3-knockdown-91 (S3KD91) based on their product codes. For the control myoblast cell line, the empty vector was transfected into C2C12 cells which we named Vector.

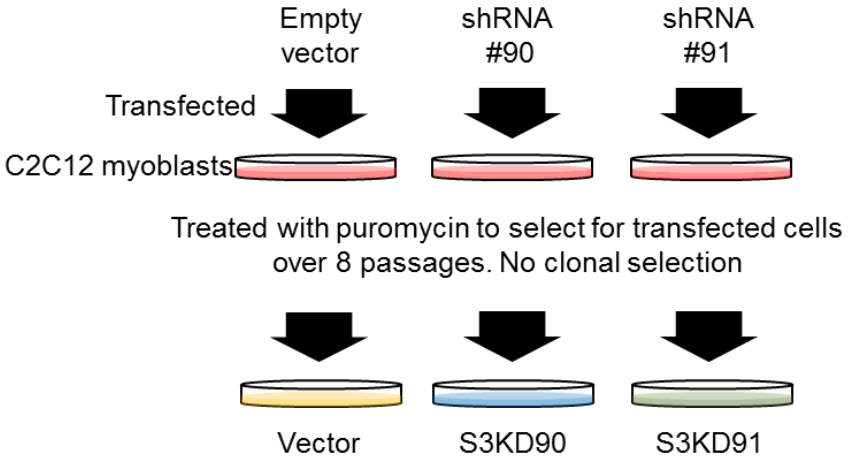

Figure 4.1: Schematic of transfection protocol for knockdown of SDC3 in C2C12 myoblasts. C2C12 myoblasts were transfected with one of three plasmids, as described in the *Methods* section 2.6, resulting in three myoblast cell lines. Vector = empty vector control, S3KD90 = SDC3-knockdown-90, S3KD91 = SDC3-knockdown-91.

The extent of SDC3-knockdown (S3KD) was verified via RT-PCR and western blotting (Fig. 4.2). RT-PCR showed a knockdown at the mRNA level of approximately 47% in the S3KD90 cells and approximately 90% in the S3KD91 cells (Fig. 4.2A). shRNA works by either inducing degradation of the mRNA or by preventing its translation, therefore it was possible that the protein knockdown achieved in S3KD90 cells was greater than what was detected via PCR. To address this question western blot analysis was performed to detect changes in the SDC3 protein level (Fig. 4.2B, C). Before testing the SDC3 knockdown myoblasts for SDC3 expression, two SDC3 antibodies were tested for their specificity, one commercially available (R&D systems) and the other gifted from Dr Alan Rapraeger (University of Wisconsin at Madison, USA). SDC3 is enriched in the brain therefore brain

tissue homogenates from wild type and *Sdc3*$^{-/-}$ mice were used as positive and negative controls respectively (Fig. 4.2B, C). Lysates were treated with heparinase III to remove heparan sulphate chains and, chondroitinase to remove chondroitin sulphate chains. This digestion allows the core SDC3 protein to resolve as a single band that can be visualised by western blot. The two SDC3 antibodies both recognised a protein at approximately >120 kDa, which is the observed mass of the SDC3 core protein after digestion with heparinase and chondroitinase (Carey *et al.*, 1992). The R&D antibody had a higher specificity for SDC3 (Fig. 4.2B) compared to the donated antibody (Fig. 4.2C) and was therefore used to detect SDC3 by western blot in subsequent experiments. Western blotting confirmed that SDC3 was knocked-down in S3KD90 myoblasts by approximately 90% compared to the Vector myoblasts (Fig. 4.2B, C). Since both cell lines showed a good knockdown of SDC3, both S3KD cell lines were taken forward for further experiments.

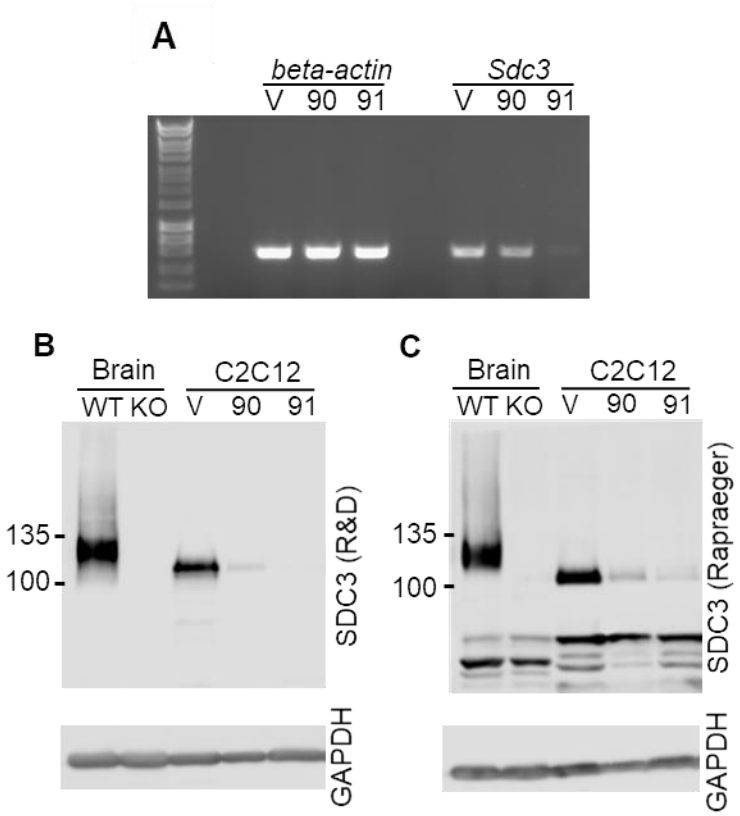

Figure 4.2: SDC3 knocked down in C2C12 cells was highly efficient. **(A)** RNA was extracted from Vector (V), S3KD90 (90) and S3KD91 (91) myoblasts, cDNA synthesised and PCR used to amplify SDC3 or beta-actin mRNA. **(B, C)** Wild type (WT), *SDC3*$^{-/-}$ (KO) brain tissues and Vector, S3KD90, S3KD91 myoblasts were lysed with RIPA buffer and treated with heparinase III and chondroitinase to remove glycosaminoglycans in preparation for western blotting. Proteins were resolved by SDS-PAGE, transferred to a nitrocellulose membrane and probed for SDC3 using two antibodies: in-house and R&D. GAPDH was used for normalisation.

4.2.2 SDC3 knockdown in S3KD90 recapitulates many of the phenotypes observed in primary *SDC3*$^{-/-}$ myoblasts

4.2.2.1 ERK1/2 phosphorylation measured in response to stimulation with FGF2 in Vector, S3KD90 and S3KD91 myoblasts.

Previously it was reported that the loss of SDC3 in satellite cell-derived myoblasts enhanced FGF2 signalling, as measured by ERK1/2 phosphorylation (Cornelison *et al.*, 2004). To test whether SDC3 knockdown in C2C12 myoblasts also increased ERK1/2 phosphorylation in response to FGF2, Vector, S3KD90 and S3KD91 myoblasts were serum-starved for 5 hours then treated with FGF2 over an 80 minutes-long time-course. Cell lysates were prepared for western blotting and probed for phosphorylated-ERK1/2 and total-ERK1/2, representative images are shown in Fig. 4.3A.

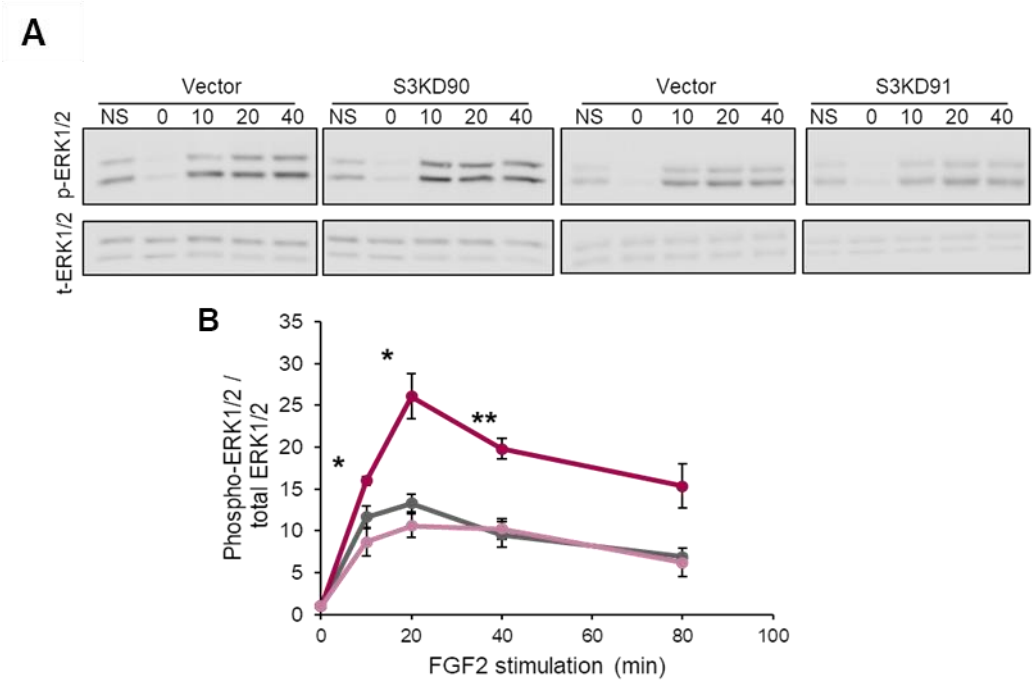

Figure 4.3: Sensitivity to FGF2 is increased in C2C12 myoblasts upon knockdown of SDC3 with one but not both shRNAs. (A) C2C12 myoblasts were serum-starved for 5 hours before treatment with 2 nM FGF2 for the indicated times. After stimulation cell lysates were prepared and analysed via western blotting to detect phosphorylated-ERK1/2 (p-ERK1/2) and total-ERK1/2 (t-ERK1/2). NS = non-starved. **(B)** Quantification of phosphorylated-ERK1/2 was performed using ImageJ, band intensity was normalised to total ERK1/2 then to 0 minutes (serum-starved). The results from three independent experiments were averaged and plotted. Error bars represent S.E.M. * = $p < 0.05$, ** = $p < 0.01$.

Phosphorylation of ERK1/2 was normalised to total ERK1/2 and then expressed as the fold change from 0 minutes of FGF2 stimulation for quantification (Fig. 4.3B). Peak phosphorylation of ERK1/2 was observed at approximately 20 minutes after FGF2 stimulation in all three cell lines. After 20 minutes of FGF2 stimulation the phosphorylation of ERK1/2 was 13 times higher than serum-starved cells in the Vector cell line, 26 times higher in S3KD90 and 10 times higher in S3KD91. After 10, 20 and 40 minutes of FGF2 stimulation the fold increase of phosphorylated-ERK1/2 in S3KD90 cells was significantly higher than in the Vector control (Fig. 4.3B). Therefore, the S3KD90 myoblasts behaved as previously hypothesised whereas the S3KD91 myoblasts showed no significant difference in response to FGF2 compared with the Vector myoblasts.

4.2.2.2 SDC3-knockdown in C2C12 myoblasts caused changes to levels of tyrosine phosphorylation

A global increase in tyrosine phosphorylation (pTyr) of satellite cell-derived *Sdc3*$^{-/-}$ myoblasts, grown under standard culture conditions, has been previously reported (Cornelison *et al.*, 2004). To test whether pTyr was also increased in C2C12 myoblasts when SDC3 was knocked-down, total pTyr levels were examined in Vector, S3KD90 and S3KD91 myoblasts under basal conditions (Fig 4.4A, NS= non-starved), after serum starvation (Fig 4.5A, 0 min), and after serum stimulation at various time points (Fig 4.4A, 10 to 80 min. Myoblast lysates were analysed for total pTyr by western blotting. The band intensity of pTyr in the entirety of each lane was measured in ImageJ then normalised to GAPDH. Quantification showed a significant increase of p-Tyr in S3KD90 myoblasts under non-starved and serum-starved culture conditions and after 10- and 20-minutes of serum stimulation, compared to Vector myoblasts (Fig. 4.4B). However, the S3KD91 myoblasts showed no significant difference in pTyr compared to the Vector myoblasts except at 80 minutes when there was a significant decrease. To summarise, after examining the response to FGF2 and serum stimulation in Vector, S3KD90 and S3KD91 myoblasts there were clear discrepancies between the two SDC3 knockdown cell lines. S3KD90 myoblasts recapitulated the previously observed FGF2 sensitivity and global increase of pTyr. However, the S3KD91 myoblasts behaved in a similar fashion to the Vector control myoblasts. To understand if the inconsistencies between the two S3KD cell lines also resulted in differences in myogenic phenotypes, the proliferation and differentiation potential of these cells were measured next.

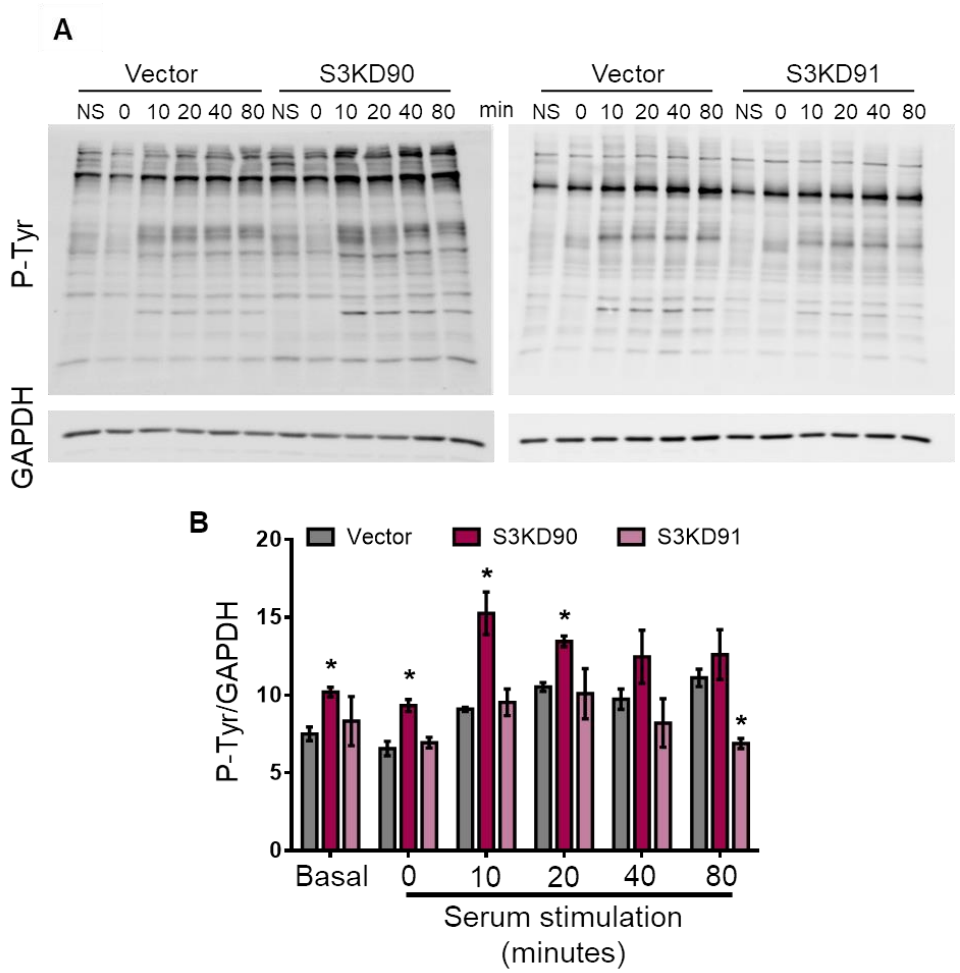

Figure 4.4: Increased global tyrosine phosphorylation upon SDC3-knockdown in C2C12 myoblasts. **(A)** SDC3-knockdown (S3KD90 and S3KD91) and Vector control cells were serum-starved and then stimulated with foetal bovine serum for 0-80 minutes. Cell lysates were prepared for western blotting to detect phosphorylated tyrosine (p-Tyr) or GAPDH. Representative western blot images shown. NS, non-starved (**B)** p-Tyr band intensity quantified using ImageJ. For each time point, the p-Tyr band intensity of the entire lane of was normalised to GAPDH band intensity. Results from two independent experiments were averaged and plotted. Error bars represent S.E.M. * = $p < 0.05$, individual S3KD myoblast lines compared to Vector myoblasts.

4.2.2.3 Effects of SDC3 knockdown on the proliferation and differentiation of C2C12 myoblasts

Myoblasts isolated from *Sdc3*$^{-/-}$ mice display aberrant proliferation and differentiation phenotypes (Cornelison *et al.*, 2004, Pisconti *et al.*, 2010). To determine if these phenotypes are cell autonomous and directly due to the loss of SDC3, the proliferation and differentiation phenotypes of S3KD90 and S3KD91 myoblasts was measured and compared to those of Vector myoblasts. The effect of SDC3 knockdown on the proliferation of C2C12 myoblasts was measured by counting the number of DAPI+ myoblasts after 24 and 48 hours of culture in growth medium (Fig. 4.5). The number of S3KD90 myoblasts counted at 24 hours was smaller ($p < 0.05$) than that of Vector myoblasts. In contrast, no

difference was observed between the S3KD91 and Vector myoblasts. After 48 hours of culture there were no longer any significant differences in myoblast numbers between Vector and either S3KD90 or S3KD91 myoblasts (Fig. 4.5). A similar behaviour is observed when comparing primary *Sdc3*$^{-/-}$ myoblasts to wild type myoblasts (Pisconti *et al.*, 2010) and suggests that S3KD90 myoblasts proliferate more slowly than Vector or S3KD91 myoblasts but this effect is lost after 48 hours of culture, when cultures have reached a level of confluence at which cell-cell contacts inhibit proliferation.

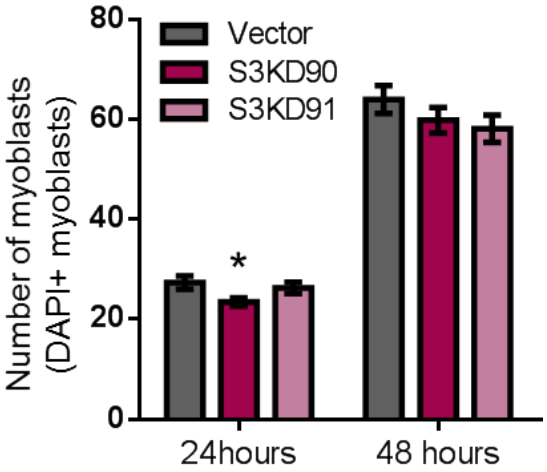

Figure 4.5: SDC3 knockdown minimally affects proliferation in C2C12 myoblasts. Vector, S3KD90 and S3KD91 myoblasts were cultured in growth medium for 24 and 48 hours. Myoblasts were fixed then stained with DAPI to visualise nuclei and the number of DAPI+ myoblasts counted. Data from three independent experiments were analysed and plotted as averages ± S.E.M. * = $p < 0.05$.

To measure the effect of SDC3 knockdown on myogenic differentiation, Vector, S3KD90 and S3KD91 myoblasts were cultured in a serum-reduced medium to induce myogenic differentiation for a period of 5 days. Cells were stained with DAPI (to visualise nuclei) and an anti-myosin heavy chain (MyHC) antibody to mark late stages of differentiation (Fig. 4.6A). Using these two markers the differentiation index, fusion index and myotube area of Vector, S3KD90 and S3KD91 cells were calculated (Fig. 4.6B), as described in the *Methods* section 2.7. The total number of nuclei per field was counted and fewer numbers were observed in both S3KD90 and S3KD91, suggesting that these myoblasts were proliferating less than the Vector during the induction of differentiation (Fig. 4.6B). The differentiation index, fusion index and myotube area were significantly increased by nearly two-fold in S3KD90 cells compared to Vector cells (Fig. 4.6B), which is consistent with what was previously observed in *SDC3*$^{-/-}$ primary myoblasts (Pisconti *et al.*, 2010). Conversely, S3KD91 failed to form mature myotubes and had a significantly lower fusion index and myotube area compared to the Vector control cells. This suggested that basic myogenic functions in the S3KD91 cell line were compromised, possibly because the shRNA used to generate this cell line had integrated in a region that controlled important myoblast function. Due to the impaired ability of S3KD91 to differentiate, leading to a cell

line that was unable to recapitulate basic myoblast functions, further experiments were only carried out with Vector and S3KD90 thereafter simply referred to as S3KD.

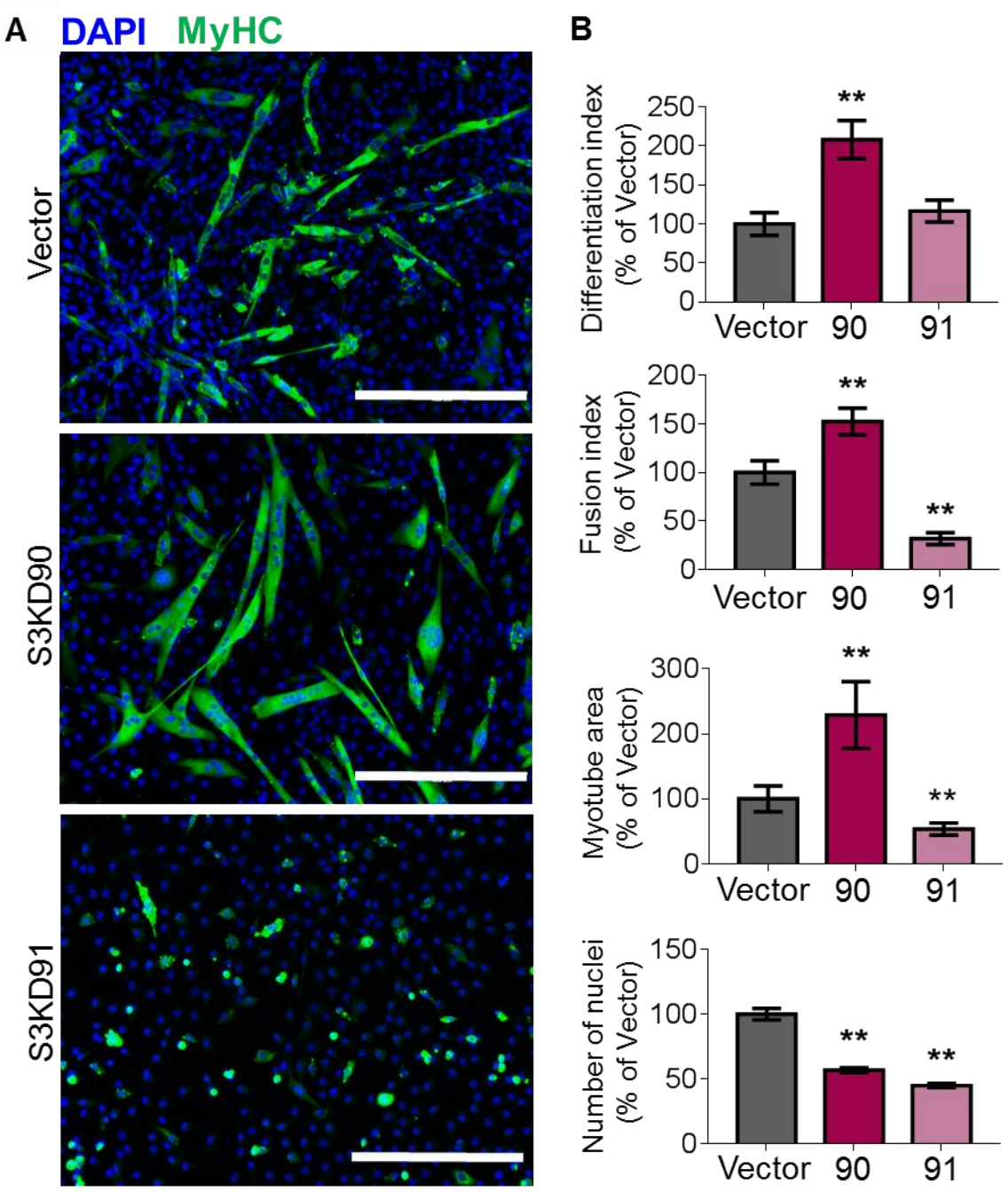

Figure 4.6: SDC3-knockdown in C2C12 myoblasts produced larger myotubes after induced differentiation. Myoblasts were grown to confluence for 2 days and then induced to differentiate for 5 days by reducing the serum concentration. **(A)** Cells were fixed then stained to detect myosin heavy chain (MyHC, green) and DNA (DAPI, blue) to visualise differentiation and nuclei respectively. Scale bar represents 400 µm. **(B)** Quantification of differentiation index, fusion index, myotube area and number of nuclei. Data expressed as a percentage of the Vector control. Results from three independent experiments were averaged and plotted. Error bars represent S.E.M. 90 = S3KD90, 91 = S3KD91, ** = $p < 0.01$.

4.2.3 SDC3 regulates adhesion of C2C12 myoblasts

Adhesion of satellite cells to the myofibre appears reduced in *Sdc3*$^{-/-}$ mice (Pisconti *et al.*, 2016). Therefore, we hypothesised that SDC3 knockdown would affect cell adhesion of C2C12 myoblasts. Myoblasts were plated onto non-coated culture dishes in the presence/absence of serum, then the number of adherent myoblasts were counted after one hour. S3KD myoblasts adhered faster than Vector myoblasts in both serum-free and serum-containing media as measured by the increase in number of myoblasts counted (Fig. 4.7). Both cell lines adhered significantly more in the presence of serum (Fig. 4.7). Moreover, the increase in S3KD myoblast adhesion compared to Vector myoblast adhesion was more pronounced in the presence of serum, suggesting that SDC3 might regulate adhesion molecules both directly and via regulating adhesion signalling cross-talk with growth factor signalling. However, these results were in contrast with what observed previously for primary *Sdc3*$^{-/-}$, which adhere less to the native myofibre *ex vivo* (Pisconti *et al.*, 2016). The experiments in Pisconti *et al.* (2016) were carried out 2.5 days after myofibre isolation, a time point at which myofibre-associated myoblasts have migrated out of the satellite cell niche and effectively adhere to the basal lamina that coats the myofibre (Siegel *et al.*, 2009).The basal lamina is rich in laminin, which is also the main ECM component to which SCs adhere. Therefore, Vector and S3KD myoblasts were tested for adhesion on laminin-coated culture dishes (Fig. 4.8). Both Vector and S3KD myoblasts adhered more to laminin in the presence of serum than without serum and again this effect was greater in S3KD myoblasts (Fig. 4.8). However, in the absence of serum S3KD myoblasts on average adhered less to laminin compared to Vector myoblasts, whereas in the presence of serum Vector and S3KD myoblasts adhered to laminin to the same extent (Fig. 4.8). These data suggest that SDC3 directly promotes adhesion to laminin and that this mechanism is overcome in the presence of growth factors.

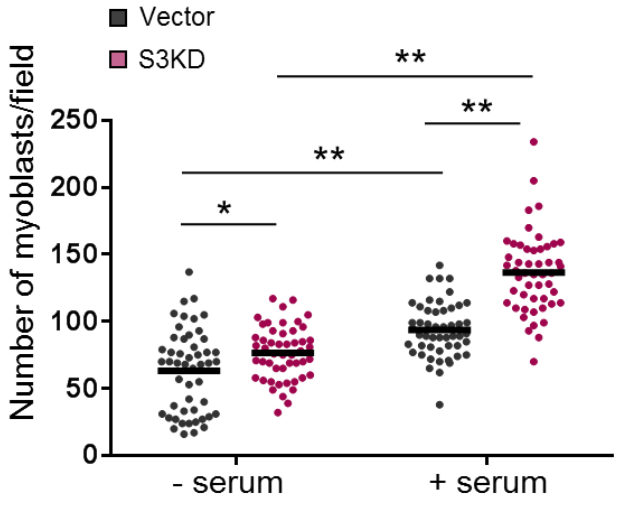

Figure 4.7: SDC3 knockdown in C2C12 myoblasts promotes adhesion. Myoblasts were plated at equal densities and allowed to adhere to the culture dish for 1 hour. Cells were washed once then fixed before staining with DAPI. DAPI+ myoblasts were counted and the average number of cells per field (each dot on the plot) were calculated as indicated by the black horizontal bar. Cumulative data from three independent experiments are plotted. * = $p < 0.05$, ** = $p < 0.01$.

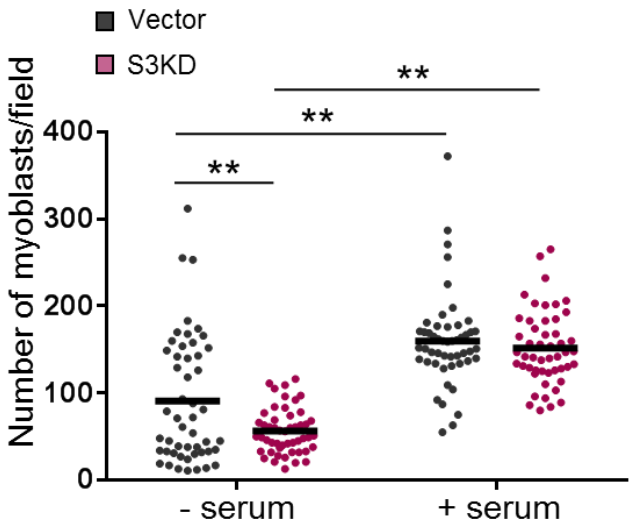

Figure 4.8: SDC3 knockdown in C2C12 myoblasts inhibits adhesion to laminin. Myoblasts were plated at equal densities onto laminin-coated dishes and allowed to adhere for 1 hour. Cells were washed once then fixed before staining with DAPI. DAPI+ myoblasts were counted and the average number of cells per field (each dot on the plot) were calculated as indicated by the black horizontal bar. Data from three independent experiments are plotted. * = $p < 0.05$, ** = $p < 0.01$.

4.2.4 Phosphatase activity in C2C12 myoblasts

In proliferating S3KD C2C12 myoblasts there was an increase in global tyrosine phosphorylation under standard growing conditions and after serum starvation and FBS stimulation. Protein phosphorylation is a reversible event and regulation is achieved through a balance of kinase and phosphatase activity. One possible explanation for an increase in tyrosine phosphorylation is a decrease in phosphatase activity when SDC3 is lost. To test this hypothesis soluble cell extracts from Vector and S3KD myoblasts were incubated with a generic phosphatase substrate (pNPP, p-Nitrophenyl Phosphate) over five hours. Serine/threonine and tyrosine phosphatases are capable of hydrolysing pNPP to form a chromogenic product which absorbs at 405 nm. Therefore, an increase in phosphatase activity leads to an increase in absorbance. Assay conditions were optimised using parental C2C12 lysate, and using methods from the literature (McAvoy and Nairn, 2010, Lorenz, 2011). To confirm specificity of phosphatase-pNPP interactions in the cell extracts a cocktail of broad-spectrum phosphatase inhibitors (PhosSTOP™) was used. Additionally, the pNPP substrate was incubated alone in phosphatase buffer to confirm that no spontaneous hydrolysis of pNPP had occurred. There were no differences in phosphatase activity between Vector and S3KD lysates, suggesting that the increase in tyrosine phosphorylation was not due to a general impairment in phosphatase activity (Fig. 4.9A). However, testing the entire cell extract may have masked subtle changes in phosphatase activity if only one or two phosphatases are affected by the loss of SDC3.

Other syndecans have been shown to regulate tyrosine phosphatases (Doody *et al.*, 2015), so it is possible that SDC3 may be a co-receptor to one or more phosphatases. To test this hypothesis SDC3 was immunoprecipitated from parental C2C12 myoblasts and phosphatase activity was measured as described before (Fig. 4.9B). Whole cell extracts

from parental C2C12 myoblasts was used as a positive control for phosphatase activity. C2C12 lysate plus PhosStop™ or pNPP alone were used as negative controls. No phosphatase activity was detected from the bead-only control, rabbit-Ig control or SDC3 pull-down samples as compared to negative controls. These results show that phosphatases do not immunoprecipitate with SDC3 or, at least, no phosphatase activity is observed under the conditions used. These results further suggest that loss of SDC3 does not directly affect phosphatase activity in proliferating C2C12 myoblasts.

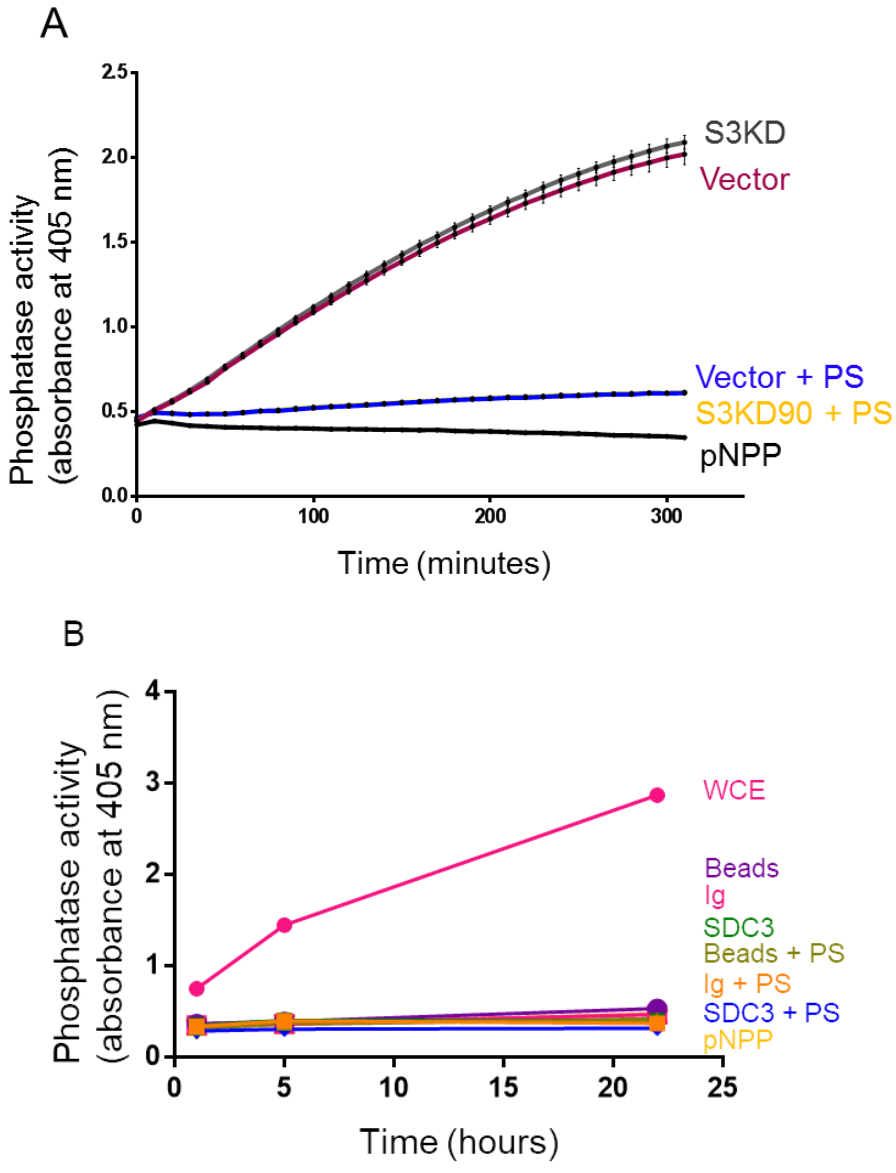

Figure 4.9: SDC3 knockdown does not affect global phosphatase activity in C2C12 myoblasts. (A) Vector and S3KD myoblasts were lysed and whole cell extracts were used to measure the global phosphatase activity. PhosSTOP (PS) was used to inhibit phosphatase activity and confirm that the substrate (pNPP) was specifically hydrolysed by phosphatases. **(B)** SDC3 was immunoprecipitated from parental C2C12 myoblasts and phosphatase activity measured using the same conditions as in (A). Whole cell extract (WCE) from C2C12 myoblasts was used as a positive control for phosphatase activity. Key: Beads = Bead-only control, Ig = Rabbit-Ig control, SDC3 = SDC3-Ig.

4.2.5 Changes to syndecan gene expression in C2C12 myoblasts

Syndecans are dynamically regulated throughout myogenesis and loss of SDC3 or SDC4 results in different muscle phenotypes (Cornelison *et al.*, 2001, Cornelison *et al.*, 2004, Pisconti *et al.*, 2012). Therefore, to confirm that SDC3-knockdown did not affect expression of the other syndecans, and consequently influence the phenotypes observed in S3KD myoblasts, real-time PCR was performed using cDNA from proliferating and differentiating Vector and S3KD cells. Results were analysed using the comparative Ct method (ΔΔ-Ct) such that each syndecan mRNA was quantified relative to GAPDH, then compared to proliferating Vector myoblasts (Fig. 4.10). The gene expression levels of SDC1-4 were compared between Vector and S3KD proliferating myoblasts and showed that SDC3 knockdown did not affect expression of SDC1 or SDC4 but SDC2 and SDC3 expression declined slightly upon SDC3 knockdown. Surprisingly the cDNA levels of SDC3 only declined by 10% when S3KD myoblasts were compared to Vector myoblasts during proliferation (Fig. 4.10C) which contradicts my previous results where SDC3 cDNA expression declined by ~47% in S3KD90 myoblasts (Fig. 4.2A) and by ~90% at the protein level (Fig 4.2B).

In differentiating cells, there appeared to be more obvious differences in the mRNA levels between Vector and S3KD cells. SDC3 knockdown increased the transcript levels of SDC1 and SDC4 compared to Vector cells whereas SDC3 and SDC2 transcript levels decreased (Fig. 4.10). These data suggest that the other syndecans are regulated in response to loss of SDC3. However, the differences in SDC1-4 mRNA levels observed between proliferating Vector and S3KD myoblasts are very small, although I observe phenotypic differences when SDC3 is knocked-down already during proliferation. Furthermore, the qPCR was only performed with one biological replicate (with three technical replicates), therefore, without further biological replicates I cannot be sure that the observed results are not false positives derived from the small variation obtained from pipetting error. Lastly, real-time PCR only measures the transcript level of gene expression therefore to further confirm these results observation of the protein level is key. Unfortunately, there are not very good commercially available antibodies to probe for mouse syndecans.

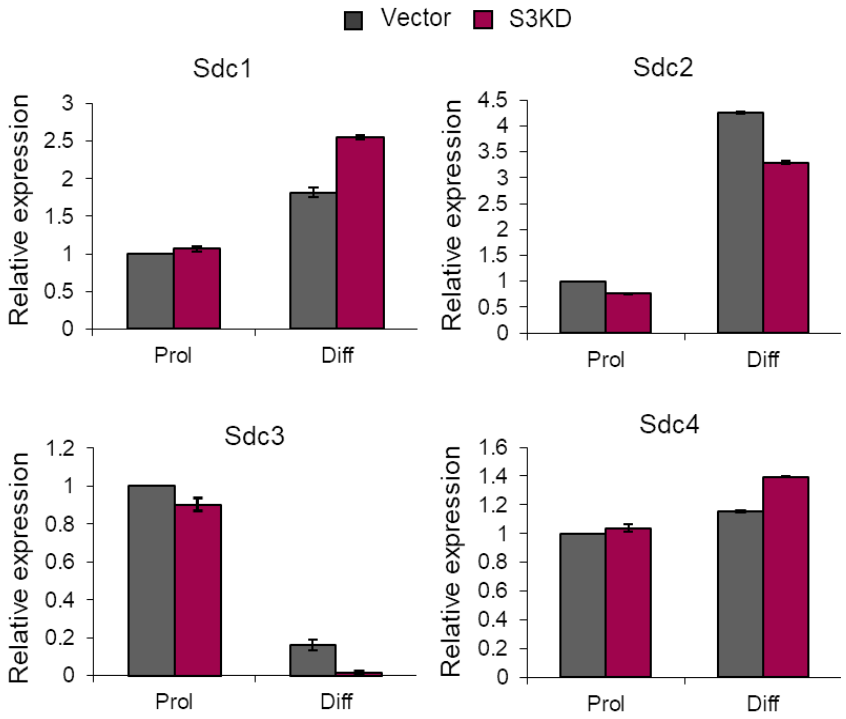

Figure 4.10: Relative expression of SDC1, SDC2, SDC3, SDC4 in proliferating and differentiating C2C12 cells. cDNA from proliferating (Prol) and differentiating (Diff) Vector and S3KD cells were used for real-time PCR. The relative quantification of Syndecan1-4 expression was calculated using the delta-delta-CT method using GAPDH as reference gene and "Vector proliferating" as reference condition. Three technical replicates are shown.

4.3 Discussion

Previous reports have shown that loss of SDC3 in mice gives rise to several interesting muscle phenotypes (Pisconti *et al.*, 2010, Pisconti *et al.*, 2016). The aims of this chapter were to determine if these phenotypes could be recapitulated in C2C12 myoblasts when SDC3 was stably knocked-down. The results shown indicate that loss of SDC3 affects cell signalling, differentiation and cell adhesion in a cell autonomous manner, as hypothesised. Using two different shRNAs, SDC3 was successfully knocked-down in C2C12 myoblasts. Two stable cell lines where SDC3 had been successfully knocked down at the protein levels were generated and named S3KD90 and S3KD91. Initially both SDC3-knockdown cell lines were characterised however it quickly became apparent that there were discrepancies between the two cell lines. Further investigation revealed that S3KD91 cells failed to form mature multi-nucleated myotubes and appeared unhealthy in culture upon induced differentiation. Therefore, I decided to disregard S3KD91 cells and focus on S3KD90 cells, which from now on will be referred to as S3KD cells.

An objective of this chapter was to determine whether S3KD myoblasts recapitulated phenotypes that had been described in primary *Sdc3*$^{-/-}$ myoblasts. All the experiments conducted indicated that S3KD myoblasts do indeed recapitulate the phenotypes of primary

Sdc3$^{-/-}$ myoblasts. More specifically, S3KD myoblasts show: enhanced differentiation, increased FGF2 sensitivity and increased global tyrosine phosphorylation when compared to Vector control myoblasts. Whilst proliferation was marginally decreased by SDC3 knockdown at 24 hours, this phenotype was lost after 48 hours which is contradictory to the previously observed results where *Sdc3*$^{-/-}$ myoblasts expanded less than wild type myoblasts in culture over a two-day time course (Pisconti *et al.*, 2010). However, when the number of cells per clone was measured at six days after isolation, *Sdc3*$^{-/-}$ and wild type cultures were comparable in number (Cornelison *et al.*, 2004), suggesting that over a longer period of time, as cell expansion reaches a plateau, primary *Sdc3*$^{-/-}$ myoblasts reach the same levels of expansion as wild type myoblasts. This is consistent with data shown here comparing S3KD myoblast expansion to Vector myoblast expansion. Altogether these data show that the general trends of the *Sdc3*$^{-/-}$ primary myoblast phenotypes and those of the S3KD myoblast phenotypes are the same, suggesting that C2C12 myoblasts are a good model to study how the loss of SDC3 impacts myogenesis.

Another key difference observed between Vector and S3KD myoblasts was a global increase in tyrosine phosphorylation. Not only under growing conditions, as observed previously (Cornelison *et al.*, 2004), but also in serum-starved myoblasts and minutes after re-stimulation of starved myoblasts. These data suggest that SDC3 might act as a general inhibitor of several signalling pathways. Alternatively, type II receptor-like protein tyrosine phosphatases (RPTPs) have shown binding affinity for heparan and chondroitin sulphate *in vitro* and *in vivo (*Aricescu *et al*., 2002, Shen *et al*., 2009), suggesting a possible role for SDC3 in controlling RPTP-mediated regulation of tyrosine phosphorylation. However, this seems unlikely since no phosphatase activity was detected upon SDC3 immunoprecipitation from C2C12 parental myoblasts, nor any difference in phosphatase activity between Vector and S3KD cell extracts. Exactly which signalling pathways are affected by this increase in tyrosine phosphorylation is unknown. There are many cellular processes in which tyrosine phosphorylation is involved such as growth factor signalling and cell adhesion via integrin signalling (Malarkey *et al.*, 1995, Vuori and Ruoslahti, 1995). Additionally, S3KD myoblasts were hypersensitive to FGF2 signalling after serum starvation. FGF2 stimulates skeletal muscle cell proliferation and strongly inhibits differentiation, suggesting dynamic FGF2-mediated cell signalling is required during myogenesis (Clegg *et al.*, 1987, Olwin and Rapraeger, 1992, Jones *et al.*, 2001). The hypersensitivity of S3KD myoblasts to FGF2 may suggest that SDC3 inhibits FGF2-mediated cell signalling, therefore, when SDC3 is lost there is an increase in ERK1/2 phosphorylation in response to FGF2 addition. Further understanding of SDC3-mediated signalling pathways will require investigation into the myoblast phosphoproteome.

Syndecans have long been thought to be important regulators of cell adhesion and migration with their ability to interact with the actin cytoskeleton and mediate integrin signalling (Culp *et al.*, 1986, Morgan *et al.*, 2007, Whiteford *et al.*, 2007, Beauvais and Rapraeger, 2010). On non-coated dishes S3KD myoblasts adhered significantly more than Vector myoblasts, with or without the presence of serum, which may be related to the increased tyrosine phosphorylation observed in S3KD. This further supports a role for SDC3 and growth factor mediated cell adhesion. The opposite effect was observed when S3KD myoblasts were plated on laminin. S3KD myoblasts displayed impaired adhesion to laminin compared to Vector myoblasts in serum-free conditions, suggesting that SDC3 might either regulate the activity of laminin receptors independently or directly bind to laminin. In both cases, independently of SDC3 regulation of growth factor signalling. Indeed, this effect was rescued in the presence of serum, suggesting that pro-adhesive growth factor signalling was capable of compensating for the loss of SDC3 in the regulation of adhesion laminin. In contrast, the presence of serum further exacerbates the enhanced adhesion to non-coated dishes, suggesting that different adhesion receptors were involved in the two experimental conditions and that SDC3 regulates these different mechanisms of cell-matrix adhesion in different ways. Previous studies have shown that loss of SDC3 impairs satellite cell adhesion to basal lamina-coated myofibres *ex vivo* and satellite cell homing to the niche *in vivo* after muscle regeneration, which further support a role for SDC3 in regulating adhesion to laminin (Pisconti *et al.*, 2016). In addition, the core SDC3 ectodomain is involved in cell adhesion and migration of endothelial cells (De Rossi and Whiteford, 2013). Further investigation into the role of SDC3 in the regulation of myoblast adhesion would be insightful. For example, it would be interesting to test how well S3KD myoblasts adhere to other components of the satellite cell niche such as fibronectin, collagen I and collagen IV.

In conclusion, the experiments conducted in this chapter identified several phenotypes when SDC3 was knocked down in C2C12 myoblasts during proliferation and differentiation, recapitulating previously observed phenotypes in primary *Sdc3*$^{-/-}$ myoblasts. These results were encouraging because C2C12 myoblasts appear to be a good model to study the molecular mechanisms regulated by SDC3, providing confidence for use of these cells in further experimentation. Several questions remain at this point including: what drives enhancement of differentiation in S3KD myoblasts? Why does loss of SDC3 affect cell adhesion in a seemingly serum-dependant manner and what other changes are occurring in S3KD cell signalling pathways? Investigation into the phosphoproteome of Vector and S3KD myoblasts may provide clues to answer these questions.

Chapter 5

Using phosphoproteomics to decipher the SDC3 signalling network

5.1 Introduction

Phosphorylation is a common reversible post-translational modification of proteins that can positively or negatively affect cell signalling cascades. The regulation of protein phosphorylation is mediated by protein kinases, which covalently add a phosphate group to a specific amino acid, and phosphatases which remove the phosphate group. Protein kinases recognise specific linear motifs within a substrate's amino acid sequence, which confers specificity to the kinase-substrate interaction. In eukaryotic cells, the most commonly phosphorylated amino acids are: serine, threonine and tyrosine, at a ratio of approximately 1000:100:1 (Raggiaschi *et al.*, 2005). Other amino acids can be phosphorylated such as histidines, arginines and lysines but these are more difficult to study and consequently little is known about these types of phosphorylation (Sickmann and Meyer, 2001). Phosphorylated proteins can recruit adaptor proteins that recognise specific phosphorylated-motifs through specialised domains such as Src homology 2 (SH2) or Mad homology 2 (MH2), which bind to phosphorylated-tyrosine (pTyr) or phosphorylated-serine (pSer) respectively (Nishi *et al.*, 2011). The addition of a phosphate group often alters the structural conformation of a protein, and when the phosphorylated protein is an enzyme, this conformational change may reveal or conceal its catalytic domain, activating or deactivating the biological function of the enzyme. Additionally, phosphorylation can cause subcellular translocation of a protein, affect the rate of protein degradation or its ability to bind other proteins. These multifunctional abilities of protein phosphorylation are critical for signal transduction and many other biological processes in cells. Therefore, in the last few decades the kinome (the entire repertoire of protein kinases present in a cell) and the phosphoproteome (the complex set of protein phosphorylations present in a cell) have been the subject of intense studies in several disciplines including cell biology, evolutionary biology, enzymology and translational medicine (Tobe *et al.*, 2012).

Recent advances in mass spectrometry have allowed unbiased global analysis of protein phosphorylation in various cellular or tissue contexts leading to the development of a whole new branch of proteomics called phosphoproteomics (Nilsson, 2012). Mass spectrometry-based phosphoproteomics has many advantages over other methods, such as immunoblotting, the main being that multiple proteins can be studied at the same time resulting in high throughput data. Study of the phosphoproteome has yielded important information regarding cell signalling networks, multi-site phosphorylation and function of specific phosphosites. For example, the idea of complex multidirectional cell signalling interactions were confirmed by phosphoproteomic studies and further proved that phosphorylation events previously considered linear components of a signalling pathway, actually participated in negative feedback mechanisms and cross-talked with other signalling pathways, thus adding several layers of complexity to the mechanisms of cell signal transduction (Raggiaschi *et al.*, 2005).

Although mass spectrometry is a powerful tool to study phosphoproteomics, several technical considerations must be made to obtain a high-quality data. From the choice of appropriate lysis buffer, to the method for phosphopeptide enrichment, data acquisition, and methods of quantification. Phosphopeptide quantification using label-free or stable isotope labelling are commonly used methods (Kumar and Mann, 2009). Stable isotope labelling can be introduced metabolically in live cells or live animals using SILAC (Stable Isotope Labelling by Amino acids in Cell culture) culture media or SILAC animal feed. Alternatively, isotope labelling can be added later in the sample preparation workflow using chemical methods such as iTRAQ (Isobaric Tag for Relative and Absolute Quantitation) (Florini *et al.*, 1991, Montarras *et al.*, 1996, Duan and Gallagher, 2009). Whilst these methods based on isotope-labelling may produce more accurate quantification results than label-free methods, they are often more complex, costly and concede to a reduced quantitative proteome coverage (Solari *et al.*, 2015). More recently label-free approaches were introduced into the global phosphoproteomics field. Label-free methods rely on either spectral counting of each peptide mapped to a certain list of proteins of interest, or, on the measurement of the mass spectrometric signal intensity of a peptide. Label-free approaches are the least accurate methods of peptide/protein quantification. However, label-free workflows require fewer time-consuming steps and therefore fewer opportunities for introducing errors and contaminations. In addition, label-free proteomics requires fewer costly reagents and poses no limit to the number of samples that can be compared in one single experiment, unlike some stable isotope labelling techniques, such as iTRAQ which is limited to 8 samples (Duan and Gallagher, 2009). Additionally, there is evidence to suggest that label-free approaches may be advantageous over labelling techniques when

studying global protein changes between experiments as label-free proteomics allows to reliably profile a wider dynamic range (Solari *et al.,* 2015).

Since phosphorylated proteins are present at low abundance in the total proteome, enrichment of phosphorylated proteins is vital to ensure reliable phosphopeptide detection by the mass spectrometer (Mann *et al.*, 2002). Immunoaffinity can be used to enrich for specific phosphopeptides using antibodies specific for phospho-tyrosine or a specific phosphorylated motif; these methods are useful if the study is focussed on a specific subset of phosphorylations. In contrast, for global phosphopeptide enrichment, chemical methods such as immobilized metal-affinity chromatography (IMAC) or Titanium dioxide (TiO_2) columns are preferable, as these will capture phosphorylated-serines (pSer), phosphorylated-threonines (pThr) and pTyr peptides. The necessity to enrich the sample prior to mass spectrometry analysis, implies that a larger amount of starting material is required for phosphoproteomic studies compared to general proteomic studies (Vyse *et al.*, 2017). Often milligrams of protein are required for large-scale discovery phosphoproteomic experiments (Ferries *et al.*, 2017) which causes difficulty in using primary myoblasts as these cannot be expanded for more than a couple of passages before beginning to spontaneously differentiate or senesce (Noujaim *et al.*, 2016). Moreover, primary myoblasts require a proteinaceous substrate to grow on (usually laminin, collagen type I or gelatin) which would be collected in large amounts alongside the cells during cell lysis, and analysed by mass spectrometry alongside the cell lysates, which may mask cell proteins that are present in the sample in low abundance.

5.1.1 Hypothesis and objectives

In the previous chapter I determined that the S3KD myoblasts recapitulated phenotypes observed in primary *Sdc3*$^{-/-}$ myoblasts. An increase in global tyrosine phosphorylation was observed in S3KD myoblasts, therefore, I hypothesised that SDC3 was involved in regulating several receptor tyrosine kinase (RTK) signalling pathways. The objectives of this chapter were:

1) To investigate the global phosphoproteome changes in Vector and S3KD myoblasts using label-free phosphoproteomics.
2) To use a bioinformatic approach to infer SDC3-mediated regulation of myoblast cell signalling.

5.2 Results

5.2.1 Experimental design and sample processing

The previous chapter confirmed that SDC3 knockdown in C2C12 myoblasts resulted in an increase in global tyrosine phosphorylation, in proliferating myoblasts exposed to growth medium, in serum-starved myoblasts, and after 10 and 20 minutes of stimulation with serum (*Chapter 4,* Fig. 4.4). The next stage of this project was to identify which proteins were differentially phosphorylated upon loss of SDC3 and infer which signalling pathways were regulated by SDC3 in myoblasts. To achieve this goal a phosphoproteomics experiment was designed to identify significantly regulated phosphopeptides in Vector and S3KD myoblasts after serum stimulation and determine which phosphopeptides were regulated by SDC3 knockdown **(**Fig. 5.1). Since the maximum difference in pTyr levels between Vector and S3KD myoblasts was detected at 10 minutes stimulation with serum after a five-hour-long serum starvation (*Chapter 3*, Fig. 3.4), I chose to investigate two time points (Time 0 = serum starved myoblasts and, Time 10 = 10 minutes of serum stimulation) as this would have given information about the role of SDC3 in the myoblast response to serum stimulation. Eight independent replicates of Vector and S3KD cells were serum-starved for five hours then either lysed (four replicates, Time 0) or stimulated with serum for 10 minutes (four replicates, Time 10) prior to being lysed. The cell lysates were then processed for phosphopeptide enrichment and prepared for LC-MS/MS analysis by the Centre for Proteome Research (University of Liverpool). Briefly, samples were digested with trypsin then enriched for phosphopeptides using titanium dioxide columns, prior to liquid chromatography followed by tandem mass spectrometry (LC-MS/MS).

Following LC-MS/MS data acquisition several data processing steps were required to obtain the final semi-quantitative results including: (1) alignment of chromatograms, (2) identification of peptides, (3) localisation of phosphorylation modifications within peptides, (4) label-free quantification of peptide abundances, and (4) statistical analysis of peptide abundance (Fig. 5.1). A problem was encountered when a peptide was rarely identified in one or more replicates, as the subsequent semi-quantitative analysis returned a value of zero when the peptide abundance was below the threshold of detectability. The presence of missing abundance values, is a common problem in data analysis of proteomics experiments (Karpievitch *et al.*, 2012). To overcome this problem, we collaborated with Prof Andy Jones, University of Liverpool, to design a Bayesian inference model that would robustly detect statistically significant differences in phosphopeptides between conditions (Fig. 5.1). For further details please refer to the *Methods* section 2.13.

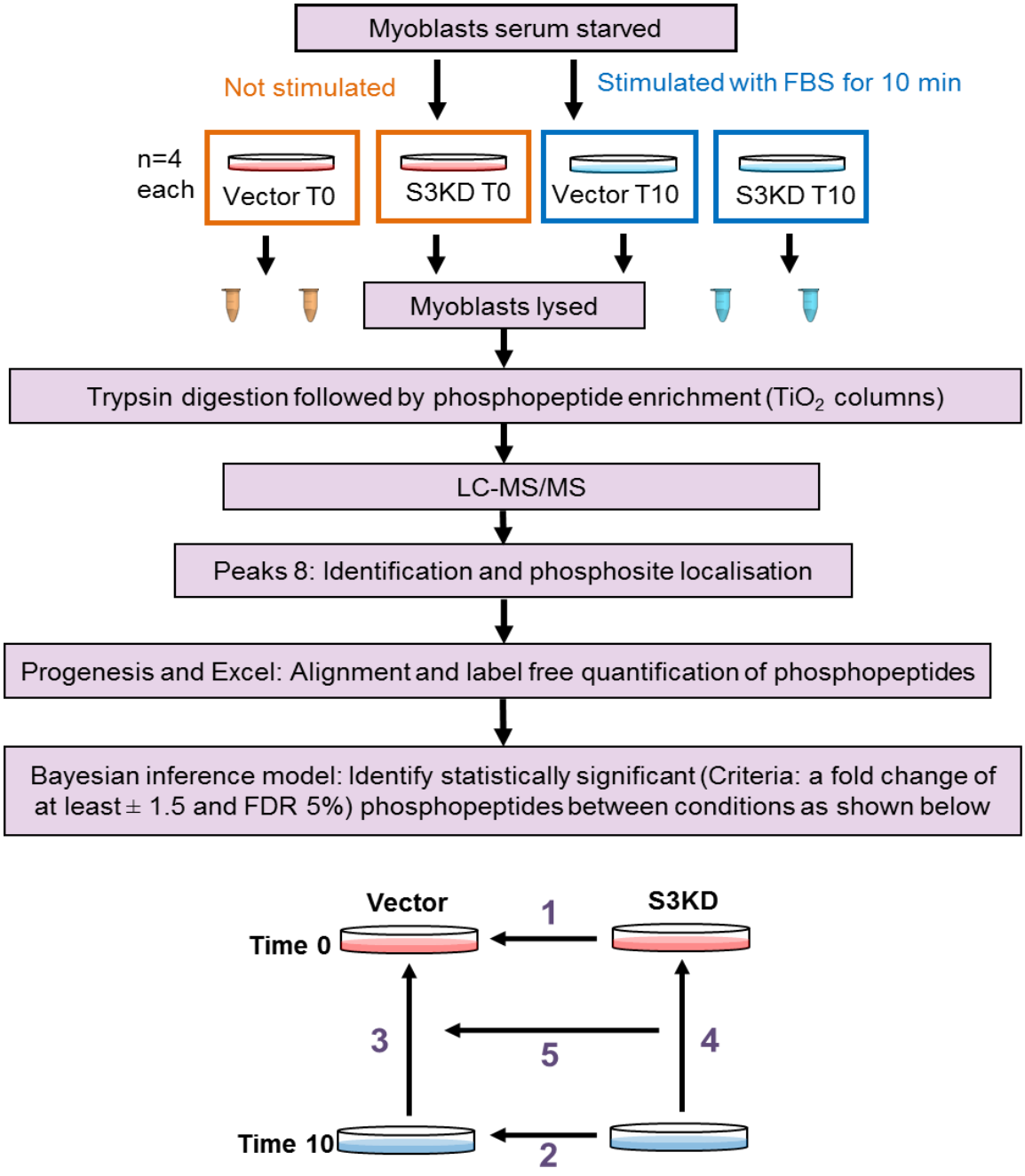

Figure 5.1: Schematic representation of the phosphoproteomcis workflow. Vector and SDC3 knockdown (S3KD) myoblasts were serum starved for 5 hours (T0 = Time 0) then either immediately lysed or serum-stimulated for 10 minutes (T10 = Time 10) prior to being lysed. Lysates were processed and peptides were analysed by LC-MS/MS. Peptides were identified and phosphosites localised using the software package Peaks 8 before chromatogram allignment and quantification of phosphpeptide abundance using the software package ProgenesisQI followed by data compiling in Microsoft Excel (please refer to the *Methods* section for further detail). A Bayesian inference model was used to identify statistically significant differences in phosphopeptide abundances between the following conditions: **1)** S3KD compared to Vector cells at Time 0, **2)** S3KD compared to Vector at Time 10, **3)** Vector at Time 10 compared to Vector at Time 0, **4)** S3KD at Time 10 compared to S3KD at Time 0, and, **5**) S3KD (Time 10/Time 0) compared to Vector (Time 10/Time 0).

5.2.2 Description of peptide results

The main aim of this chapter was to identify changes in the phosphoproteome upon loss of SDC3, therefore a large focus was placed on the phosphopeptides rather than all peptides identified. By using TiO_2 columns a good enrichment of phosphopeptides was obtained from total peptides, as > 60% of all the peptides identified (corresponding to > 67% of all proteins identified) were phosphorylated (Fig. 5.2A). This is a substantial enrichment when considered that without phosphopeptide enrichment approximately less than 1% of all peptides identified in a whole cell lysate are phosphorylated (Alessi *et al.*, 1997). The majority of the 7,190 phosphopeptides identified contained only one phosphorylated site with relatively fewer containing two or three phosphorylated sites (Table 5.1). In total 8,493 phosphorylated sites were identified and approximately half of these sites were assigned a phosphosite localisation score (Ascore) >13, indicating that the probability of correct phosphosite localisation within the peptide exceeded 95% (Fig. 5.3B) (Beausoleil *et al.*, 2006). A breakdown of the number of singly, doubly or triply phosphorylated peptides are shown in Table 5.1 along with the number of pSer, pThr and pTyr phosphosites identified. Very few tyrosine phosphorylations were identified compared with pSer and pThr, which was expected considering tyrosine phosphorylation is much rarer than serine or threonine phosphorylation (Raggiaschi *et al.*, 2005).

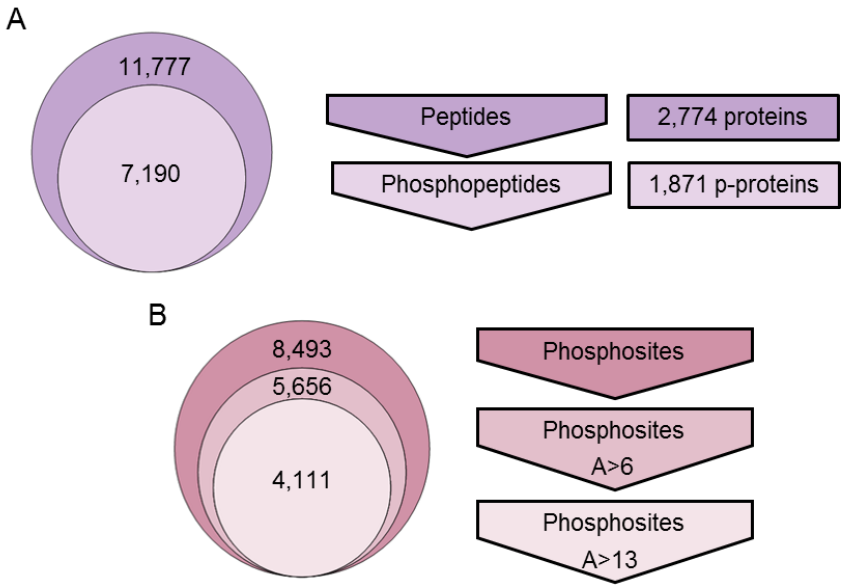

Figure 5.2: Number of confidently identified peptides, phosphopeptides and phosphosites from all data obtained. (A) The Venn diagram shows the numbers of total peptides (dark purple) and phospho-peptides (light purple) identified with a false discovery rate of 1%. The corresponding number of proteins identified are shown in rectangles. **(B)** The total number of phosphosites identified and confidently localised according to the indicated Ascore are shown. An Ascore (A) of > 6 is equivalewnt to a p-value of 0.25 and an A > 13 is equivalent to a p-value of 0.05.

Table 5.1 Number of of phosphorylated sites identified.
The number of phosphopeptides with 1, 2 or 3 phosphorylated sites per phosphopeptide are shown in the first three columns, while the numbers of confidently localised S/T/Y phosphorylations are shown in the third through fifth columns; only phospphopeptides with an Ascore larger than 13 were considered correctly localised.

Number of phosphosites per phosphopeptide			Number of phosphorylated serines, threonines or tyrosines identified		
1	2	3	Serine	Threonine	Tyrosine
6,022	1,033	135	3,674	420	18

After calculating the total number of phosphopeptides and phosphosites identified, the number of differentially abundant phosphopeptides in each comparison was identified (Fig 5.3A) as described in the *Methods* section 2.14. The largest number of phosphopeptide changes occurred between serum-starvation (Time 0) and serum-stimulation (Time 10) in both Vector and S3KD myoblasts. These results represented all the phosphorylation events that were detected after the myoblasts were stimulated with serum. Serum is rich in growth factors, nutrients, hormones and other signalling molecules that stimulate a myriad of phosphorylation cascades in the cell, involved in cell signalling and would explain why a large number of phosphorylation events were detected in both cell lines in response to serum stimulation after a period of serum starvation. Next, I looked at the phosphopeptides that had changed in abundance compared between Vector and S3KD myoblasts at the individual time points (Time 0 and Time 10). Based from my data in the previous chapter where increased pTyr was observed in S3KD myoblasts after 10 minutes of serum stimulation compared to Vector myoblasts, and less so when serum starved, I expected to see a larger number of phosphopeptides differentially abundant between Vector and S3KD myoblasts at Time 10 compared to Time 0. However, only 103 phosphopeptides were differentially abundant at Time 10 and, interestingly, even more (355) phosphopeptides were differentially abundant in S3KD and Vector myoblasts after serum-starvation. Next I asked: how many of these phosphopeptides that had changed in response to serum in both cell lines, had differentially changed in Vector versus S3KD myoblasts? Surprisingly, only 59 phosphopeptides were significantly changed between Vector and S3KD myoblasts in response to serum stimulation, and most of them were phosphopeptides that had increased less in S3KD myoblasts compared to Vector myoblast in response to serum stimulation.

Using these five sets of differentially abundant phosphopeptides (Fig. 5.3A), several functional analyses were completed for each set of conditions compared including: signalling pathway analysis, gene ontology enrichment and identification of overrepresented phosphorylation motifs. A schematic of the downstream analysis workflow is shown in Figure 5.3B. For some of the bioinformatic analysis, a filter was applied so that

only phosphopeptides with a confident localisation score were used. This was imperative for analyses where the position of the phosphosite was important such as substrate motif analysis. In the case of pathway enrichment, where the phosphosite position was not important, but rather the evidence of a phosphorylation event occurring somewhere in the peptide, no filtering was applied.

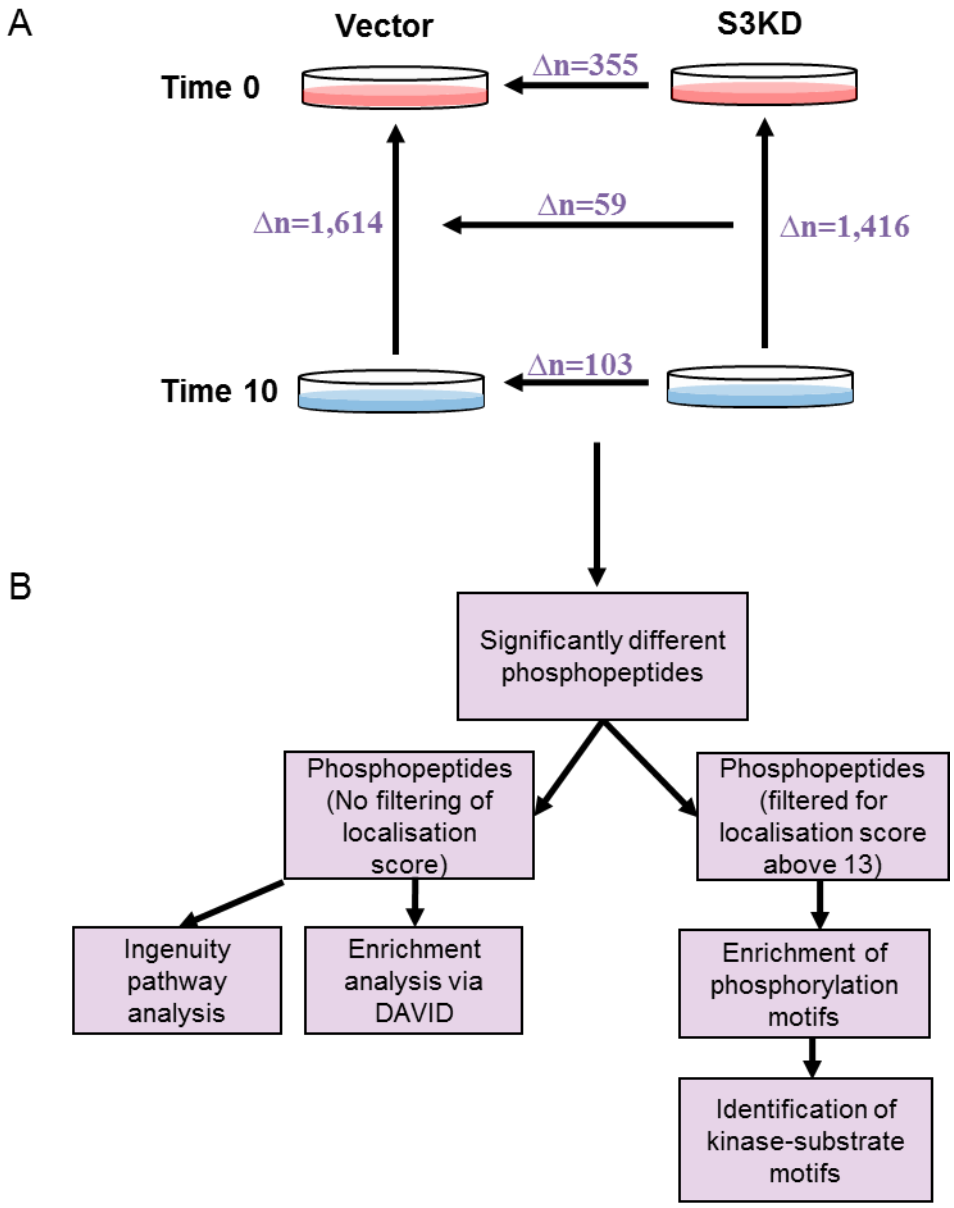

Figure 5.3: Workflow of downstream analysis (A) Number of significantly regulated phosphopeptides identified within each of the 5 comparisons analysed. **(B)** Bioinformatic workflow followed to functionally analyse the phosphopeptides that significantly change in the comparisons shown in (A).

5.2.3 Phosphopeptide changes mediated by SDC3 knockdown at Time 0 and at Time 10

To formulate a biological interpretation of the differences in phosphopeptide abundance observed when comparing Vector and S3KD cells, both at Time 0 and at Time 10, multiple types of functional analysis were conducted. The fold change versus q-value of the phosphopeptides were plotted on volcano plots to visualise the spread of the data and identify any obvious skews which may have indicated a change towards increased or decreased phosphorylation of peptides when SDC3 was knocked down (Fig. 5.4). At Time 0 the number of phosphopeptides with increased phosphorylation in S3KD compared to Vector myoblasts was ~40% greater than the number of phosphopeptides with decreased phosphorylation in S3KD compared to Vector myoblasts (Fig. 5.4A), which is consistent with the finding that the levels of phosphorylated tyrosine in serum-starved S3KD cells is greater than in Vector cells (*Chapter 4,* Fig. 4.4). Similarly, the number of phosphorylated peptides that were increased in S3KD compared to Vector myoblasts at Time 10 was almost twice the number of phosphopeptides whose abundance was decreased in S3KD versus Vector myoblasts (Fig. 5.4B), which is consistent with the previous observation that the levels of pTyr further increases in S3KD myoblasts compared to Vector myoblasts after stimulation with FBS. A complete list of all differentially abundant phosphopeptides at Time 0 and Time 10 can be found in Appendix 2.1 and 2.2.

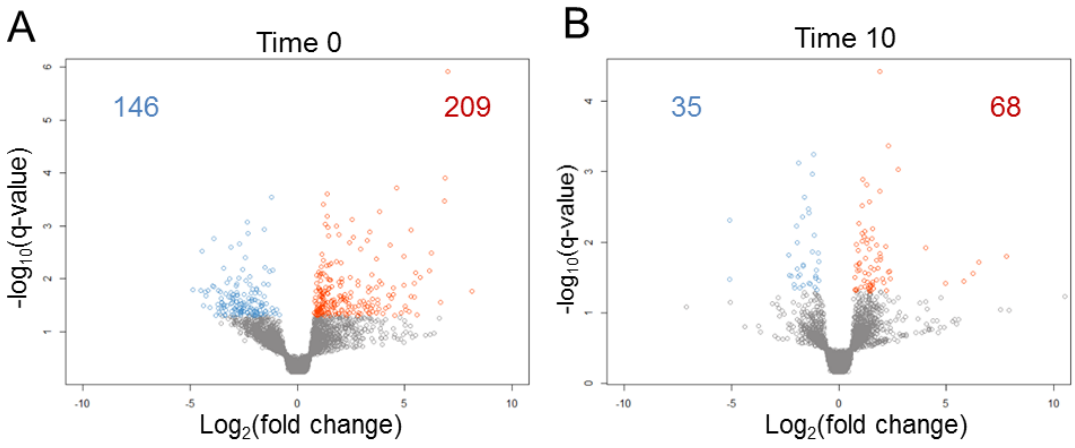

Figure 5.4: Volcano plots of phosphopeptides identified at Time 0 and Time 10. Grey dots show phosphopeptides with no signifcant change in abundance between Vector and S3KD myoblasts. Red indicates S3KD phosphopeptides with an increase in abundance compared to Vector control and blue shows decreased phosphorlyation in S3KD myoblasts compared to Vector myoblasts.

5.2.3.1 Over-represented phosphorylation motifs

Protein kinases recognise short linear motifs within an amino acid sequence of a substrate which preferentially allows them to engage and phosphorylate a residue within that amino acid sequence (Chou and Schwartz, 2011). Different kinases recognise different motifs and many of these motifs have been identified, which allows prediction of kinase-substrate interactions (Chou and Schwartz, 2011, Lee*, et al.*, 2011). One way to analyse phosphoproteomics datasets is to search for specific motifs that are enriched (over-represented) in each set of samples as this gives an indication of which upstream kinases, and therefore signalling pathways, are more or less active in one set of samples versus another. Motif-x is a bioinformatic tool that uses an algorithm to identify statistically over-represented motifs from a data set (Schwartz and Gygi, 2005, Chou and Schwartz, 2011). Using this information, the aim was to identify potential kinases that had differing activity upon SDC3 knockdown in myoblasts, indicating kinase-mediated changes in cell signalling. Phosphopeptides with a confident localisation score, (Ascore >13), were grouped by increased or decreased phosphopeptide abundance then analysed using Motif-x to identify statistically over-represented motifs in the Time 0 and Time 10 data (Table 5.2). No motifs were identified for pTyr, likely because pTyr is a fairly rare modification and only a few peptides containing phosphorylated tyrosines were identified. Only one over-represented pThr motif was identified, likely because relatively few pThr phosphopeptides were differentially abundant. Fewer over-represented pThr motifs were identified at Time 10, this may have been because serum stimulation caused activation of several signalling pathways and many different kinases were activated resulting in phosphorylation of a vast range of motifs and only few motifs could be grouped together.

Table 5.2: Number of statistically over-represented motifs identified in phosphopeptides that were differentially abundant between S3KD and Vector myoblasts at either Time 0 or Time 10. The arrows pointig up indicate that the indicated phosphosite is increased in S3KD versus Vector cells. The arrows pointing down indicate that the indicated phosphosite is decreased in S3KD versus Vector cells. pS = phosphorylated serine motifs, pT = phosphorylated threonine motifs, pY = phosphorylated tyrosine motifs.

Time 0						Time 10					
↑ pS	↑ pT	↑ pY	↓ pS	↓ pT	↓ pY	↑ pS	↑ pT	↑ pY	↓ pS	↓ pT	↓ pY
3	1	0	3	0	0	0	0	0	1	0	0

Four over-represented motifs were identified amongst phosphopeptides that were increased in S3KD myoblasts compared to Vector myoblasts at Time 0 and three motifs were identified amongst phosphopeptides that were decreased in S3KD myoblasts compared to Vector myoblasts at Time 0 (Fig. 5.5). In contrast, no significant motif enrichment was found at Time 10 amongst the phosphopeptides that were increased in

S3KD myoblasts compared to Vector myoblasts and only one motif was significantly over-represented amongst the phosphopeptides that were decreased in S3KD myoblasts compared to Vector myoblasts at Time 10 (Fig. 5.5).

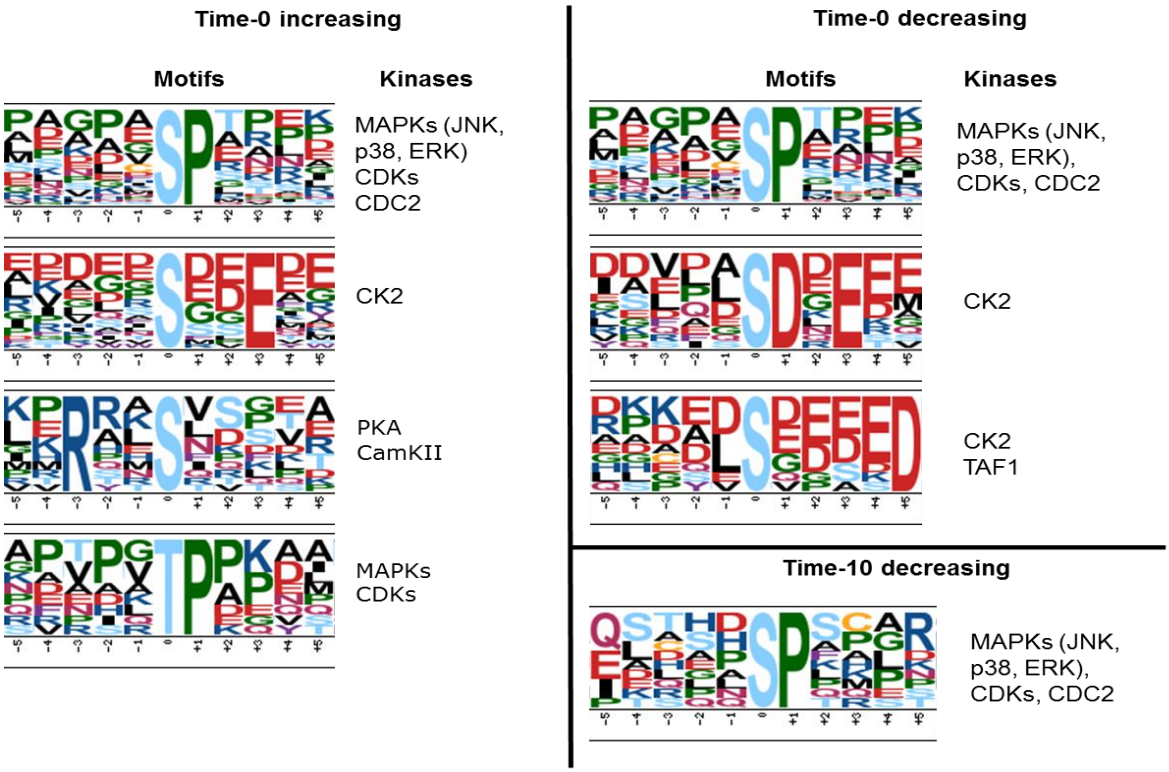

Figure 5.5: Over-represented phosphorylation motifs from Time 0 and Time 10. Phosphopeptides differentiatlly abundant between Vector and S3KD at Time 0 and Time 10 were separated into increasing and decreasing phosphorylation then submitted to Motif-x to identify over-represented motifs. Putative kinases responsible for the phosphorylation of the identified motifs are shown to the right.

Using the literature, it is possible to identify potential kinases that are predicted to phosphorylate the enriched motifs (Fig. 5.5). Many of the motifs identified have been biologically well-characterised and are recognised by kinases belonging to the family of mitogen-activated kinases (MAPKs). The p[S/T]P motifs are commonly found in motif enrichment studies because a large number of peptides are phosphorylated by proline-directed kinases, such as kinases belonging to the MAPK superfamily (Schwartz and Gygi, 2005, Schmutz *et al.*, 2013). However, because the p[S/T]P motif is very common, it is recognised by several kinases and it is over-represented in all the sets of data (Time 0 increasing, Time 0 decreasing and Time 10 decreasing), it is difficult to infer from these data which signalling pathways might be regulated by SDC3 and whether they are inhibitory or activating.

The second most recurrent motif was pS[D/E]xE which is found in acidophilic substrates phosphorylated by casein kinase 2 (CK2). Since CK2 is ubiquitously and constitutively

expressed and is able to phosphorylate a substantial proportion of the eukaryotic phosphoproteome (Litchfield, 2003), the fact that CK2 substrates were over-represented in our Time 0 dataset suggests that loss of SDC3 affects CK2 activity upon serum starvation, but SDC3 seems dispensable for CK2 activity in the presence of serum (Fig. 5.5).

In contrast to MAPK and CK2 targets, which were over-represented in phosphopeptides that were both increased and decreased in S3KD myoblasts compared to Vector myoblasts at Time 0, the motif RxxpS, which can be recognised and phosphorylated by Protein kinase A (PKA) and Ca2+/calmodulin-dependent protein kinase II (CamKII) (Pearson and Kemp, 1991), was over-represented only within phosphopeptides that had significantly increased in phosphorylation in S3KD myoblasts compared to Vector myoblasts at Time 0 (Fig. 5.5). This result indicates that PKA and/or CamKII activity is increased in S3KD myoblasts under serum starvation, suggesting a role for SDC3 in either inhibiting upstream signalling pathways that lead to CamKII and/or PKA activation or promoting signalling pathways that lead to PKA and/or CamKII inhibition.

These data provided information regarding possible SDC3-mediated regulation of downstream kinases, such as MAPKs, CK2 and PKA, but limited information regarding specific signalling pathways involved. Therefore, next I investigated the biological function of the differentially abundant phosphopeptides.

5.2.3.2 Functional enrichment of phosphopeptides from Time 0 and Time 10

Gene Ontology (GO) is a collaborative project that collects and collates descriptions of gene function from several databases then organises these data into structured and controlled vocabularies called ontologies; this allows functional inference of a gene product (protein). GO is organised in a hierarchical way with three main ontologies: Biological Processes, Molecular Function and Cellular Component. Each one of these three main ontologies are further divided into several functional categories to which genes and gene products are mapped. Each one of these functional categories is called a GO term. Many bioinformatic tools, such as DAVID, make use of GO terms to perform functional enrichment analyses, which can help infer changes in biological function between conditions when a list of differentially expressed/abundant genes or gene products is analysed. Functional enrichment encompasses several steps: mapping of genes or gene products to a functional term, grouping the identified terms according to a common function, then comparing these groups to a reference dataset also called the background dataset, which is usually the entire species genome or proteome (depending on whether a gene list or a protein list is being analysed). Using the background dataset, an algorithm calculates how enriched a functional group is in the experimental dataset considering the probabilities of a specific functional

term occurring within the background. Lastly, a p-value is calculated to determine the significance of the enrichment.

In these analyses, I enriched for GO terms using DAVID ((Huang da *et al.*, 2009, 2009) Version 6.8, last update Oct 2016) to identify changes in biological functions of the phosphopeptides found differentially abundant between Vector and S3KD myoblasts at Time 0 and Time 10. DAVID does not recognise phosphopeptide data therefore I mapped each differentially abundant phosphopeptide to its corresponding protein and carried out functional enrichment analysis of the resulting phosphoprotein lists. As part of the experimental workflow, samples were passed through a titanium dioxide column to enrich the sample in phosphopeptides. Therefore, when all the phosphoproteins identified in this study were functionally analysed against the whole mouse proteome, not surprisingly the most significantly enriched Biological Process was protein phosphorylation and the most enriched Molecular Function was protein kinase activity (Appendix 3.1). This was clearly due to a bias introduced in the statistical analysis of the functional enrichment by the biochemical enrichment of the samples carried out before LC-MS/MS. Therefore, to provide an unbiased approach to the functional enrichment analysis, the differentially abundant phosphoproteins were analysed against a background dataset containing all the phosphoproteins identified in this study, across all conditions and all replicates.

At Time 0 the most significantly enriched Biological Process in the phosphoproteins that were differentially abundant between S3KD and Vector myoblasts was ‘cell-cell adhesion’ followed by ‘mTOR signalling’ (Fig. 8A). The identified phosphoproteins that mapped to these Biological Processes are shown in Appendix 2.1.1 with their phosphosite(s) and fold change. Enriched mTOR signalling proteins included: La-related protein 1 (Larp-1), Eukaryotic translation initiation factor 4E-binding protein 1 (4E-BP1), eukaryotic translation initiation factor 4E binding protein 2 (4E-BP2), Girdin and Ribosomal protein S6 (RPS6). All of these, except Girdin, act downstream of mTOR signalling and are involved in protein translation, while Girdin is an AKT-binding protein. Additionally, the phosphosites identified for these proteins indicated increased activation of the mTOR signalling pathway in S3KD myoblasts compared to Vector myoblasts, suggesting that loss of SDC3 in myoblasts activates mTOR signalling in the absence of serum. Interestingly, Girdin is also involved in cell adhesion and migration (Gu *et al.*, 2014), which is consistent with the other Biological Process and Molecular Function categories identified, such as: ‘cell adhesion’, ‘cadherin binding in cell-cell adhesion’ and ‘actin binding’. NEDD4 was enriched in ‘Protein K63-linked ubiquitination’ suggesting NEDD4 phosphorylation is regulated by loss of SDC3. This was particularly interesting as NEDD4 regulates PAX7 protein levels in myoblasts (Bustos

et al., 2015). Unfortunately, little is known about the function of the NEDD4 phosphosites identified in this study.

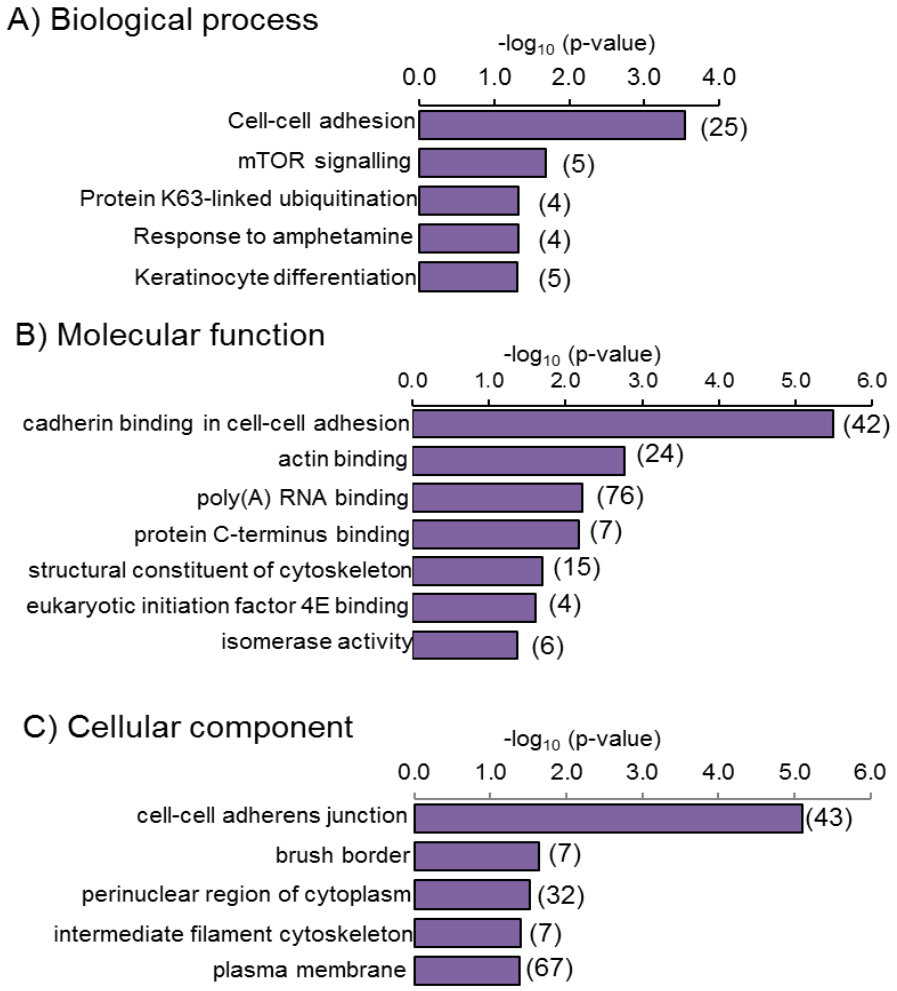

Figure 5.6: Enriched GO terms identified at Time 0 divided by GO category. Phosphopeptides that were significantly regulated between Vector and S3KD myoblasts at Time 0 were mapped to phophoprotein identifiers and then functional enrichment analysis was performed using DAVID (https://david.ncifcrf.gov/). P-values less than 0.05 were considered significant. Numbers in brackets indicate the number of proteins mapped to each indicated GO term.

In addition to 'cell-cell adhesion', as the most significantly enriched sub-category within the Biological Process category at Time 0, the most enriched Molecular Function and Cellular Component sub-categories at Time 0 were 'cadherin binding in cell-cell adhesion' and 'cell-cell adherens junction' (Fig. 5.6B and 5.6C). Syndecans have been shown to regulate both cell-cell adhesion and growth factor signalling pathways (Lambaerts *et al.*, 2009). The fact that sub-categories related to cell-cell adhesion are enriched with phosphoproteins differentially abundant in S3KD compared to Vector myoblasts at Time 0 (serum-starved cells) suggests that SDC3 directly regulates cell-cell adhesion in myoblasts, in the absence of growth factors. The Cellular Component sub-category 'plasma membrane' contained the largest fraction of differentially abundant phosphoproteins (25%,

p = 0.04) suggesting that many of the cell signalling changes had occurred at the cell membrane, which is consistent with SDC3 being a transmembrane proteoglycan.

Fewer significantly enriched groups were identified in the Time 10 data set (Fig. 5.7), possibly because fewer phosphoproteins were submitted for analysis compared to Time 0 or because fewer phosphoproteins could be grouped together. Significantly enriched Biological Processes included 'phosphatidylinositol signalling' and 'regulation of mesenchymal cell proliferation', suggesting changes to PI3K signalling and cell proliferation upon loss of SDC3. Interestingly, IRS1 (Insulin receptor substrate 1) and IRS2 (Insulin receptor substrate 2) mapped to both these GO terms (Fig. 5.7A). IRS1 had one significantly increased phosphosite (S1096 or human S1100, Ascore = 12.81, fold change = 2.7), which has been linked to insulin resistance in diabetic muscle (Langlais *et al.*, 2011). IRS2 also had one significantly increased phosphosite (S675 or human S679, Ascore = 14.04, fold chance = 3.8) however the biological function of this phosphosite is unknown. IRS1 and IRS2 are primary modulators of the insulin and IGF signalling pathways. These changes in IRS1 and IRS2 phosphorylation between Vector and S3KD at Time 10, and the changes observed in mTOR and PI3K signalling pathways, which are downstream of insulin/IGF signalling, suggest that insulin or IGF signalling may be regulated by SDC3 in C2C12 myoblasts.

Two Molecular Function GO terms were identified at Time 10: 'actin binding' and 'protein domain specific binding' (Fig. 5.7B). Neither of these functions helped identify SDC3-mediated signalling pathways, however, the enrichment of 'actin binding' in Molecular Function and 'actin cytoskeleton' in Cellular Component, suggests a role for SDC3 in cytoskeleton rearrangement, which is important for cell adhesion and migration. Similar to Time 0, a large proportion (40%) of plasma membrane-associated proteins were enriched at Time 10 (Fig. 5.7C). Two muscle specific Cellular Component GO terms were enriched (Z-disc and sarcolemma) which was expected as myoblasts were used for these experiments.

Surprisingly three neuro-specific components were also significantly enriched at Time 10 including 'neuronal cell body', 'postsynaptic density' and 'dendrite'. Investigation of the proteins which mapped to these Cellular Components indicated many with a role in cytoskeleton rearrangement such as: Synaptopodin, Drebrin-like protein, Dystonin and Brain-specific angiogenesis inhibitor 1-associated protein 2 (Baiap2). From a strictly functional perspective, these proteins are consistent with cytoskeletal rearrangement and therefore with the enriched Molecular Function GO term 'actin-binding' observed at Time 10. However, the "neuronal" nature of these proteins might appear puzzling. A caveat of

using GO for functional enrichment analysis is that a protein may be 'mapped' to a neuro-related group because there is more information in the literature about the protein's role in neurons but very little information in other cellular systems, such as myoblasts, even if that protein may be expressed in myoblasts as well. For example Dystonin is upregulated during myogenesis and crosslinks actin and desmin filaments; Dystonin-deficient myoblasts form incompletely assembled myofibrils (Dalpe *et al.*, 1999).

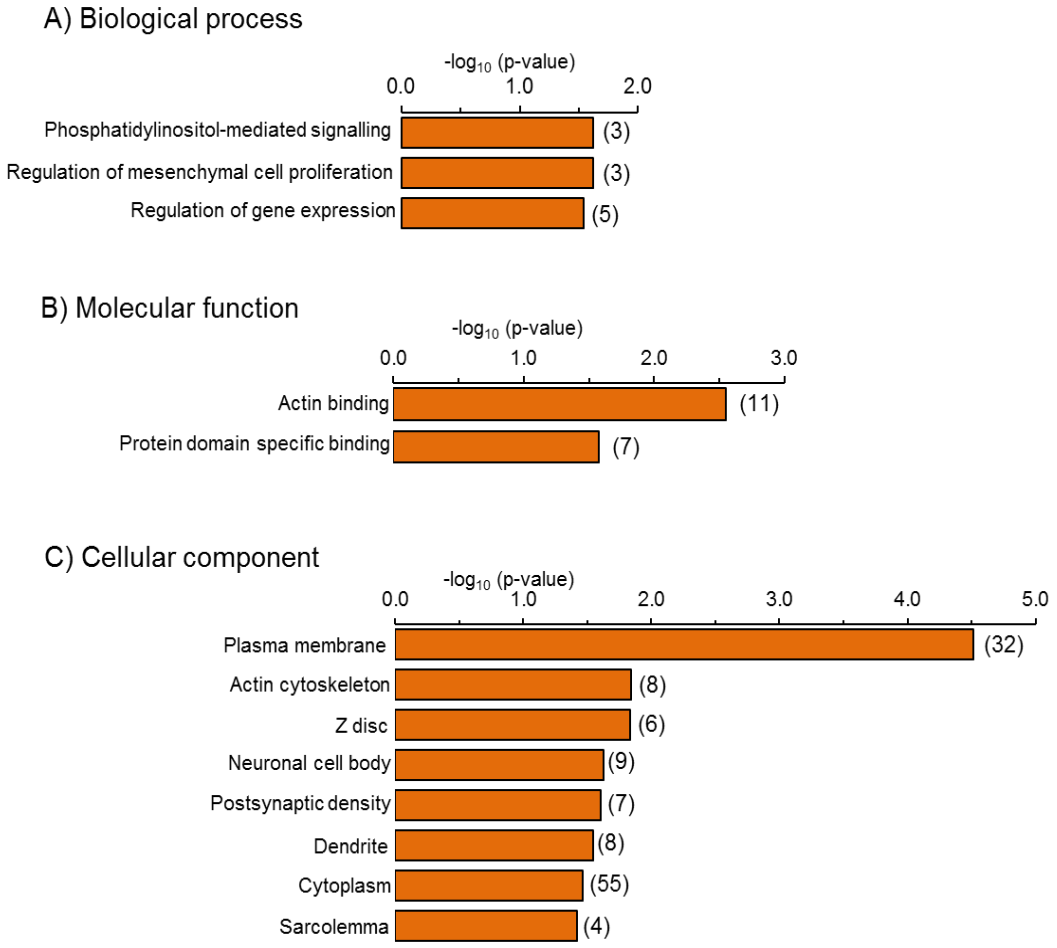

Figure 5.7: Enriched gene ontology categories identified at Time 10. Phosphopeptides that were significantly regulated between Vector and S3KD at Time 10 were mapped to phosphoproteins and then functional enrichment analysis was performed using DAVID. P-values less than 0.05 were considered significant. Numbers in brackets indicate the number of proteins mapped to each indicated GO term.

5.2.3.3 Pathway enrichment analysis of phosphopeptides differentially abundant between S3KD and Vector myoblasts at Time 0 and Time 10

The main goal of the phosphoproteomics experiment was to identify changes in cell signalling pathways in S3KD myoblasts. Ingenuity Pathway Analysis (IPA) is a comprehensive, manually curated knowledge database designed to extract biological meaning from large datasets. A recent IPA update allowed analysis of phosphoproteomic

data. This new IPA feature focuses on phosphosite-phosphoprotein regulation rather than gene regulation. Differentially regulated phosphoproteins, with their corresponding phosphosites and semi-quantitative values, were subjected to canonical pathway enrichment analysis using IPA (Fig. 5.8). Enrichment scores and adjusted p-values were obtained using an inbuilt Fisher's exact test. As I was particularly interested in pTyr mediated signalling, canonical pathways were restricted to Receptor Tyrosine Kinase (RTK) pathways or closely related pathways (see *Methods* section 2.13.8 for a list of pathways included in the IPA analysis)**.** At Time 0, mTOR signalling, ERK signalling, Insulin receptor signalling and Ephrin receptor signalling were significantly enriched (Fig. 5.8A) with phosphopeptides that were differentially regulated between S3KD and Vector myoblasts. This result was consistent with what previously found using DAVID/GO (Figs. 5.6 and 5.7).

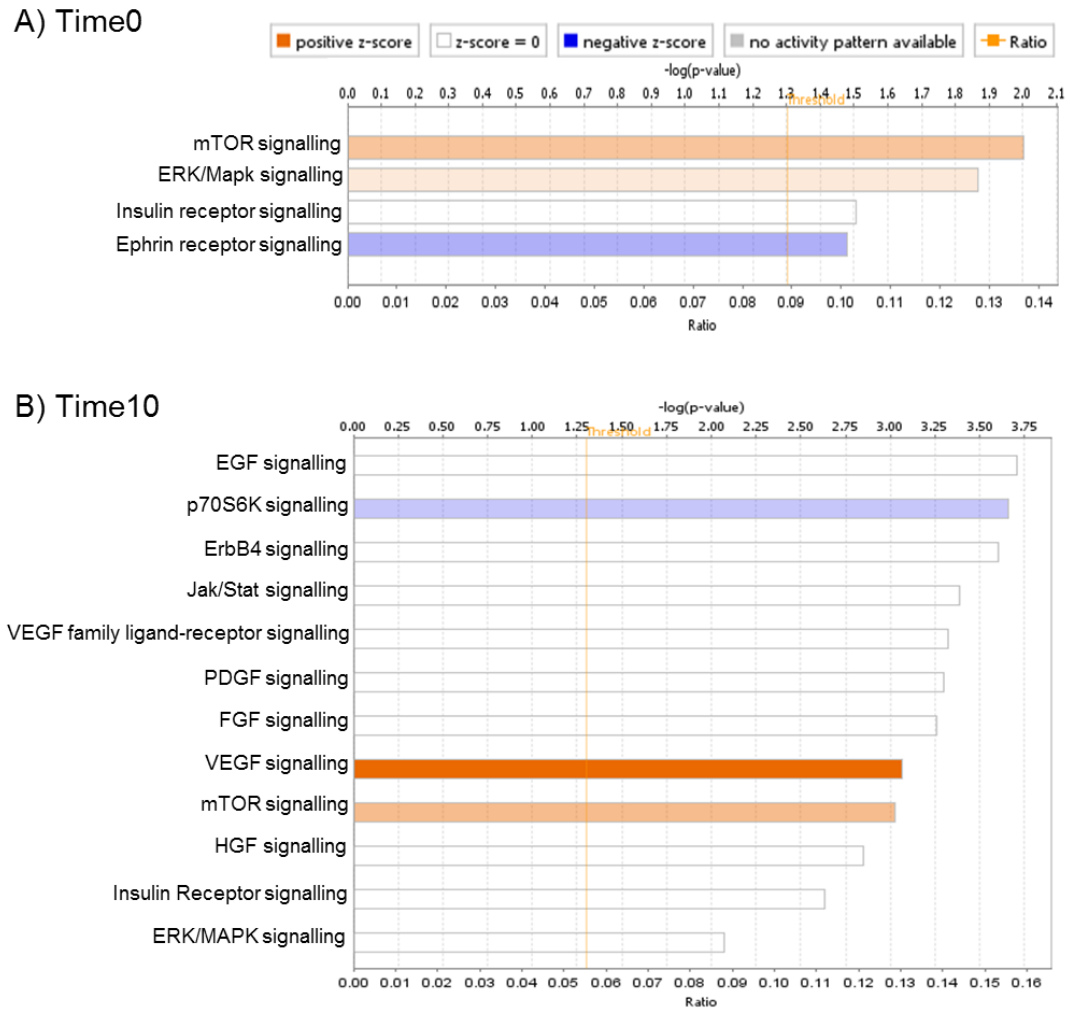

Figure 5.8: Pathway enrichment analysis of phosphoproteins and phosphosites found differentially abundant between S3KD and Vector myoblasts at Time 0 and Time 10. Differentially abundant phosphopeptides at Time 0 **(A)** and Time 10 **(B)** were analysed using Ingenuity Pathway Analysis to enrich for Receptor Tyrosine Kinase pathways. Z-score indicates whether a pathway is activated (positive score, orange) or deactivated (negative score, blue). Pathways with a p-value of less than 0.05 were considererd significant.

At Time 0, the Z-score, a means of predicting the activation or deactivation of a signalling pathway, was increased in mTOR and ERK signalling, neutral for Insulin receptor signalling, and decreased for Ephrin signalling. These data supported the results obtained from the DAVID analysis suggesting that mTOR and insulin signalling activity were increased in serum-starved S3KD myoblasts compared to serum-starved Vector myoblasts. At Time 10, several significantly enriched RTK pathways were identified including EGF, FGF, HGF and Insulin receptor signalling (Fig. 5.8B). This is consistent with our hypothesis that SDC3 regulates several RTK signalling pathways simultaneously. However, only three signalling pathways had a positive or negative Z-score, these were 'p70S6K signalling', 'VEGF signalling' and 'mTOR signalling'. The lack of a Z-score for the other enriched pathways was possibly because too few proteins were submitted for analysis at Time 10 to confidently assign a Z-score. Alternatively, it is possible that the phosphorylation associated with those proteins was not well characterised. Upon closer inspection of these enriched pathways in the Time 0 and Time 10 datasets, many of the same proteins were associated with these pathways including ERK1, IRS1, IRS2 and PKCα, suggesting that SDC3 knockdown commonly affects these downstream signalling effectors, likely because of pathway cross-talk (Appendix 3.2).

The IPA function "Upstream analysis" predicts upstream regulators of proteins that are differentially abundant across datasets. With phosphoproteomics data, IPA recognises and records the predicted "activation or deactivation" of a phosphoprotein depending on whether the phosphorylation of that protein has increased or decreased when compared across conditions. This is a useful feature for phosphoproteomics analysis as often an increase in phosphorylation does not necessarily lead to activation of a protein, similarly a decrease in phosphorylation may not lead to deactivation of a protein. Molecules identified as upstream regulators in our datasets comparing Vector and S3KD myoblasts at Time 0 and Time 10 with an adjusted p-value < 0.05 and their protein targets were displayed as networks in Figure 5.9 for Time 0 and Figure 5.10 for Time 10. SDC3 is a membrane protein and as such I was interested in possible regulators that were either on the membrane or in close proximity; these proteins are more likely to be regulated by SDC3. Potential upstream regulators at Time 0 include:

1) PTP-RM (protein tyrosine phosphatase, receptor type, M) and MC4R (melanocortin 4 receptor) are plasma membrane receptors that are predicted to regulate catenin-delta-1 and IRS1 phosphorylation respectively. Interestingly, SDC3 was previously reported to act as a co-receptor for MC4R in the context mouse feeding behaviour regulation (Reizes *et al.*, 2003).

2) TGFβ1 is another plasma membrane receptor which is predicted to regulate regulates RB1 (RB transcriptional corepressor 1, also known as pRB).

3) Interferon-α is predicted to regulate phosphorylation of 4E-BP1, and MAPK1.

4) Proinsulin, Raptor, mTOR, Rheb, NR4A1, Sirt3 and Sik2 are predicted to regulate IRS1. Although no activation/deactivation score was assigned to IRS1 by IPA (Fig. 5.9). Five different IRS1 phosphopeptides were differentially abundant in S3KD and Vector myoblasts at Time 0. For two of these five IRS1 phosphosites ($IRS1^{S3}$ and $IRS1^{T525}$) no functional information is available. Whereas for $IRS1^{S302}$, $IRS1^{S307}$ and $IRS1^{S522}$ phosphosites the literature suggests that these sites become phosphorylated as part of an S6K/mTOR or PI3K/AKT mediated negative feedback mechanism (Shah and Hunter, 2006, Giraud *et al.*, 2007).

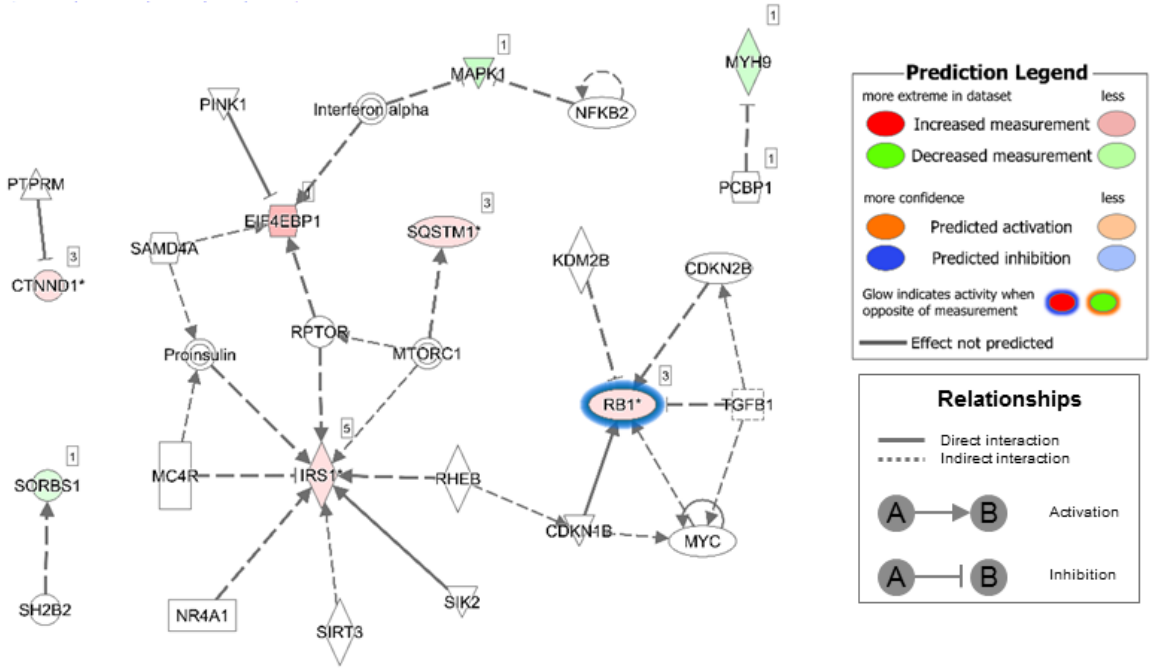

Figure 5.9: Upstream regulator analysis of differentially expressed phosphopeptides at Time 0. Phosphopeptides found differentially abundant between S3KD and Vector myoblasts at Time 0 were analysed using the IPA function "Upstream Regulator Analysis". Proteins with a boxed number were differentially abundant between Vector and S3KD; the number in the box represents the number of phosphosites differentially regulated. Increased/decreased phosphorylation measurement (red/green) and predicted activation/inhibition (orange glow/ blue glow) are reported.

Also at Time 10, the most highly connected protein in the upstream regulators network was IRS1, which was functionally connected to 19 proteins (Fig. 5.10). However, whether this network activated or inactivated IRS1 could not be determined by IPA. Moreover, scrutiny of the IRS1 phosphosite that was differentially abundant between Vector and S3KD myoblasts (S1096 equivalent to S1100 in humans) yielded no functional information.

Predicted membrane proteins, or proteins in close proximity to the membrane, that regulated IRS1 included: JNK (c-Jun N-terminal kinase), PTPRF (PTP type F), NR4A1 (nuclear receptor subfamily 4, group A, member 1), proinsulin, PTPN1 (PTP non-receptor type 1), PTPRE (PTP receptor type E), suggesting that this whole network might be functionally linked to SDC3 and work as an upstream regulator of the phosphoproteins identified as differentially abundant in our Time 10 dataset. Similar to observations at Time 0, several components of the mTOR signalling pathway were predicted to regulate IRS1 at Time 10. Both the Time 0 and the Time 10 networks indicated that IRS1 was a common target for many predicted upstream regulators and may explain why IRS1 was associated with other RTK pathways (Appendix 3.2) and not just insulin receptor signalling.

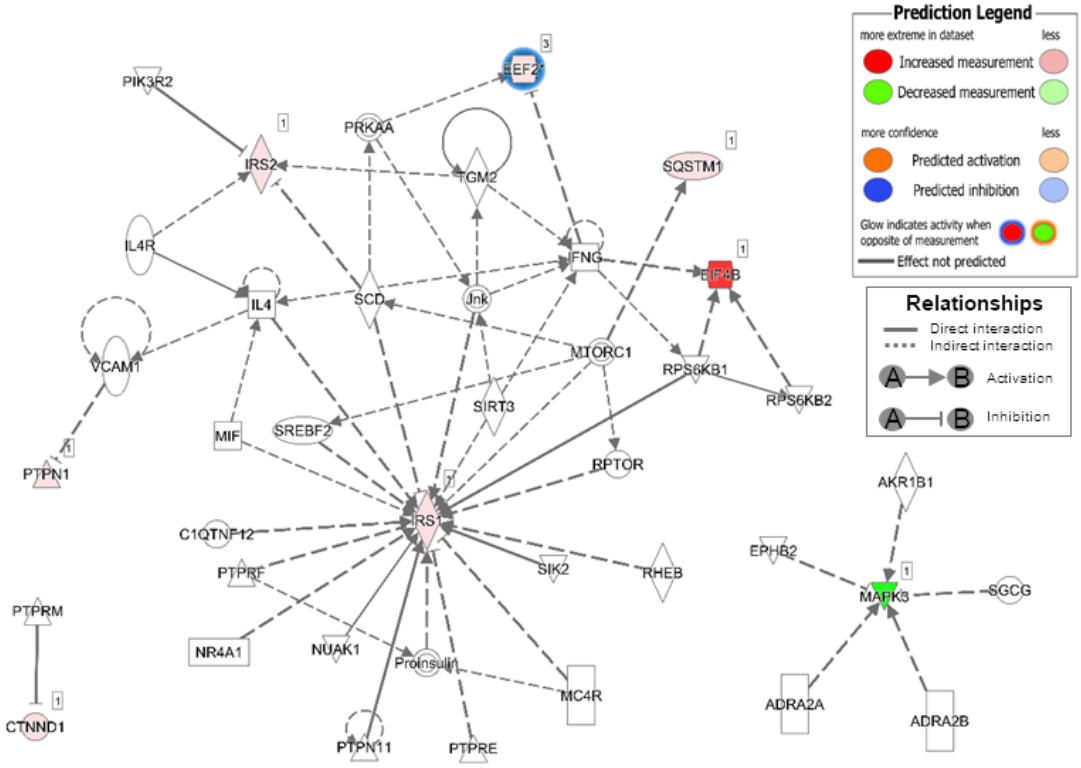

Figure 5.10: Upstream regulator analysis of differentially expressed phosphopeptides at Time 10. Phosphopeptides found differentially abundant between S3KD and Vector myoblasts at Time 10 were analysed using the IPA function "Upstream Regulator Analysis". Proteins with a boxed number were differentially abundant between Vector and S3KD; the number in the box represents the number of phosphosites differentially regulated. Increased/decreased phosphorylation measurement (red/green) and predicted activation/inhibition (orange glow/ blue glow) are reported.

5.2.4 Phosphopeptide changes mediated by serum-stimulation in Vector and S3KD myoblasts

After analysing phosphopeptide changes between Vector and S3KD myoblasts at the two distinct time points (Time 0 and Time 10), analysis of the serum-mediated changes in both cell lines was conducted. Firstly, the responses of Vector and S3KD myoblasts to serum stimulation were analysed separately to determine which phosphopeptides had undergone changes in their phosphorylation levels after stimulation with serum. The fold change versus q-value of phosphopeptides identified in Vector and S3KD myoblasts were plotted in Figure 5.11. In response to serum there is a small skew towards the number of phosphopeptides with increased phosphorylation compared to decreased phosphorylation in both Vector and S3KD myoblasts; this skew was slightly more pronounced in S3KD myoblasts. The large number of significantly regulated phosphopeptides (1,614 in Vector cells and 1,416 in S3KD cells) meant that many different Biological Processes, Molecular Functions and motifs were enriched in these data sets which was not particularly useful, as many of these enriched functions were the same in both cell lines. Therefore, I decided to focus on pathway enrichment analysis and differences in the activation levels of these pathways using IPA.

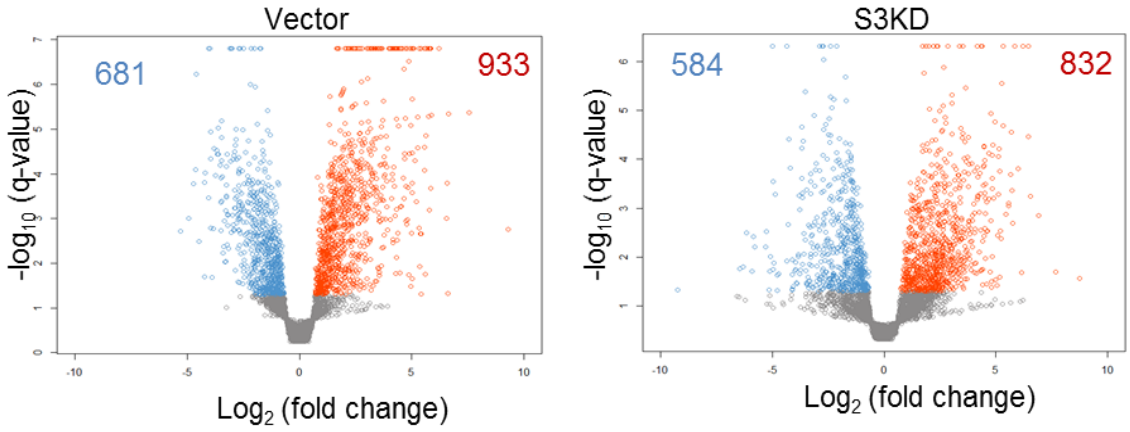

Figure 5.11: Volcano plots of phphopeptides identified in Vector and S3KD myoblasts after serum stimulation. Grey dots show phosphopeptides with no signifcant change in abundance after serum stimulation. Red dots indicate phosphopeptides at Time 10 with increased phosphorylation compared to Time 0. Blue dots indicate phosphopeptides at Time 10 with decreased phosphorylation compared to Time 0. Phosphopeptides with a q-value < 0.05 were considered statistically significant.

5.2.4.1 Comparison of pathway enrichment

The same RTK pathways were significantly enriched (p-value < 0.01) and were activated in the same direction in both Vector and S3KD myoblasts between Time 0 and Time 10, although to different extents (Fig. 5.12). Insulin receptor signalling was the most significantly enriched RTK pathway in both cell lines (Fig. 5.12A). This was particularly interesting as previous observations show that IRS1 phosphorylation levels are different in S3KD cells

compared to Vector cells, with some different phosphosites at Time 0 and Time 10, suggesting Insulin/IRS1 signalling is altered in S3KD myoblasts. However, the Z-scores of enriched S3KD signalling pathways were more often lower than the Z-scores of the Vector signalling pathways, suggesting lesser activation of RTK pathways in S3KD myoblasts upon serum stimulation (Fig. 5.12B).

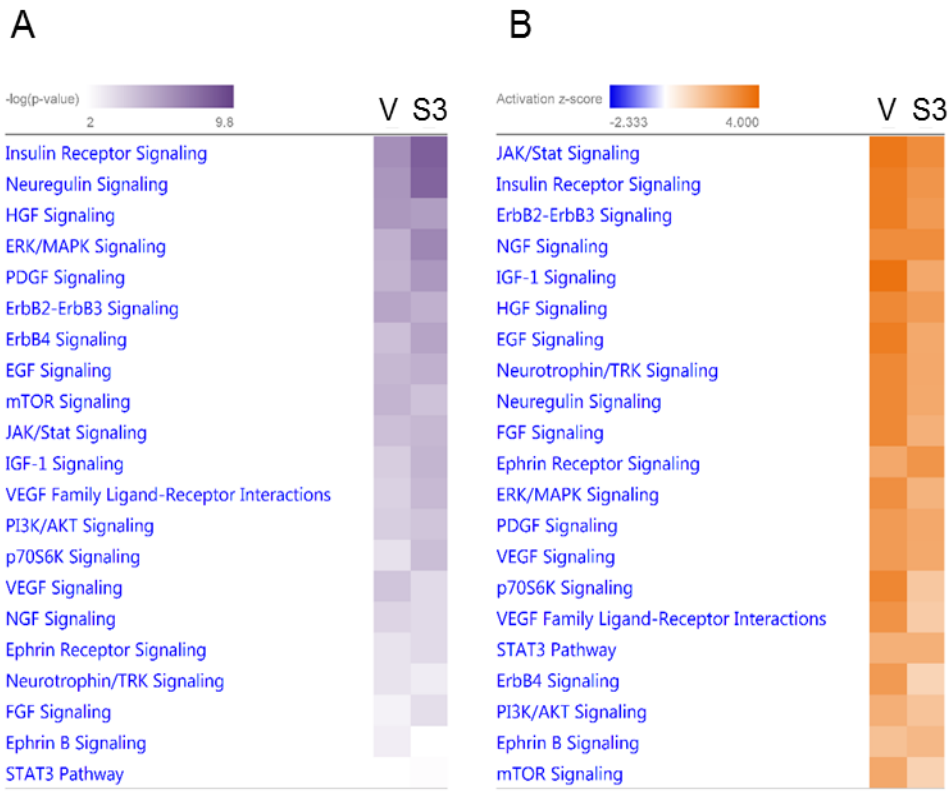

Figure 5.12: Comparison of significantly enriched receptor tyrosine kianse pathways. (A) RTK signalling pathways sorted by enrichment score. **(B)** RTK signalling pathways sorted by Z-score. Positive z-scores indicate activated pathways, negative z-scores indicate deactivated pathways. V = Vector, S3 = SDC3 knock-down.

Upon closer inspection there were evident differences in the phosphopeptide abundance of proteins that mapped to the insulin receptor signalling pathway (Fig. 5.13 and Fig. 5.14). The most obvious differences were clustered around the insulin receptor including the proteins: IRS1, IRS2, Nck, Ptp1b, and PI3K and further downstream of the AKT pathway including proteins: 4E-BP1, PP1 (serine/threonine protein phosphatase) and PKA.

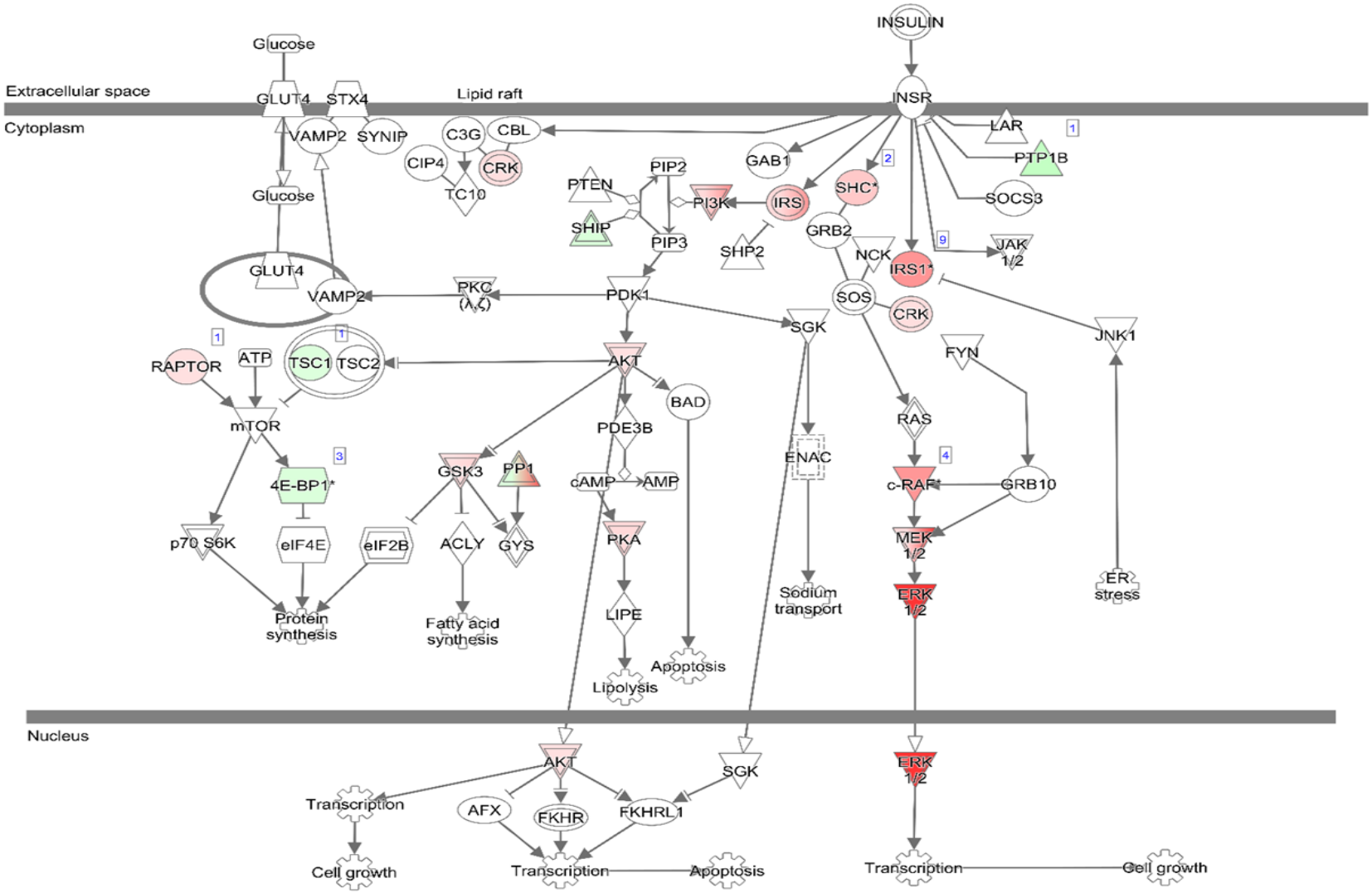

Figure 5.13: Changes to insulin receptor signalling in Vector myoblasts after serum stimulation. Proteins with significant phosphopeptide changes between Time 0 and Time 10 were mapped to the insulin signalling pathway using IPA. Red coloured proteins show increased phosphorylation. Green coloured proteins show decreased phosphorylation. Non-coloured proteins were not identified in this phosphoproteomic study. Blue numbers in boxes represent the number of phosphopeptides identifed per protein.

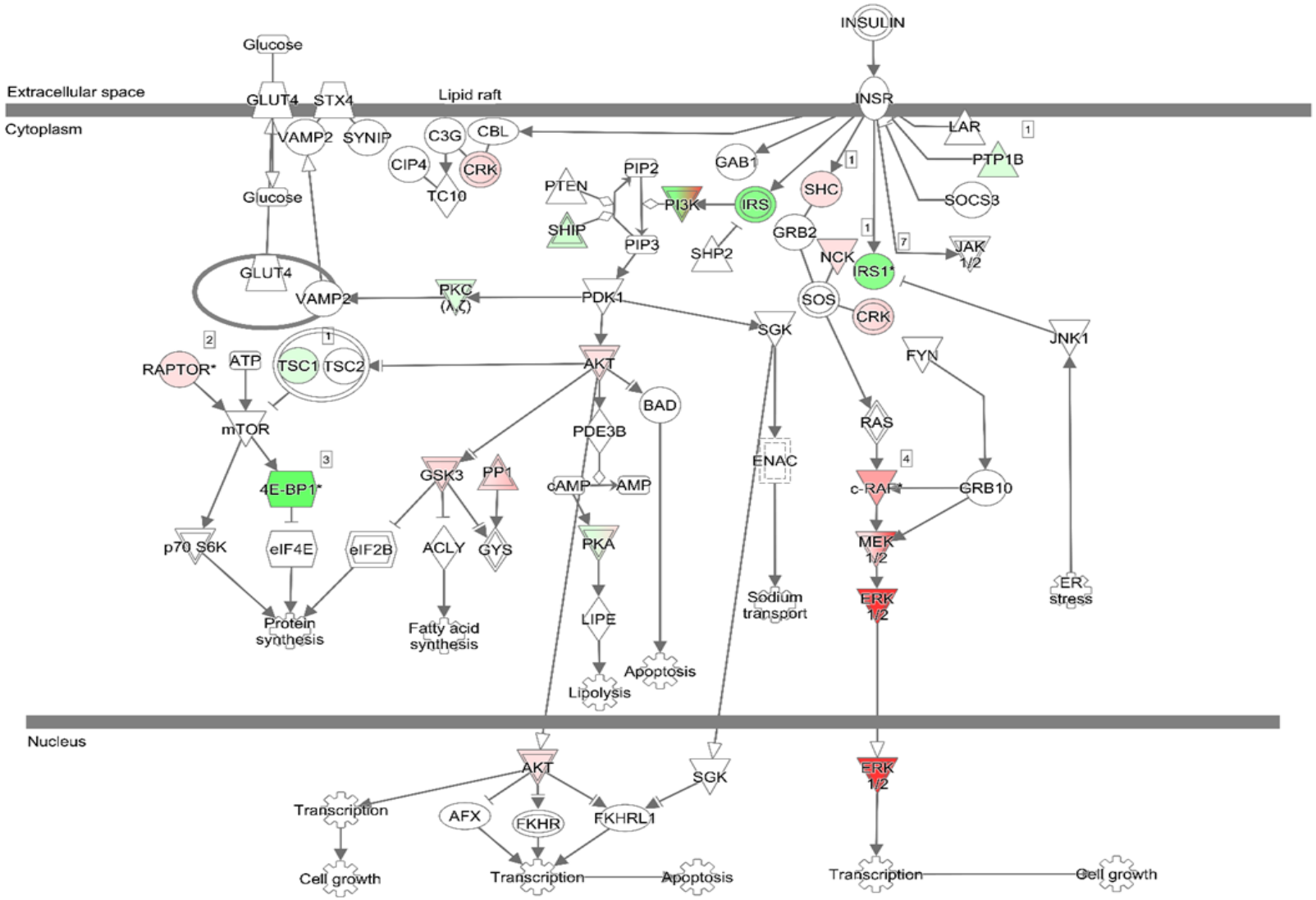

Figure 5.14: Changes to insulin receptor signalling in S3KD myoblasts after serum stimulation. Proteins with significant phosphopeptide changes were mapped to the insulin signalling pathway using IPA. Red coloured proteins show increased phosphorylation. Green coloured proteins show decreased phosphorylation. Non-coloured proteins were not identified in this phosphoproteomic study. Blue numbers in boxes represent the number of phosphopeptides identifed per protein.

IPA automatically selects one phosphosite to colour code the proteins mapped to the signalling pathway based on which phosphosite has the largest fold change; this is not useful when multiple phosphosites are identified per protein and each phosphosites might change in different directions and/or might be activating or inhibitory. Table 5.3 includes all the phosphosites/proteins mapped to the insulin receptor signalling pathway. Some phosphoproteins were uniquely identified in S3KD myoblasts such as PRKCI (protein kinase C-iota) T411, which was desphosphorylated in response to serum indicating inactivation of PKCI upon serum stimulation. Additionally, PRKACA (protein kinase A catalytic subunit) T198 was also dephosphorylated indicating deactivation of PKA. These data further suggested that SDC3 knock-down led to a reduction in the activation of insulin signalling in response to serum (Fig. 5.12), although at Time 0 the insulin signalling pathway seemed to be more active in S3KD cells than in Vector cells (*Chapter 5,* section: *5.2.3.2*). There were also differences in the abundance of phosphosites common to Vector and S3KD myoblasts, for example phosphorylation of IRS1$^{S302\text{-}S307}$ increased by 12.94 times in Vector cells in response to serum but only 4.1 times in S3KD myoblasts, again suggesting that SDC3 knock-down reduced myoblast responsiveness to serum stimulation via the insulin signalling pathway. However, at Time 0 IRS1$^{S302\text{-}S307}$ was significantly increased in S3KD compared to Vector myoblasts. A possible explanation for why there is a smaller fold change in IRS1$^{S302\text{-}S307}$ phosphorylation upon serum stimulation in S3KD myoblasts is that the phosphorylation levels of those phosphosites were already significantly higher in S3KD myoblasts at Time 0. Therefore serum-stimulation of S3KD myoblasts does not increase phosphorylation of IRS1$^{S302\text{-}S307}$ as much as it does in Vector myoblasts because S3KD myoblasts might have already been close to maximal phosphorylation when serum-starved. Although this is not the case for every phosphopeptide identified, a general trend was observed that an increase in phosphorylation levels in S3KD myoblasts compared to Vector myoblasts at Time 0 was associated with a smaller fold change in phosphorylation upon serum stimulation in S3KD myoblasts.

Table 5.3: Proteins and corresponding phosphopeptides that mapped to the insulin signalling pathway and were regulated by serum stimulation in Vector and S3KD myoblasts. Red represents increasing phoshphopeptide abundance, blue represents decreasing phoshopeptide abundance. FC = fold change.

Vector			S3KD		
Protein	**Phosphosite(s)**	**FC**	**Protein**	**Phosphosite(s)**	**FC**
AKT2	T451	2.41	AKT2	T451	2.18
CRK	-	-	CRK	S194	5.47
CRKL	Y207	3.82	CRKL	Y207	2.89
EIF4EBP1	T45 S82-S95-S100 T69 - -	-4.01 3.25 -2.27 - -	EIF4EBP1	- S82-S95-S100 - S64-S69-S100 S64-S69	- 3.67 - -16.95 6.23
GSK3B	S9 -	4.18	GSK3B	S9 S21	4.95 4.44
IRS1	S265 S302-S307 S522-T525 S343 S1096 S325 S325-S343 S887	2.75 12.94 4.10 -8.25 -3.35 8.17 3.16 1.90	IRS1	S265 S302-S307 - S343 S1096 S325 S323-S343 -	2.33 4.10 - -12.81 -1.99 5.87 11.13 -
IRS2	S556 S675 S590	3.97 4.48 3.03	IRS2	- - -	- - -
MAP2K1	S385	4.26	MAP2K1	S385	3.74
MAP2K2	S226 S222-S226	47.94 12.55	MAP2K2	S226 S222-S226	16.44 40.04
MAPK1	T183-Y185	42.52	MAPK1	T183-Y185	92.76
MAPK3	T202-Y204 -	186.79 -	MAPK3	- Y204	- 10.59
NCK1	-	-	NCK1	S85	3.25
PIK3C2A	S261	14.15	PIK3C2A	S261	21.98
PPP1CA	T320	-1.97	PPP1CA	-	-
PPP1R10	S313	1.90	PPP1R10	S313	2.61
PPP1R12A	S507 S422	19.89 -2.56	PPP1R12A	S507 S422	9.49 -2.86
PRKACA	-	-	PRKACA	T198	-3.35
PRKAR1A	S77-S83	4.57	PRKAR1A	S77-S83	4.01
PRKCI	-	-	PRKCI	T411	-3.29
PTPN1	S335	-6.55	PTPN1	S335	-4.10
RAF1	S29 S301 S43 S642	12.68 3.90 3.60 3.97	RAF1	S29 S301 S43 S642	11.47 9.21 5.58 6.49
RPTOR	S863 -	3.00 -	RPTOR	S863 S859-S863	2.75 -2.66
SHC1	S139 Y423	4.22 6.62	SHC1	S139 -	3.00 -
TSC1	S502	-3.06	TSC1	S502	-3.74

5.2.5 Analysis of phosphopeptides regulated by both serum stimulation and SDC3-knockdown.

The previous section showed that both Vector and S3KD myoblasts responded robustly to serum stimulation as measured by the number of differentially abundant phosphopeptides between Time 0 and Time 10. Comparison of the signalling pathways regulated by serum stimulation in both cell lines showed that the same signalling pathways were enriched in both cell lines in response to serum stimulation. However, the extent and, in some cases, the direction of the change in phosphorylation levels of phosphoproteins in these pathways were different between Vector and S3KD myoblasts. To better understand how differently Vector and S3KD myoblasts responded to serum stimulation, I compared Vector myoblast response to serum-stimulation to S3KD myoblast response to serum-stimulation (comparison No. 5, Fig. 5.1) and identified phosphopeptides that had a fold change of at least ± 1.5 fold between Vector and S3KD myoblasts. From this analysis 59 phosphopeptides were considered significantly regulated by both serum stimulation and loss of SDC3. Of these phosphopeptides 71% had a smaller fold change in S3KD serum-stimulated myoblasts compared to Vector-stimulated myoblasts (Fig. 5.15).

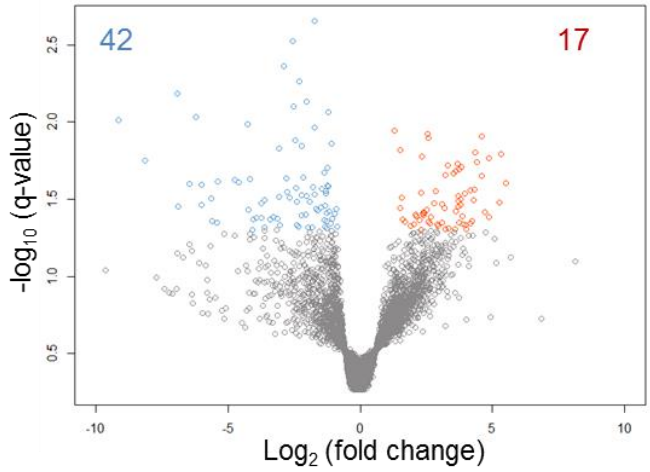

Figure 5.15: Volcano plot of phosphopeptides significantly regulated by both serum stimulation and S3KD. Statistical analysis of changes in phosphorylation as a response to serum and SDC3 loss resulted in identification of 59 statistically significant phosphopeptides whose phosphoryltion abundances change in different ways or to different extents in Vector and S3KD myoblasts in response to serum. Blue dots indicate S3KD phosphopeptides that decrease in phosphorylation in response to serum compared to Vector myoblasts in response to serum or S3KD phosphopeptides that increase less in response to serum compared with Vector myoblasts stimulated with serum. Red dots indicate S3KD phosphopeptides that increase in phosphorylation in response to serum compared to Vector myoblasts in response to serum or S3KD phosphopeptides that increase more in response to serum compared with Vector myoblasts stimulated with serum. Phosphopetide abundance changes with a q-value < 0.05 were considered statistically significant.

This supported the observations made previously that an increase in phosphopeptides at Time 0 in S3KD myoblasts was associated with little to no difference at Time 10 between S3KD and Vector myoblasts, resulting from a smaller degree of change in S3KD myoblasts in response to serum (Table 5.4). The most significantly regulated phosphopeptide mapped to RPS6 which is a downstream target of mTOR and regulates processes such as cell size, proliferation and glucose homeostasis (Ruvinsky *et al.*, 2005, Biever *et al.*, 2015). Additionally, RPS6 phosphorylation is often used as a measurement of mTORC1 activity (Ma and Blenis, 2009) instead of measuring mTOR phosphorylation itself, since mTOR phosphorylation is highly dynamic and mTOR phosphorylations are not fully understood (Figueiredo *et al.*, 2017). IRS1, which I previously identified as a key phosphoprotein regulated by SDC3 at both Time 0 and Time 10 (section 5.2.3.2 and 5.2.3.3), was also one of the most significantly regulated phosphoproteins when changes in response to both serum stimulation and SDC3 loss were analysed. Phosphorylation of IRS1$^{S522\text{-}T525}$, which has been associated with inhibition of insulin signalling via negative feedback (Giraud *et al.*, 2007), increased less in S3KD myoblasts than in Vector myoblasts in response to serum (Table 5.4). This was particularly interesting as changes in IRS1 and mTOR signalling had been observed in every section of this phosphoproteomics analysis. Scrutiny of the other proteins identified when the effect of both SDC3 loss and serum stimulation were examined, revealed that other changes mapped to either insulin receptor signalling or glycogenesis such as Dok1 (docking protein 1), Sik3 (SIK family kinase 3), 4E-BP1, PKCα and Mek2. Several cell adhesion and cell migration proteins were also identified including cortactin, Larp1, Catenin-delta-1, Tjp1 (tight junction protein 1), Lrrfip1, Girdin and Ahnak.

Table 5.4: List of phosphopeptides significantly regulated by SDC3 knock-down and serum stimulation. FDR = false discovery rate. Ascore represents the probability of correct phosphosite localisation, bigger than 13 represents $p < 0.05$. Phosphopeptides ordered by q-value.

Uniprot Accession	Gene name	Protein name	Phosphosite	Fold Change	FDR	Ascore p1	Ascore p2	Ascore p3
P62754	RPS6	40S ribosomal protein S6	S236-S240-S244	**-3.35**	0.002	0	0	9.42
P97465	Dok1	Docking protein 1	S290	**-5.87**	0.003	76.17		
P62754	RPS6	40S ribosomal protein S6	S236-S240	**-7.39**	0.004	17.01	12.28	
Q543V3	IRS1	Insulin receptor substrate 1	S522-T525	**-4.95**	0.005	5.55	0	
Q6P4S6	Sik3	Serine/threonine-protein kinase SIK3	T411	**-4.06**	0.007	1000		
E0CXA0	Hdgf	Hepatoma-derived growth factor	S100-S101	**-5.75**	0.007	0	0	
P43276	Hist1h1b	Histone H1.5	S18	**-2.32**	0.008	77.76		
E9Q784	Zc3h13	Zinc finger CCCH domain-containing protein 13	S110	**-3.32**	0.009	0		
E9Q616	Ahnak	Protein Ahnak	S5522-S5525-S5536	**2.46**	0.010	4.08	2.37	9.34
Q9R020	Zranb2	Zinc finger Ran-binding domain-containing protein 2	S120	**5.81**	0.011	0		
E9QAS4	Chd4	Chromodomain-helicase-DNA-binding protein 4	S408	**6.05**	0.012	1000		
Q60749	Khdrbs1	KH domain-containing, RNA-binding, signal transduction-associated protein 1	S20	**-2.14**	0.013	8.22		
A6PWC3	Nrd1	Nardilysin	S85	**-4.71**	0.014	1000		
P30999	Ctnnd1	Catenin delta-1	S920	**2.83**	0.014	1000		
Q6PHZ2	Camk2d	Calcium/calmodulin-dependent protein kinase type II subunit delta	S330	**5.05**	0.015	0		
P70445	Eif4ebp2	Eukaryotic translation initiation factor 4E-binding protein 2	T70	**-2.39**	0.016	29.96		
G3UX48	Prrc2a	Protein PRRC2A	S706	**-2.59**	0.018	6.59		
Q6A026	Pds5a	Sister chromatid cohesion protein PDS5 homolog A	S1174	**-2.39**	0.019	5.08		

Q80XU3	Nucks1	Nuclear ubiquitous casein and cyclin-dependent kinase substrate 1	S214	**-2.32**	0.020	44.69		
Q5SNZ0	Ccdc88a	Girdin	T1419	**-3.49**	0.021	0		
Q80TM9	Nisch	Nischarin	S543	**-5.37**	0.022	5.47		
P25206	Mcm3	DNA replication licensing factor MCM3	S672	**-2.75**	0.023	25.11		
Q5SW19	Cluh	Clustered mitochondria protein homolog	S1300	**4.95**	0.024	38.16		
P20152	Vim	Vimentin	S39	**-2.46**	0.025	7.32		
P15532	Nme1	Nucleoside diphosphate kinase A	S120	**-3.29**	0.026	10.42		
Q3UZ39	Lrrfip1	Leucine-rich repeat flightless-interacting protein 1	S649	**-4.71**	0.026	37.5		
Q80VI1	Trim56	E3 ubiquitin-protein ligase TRIM56	S6	**-3.78**	0.027	0		
Q6NXJ0	Wwc2	Protein WWC2	T999	**-5.26**	0.028	11.1		
Q9D8C8	Ppp1r35	Protein phosphatase 1 regulatory subunit 35	S85	**-2.53**	0.029	1000		
P05132	Prkaca	cAMP-dependent protein kinase catalytic subunit alpha	T198	**-2.83**	0.030	0		
P47930	Fosl2	Fos-related antigen 2	S19	**2.86**	0.031	0		
Q7TSG2	Ctdp1	RNA polymerase II subunit A C-terminal domain phosphatase	S830	**-1.86**	0.032	33.18		
E9Q616	Ahnak	Protein Ahnak	T5567	**-3.19**	0.033	0		
Q5SW15	Mettl16	Methyltransferase-like protein	T499	**-3.10**	0.033	61.69		
D3Z069	Phldb2	Pleckstrin homology-like domain family B member 2	S248	**-2.25**	0.034	7.21		
Q5EBP8	Hnrnpa1	Heterogeneous nuclear ribonucleoprotein A1	S2-S4-S6	**-2.41**	0.035	1000	1000	0
P39447	Tjp1	Tight junction protein ZO-1	S912	**-1.95**	0.036	79.54		
Q8BYI8	Fam234b	Protein FAM234B	S30-S33	**5.10**	0.036	11.12	8.82	
Q80X82	Sympk	Symplekin	S494	**-4.18**	0.037	50.34		
Q60875	Arhgef2	Rho guanine nucleotide exchange factor 2	S931	**4.22**	0.038	1000		
P83917	Cbx1	Chromobox protein homolog 1	S89	**4.35**	0.038	14.04		

Q9JJ89	Ccdc86	Coiled-coil domain-containing protein 86	S18	**3.00**	0.039	72.22		
Q6P542	Abcf1	ATP-binding cassette sub-family F member 1	S138	**4.71**	0.040	1000		
E9Q616	Ahnak	Protein Ahnak	S4906	**-2.56**	0.040	8.14		
Z4YJT3	Larp1	La-related protein 1	T503	**-2.44**	0.041	48.12		
Q8BJU0	Sgta	Small glutamine-rich tetratricopeptide repeat-containing protein alpha	T305	**3.22**	0.042	11.1		
Q5SVQ0	Kat7	Histone acetyltransferase KAT7	T90	**-2.16**	0.042	16.66		
Q9CY58	Serbp1	Plasminogen activator inhibitor 1 RNA-binding protein	S197	**4.06**	0.043	14.04		
Q9Z0W3	Nup160	Nuclear pore complex protein Nup160	S1123	**3.78**	0.043	16.36		
P62754	RPS6	40S ribosomal protein S6	S235-S236-S240	**-2.51**	0.044	7.97	9.3	12.28
E9QN31	Nop2	Probable 28S rRNA	S59	**-1.84**	0.045	1000		
Q921L6	Cttn	Cortactin, isoform CRA_a	S33	**-3.90**	0.045	0		
Q9JIK5	Ddx21	Nucleolar RNA helicase 2	S192	**-3.56**	0.046	3.64		
Q6P5H2	Nes	Nestin	S963	**-2.41**	0.047	1000		
Q6P9Q4	Fhod1	FH1/FH2 domain-containing protein 1	S524-S527	**-2.16**	0.047	1000	1000	
Q91YS7	Map2k2	Dual-specificity mitogen-activated protein kinase 2	S226	**-2.92**	0.048	35.13		
H3BIY7	Mta3	Metastasis-associated protein MTA3	S176	**3.97**	0.048	17.01		
P83741	Wnk1	Serine/threonine-protein kinase WNK1	S2027	**-1.92**	0.049	17.32		
Q05D44	Eif5b	Eukaryotic translation initiation factor 5B	S114	**3.86**	0.050	30.1		

5.2.5.1 Functional enrichment and motif analysis

Next, I performed functional enrichment on the 59 phosphopeptides that were significantly regulated by serum and SDC3 loss in order to elucidate any common (enriched) function. Gene ontology analysis revealed that the only Biological Process significantly enriched in this data set was mTOR signalling ($p = 0.001$). The proteins mapped to this process were Girdin, RPS6, 4E-BP2 and Larp1; all these proteins had a significantly smaller change in phosphorylation upon serum stimulation in S3KD compared to Vector myoblasts. To further understand how loss of SDC3 affected the myoblast phosphoproteome in response to serum, significantly enriched phosphopeptides were submitted to Motif-x and identified motifs were matched to predicted kinases (Fig. 5.16). No motifs were enriched in phosphopeptides that increased more or only in S3KD cells compared to Vector cells in response to serum. In contrast, three motifs, [pS]P, Rxx[pS] and [pS]xxE, were significantly enriched in phosphopeptides that increased more or only in Vector cells compared to S3KD cells (Fig. 17). These were motifs recognised by protein kinases in the MAPK family (such as JNK, p38, ERK), AKT, CK2, PKA and CamKII. CamKII-delta S330 had a significantly larger change in phosphorylation in S3KD myoblasts compared to Vector myoblasts. However, whether S330 is an activating or inhibiting phosphorylation is unknown. AKT recognises a conserved motif of RxxRxx[pS/T] and although this motif was not specifically enriched in this data-set, many phosphopeptides containing this sequence were identified in this dataset (Fig. 5.16), indicating that changes in AKT activity may be influenced by SDC3 knock-down.

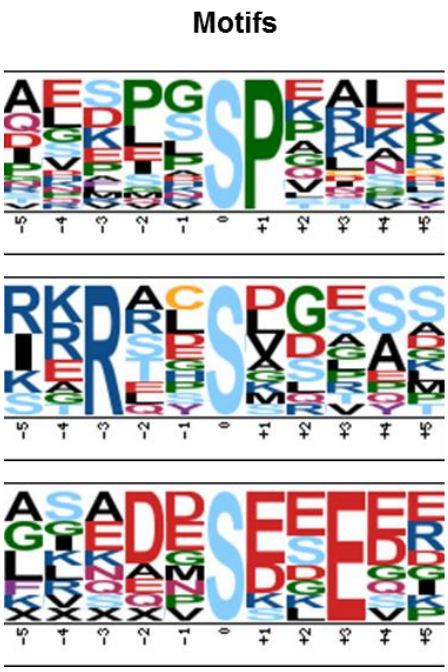

Figure 5.16: Over-represented phosphorylation motifs in phosphopeptides regulated by both serum stimulation and S3 knockdown. Phosphopeptides that either decreased or increased to a lesser extent upon serum stimulation in S3KD cells compared to Vector cells were submitted to Motif-x to identify over-represented motifs. Putative kinases responsible for the phosphorylation of the identified motifs are shown on the left.

5.2.6 Validation of phosphoproteomics data by western blotting

Altogether, the data in this chapter indicated a role for SDC3 in Insulin/IRS1/AKT/mTOR signalling. Therefore, I decided to validate the abundance of phosphorylation in proteins that mapped to the insulin signalling pathway and were differentially abundant between Vector and S3KD myoblasts in the phosphoproteomics data. For this purpose, Vector and S3KD myoblasts were serum-starved then immediately lysed (Time 0) or re-stimulated with serum for 10 minutes (Time 10) before lysis, as done previously for the phosphoproteomics experiment (*see Methods*). Lysates were analysed by western blotting to quantify the change in abundance of specific phosphosites compared to the abundance of the total protein. Unfortunately, only very few of the phosphosites identified in this study were recognised by commercially available antibodies leaving only four phosphosites that could be quantified by western blotting. These included RPS6$^{S235/S236}$, RPS6$^{S240/S244}$, IRS1^{S302} and IRS1^{S307} (Fig. 5.17). Western blot analysis confirmed increased phosphorylation of both RPS6 phosphosites in S3KD myoblasts compared to Vector myoblasts at Time 0 (Fig. 5.17B and C). At Time 10, RPS6$^{S235/S236}$ was still significantly increased in S3KD myoblasts compared to Vector Myoblasts (Fig. 5.17B), however the phosphorylation levels of both RPS6 phosphosites increased upon serum stimulation in both Vector and S3KD myoblasts, although to a slightly lesser extent in S3KD myoblasts compared to Vector myoblasts (Fig. 5.17B and C). Similarly, the increase in RPS6$^{S240/S244}$ in S3KD myoblasts due to serum stimulation was smaller than the increase observed in Vector myoblasts and the abundance of RPS6$^{S240/S244}$ was not significantly increased between Vector and S3KD myoblasts at Time 10 (Fig. 5.17C). which is consistent with the phosphoproteomics analysis.

Of all the IRS1 phosphosites identified in this study only two were recognised by commercially available antibodies at the time of validation: IRS1^{S302} and IRS1^{S307}. Both these phosphosites were identified on the same peptide with a low Ascore (Appendix 2.1 and 2.2), nonetheless both were tested for abundance. IRS1^{S307} was not detected by the antibody and could not be quantified. IRS1^{S302} was poorly detected, and, indicated that there were no changes in phosphorylation when normalised to total IRS1 (Fig. 5.17E). This was not expected as after serum stimulation in Vector and S3KD myoblasts a significant increase in IRS1 phosphorylation was observed by mass spectrometry (Table 5.3). When total IRS1 was quantified and normalised to GAPDH the results showed a significant increase in IRS1 between S3KD and Vector myoblasts at both Time 0 and Time 10 (Fig.5.17F). Moreover, IRS1 was also significantly increased upon serum stimulation in both Vector and S3KD myoblasts, though to a lesser extent in S3KD myoblasts, suggesting that regulation of cell signalling by IRS1 is largely mediated by rapid regulation of IRS1 protein levels, which in turn is regulated by phosphorylation (Copps and White, 2012).

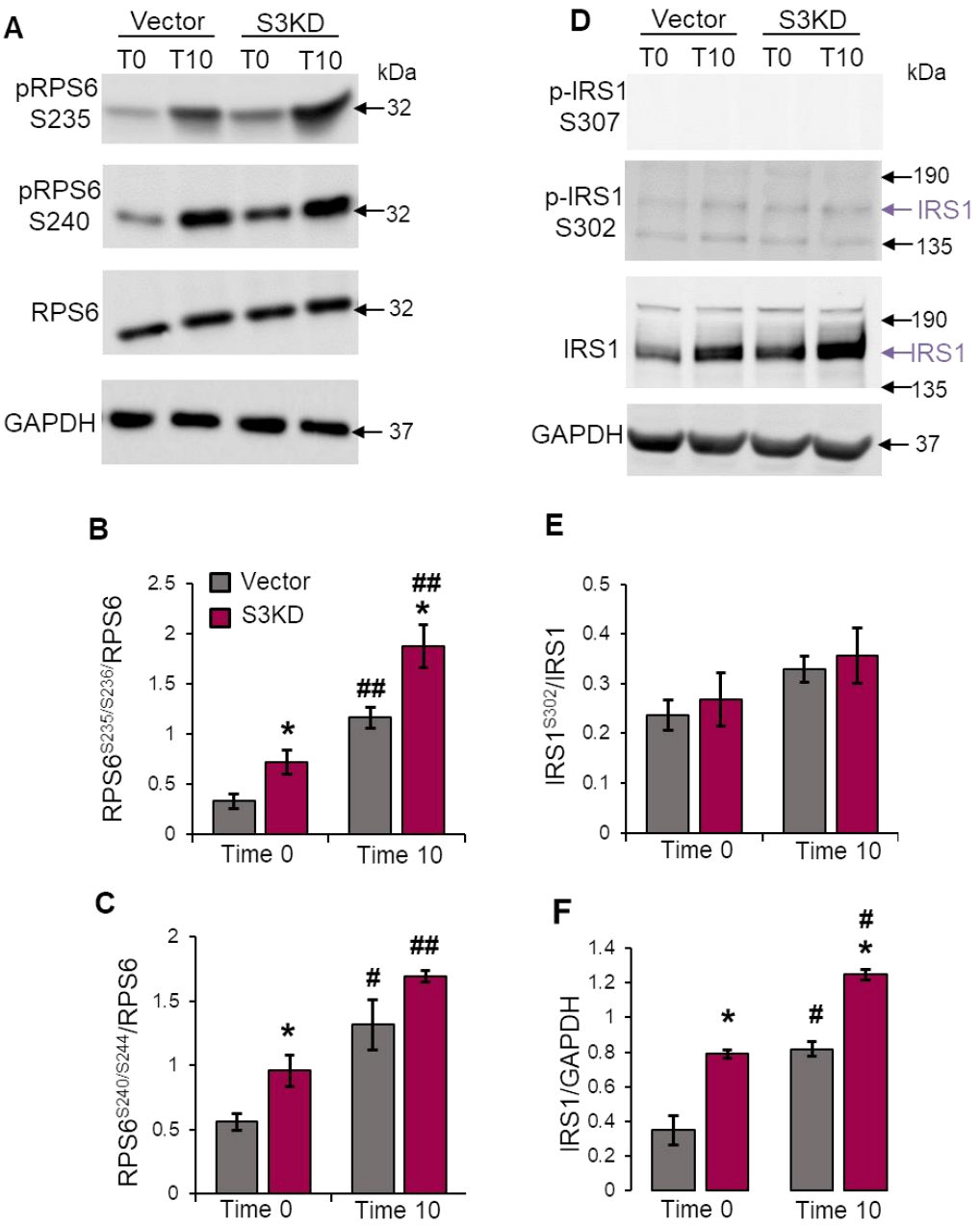

Figure 5.17: Validation of phosphoproteomics data using western blotting. Vector and S3KD myoblasts were serum-starved (Time 0, T0) then stimulated with 10% FBS for 10 minutes (Time 10, T10). Myoblasts were lysed then prepared for western blotting. **(A)** Representative western blots of total RPS6, phosphorylated-RPS6 at two phosphosites (S235 and S240) and GAPDH. **(B-C)** Quantification of phospho-RPS6$^{S235/S236}$ **(B)** and phospho-RPS6$^{S240/S244}$ **(C)** normalised to total RPS6. **(D)** Rpresentative western blots of IRS1 and phosphorylated-IRS1. **(E)** Quantification of phosphorylated IRS1^{S302} compared to total IRS1. **(F)** Quantification of total IRS1 normalised to GAPDH. * = $p < 0.05$ between Vector and S3KD cells at both time points; # = $p < 0.05$ between Vector at Time 0 and Vector at Time 10 or between S3KD at Time 0 and S3KD Time 10; ## = $p < 0.01$ between Vector at Time 0 and Vector at Time 10 or S3KD at Time 0 and S3KD at Time 10. n=3.

5.3 Discussion

In this chapter, a phosphoproteomics experiment was designed to identify key signalling pathways that are altered in serum-starved and serum-stimulated myoblasts when SDC3 was knocked-down. The initial stages of data processing were more challenging than expected due to the problems encountered with missing peptide abundances and quantification. However, these issues were resolved once we established a collaboration with Professor Andrew Jones (University of Liverpool, UK) to develop a Bayesian method to analyse the phosphoproteomic datasets that contained missing data and this provided us with a list of significantly regulated phosphopeptides. Overall it was clear that there were many changes in the phosphoproteome of Vector and S3KD myoblasts upon serum stimulation. This was expected because serum contains many different growth factors which were expected to activate several signalling pathways simultaneously leading to large changes in signal transduction networks. However, it was unexpected that the same signalling pathways were significantly enriched in both Vector and S3KD myoblasts, and that those pathways were all activated in the same direction. Direct comparison of the pathways activated by serum, in both cell lines, indicated subtle differences between Vector and S3KD myoblasts. As a general trend the activation scores of S3KD myoblasts in response to serum stimulation were generally lower than those observed in the Vector myoblasts. This suggested that when SDC3 is knocked-down, the response to serum is blunted in myoblasts, which contradicted previous results showing a global increase in tyrosine phosphorylation in S3KD myoblasts compared to Vector myoblasts (*Chapter 4*, Fig.4.4). Therefore, my hypothesis that loss of SDC3 activates several signalling pathways in myoblasts appeared to be wrong. However, a different interpretation presented itself when phosphopeptide differences between S3KD cells and Vector cells at Time 0 and at Time 10 were investigated. Under serum-starved conditions (Time 0) there was an increase in phosphorylated proteins such as IRS1 and RPS6 in S3KD myoblasts, but upon serum stimulation (Time 10) these significant increases were lost. Therefore, I speculated that the smaller degree of cell signalling activation in S3KD myoblasts in response to serum was due to these pathways being already more active in serum-starved S3KD myoblasts compared to Vector myoblasts and that SDC3 acts an inhibitor for several signalling pathways.

To initiate serum-starvation the cells are washed extensively with serum-free medium which removes the majority of growth factors found in the serum and therefore cell signalling should be less active. However, this is not the case when comparing S3KD and Vector myoblasts. There are several possibilities that could explain the increased signalling activity observed in S3KD myoblasts (Fig 5.18). The syndecans have been reported to regulate internalisation and trafficking of integrins and growth factor receptors which regulates cell signalling (Tkachenko *et al.*, 2004, Elfenbein *et al.*, 2012, Morgan *et al.*, 2013). Therefore,

a possible explanation for the increased signalling pathway activation in serum-starved S3KD myoblasts, is that SDC3 promotes receptor internalisation and recycling, which normally leads to pathway de-activation. However, in the absence of SDC3, such internalisation is decreased, and the receptors remain active on the membrane and still signal upon occasional ligand binding from the residual growth factors. A second possibility is that SDC3 decreases ligand-receptor binding affinity, as previously shown for other heparan sulphate proteoglycans (Choi *et al.*, 2011, Astudillo *et al.*, 2014, Lin *et al*., 2016). In the absence of SDC3, ligands have greater affinity for their receptors which become more active. Lastly, it is possible that SDC3 is involved in inhibiting intracellular signal transduction. Therefore, another possibility is that SDC3 recruits adaptor proteins involved in inhibition of receptor activity to the membrane and when SDC3 is lost this inhibition of cell signalling is lost (Fig 5.18). This hypothesis seems more likely as the phosphoproteins identified in this study were mostly intracellular proteins involved in cell signalling.

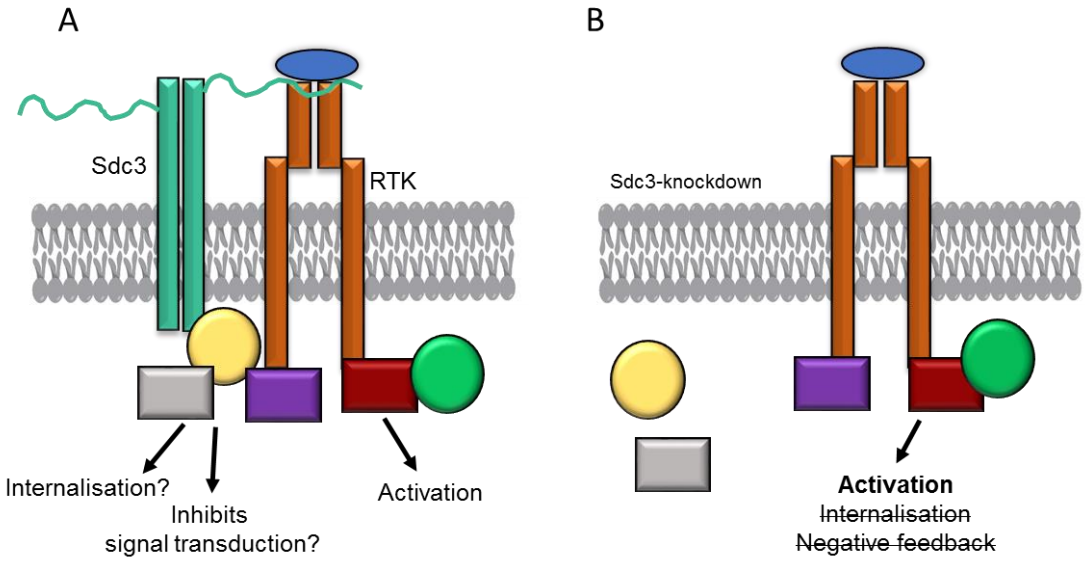

Figure 5.18: Hypothetical model explaining the increase in RTK signalling activation mediated by SDC3 knockdown in serum-starved myoblasts. (A) When myoblasts are serum-starved, SDC3 supports the internalisation of receptor tyrosine kinases (RTKs) and their ligands or mediates interactions between adaptor molecules that inhibit RTK signal transduction. **(B)** The loss of SDC3 results in disruption of interactions between adaptor molecules and RTKs leading to sustained RTK signal transduction.

Some of the more notable changes that recurred throughout the analysis were differences in IRS1 and insulin receptor signalling. Insulin receptor signalling was the most enriched RTK signalling pathway in S3KD myoblasts upon serum-stimulation and was enriched at both Time 0 and Time 10. Upon further investigation of the proteins that mapped to the insulin signalling pathway, there were obvious differences in the abundance of phosphopeptides between Vector and S3KD myoblasts in response to serum for example IRS1, IRS2, RPS6 and PKA. The kinase-substrate motif analysis of phosphopeptides

differentially abundant between Vector and S3KD in response to serum suggested changes in activity of PKA and AKT, strengthening the hypothesis that SDC3 is involved in regulating the Insulin/AKT signalling pathway. At the individual time points (Time 0 and Time 10) other proteins involved in insulin signalling had differentially abundant phosphopeptides between Vector and S3KD myoblasts such as: Ptp1b, 4E-BP1, Mek and ERK. Furthermore, the most enriched biological process at Time 10 was phosphatidylinositol signalling, while at Time 0 mTOR signalling was most enriched, suggesting SDC3-knockdown causes changes in PI3K and mTOR signalling. Altogether these data suggest that SDC3 regulates the insulin signalling pathway primarily via the PI3K/AKT/mTOR signalling pathway. SDC3 has been implicated in insulin signalling previously; *Sdc3*$^{-/-}$ mice had leaner bodies, improved glucose tolerance and increased insulin sensitivity compared to wild type mice when fed on a high fat diet (Strader *et al.*, 2004). Glucose uptake by GLUT4 is mainly stimulated via the insulin signalling pathway but neuregulin signalling in skeletal muscle has also been shown to stimulate glucose uptake by recruitment of glucose transporters to the membrane (Suarez *et al.*, 2001). Neuregulin signalling was the second most enriched RTK pathway in S3KD myoblasts stimulated with serum (Time 10/Time 0) suggesting that SDC3 may be involved in glucose transport either via insulin receptor or neuregulin signalling.

IRS1 is one of the main intracellular protein adaptors of insulin receptor tyrosine kinase activity and is the most upstream protein in signal transduction mediated by insulin, IGF-1 and interleukin-4 (White and Kahn, 1994). Significantly regulated phosphosites of IRS1 were identified throughout the phosphoproteomic analysis, and IRS1 was the main hub of the upstream regulators network at Time 0 and Time 10, suggesting that knockdown of SDC3 significantly affected the phosphorylation of IRS1 likely via the insulin/IGF receptor. IRS1 has many potential phosphorylation sites, and depending on the residue, phosphophorylation can either positively or negatively regulate its function with the insulin receptor and downstream proteins (Gual *et al.*, 2005). Tyrosine phosphorylation allows downstream proteins to dock with IRS1 and positively transduce signals, whereas many serine/threonine phosphorylations can produce both positive and negative effects on IRS1 (Gual *et al.*, 2005, Copps and White, 2012). IRS1^{S302} was significantly increased in S3KD myoblasts at Time 0 in the phosphoproteomics analysis. Interestingly, phosphorylation of IRS1^{S302} is observable in serum-starved C2C12 myoblasts, peaks at 10 minutes after insulin stimulation but then declines after 30 minutes (Weigert *et al.*, 2008). In this scenario IRS1^{S302} enhances signalling downstream of IRS1 as measured by phospho-AKT activity (Weigert *et al.*, 2008). IRS1^{S302} and IRS1^{S522}, which were both significantly increased at Time 0 but not Time 10 in S3KD myoblasts, have been implicated in IRS1 degradation via over-activation of the mTOR/S6K and PI3K/AKT signalling pathways respectively (Shah and Hunter, 2006, Giraud *et al.*, 2007). However, from my western blot analysis it appeared that significant accumulation of IRS1 had occurred in S3KD myoblasts compared to Vector

myoblasts at Time 0 and Time 10 contradicting reports that IRS1^{S302} promotes degradation. The Rheb/mTOR signalling pathway inhibits myoblast differentiation by reducing the total protein levels of IRS1, which in turn leads to reduced PI3K/AKT activity (Ge *et al.*, 2011). Therefore it is possible that degradation of IRS1 failed when SDC3 was knocked-down which led to sustained signalling via IRS1, increased AKT phosphorylation and enhanced downstream effects.

Proteins involved in ubiquitination were significantly enriched at Time 0 when comparing Vector and S3KD myoblasts, including NEDD4 which had decreased phosphorylation at S2 and S16 in S3KD myoblasts, although, the functional role of these two phosphorylations is unknown. NEDD4 is an E3 ubiquitin ligase and an important regulator of autophagy via interaction with Microtubule-associated proteins 1A/1B light chain 3B (MAP1LC3-II). NEDD4 knockdown in cancer cells inhibits autophagy as measured by seqestosome-1 (SQSTM1) degradation and causes impaired mitochondrial structure (Sun *et al.*, 2017). NEDD4 is expressed in quiescent and activated satellite cells and mono-ubiquitinates PAX7 *in vitro* leading to its degradation and increased muscle differentiation (Bustos *et al.*, 2015). NEDD4 regulates NOTCH1 in a ubiquitin-dependent manner and downregulates NOTCH1 activity. SDC3 is reportedly in complex with NOTCH1 and is required for NOTCH1-cleavage and subsequent signalling (Koncarevic *et al.*, 2007, Pisconti *et al.*, 2010). NEDD4 is also involved in ubiquitin-mediated intracellular trafficking of RTKs, such as IGF-1R, insulin receptor and EGFR, which is interesting given the pTyr phenotypes observed in S3KD myoblasts (Morrione *et al.*, 1999, Katz *et al.*, 2002, Cornelison *et al.*, 2004, Marmor and Yarden, 2004). Furthermore, NEDD4 regulates insulin/IGF signalling and IRS1/2 ubiquitination via PTEN, suggesting a potential role for SDC3 in insulin, IRS1 and IRS2 regulation via NEDD4 (Shi *et al.*, 2014, Fukushima *et al.*, 2015, Li *et al.*, 2015). One hypothesis could be that SDC3 recruits NEDD4 to the membrane allowing ubiquitination of IRS1 and therefore degradation. However, when SDC3 is lost this process is non-functional which leads to an accumulation of IRS1, as observed by western blotting (Fig. 5.17).

mTOR signalling is known for regulating biological processes such as: cell growth, glycolysis, lipogenesis, glucose metabolism and autophagy in response to stimulation by growth factors, nutrients and changes in energy status (Chang et al., 2009, Sengupta et al., 2010, Hagiwara et al., 2012). Autophagy is the highly selective process of recycling cytoplasmic components to generate nutrients and energy to maintain cellular homeostasis (Jung *et al.*, 2010). Unc-51 like kinase 1 (ULK1) is a key regulator of autophagy in mammals and phosphorylation of ULK1^{S757} by mTORC1 inactivates ULK1 under high glucose conditions (Kim *et al.*, 2011). In our study phosphorylation of ULK1^{S622} was significantly higher in S3KD myoblasts at Time 0. No information is available for this particular ULK1

phosphosite but our data suggest that mTOR-mediated regulation of autophagy might be altered in S3KD myoblasts. Autophagy is upregulated in an mTORC1-independent manner during differentiation of satellite cell-derived myoblasts and inhibition of autophagy, via Beclin-1 silencing, drastically reduces myocyte fusion (Fortini *et al.*, 2016). Additionally, another study investigated the role of mitochondrial degradation via autophagy in C2C12 myoblasts and found that when SQSTM1, an autophagosome cargo protein, was silenced C2C12 cell differentiation was inhibited (Sin *et al.*, 2016). Two phosphosites on SQSTM1, S330 and S334, were significantly increased in S3KD myoblasts at Time 0 and two different phosphosites, S357-S368, were significantly increased in S3KD myoblasts at Time 10. Again, limited functional information is available about these phosphosites but it is suggested that SQSTM1^{S334} (corresponding to human S332) may be involved in MAP1LC3-II- mediated protein-protein interactions, which are essential for protein-autophagosome binding (Rigbolt *et al.*, 2014). Although it is not clear what the biological function of increased ULK1 and SQSTM1 phosphorylation in S3KD myoblasts is, it does suggest that autophagy is dysregulated, possibly increased, in S3KD myoblasts which may lead to the enhanced differentiation and fusion phenotypes observed. Moreover, autophagy has been associated with increased satellite cell activation and *Sdc3*$^{-/-}$ myoblasts show increased activation (Tang and Rando, 2014, Pisconti *et al.*, 2016).

Cell-cell adhesion is an important step for the formation of nascent and mature myotubes and for adhesion to the myofibre (Abmayr and Pavlath, 2012). At Time 0 several GO terms related to cell-cell adhesion were significantly enriched, including ‘cell-cell adhesion’, ‘cadherin binding’ and ‘cell-adherens junction’. Additionally, non-RTK pathways, such as integrin signalling, were significantly enriched at Time 0 (Appendix 3.3). Syndecans are able to regulate cell-cell adhesion and cell-matrix adhesion via integrins and cadherins as reviewed by Rapraeger (2000). In particular the loss of SDC3 from satellite cells impairs their ability to adhere to the myofibre (Pisconti *et al.*, 2016). Phosphorylation of catenin-delta-1 (also termed p120) was significantly regulated at Time 0 and Time 10 by SDC3 knockdown, with different phosphosites being differentially phosphorylated at each time point. p120 is an adaptor protein that interacts with the cytoplasmic domains of cadherins to transduce signals associated with the formation of adherens junctions, cell-cell adhesion and regulation of E-cadherin turnover (Thoreson and Reynolds, 2002, Davis *et al.*, 2003). There is no functional information about the significantly regulated p120 phosphosites identified in this study and generally little is known about the many S/T phosphorylations, however, there is evidence that tyrosine phosphorylation of p120 enhances cadherin function (Alema and Salvatore, 2007). At Time 0, p120^{Y865} was significantly increased in S3KD myoblasts which may enhance cadherin-mediated cell-cell adhesion in S3KD myoblasts. Therefore this might be one of the mechanisms that eventually lead to the

observed increase in S3KD and primary *Sdc3*$^{-/-}$ myoblast fusion compared to Vector and primary wild type myoblast fusion.

Phosphoproteomics is a high throughput analytical tool and using this method coupled with bioinformatic analysis provided us with a list of potential SDC3-regulated signalling, which can be followed up in subsequent experiments. However, there were some limitations in this study. Only relatively few pTyr-peptides were identified (33), of these only 18 were confidently localised and even fewer were significantly regulated by SDC3. This was not unexpected as tyrosine phosphorylation is a relative rare event compared to serine and threonine phosphorylation (Raggiaschi *et al*., 2005). In order to enrich for pTyr-peptides alternative sample preparation workflows would be required such as immunoaffinity purification. However, utilising these techniques require larger quantities of starting material and the loss of pSer and pThr would have resulted in less information. Considering that very little is known about SDC3-mediated cell signalling networks, removing pSer- and pThr-peptides would have hindered our efforts to understand the SDC3 phosphoproteome.

High throughput shotgun phosphoproteomics is a relatively new discipline, which faces many challenges (Solari *et al.*, 2015). The biggest challenge in phosphoproteomics is the lack of information about the biological function of specific phosphosites. There are many tools available for analysing phosphoproteomic data at the protein level which use either open source databases (e.g. DAVID, PANTHER, Cytoscape, etc.) or subscription databases (e.g. IPA). All these databases are manually curated and the function of proteins are constantly being updated as new knowledge is acquired. In contrast, phosphorylation databases are still poorly annotated. Another challenge lies with validation of the phosphopeptide quantification. The majority of phosphosites identified in our study were not recognised by a commercially available antibody which meant that only few phosphosites identified as interesting through bioinformatic analysis could be validated by western blotting. For future experiments, antibodies targeting specific phosphosites could be generated however, these methods can be costly and time consuming, as the newly generated antibodies need to be validated.

A third challenge of phosphoproteomics is phosphosite localisation. Although mass spectrometry is highly sensitive and often identifies the correct peptide, phosphosite localisation is more difficult, particularly if a peptide contains two or more phosphosites that are in close proximity. This causes additional problems as it is unknown what percentage of the quantification change is due to one phosphosites, or to a second or third one, or to some or all of them. This was evident from the IRS1 western blots where a phosphopeptide containing two phosphosites, S302 and S307, was identified by mass spectrometry but no signal was observed from an antibody raised against IRS1^{S307}, suggesting that the majority

of changes in the phosphopeptide identified as IRS1$^{S302/S307}$, actually occurred at the S302 site. It is also possible that the IRS1^{S302} antibody poorly detected that particular phosphorylation residue. Similarly, RPS6 peptides often contained a mixture of phosphosites that were detected by two different antibodies and therefore it was difficult to determine how accurate the quantification from the phosphoproteomics was compared to the western blotting validation. Nonetheless, it was evident in the case of RPS6 that the same trends were being observed by western blot and mass spectrometry, which was most important.

Lastly, no information about SDC3-mediated changes were obtained at the whole proteome level as the phosphoproteomics experiment designed did not measure levels of whole protein abundance. This was done for two reasons: (1) I thought that the majority of phosphoproteins identified would not significantly change in total protein abundance between conditions, rather the changes in phosphorylation would be more important; (2) signalling proteins are rarely detected by label-free shotgun proteomics because they are present in low abundance, although they are detected upon enrichment such as the one we performed on a titanium-dioxide column to enrich for phosphopeptides. Thus, a mass spectrometry analysis of the unfractionated lysates to detect total protein abundance, would have yielded only very few hits amongst those of interest. Furthermore, I planned to validate by western blotting the change in phosphopeptide abundance observed by phosphoproteomics. When IRS1^{S302} phosphorylation was normalised to total IRS1 there was no significant difference between Vector and S3KD myoblasts which contradicted the phosphoproteomic results. It is likely that, because a significant increase in IRS1 total protein was observed, this naturally led to detection of an increased abundance of the IRS1^{S302} phosphopeptide by mass spectrometry.

In conclusion, the investigation into the phosphoproteomes of Vector and S3KD myoblasts yielded important insights concerning SDC3-mediatated signalling pathways. Several signalling pathways were significantly altered by SDC3-knockdown, which has provided us with various avenues to explore in the future. Analysis at Time 0 and Time 10 indicated that components of the mTOR signalling pathway and cell-cell adhesion were significantly regulated by SDC3 knockdown. Lastly, changes in IRS1 phosphorylation appeared throughout the analysis and the insulin receptor signalling pathway was significantly altered by SDC3 knockdown. Altogether the data in this chapter confirm that SDC3 is involved in the regulation of many myoblast signalling pathways, as previously hypothesised, and points towards insulin signalling as a novel SDC3-regulated pathway that is worth further examination.

Chapter 6

SDC3-mediated regulation of insulin signalling

6.1 Introduction

Insulin signalling is a highly conserved pathway that regulates several biological functions in mammals such as: lipid, carbohydrate and amino acid metabolism and maintenance of glucose homeostasis (Pessin and Saltiel, 2000). Total loss of the insulin receptor (IR) is postnatally lethal, whereas tissue-specific IR loss causes several phenotypes such as: glucose intolerance, insulin resistance and changes in body weight, depending on the tissue (Li and Zhang, 2000). Dysregulation of the insulin signalling pathway occurs in a variety of pathological conditions associated with insulin resistance, such as type II diabetes, non-alcoholic fatty acid liver disease and even some types of cancer (Wilcox, 2005).

IR is a member of the receptor tyrosine kinase family and has two isoforms, IR-A and IR-B, which are formed from alternative splicing of the same primary transcript and are present in virtually all mammalian tissue (Bailyes *et al.*, 1997). The IR is a heterotetramer composed of two alpha-subunits, which lie extracellularly and bind ligands, and two beta-subunits, which cross the plasma membrane and contain the tyrosine kinase activity on the intracellular side. IR is translated as one single proreceptor precursor then undergoes disulphide bond formation, proteolytic cleavage, and glycosylation upon maturation (Hedo *et al.*, 1983). The insulin receptor family contains the insulin-like growth factor 1 receptor (IGF1R), which shares high homology with IR particularly within the tyrosine kinase domains (Nakae, *et al.*, 2001). Insulin and IGF1 preferentially bind to their own receptors, however, they also bind to each other's receptor albeit with significantly lower affinity (Belfiore *et al.*, 2009). Additionally, IGFs have a markedly increased affinity for IR-A over IR-B. Hybrid heterotetramers consisting of one α/β IR dimer and one α/β IGF1R dimer commonly exist throughout the several tissues and these hybrid receptors preferentially bind IGF1 (Siddle, 2011). Although there appears to be crosstalk between IR and IGFR signalling as similar pathways are activated downstream of ligand binding, it is hypothesised that tissue-specific expression of IGFs and insulin, differences in ligand binding affinity and the preference of some adaptor proteins to bind to IR over IGFR, play

important roles in modulating these two pathways and regulating biological function (Werner *et al.*, 2008).

IR-ligand binding induces IR conformational changes and stimulates the tyrosine kinase activity intrinsic to the β-subunit, which subsequently auto-phosphorylates tyrosine (Tyr) residues in the β-subunits (Boucher *et al.*, 2014). Auto-phosphorylation of three Tyr residues is a key step to IR activation and downstream signalling as mutations in these specific Tyr residues result in reduced insulin-mediated signalling and loss of biological activity (Nakae*, et al.*, 2001). Activation of the IR leads to recruitment of adaptor proteins and transduction of the insulin signalling (Fig. 6.1). The first proteins activated after IR phosphorylation are the insulin receptor substrate (IRS) proteins which are recruited to the membrane and are phosphorylated on multiple Tyr residues by the IR (Sun *et al.*, 1991). In addition to IRS proteins, the IR can phosphorylate other cytoplasmic adaptor proteins such as Shc (SHC adaptor protein 1), which leads to activation of the Ras/ERK pathway and DOK proteins (Boucher*, et al.*, 2014). IRS proteins act as cytoplasmic adaptor proteins to recruit additional downstream signalling molecules containing SH2 (Src Homology 2) domains via their pTyr residues. Six IRS proteins have been identified however little is known about the biological roles of Irs3, Irs4, Irs5 and Irs6 in insulin signalling compared to what is known about IRS1 and IRS2. Activation of IRS proteins leads to two major signalling arms of the insulin pathway: Ras/ERK and PI3K/AKT signalling. The Ras/ERK pathway is generally involved in cell proliferation by regulating mitogenic gene expression (Gonzalez*, et al.*, 2004). The PI3K/AKT pathway is considered the major effector of the insulin signalling pathway by phosphorylating several downstream targets, which then regulate gluconeogenesis, lipid synthesis, protein synthesis, glycogen synthesis, metabolism, survival and glucose uptake (Fig. 6.1). IRS proteins recruit PI3K which in turn phosphorylates phosphatidylinositol 4,5-bisphosphate (PIP2) generating phosphatidyl-inositol (3,4,5)-triphosphate (PIP3), and recruits AKT to the plasma membrane. AKT is then phosphorylated by PDK1 on Thr308 and by mTORC2 on Ser473, these two phosphosites are required for full activation of AKT and subsequent downstream signalling (Alessi*, et al.*, 1997, Sarbassov *et al.*, 2005).

Downstream targets of AKT include tuberous sclerosis complex protein 2 (TSC-2) and PRAS40 (proline-rich AKT substrate 40 KDa), which relieves inhibition of the mTORC1 complex land leads to activation of S6K and 4E-BP2, thus promoting protein synthesis (Siddle, 2011). The Forkhead family of transcription factors are phosphorylated in response to AKT activation and prevent the Forkhead transcriptional activity by excluding it from the nucleus, consequently regulating genes involved in gluconeogenesis (Li and Zhang, 2000). Proteins involved in glucose transport include the GTPase-activating protein AKT substrate

of 160 kDa (AS160 or TBC1D4) and glycogen synthase kinase 3 (GSK-3). AKT negatively regulates TBC1D1 and GSK3 via phosphorylation to allow translocation of GLUT4, an insulin-regulated glucose transporter, to the plasma membrane and consequently increased glucose uptake (Boucher *et al.*, 2004).

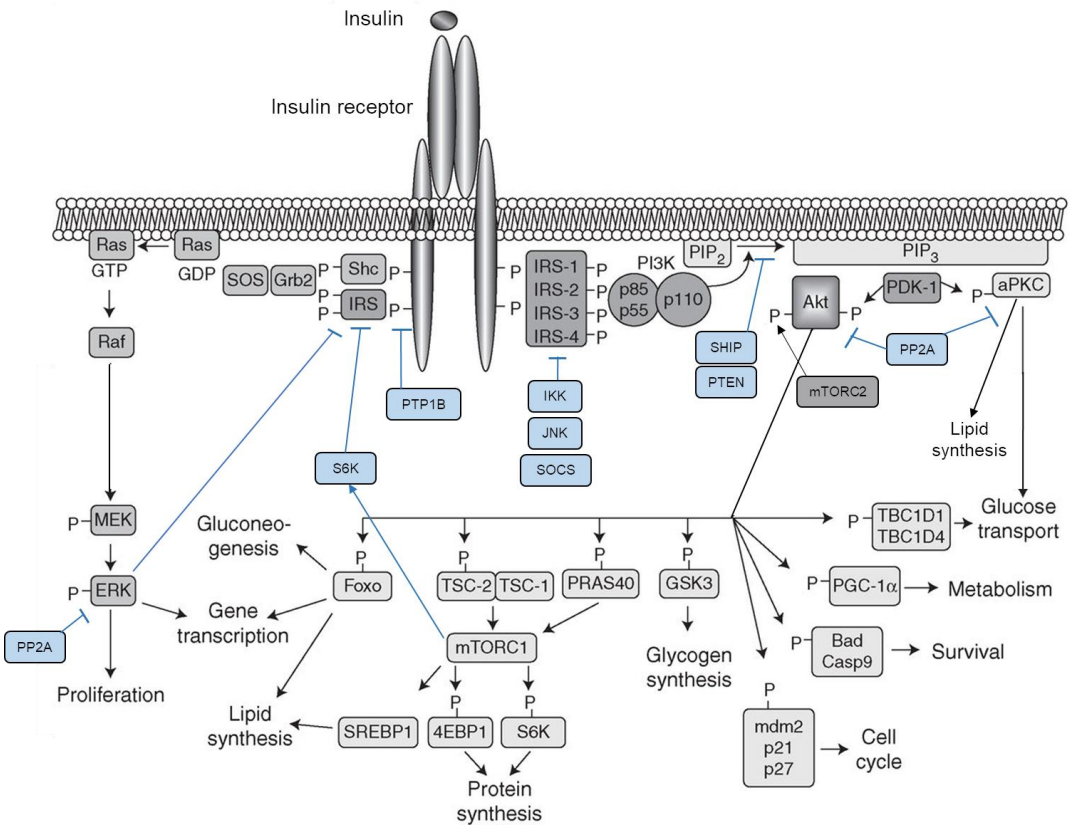

Figure 6.1: The insulin signalling pathway. Upon insulin binding to the insulin receptor, Shc and IRS proteins bind to the phosphorylated tyrosines present in the β-subunit of the insulin receptor initiating a cascade of phosphorylation events. Shc will activate the Ras/ERK pathway leading to proliferation. The IRS proteins can also activate the Ras/ERK pathway but predominantly activate the PI3K/AKT signalling pathway. The AKT pathway mediates most of insulin's metabolic effects such as glycogen synthesis, protein synthesis, glucose transport, lipid synthesis and gluconeogenesis. Figure adapted from Boucher et al. (2014).

Negative feedback of the insulin signalling pathway is equally important to ensure tightly controlled insulin-mediated activity which otherwise may lead to severe metabolic dysfunctions. Additionally, cells must be able to respond to changes in the environment and rapidly turn off insulin signalling. Several phosphatases are involved in regulation of the insulin signalling pathway, such as PTP1B, PTPRF (PTP-receptor type F), PP1 (Protein phosphatase 1), PP2A (protein phosphatase 2 phosphatase activator), SHIP (inositol polyphosphate-5-phosphatase) and PTEN (phosphatase and tensin homolog). These phosphatases directly dephosphorylate the IR, IRS proteins and AKT (Fig. 6.1). Other negative regulators include the suppressor of cytokine signalling (SOCS) family which negatively regulate cytokine and growth factor signalling (Emanuelli *et al.*, 2000). Grb10 (growth factor receptor bound protein 10) and Grb14 (growth factor receptor bound protein

14) inhibit protein binding to the IR preventing downstream signalling; loss of Grb10 is not lethal but leads to enhanced insulin signalling and growth in mice (Smith *et al.*, 2007). Lastly, activation of S6K, via mTORC1 or PDK1, phosphorylates IRS1 on Ser residues which negatively regulate IRS1 activity (Gual *et al.*, 2003).

Skeletal muscle, along with liver and fat tissues, are known as insulin-sensitive tissues. Skeletal muscle is highly responsive to insulin and consequently most of the glucose that is circulating in the blood is transported via GLUT4 transporters into the muscle where it is either immediately used to produce energy or stored as glycogen (Jue *et al.*, 1989). Skeletal muscle expresses both IR isoforms but predominantly IR-B (Moller *et al.*, 1989). At the cellular level IR expression is increased 5-10 fold during differentiation of C2 and BC3H-1 myoblasts accompanied by an increase in insulin binding to cells (Brunetti *et al.*, 1989). Furthermore, insulin stimulates differentiation of C2C12 myoblasts through activation of the PI3K/AKT/S6K pathway (Jiang*, et al.*, 1999, Conejo*, et al.*, 2001). However, in low glucose conditions, insulin is unable to exert a strong myogenic phenotype, suggesting that glucose availability is critical for insulin-mediated differentiation (Nedachi *et al.*, 2008). Interestingly, insulin has also been shown to promote cell cycle progression at S, G1 and G2 phases resulting in increased myoblast proliferation (Grabiec*, et al.*, 2014).

Investigation of heparan sulphate-interacting proteins revealed that IR interacts with heparan sulphate, suggesting that the syndecans may bind to the IR via heparan sulphate (Ori *et al.*, 2011). Furthermore, insulin stimulation of osteoblast-like cells promotes SDC1 and IR interaction, which results in activation of ERK1/2 and integrin-linked kinase (ILK) (Yoon *et al.*, 2015). However this activity is abolished when cells are treated with heparinase, a bacterial enzyme that degrades heparan sulphate, suggesting that heparan sulphate is important for IR/SDC1 interaction (Yoon*, et al.*, 2015, Ramalingam and Kim, 2016). Interestingly, heparinase treatment does not affect AKT phosphorylation following insulin stimulation suggesting that heparan sulphate is dispensable for activation of the insulin/AKT pathway (Ramalingam and Kim, 2016). Investigation on the role of syndecans in insulin signalling is scarce, but these data from the literature suggest that syndecans have the potential to regulate insulin signalling.

6.1.1 Chapter hypothesis and objectives

In the previous chapter, insulin signalling was identified as the most significantly enriched RTK pathway that was altered in Vector and S3KD myoblasts upon serum stimulation. In S3KD myoblasts phosphoproteins involved in the regulation of the insulin signalling pathway were differentially phosphorylated compared to Vector myoblasts at any time point considered, therefore we hypothesised that SDC3 may regulate insulin signalling in

myoblasts. The aim of this chapter was to determine how SDC3 knockdown affects myoblast proliferation and differentiation in an insulin-dependent manner. To do this, Vector and S3KD myoblasts were treated with insulin during proliferation and differentiation and both phenotypic and cell signalling readouts were measured. Wild type and *Sdc3*$^{-/-}$ primary mouse satellite cell-derived myoblasts were used to validate any differences observed in the C2C12-derived Vector and S3KD myoblasts.

6.2 Results

6.2.1 Insulin promotes proliferation of Vector but not S3KD myoblasts

The results from the phosphoproteomics data indicated that SDC3 regulates insulin signalling but how this translated to myoblast function was undetermined. The literature suggests that insulin promotes proliferation and differentiation in myoblasts (Grabiec *et al.*, 2014), which is counter-intuitive since proliferation and differentiation are mutually exclusive events. Proliferating Vector and S3KD myoblasts were treated with insulin to understand how SDC3 knockdown affects myoblast proliferation and differentiation in the presence of insulin. Myoblasts were cultured in growth medium for 24 hours with or without the addition of insulin, then fixed and stained with DAPI to visualise nuclei and counted. Insulin-mediated proliferation was measured as the percentage of insulin-treated myoblasts compared to non-treated myoblasts (Fig. 6.2). Upon stimulation with insulin Vector myoblasts proliferated up to 40% more in a dose-dependent manner whereas S3KD myoblasts did not significantly proliferate more in response to insulin (Fig. 6.2). Therefore, I hypothesised that SDC3 promotes insulin signalling because S3KD myoblast proliferation does not increase in response to insulin as it does in Vector myoblasts (Fig. 6.2).

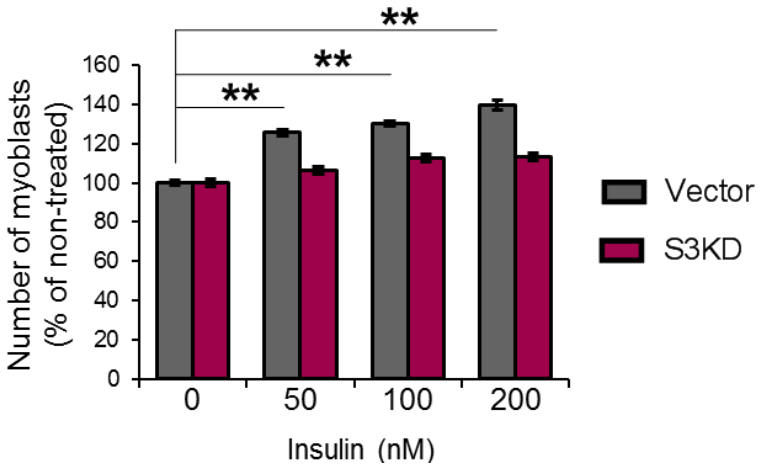

Figure 6.2: Vector myoblasts proliferate more in response to insulin compared to S3KD myoblasts. Myoblasts were cultured in growth medium for 24 hours with or without increasing concentrations of insulin. Myoblasts were then fixed and stained for DAPI to visualise nuclei. Random images (a minimum of 90) were taken using an EVOS FL microscope and the number of DAPI+ myoblasts counted in each image. Averages across 3 independent experiments were plotted ± SEM. ** = p <0.01; S3KD = SDC3 knock-down.

6.2.2 SDC3 knock-down increases activation of AKT in C2C12 myoblasts

To test whether SDC3 promotes insulin signalling in proliferating myoblasts, the phosphorylation levels of proteins in the insulin signalling pathway were quantified in Vector and S3KD myoblasts that had been treated with insulin or PBS for 48 hours under proliferating conditions. These proteins included: AKT, ERK1/2 and RPS6. Phosphorylation of RPS6$^{S240/244}$ was chosen as this site is primarily phosphorylated by S6K, which is activated by mTOR downstream of insulin/AKT (Biever *et al.*, 2015). Myoblasts were lysed and the lysates processed for western blotting (Fig. 6.3A). In non-treated proliferating myoblasts no significant differences in phosphorylation of AKT, ERK or RPS6 were observed between Vector and S3KD myoblasts (Fig 6.3). Upon insulin stimulation, AKT phosphorylation significantly increased in both myoblast cell lines but significantly more in S3KD myoblasts compared to Vector myoblasts (Fig. 6.3B). This result was surprising and contradicted the proliferation phenotype of insulin-treated S3KD myoblasts, suggesting that either insulin-mediated stimulation of proliferation does not occur via AKT or that my hypothesis that SDC3 promotes insulin signalling is wrong. The first explanation was supported by the fact that AKT signalling is well known to promote myoblast differentiation, which is mutually exclusive to proliferation. In contrast, ERK1/2 signalling, which is also activated by insulin in many cell types, promotes myoblast proliferation (Jones *et al.*, 2001). Moreover, RPS6 phosphorylation, which is downstream of insulin/AKT/mTOR was also unaltered by either insulin stimulation or SDC3 loss in proliferating cells (Fig. 6.3), further supporting that insulin does not signal via AKT in proliferating myoblasts.

If the inconsistency between the insulin-mediated increase in AKT activation and the proliferation phenotype observed in S3KD myoblasts can be explained by the fact that insulin promotes myoblast proliferation via ERK1/2 rather than AKT, I predicted that ERK1/2 phosphorylation should increase in response to insulin in Vector myoblasts but not in S3KD myoblasts. However, phosphorylation of ERK1 (Fig. 6.3D) and ERK2 (Fig. 6.3E) was not affected by insulin stimulation in either Vector or S3KD proliferating myoblasts. This suggested that the inconsistency between insulin-mediated AKT activation and the proliferation phenotype in S3KD myoblasts was not due to increased ERK phosphorylation. Instead, this suggested that my original hypothesis, that SDC3 promotes proliferation, was wrong.

An alternative explanation for these seemingly inconsistent results is that, in the absence of SDC3, insulin-mediated activation of AKT pushes myoblasts towards differentiation. Previous work has shown that myoblast differentiation induced by serum-reduction is enhanced in *Sdc3*$^{-/-}$ primary myoblasts (Pisconti, 2010) and in my work where SDC3 was knocked-down in myoblasts (*Chapter 4*, Fig. 4.6). Therefore, I decided to

investigate the role of SDC3 in the regulation of insulin-mediated promotion of differentiation.

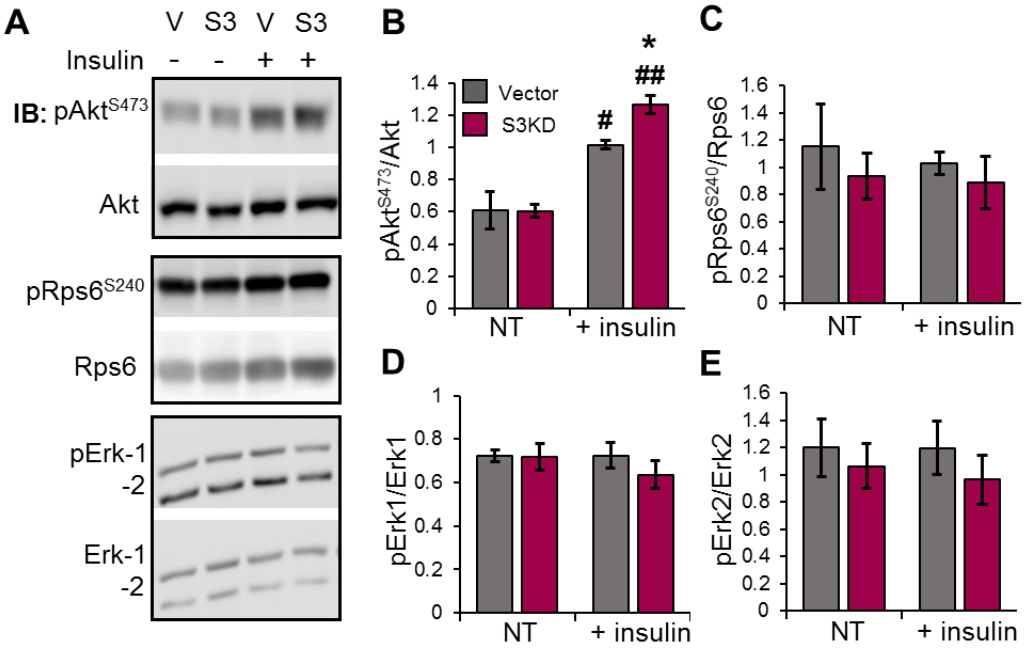

Figure 6.3: AKT phosphorylation is increased in S3KD myoblasts upon insulin stimulation. Myoblasts were cultured in growth medium with or without insulin then lysed in RIPA buffer. **(A)** Proteins were separated by SDS-PAGE and analysed by western blotting with protein- and phospho-specific (p) antibodies as indicated. **(B)** Quantification of three independent experiments. Averages plotted with ±SEM. * represents differences between Vector and S3KD; * = p <0.05. # represents differences between insulin treated and non-treated; # = p <0.05. V = Vector, S3 = SDC3 knockdown.

6.2.3 SDC3 knockdown increases differentiation and fusion of C2C12 cells via the Insulin-AKT signalling pathway

Insulin is known to promote myoblast differentiation (Jiang *et al.*, 1999, Conejo *et al.*, 2001). To determine how SDC3 knockdown affects insulin-promoted myoblast differentiation, Vector and S3KD myoblasts were grown to confluence then induced to differentiate by reducing the serum content in the medium. Insulin was added to the medium after induction of differentiation for three days. Cells were fixed, stained with DAPI and an anti-MyHC antibody to visualise nuclei and late stage differentiation, respectively. S3KD cells differentiated and fused more than Vector cells in the absence of added insulin (Fig. 6.4A, left panels). With the addition of insulin both Vector and S3KD cells significantly differentiated and fused more (Fig. 6.4A, right panels), although there was a much smaller response to insulin in the S3KD cells (2.5 times more differentiation than vehicle-treated) compared to Vector cells (12.5 times more differentiation than vehicle-treated) (Fig. 6.4B). The smaller response to insulin in the S3KD cells compared to Vector cells recapitulates the same trend as previously observed in the activation of the insulin/PI3K/mTOR signalling

pathway in the phosphoproteomics dataset, when S3KD myoblasts were compared to Vector myoblasts after serum stimulation in (*Chapter 5*).

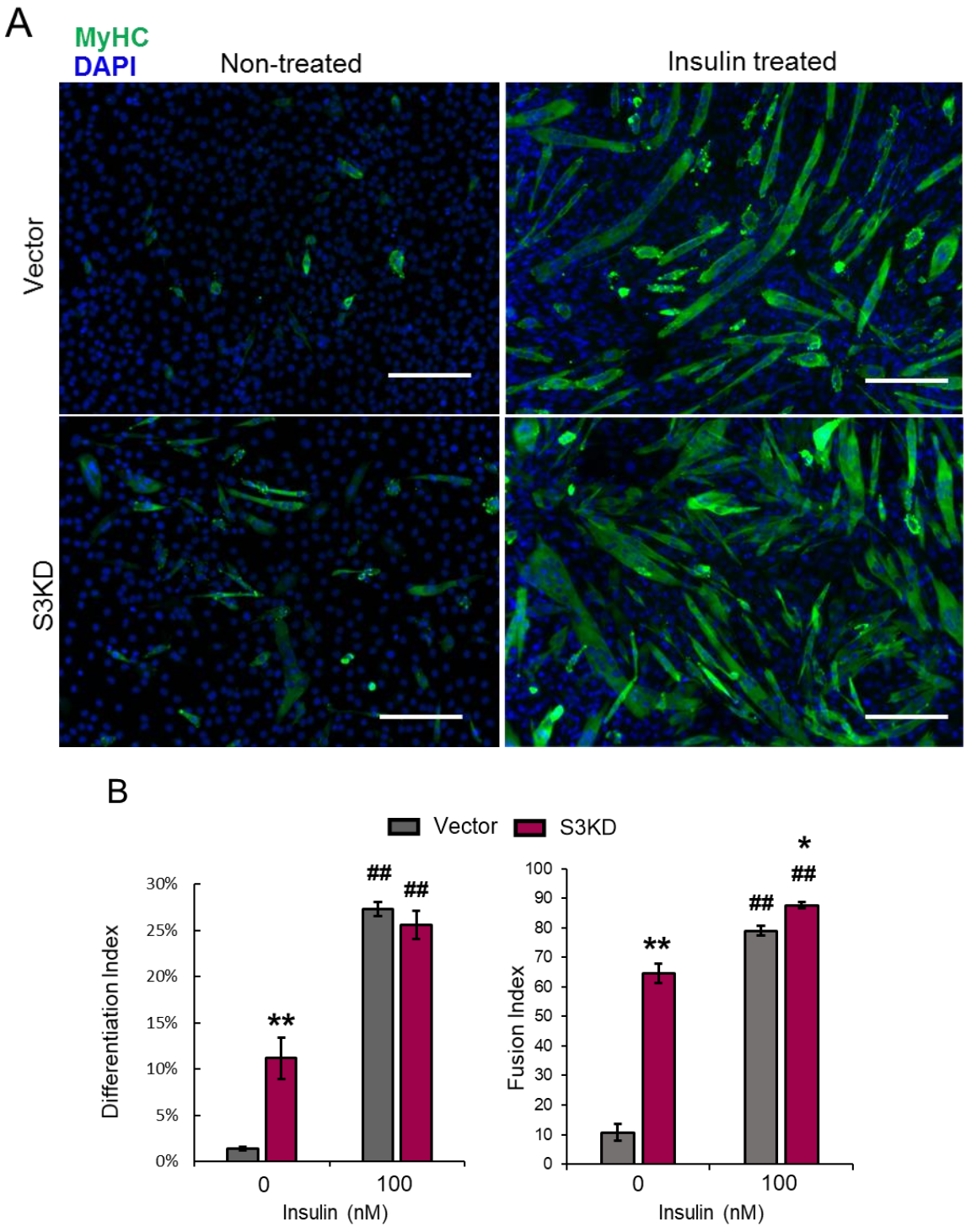

Figure 6.4: Vector cells are more responsive to insulin than S3KD cells during differentiation. Myoblasts were grown to confluence and then induced to differentiate for three days with or without insulin. **(A)** Cells were fixed then stained to detect myosin heavy chain (MyHC) and DNA (DAPI) to visualise late stage differentiation and nuclei respectively. Scale bar represents 200 µm. **(B)** Differentiation and fusion index were calculated from three independent experiments. Averages were plotted ± SEM. * represents differences between Vector and S3KD; * = p <0.05; ** = p <0.01. # represents differences between insulin treated and non-treated; ## = p <0.01. V = Vector, S3 = SDC3 knock-down.

Next I investigated how SDC3 knockdown affects the phosphorylation levels of proteins in the insulin signalling pathway in differentiating cells. Vector and S3KD cells were cultured to confluence then induced to differentiate by reducing the serum content in the medium before addition of insulin for three days. Cells were then lysed and the lysates processed for western blotting (Fig. 6.5A). In non-treated differentiating S3KD cells a significant increase in pAkt was observed compared to Vector cells (Fig. 6.5B). AKT phosphorylation was also significantly increased upon insulin stimulation in both Vector and S3KD cells. However, the response to insulin in S3KD cells (1.6 times) was much reduced compared with Vector cells treated with insulin (4 times) (Fig. 6.5B). Phosphorylation of RPS6 followed a similar trend as phosphorylation of RPS6 was increased in non-treated S3KD cells compared to non-treated Vector cells (Fig. 6.5C), however there was no significant difference in pRPS6 in response to insulin between both cell lines. This trend of increased AKT phosphorylation in S3KD cells and a reduced response to insulin was consistent with the differentiation phenotype observed in S3KD cells, suggesting that SDC3 inhibits differentiation by inhibiting the insulin/AKT signalling pathway.

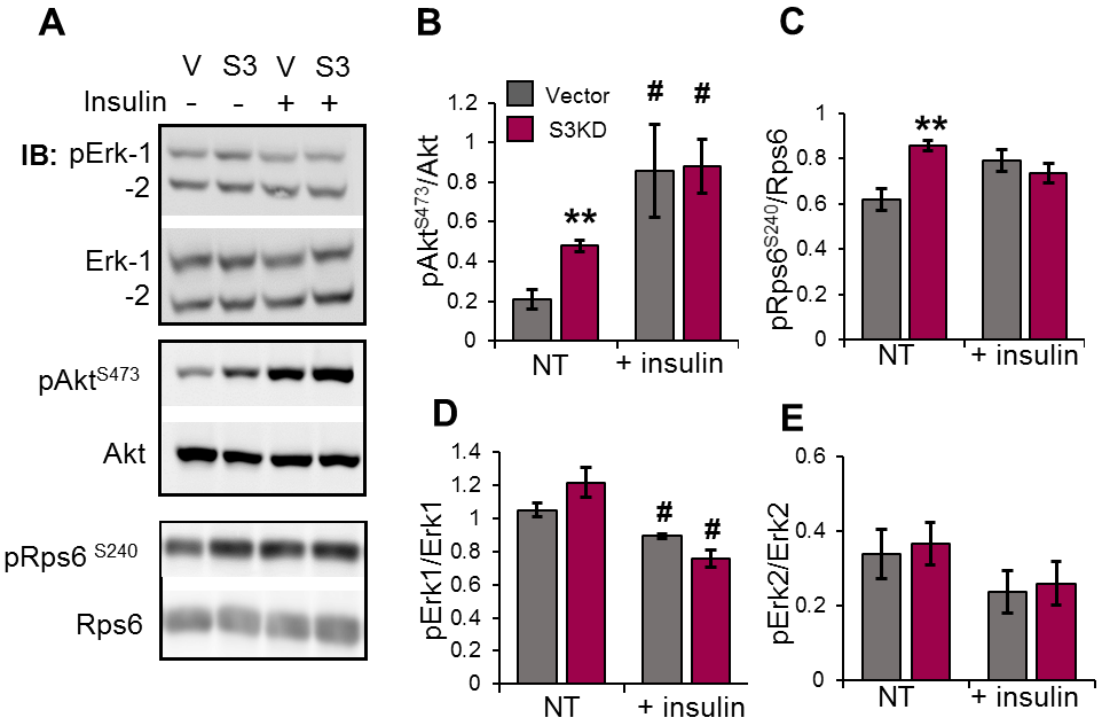

Figure 6.5: S3KD-mediated changes in phosphoproteins after insulin stimulation. Myoblasts were grown to confluence and then induced to differentiate for three days with or without insulin. **(A)** Cells were lysed then proteins were separated by SDS-PAGE and analysed by western blotting with protein- and phospho-specific (p) antibodies as indicated. **(B)** Quantification of three independent experiments. Averages plotted with ±SEM. * represents differences between Vector and S3KD myoblasts; * = p <0.05, ** = p <0.01. # represents differences between insulin treated and non-treated myoblasts; # = p <0.05. V = Vector myoblasts, S3 = SDC3 knockdown myoblasts.

I have shown that S3KD myoblasts do not proliferate more in response to insulin in contrast to Vector myoblasts when both are maintained in growth medium (Fig. 6.2). This is accompanied by increased AKT phosphorylation in proliferating cells, which is associated with insulin-mediated promotion of induced differentiation (Fig. 6.4, (Conejo *et al.*, 2001)). Moreover, ERK1 phosphorylation is significantly decreased in insulin-treated Vector and S3KD cells maintained in low serum medium (Fig. 6.5D), which is consistent with the fact that ERK1/2 phosphorylation promotes myoblast proliferation (Jones *et al.*, 2001). These results, coupled with the information that SDC3 knockdown increased AKT phosphorylation in proliferating myoblasts when stimulated with insulin compared to Vector myoblasts (Fig. 6.3), I hypothesised that S3KD myoblasts would have an increased propensity to spontaneously differentiate in growth medium (high serum conditions) compared to Vector myoblasts, and that spontaneous differentiation was due to overactivation of the insulin/AKT signalling pathway when SDC3 was knocked-down.

6.2.4 SDC3 inhibits myoblast spontaneous differentiation in growth medium via AKT

Traditional protocols to induce myogenic differentiation of C2C12 or primary myoblast cells require a reduction in the serum concentration of the culture medium. However, both C2C12 and primary myoblasts also spontaneously differentiate in the presence of high serum concentrations when they become confluent. To test if SDC3 knockdown promotes myoblast spontaneous differentiation via AKT activation, myoblasts were cultured in growth medium, with or without insulin and with or without an AKT inhibitor (AZD5363) for a prolonged period (Fig 6.6, 6.7). After five days small myotubes were visible in non-insulin treated cells, using bright-field microscopy, and were fixed for staining with DAPI and an anti-MyHC antibody. Random areas of the culture plates were imaged and the fusion and differentiation index were calculated (Fig. 6.6). This experiment provided several key points regarding SDC3-mediated regulation of insulin/AKT signalling and its effect on spontaneous myoblast differentiation in high-serum medium. Firstly, insulin significantly promoted differentiation and fusion in both Vector and S3KD myoblasts in high serum medium (Fig. 6.6). Vector myoblasts differentiated (Fig. 6.6A) and fused (Fig. 6.6B) three times more when stimulated with insulin compared to when insulin was not added, whereas S3KD myoblasts differentiated twice more (Fig. 6.6A) and fused less than twice more (Fig. 6.6B) in response to insulin, indicating that the response to insulin in S3KD myoblasts was reduced. However, S3KD myoblasts spontaneously differentiated almost twice as much as Vector myoblasts (Fig. 6.6A) and fused almost three times more than Vector myoblasts in DMSO control conditions (Fig. 6.6B). A trend of increased differentiation and fusion in S3KD cells compared to Vector cells was observed in almost all conditions. In DMSO-treated control cells supplemented with 100 nM insulin no significant difference between S3KD and Vector cells was found suggesting that a maximal response to insulin was reached. Lastly,

the inhibition of AKT in S3KD and Vector cells reduced differentiation and fusion in a dose-dependent manner (Fig. 6.6). This effect was also observed when the cells were treated with insulin, although with fusion of S3KD cells to a lesser extent. S3KD cells still significantly differentiated and fused more in the presence of the AKT inhibitor, suggesting that AKT activity is increased in the S3KD cells and would require a higher dose of AKT inhibitor to prevent differentiation to the same extent observed in Vector cells. Altogether these data suggest that activation of the insulin/AKT signalling pathway, which promotes differentiation, is enhanced when SDC3 is knocked down, leading to increased differentiation and fusion under all culture conditions, further supporting the idea that SDC3 is a negative regulator of the insulin signalling pathway.

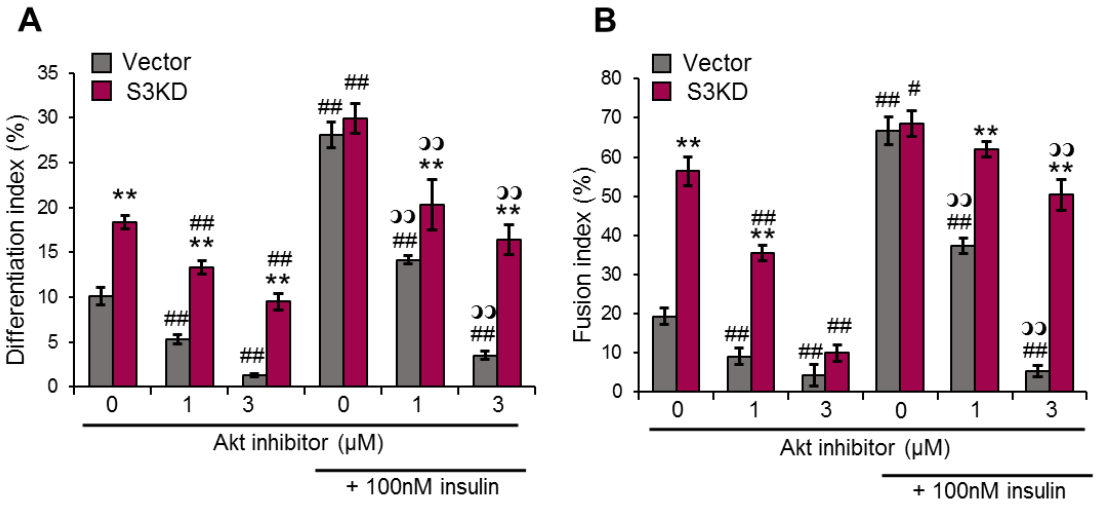

Figure 6.6 Quantification of spontaneous differentiation and fusion in C2C12 myoblasts. Average of differentiation and fusion index for each condition across three independent experiments, with >10 images scored in each experiment (n > 30) was plotted ± SEM. * represents the p-value of the differences between Vector and S3KD myoblasts; ** = p <0.01. # represents the p-value of the differences between cells treated AKT inhibitor and cells not treated with AKT inhibitor, # = p <0.05, ## = p < 0.01. ɔ represents differences between AKT inhibitor plus insulin compared to 0 μM AKT inhibitor plus insulin. ɔɔ = p < 0.01.

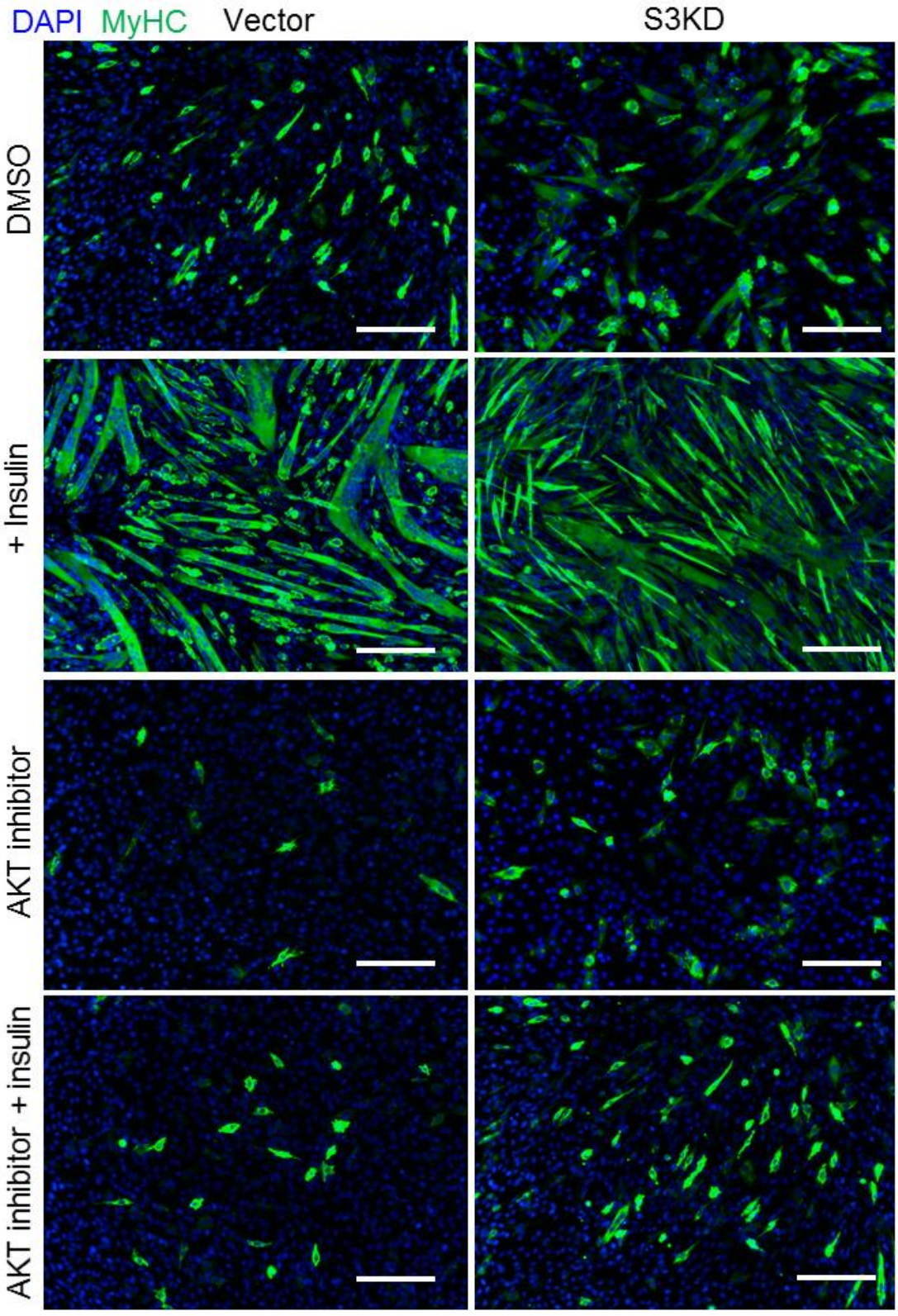

Figure 6.7: Representative images showing the effects of insulin stimulation and AKT inhibition on spontaneous differentiation of C2C12 myoblasts. Vector and SDC3 knock-down (S3KD) myoblasts were plated at a high density (~80%) and cultured in growth medium to measure spontaneous differentiation. Dimethyl sulfoxide (DMSO), insulin and/or AZD5363 (AKT inhibitor) were added to the growth medium couple of hours after plating and myoblasts were cultured for five days. Cells were fixed then stained to detect myosin heavy chain (MyHC, green) and DNA (DAPI, blue) to visualise late stage differentiation and nuclei respectively. Scale bar represents 200 µm.

6.2.5 The effects of SDC3 knock-down in C2C12 cells are recapitulated in primary satellite cell-derived cells

As discussed in *Chapter 4*, there are many similarities between C2C12 myoblasts and satellite cell-derived myoblasts making them a useful tool to study myogenesis. However, there are discrepancies between these two cell types therefore it is important to validate findings obtained using C2C12 cells in primary satellite cell-derived myoblasts. In the previous sections, significant differences were observed in the proliferation and differentiation of Vector and S3KD cells treated with insulin. Using primary mouse satellite cell-derived myoblasts the effects of SDC3-mediated insulin signalling on the proliferation, induced differentiation and spontaneous differentiation were validated.

Primary wild type and *Sdc3*$^{-/-}$ myoblasts were isolated from mice using the differential plating method and, after two days of expansion on gelatin-coated plates, were passaged for proliferation experiments. Myoblasts were treated with increasing concentrations of insulin for 24 hours, fixed and stained for DAPI to visualise nuclei. Random areas of the culture plates were imaged and the numbers of DAPI+ myoblasts were counted. Wild type myoblasts proliferated by up to 40% more when stimulated with insulin however this effect was only significant at 100 nM insulin (Fig. 6.8). In contrast, higher concentrations of insulin (200 nM) did not significantly increase proliferation of wild type myoblasts compared to the non-treated control. *Sdc3*$^{-/-}$ myoblasts did not proliferate more in response to insulin stimulation at any concentration (Fig. 6.8), indicating that SDC3 plays similar roles in insulin-mediated regulation of primary myoblast proliferation as it does in C2C12 myoblasts.

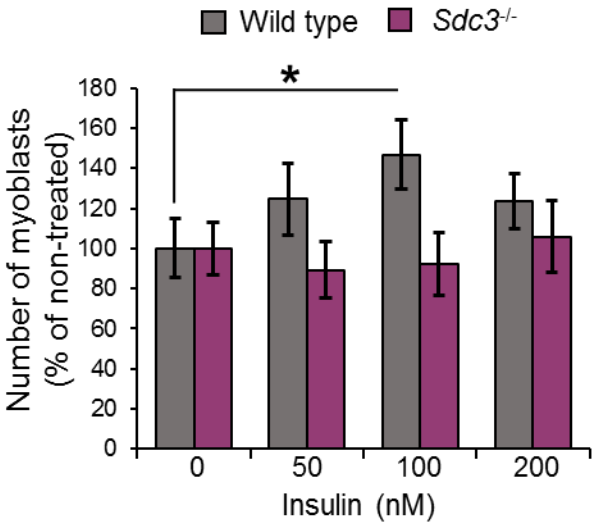

Figure 6.8: Wild type satellite cell-derived myoblasts proliferate more in response to insulin compared to *SDC3*$^{-/-}$ myoblasts. Myoblasts were cultured in growth medium for 24 hours with or without insulin. Myoblasts were then fixed and stained for DAPI to visualise nuclei. Random images were taken using a EVOS FL microscope and number of DAPI+ myoblasts counted. Quantification of 3 independent experiments is shown. Averages plotted ± SEM. * = $p < 0.05$.

Wild type and *Sdc3*$^{-/-}$ myoblasts were induced to differentiate for three days in the presence or absence of insulin. Only two insulin concentrations were used as not enough primary myoblasts could be obtained for a third condition. As the wild type myoblasts stopped proliferating in response to insulin at the highest dose, the two lower doses (50 nM and 100 nM) were used. Cells were fixed after three days in differentiation medium, stained with DAPI and to detect MyHC (Fig. 6.9) and differentiation and fusion index were calculated (Fig. 6.10). Wild type myoblasts significantly differentiated and fused more in response to serum reduction as described previously (Pisconti *et al.*, 2010) and also responded to insulin stimulation in a dose dependant manner (Fig. 6.10). However, insulin treatment promoted both differentiation and fusion in wild type and *Sdc3*$^{-/-}$ cells but to different extents. Wild type cells differentiated and fused significantly more in response to insulin whereas *Sdc3*$^{-/-}$ cells did not significantly differentiate more in response to insulin but did fuse more at the highest concentration of insulin treatment (Fig. 6.10B). This trend is the similar to that observed in C2C12 myoblasts where S3KD cells responded less to insulin treatment compared to Vector cells.

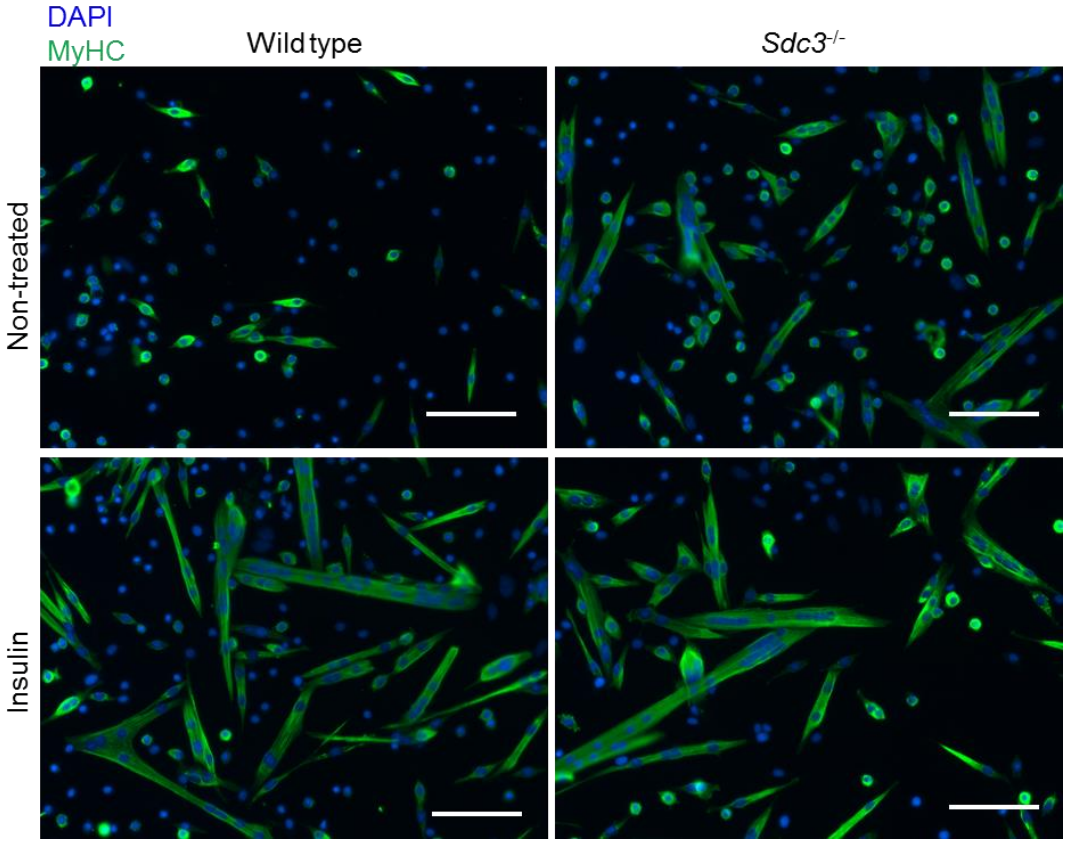

Figure 6.9: Representative images showing that insulin stimulation enhances myoblast differentiation. Myoblasts were cultured for two days before induced to differentiate for three days with or without 100 nM insulin. Cells were fixed then stained to detect myosin heavy chain (MyHC) and DNA (DAPI) to visualise late stage differentiation and nuclei respectively. Imaged on 20X magnification Scale bar represents 100 µm.

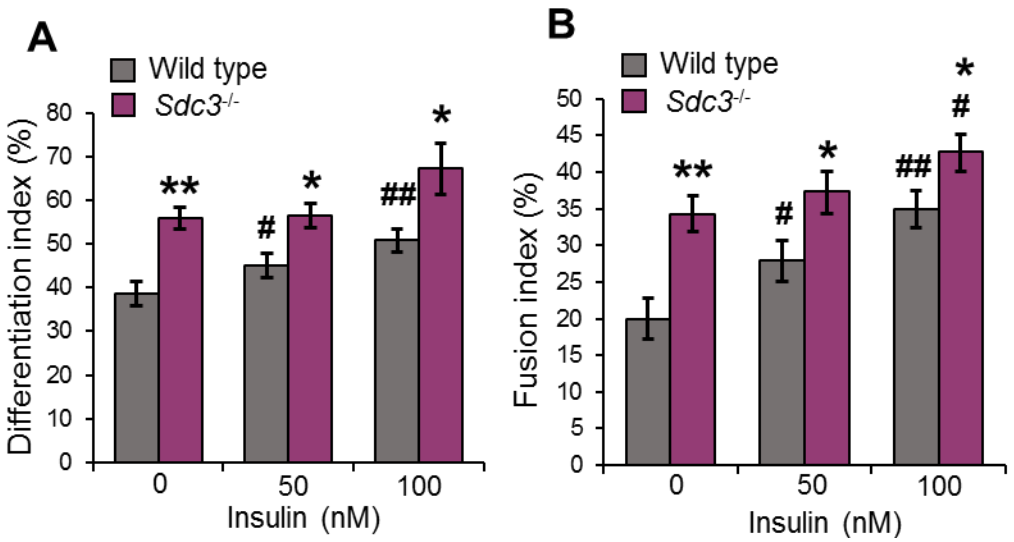

Figure 6.10: Insulin stimulation increases induced differentiation and fusion of wild type and *SDC3*$^{-/-}$ primary myoblasts at different extents. Quantification of three day differentiating cells with and without chronic insulin treatment (a minimum of 15 images were taken over 3 experiments, n = >45). Differentiation and fusion index were calculated from three independent experiments. Averages were plotted ± SEM. * represents the p-value of the differences between wild type and *SDC3*$^{-/-}$ myoblasts; * = $p < 0.05$; ** = $p < 0.01$. # represents the p-value of the differences between insulin-treated and non-treated cells; # = $p < 0.05$; ## = $p < 0.01$.

So far the phenotypes observed for SDC3-mediated proliferation and induced differentiation in response to insulin treatment are consistent between the C2C12 myoblast cell line and the primary myoblasts. Another key phenotype observed in C2C12 cells upon SDC3 knockdown is an AKT-dependent increase in spontaneous differentiation under growth conditions. Therefore to validate those results in primary cells, myoblasts were grown to confluence then treated with insulin and/or AKT inhibitor for two days. Cells were fixed then stained with DAPI and an anti-MyHC antibody (Fig. 6.11) then average differentiation and fusion index were calculated (Fig. 6.12). *Sdc3*$^{-/-}$ myoblasts spontaneously differentiated more than wild type myoblasts in an AKT-dependent manner (Fig. 6.12A). Additionally, as previously observed in C2C12 cell cultures, *Sdc3*$^{-/-}$ myoblasts differentiated less in response to insulin compared with wild type cells. (Fig. 6.12A).

The effect of insulin treatment on myoblast fusion was less clear (Fig. 6.12B). In wild type myoblasts insulin promoted fusion, which was not inhibited by the AKT inhibitor (Fig. 6.12B). This result was unexpected because in C2C12 myoblasts the AKT inhibitor does prevent fusion consequent to spontaneous differentiation (Fig. 6.6B). The AKT inhibitor did not significantly prevent fusion in the *Sdc3*$^{-/-}$ myoblasts either (Fig. 6.12B). In the absence of insulin and AKT inhibitor *Sdc3*$^{-/-}$ myoblasts fused significantly more than wild type myoblasts, which is consistent with observations in Vector and S3KD cells (Fig. 6.6) However, *Sdc3*$^{-/-}$ myoblasts did not fuse more in response to insulin, which contradicts previous observations in S3KD C2C12 myoblasts (Fig. 6.6B).

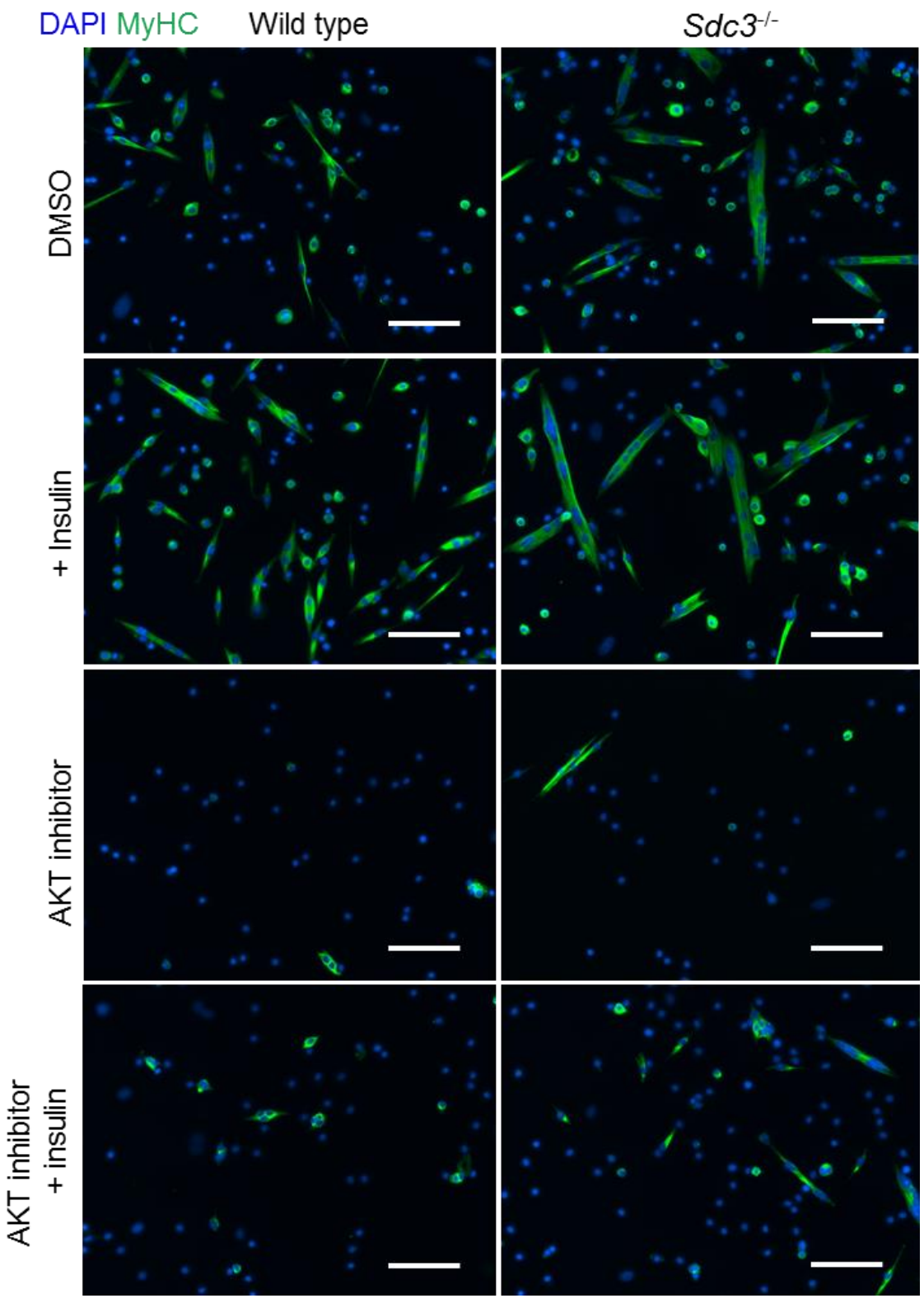

Figure 6.11 Representative images showing the effects of insulin stimulation and AKT inhibition on spontaneous differentiation in primary myoblasts. Myoblasts were cultured for two days in growth medium before FGF2 was removed and treatments were added for an additional two days. Cells were fixed then stained to detect myosin heavy chain (MyHC) and DNA (DAPI) to visualise late stage differentiation and nuclei respectively. Imaged on 20X magnification. Scale bar represents 100 µm.

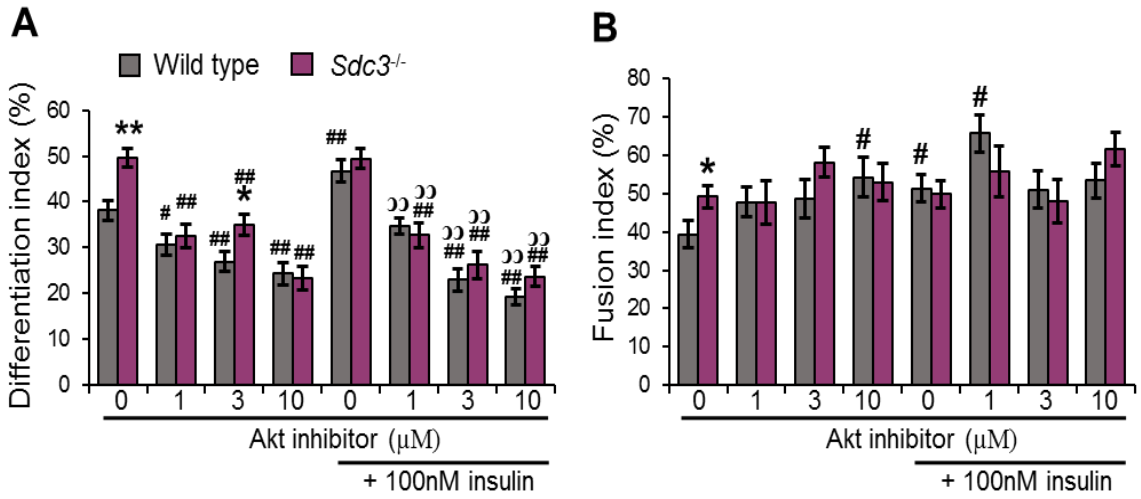

Figure 6.12: Quantification of spontaneous differentiation and fusion index in primary myoblasts in response to insulin and AKT inhibitor. Average of differentiation and fusion index for each condition was plotted ± SEM (A minimum of 15 images per experiment n = > 45). * represents the p-value of the differences between WT and *SDC3*$^{-/-}$ myoblasts; ** = p <0.01. # represents the p-value of the differences between AKT inhibitor and non-treated; # = p <0.05; ## = p <0.01. ɔ represents the p-value of the differences between AKT inhibitor plus insulin compared to 0 μM AKT inhibitor plus insulin. S3, SDC3 knockdown; ɔɔ = p <0.01. Quantification of three independent experiments.

The difference in fusion phenotype between the C2C12 myoblasts and the primary myoblasts seemed unusual and I hypothesised that the AKT inhibitor was added too late to the growth medium (only after cells had reached confluence), allowing time for a population of myoblasts to differentiate and fuse before the treatments were added. To test this hypothesis the spontaneous differentiation experiments were repeated but in this second experiment insulin and/or the AKT inhibitor were added only a few hours after plating. Due to time restraints this experiment could only be repeated with three wild type mice and one *Sdc3*$^{-/-}$ mouse. Additionally, fewer myoblasts were obtained from these myoblast preparations so I opted to only test the highest concentration of AKT inhibitor (10 μM). The preliminary results in Figure 6.13 show that inhibition of AKT leads to differentiation and fusion inhibition in both wild type and *Sdc3*$^{-/-}$ myoblasts when added at an earlier time point as hypothesised.

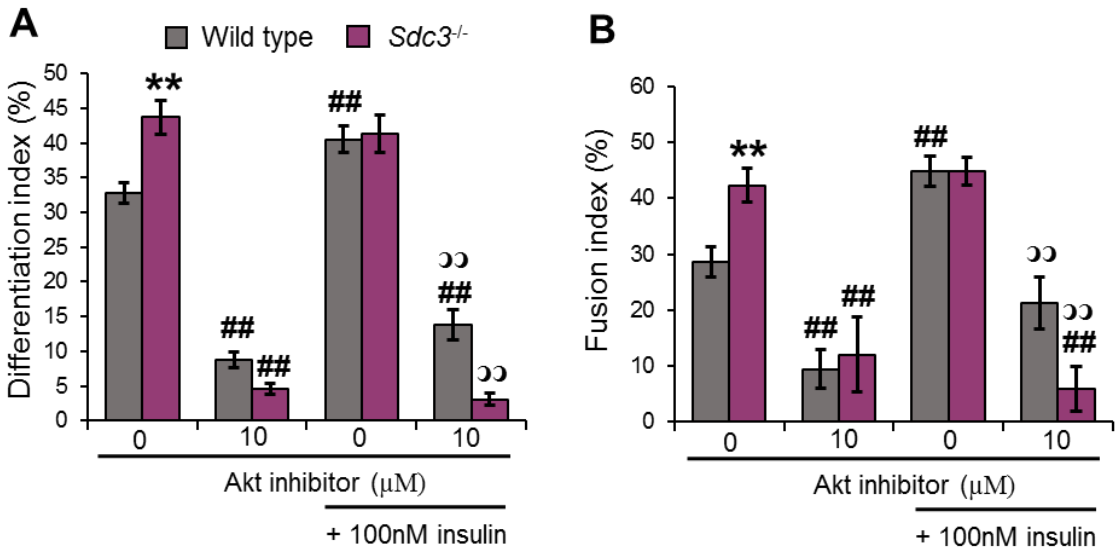

Figure 6.13: Quantification of spontaneous differentiation and fusion in primary myoblasts in response to insulin and AKT inhibitor. Myoblasts were cultured for two days in growth medium plus treatments (insulin and/or AKT inhibitor) before FGF2 was removed and myoblasts were cultured for an additional two days still in the presence/absence of insulin and/or AKT inhibitor. Cells were fixed then stained to detect myosin heavy chain (MyHC) and DNA (DAPI) to visualise late stage differentiation and nuclei respectively. Average of differentiation and fusion index for each condition was plotted with ± SEM. * represents the p-value of the differences between WT and *SDC3*$^{-/-}$ myoblasts; ** = p <0.01. # represents the p-value of the differences between AKT inhibitor and non-treated; ## = p <0.01. ↄ represents differences the p-value of the between AKT inhibitor plus insulin compared to 0 μM AKT inhibitor plus insulin.; ↄↄ = p <0.01. Quantification of three independent experiments (wild type), one experiment for *SDC3*$^{-/-}$

6.2.6 SDC3 knockdown regulates IRS1 phosphorylation in C2C12 myotubes

SDC1 and SDC3 are considered more homologous to each other than compared with the other syndecans (Couchman, 2003). Previous studies have shown that SDC1 and IGFR interact (Beauvais and Rapraeger, 2010) and given that IGFR and IR share considerable homology, I hypothesised that SDC3 may interact with IR. Moreover, I hypothesised that SDC3 knockdown caused an over-activation of the insulin receptor resulting in higher tyrosine kinase activity and subsequent increased downstream signalling. To test this hypothesis insulin-stimulated cells were lysed and lysates prepared for western blotting. An antibody that targets IGFR/IR pTyr was used to measure the pTyr of the insulin receptor. Unfortunately, after multiple attempts, no bands were visible corresponding to the pTyr insulin receptor either at basal levels or upon insulin stimulation (Appendix 4). However, the insulin receptor was expressed in Vector and S3KD cells as observed with a different antibody (Appendix 4).

One of the first proteins to be recruited and phosphorylated downstream of the insulin receptor in response to insulin is the adaptor protein IRS1 (Sun *et al.*, 1991). We used an antibody that recognises IRS1^{Y608} (human: IRS1^{Y612}) which is indicative of IRS1 activation in response to insulin and is required for full activation of Pi3K (Esposito et al., 2001). No change in phospho-IRS1^{Y608}/IRS1 was observed in either Vector or S3KD myoblasts during proliferation or in response to insulin treatment (Fig. 6.14). This was unexpected considering that Vector myoblasts proliferate in response to insulin (Fig. 6.2, 6.8) and that AKT phosphorylation is increased in both Vector and S3KD myoblasts in response to insulin (Fig. 6.3). The results obtained with differentiating myoblasts were even more confusing. In differentiating Vector and S3KD cells the levels of phospho-IRS1^{Y608} significantly decreased in response to insulin stimulation (Fig. 6.14). Additionally, non-treated S3KD myoblasts showed significantly reduced levels of phospho-IRS1^{Y608}/IRS1 levels, which is in contradiction with increased AKT phosphorylation observed in both Vector and S3KD differentiating myoblasts in response to insulin (Fig. 6.5).

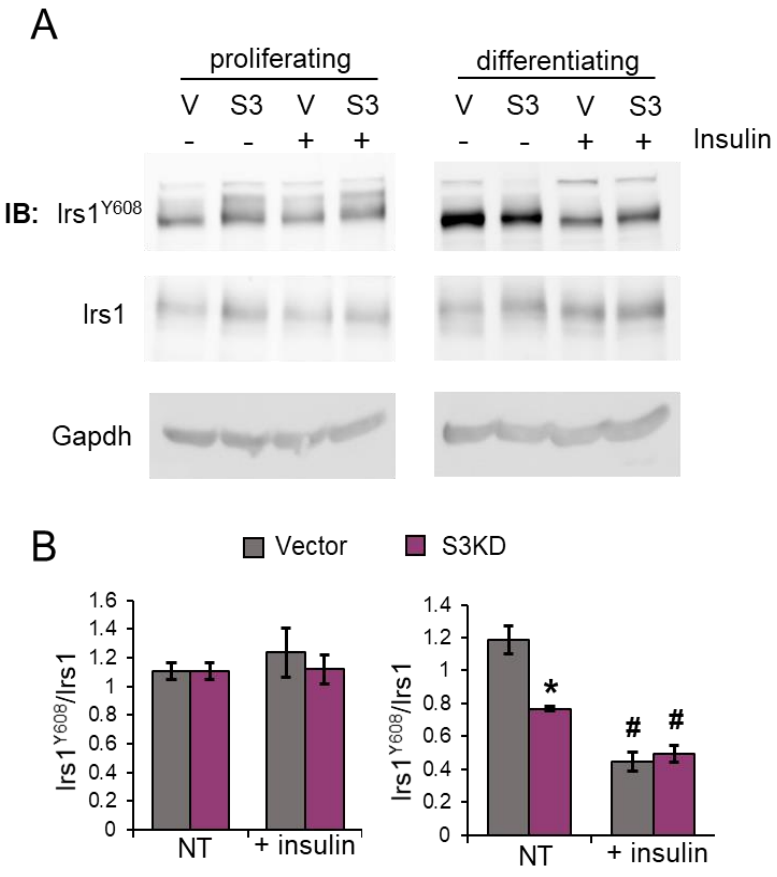

Figure 6.14: Effect of insulin stimulation on IRS1^{Y608} phosphorylation in Vector and S3KD cells. Proliferating and differentiating Vector and S3KD cells were chronically stimulated with insulin then lysed. (A) Proteins were separated by SDS-PAGE and analysed by western blotting to detect IRS1^{Y608}, IRS1 and GAPDH. (B) Quantification of three independent experiments. Averages plotted ± SEM. * represents the p-value of differences between Vector and S3KD myoblasts; * = p <0.05. # represents the p-value of differences between insulin-treated and non-treated; # = p <0.05.

These results appear contradictory with what was mentioned above because insulin signalling should promote IRS1 activation and phosphorylation of IRS1^{Y608} via the IR (Esposito *et al.*, 2001). Furthermore, I hypothesised that SDC3 was an inhibitor of the Insulin-AKT signalling pathway and I expected a greater increase in IRS1^{Y608} in S3KD cells stimulated with insulin compared to Vector cells. A possible explanation for this lies with the prolonged time of insulin treatment in these cells (48 hours for proliferating myoblasts and 72 hours for differentiating cells). Previous work has shown that prolonged treatment with insulin causes rapid loss of total pTyr IRS1 phosphorylation after approximately four hours (Sun *et al.*, 1999). Additionally, the protein levels of IRS1 eventually decline with prolonged insulin treatment although this is not as fast as the loss of initial pTyr IRS1 levels. Possibly, in low-serum conditions, insulin treatment eventually feeds-back to IRS1 and inhibits its Tyr phosphorylation. pIRS1 levels may have declined in S3KD cells in low serum conditions compared to Vector cells because of an over-activation of insulin-IRS1 signalling which in turn activates a negative feedback loop to inhibit further IRS1 signalling.

6.2.7 The insulin receptor and SDC3 might co-immunoprecipitate in myoblasts

The data in this chapter suggests that SDC3 knockdown in C2C12 myoblasts and knockout in primary myoblasts increases activation of the insulin/AKT signalling pathway, consequently promoting myoblast differentiation. SDC3 expression rapidly declines with the onset of differentiation in C2C12 myoblasts (Fuentealba*, et al.*, 1999) particularly between days 1 and 3 of induced differentiation (Appendix 5). Therefore, I hypothesised that SDC3 negatively regulates insulin signalling and therefore negatively regulates myoblast differentiation. This could be mediated by two possible mechanisms: 1) SDC3 might bind the insulin receptor via the core protein or heparan sulphate chains and inhibit receptor function, or 2) SDC3 might bind to and sequester insulin in the extracellular matrix preventing ligand binding. Previous studies have shown that heparan sulphate binds to the insulin receptor (Ori *et al.*, 2011) therefore I hypothesised that SDC3 may bind to the insulin receptor via its heparan sulphate chains and inhibit downstream signalling. To test this hypothesis fully glycosylated SDC3 was immunoprecipitated from parental C2C12 myoblasts and the resultant immunocomplexes were probed for IR by western blotting (Fig. 6.15A). Immunoprecipitation with a previously validated SDC3 antibody (Pisconti *et al.*, 2010) indicated that a band corresponding to the beta-subunit of insulin receptor (95 kDa) immunoprecipitated with SDC3. However, a fainter band at approximately the same molecular weight was also observed in the rabbit-IgG control. Three other bands were detected in the SDC3 immunoprecipitation, two of these did not correspond to any known Insulin receptor species but one ~220 kDa band corresponded to the uncleaved pro-receptor. To confirm that SDC3 was successfully immunoprecipitated, immunoblots were probed using the 3G10 antibody, which recognises a cleaved heparan sulphate stub on

proteoglycans and detects SDC3 in myoblasts at ~120 kDa after digestion with heparinase-III (Pisconti 2010). Additionally, a SDC3 antibody different from the one used to immunoprecipitate was also used to detect SDC3 in the immunocomplexes (Fig. 6.15A). No bands were detected using the SDC3 antibody apart from in the input lysate. However, the 3G10 antibody confirmed that SDC3 was present in the immunocomplexes, though at very low levels, which might have been below the threshold of detectability of the SDC3 antibody. Next, a reciprocal immunoprecipitation was performed using an insulin-receptor antibody followed by western blotting for SDC3 and 3G10 (Fig. 6.15B). This time SDC3 was recognised in the bead and rabbit IgG controls alongside the insulin receptor immunoprecipitation using the SDC3 and 3G10 antibodies suggesting a problem during immunoprecipitation might have occurred. However, more SDC3 was recognised in the insulin receptor immunoprecipitation compared to the controls and less SDC3 was observed in the unbound fraction of the insulin receptor immunoprecipitation, suggesting that a SDC3-IR interaction might indeed exist, however optimisation of the immunoprecipitation method is required to confirm this.

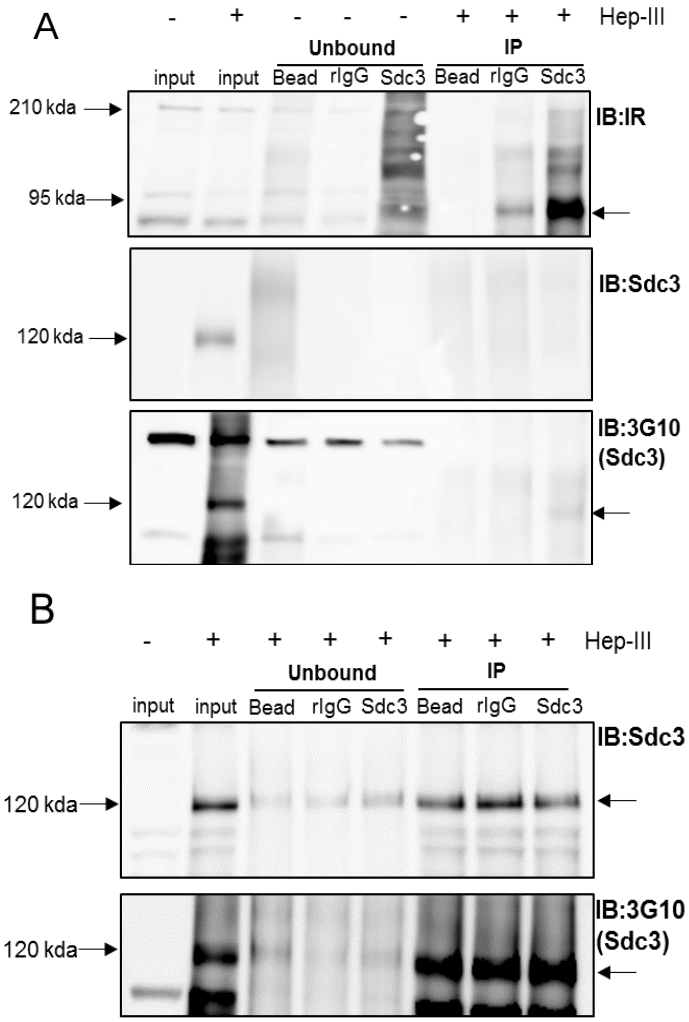

Figure 6.15: Immunoprecipitation of SDC3 and insulin receptor. Proliferating parental C2C12 myoblasts were cultured and lysed in HSPG buffer. Immunoprecipitation (IP) with **(A)** SDC3 antibody and **(B)** Insulin receptor antibody. 1 mg of C2C12 lysate was incubated with control beads, normal rabbit immunoglobulin (rIgG) or target antibody overnight. Immunocomplexes were collected and digested with heparinase III (Hep-III) then resolved by SDS-PAGE and transferred to PVDF membranes. Insulin receptor (IR), SDC3 or 3G10 proteins were detected by immunoblot (IB) analysis. Hep-III digested and non-digested input was used to identify heparan sulphate proteoglycans.

6.3 Discussion

The results in this chapter show that loss of SDC3 impairs insulin-mediated proliferation of C2C12 myoblasts and primary satellite cell-derived myoblasts, while promoting their differentiation. In proliferating myoblasts the addition of insulin promoted proliferation however when SDC3 was knocked out or down, myoblasts no longer proliferated in response to insulin, which suggested that SDC3 was required for IR-mediated signalling. However, insulin-mediated AKT phosphorylation was increased in insulin-stimulated S3KD myoblasts compared to insulin-stimulated Vector myoblasts, contradicting the hypothesis that SDC3 is required for IR signalling activation. Since the insulin/AKT pathway promotes differentiation in myoblasts and is increased in the absence of SDC3, I hypothesised that SDC3 inhibits myoblast differentiation via inhibiting insulin/AKT signalling. In the absence of SDC3, the insulin/AKT pathway is hyperactivated by the insulin present in the culture medium serum and promotes differentiation rather than proliferation. This would also explain why further stimulation with additional insulin potently promotes induced and spontaneous differentiation of Vector and WT myoblasts, whilst the response to insulin in S3KD and *Sdc3*$^{-/-}$ myoblasts is much smaller. I tested this hypothesis and validated it by using a selective AKT inhibitor.

The fact that insulin increased both proliferation and differentiation of Vector myoblasts was counter-intuitive as they are mutually exclusive events. This could be explained by assuming that SDC3 inhibits AKT activation or downstream signalling. In growth medium (high serum content) mitogenic growth factors are in high abundance and promote proliferation and supress differentiation (Fig. 6.16). In this context, SDC3 inhibits Insulin/AKT signalling, and therefore myoblast differentiation, which overall tips the balance to favour proliferation in growth medium (Fig. 6.16A). When Vector myoblasts are stimulated with insulin, again the pathway tries to activate both ERK1/2 and AKT, but AKT is inhibited by SDC3 and therefore this further promotes proliferation, possibly via ERK signalling, further blocking AKT activation and therefore differentiation (Fig. 6.16C). However, when SDC3 is lost insulin/AKT signalling is no longer being inhibited and therefore a small shift towards less proliferation and, possibly, beginning of spontaneous differentiation occurs (Fig. 6.16B and Chapter 4, Fig. 4.5, which is further exacerbated when S3KD cells are stimulated with insulin (Fig. 6.16D).

In differentiation medium, where there is a low serum content, the reduction in growth factors leads to a loss in proliferative ability of the myoblasts and instead differentiation is activated (Fig. 6.17A). Furthermore, SDC3 is downregulated in low serum medium (Appendix 5) increasingly alleviating the insulin/AKT inhibition and further promoting differentiation when the Vector myoblasts are treated with insulin (Fig. 6.17C). When SDC3

is lost via knockdown or knockout, the insulin/AKT pathway is no longer repressed allowing hyperactivation of insulin/AKT signalling pathway which further promotes differentiation (Fig. 6.17B). Lastly, insulin stimulation of S3KD cells yields a much smaller differentiative response in comparison to Vector cells because the insulin/AKT pathway is already hyperactivated in S3KD cells by insulin contained in the medium and upon addition of exogenous insulin a maximal response is obtained (Fig 6.17D).

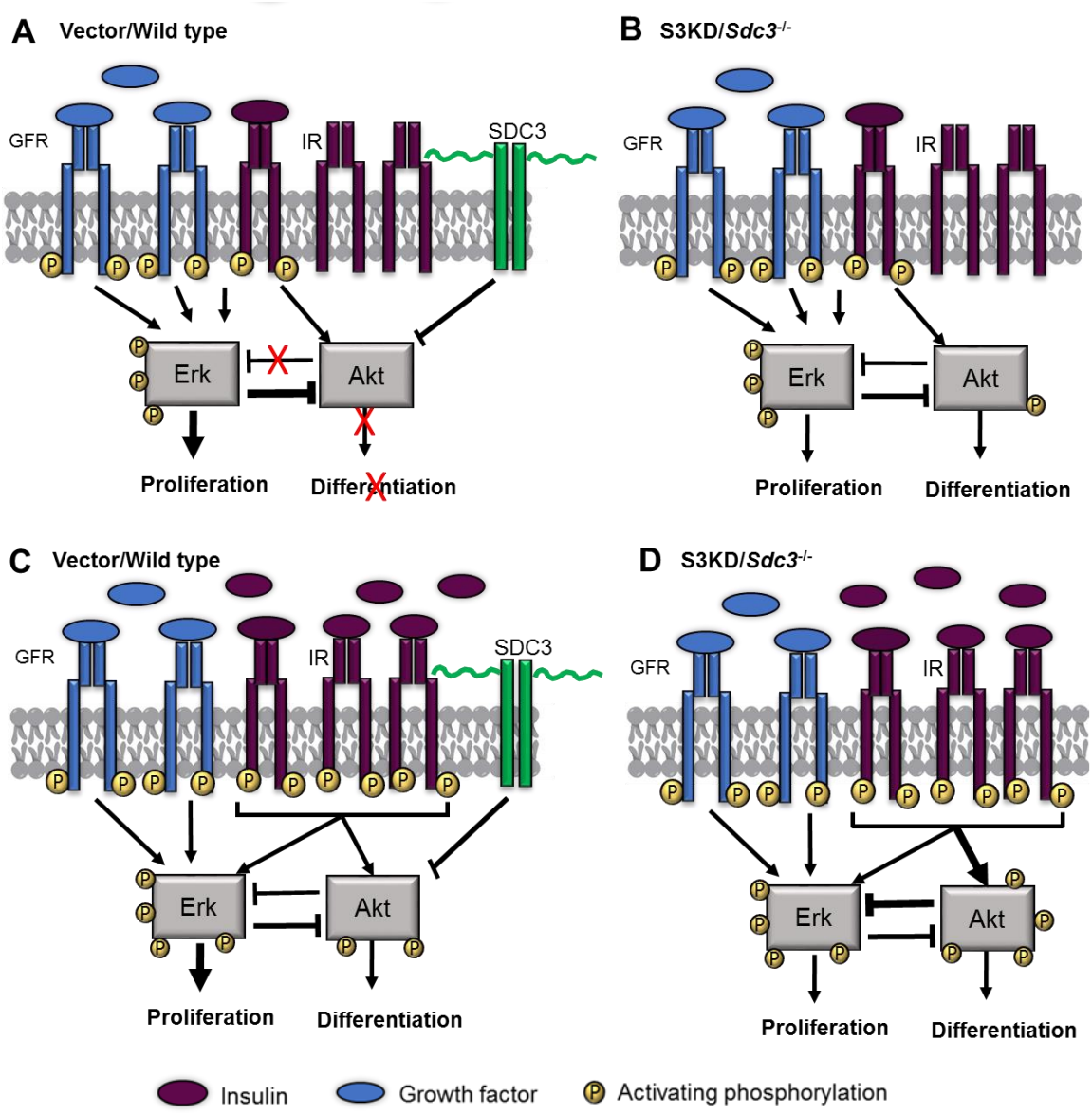

Figure 6.16: Working model depicting SDC3-mediated regulation of myoblast function in high serum conditions. (A) In Vector cell cultures, growth factors from the serum promote proliferation whilst suppressing differentiation. SDC3 inhibits insulin/AKT-mediated differentiation. **(B)** Loss of SDC3 no longer inhibits AKT but growth factors promote proliferation although now to a lesser extent since AKT inhibits ERK1/2 and promotes differentiation. **(C)** Addition of insulin increases proliferation in Vector cells as SDC3 stills blocks insulin/AKT-mediated myoblast differentiation. **(D)** Loss of SDC3 allows strong activation of AKT but proliferation/differentiation is balanced by other growth factors in the serum resulting in no increase in proliferation and the onset of differentiation in a small percentage of cells, despite the high concentration of growth factors. Key: IR = insulin receptor, GFR = growth factor receptor, P = phosphorylation of the same phosphorylated residue, leading to activation of downstream signalling.

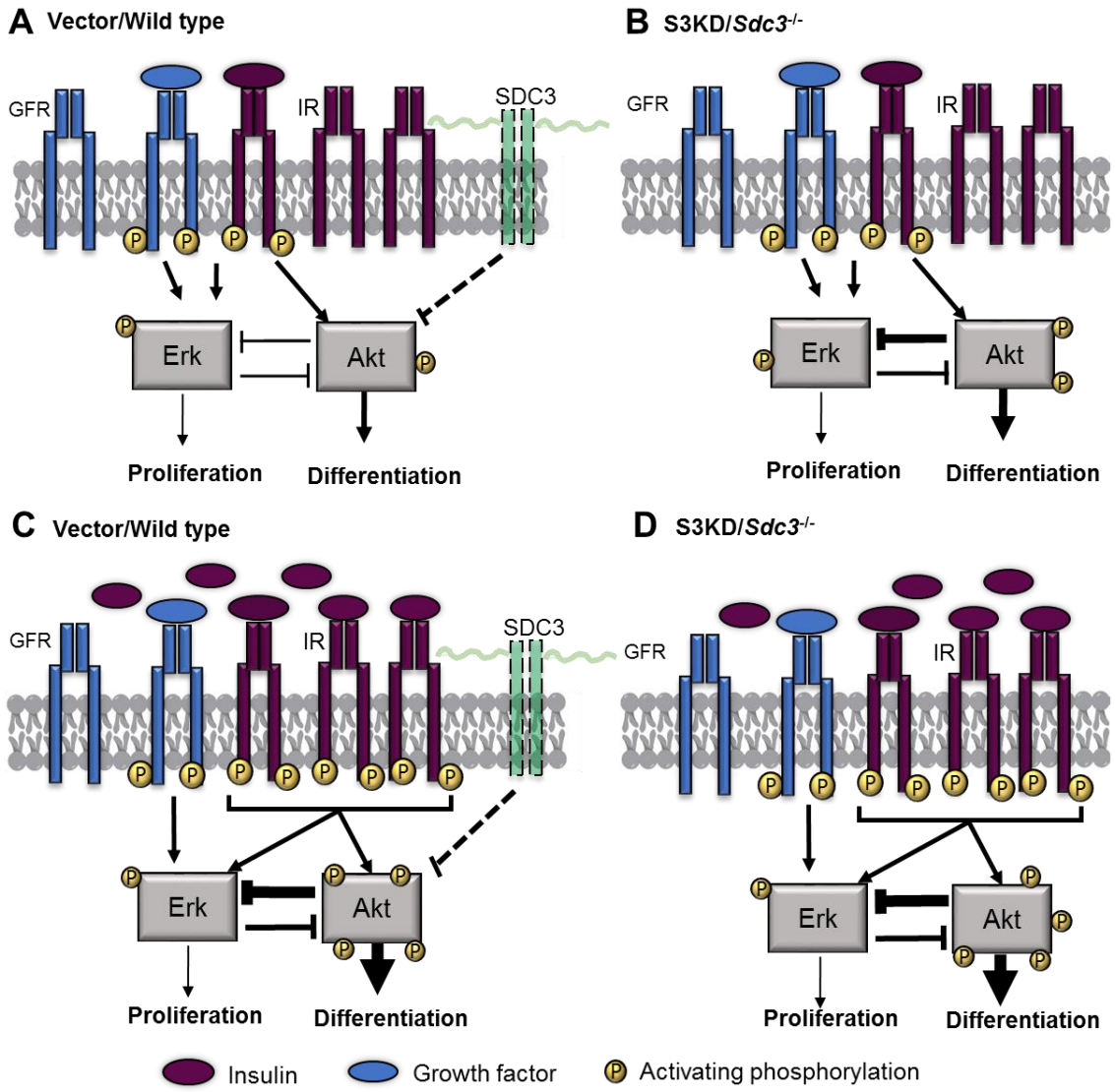

Figure 6.17: Working model depicting SDC3-mediated regulation of myoblast function in low serum conditions. (A) In Vector cells SDC3 becomes downregulated in response to serum reduction (depicted here as semi-transparent) and inhibition of insulin/AKT signalling is lessened (depicted as a dotted line). Fewer growth factors in the serum promote proliferation and differentiation can take place. **(B)** Complete or near complete loss of SDC3 leads to increased activation of insulin/AKT signalling further promoting differentiation. **(C)** Addition of insulin to Vector cells promotes differentiation as growth factors are no longer able to support proliferation and as SDC3 expression declines SDC3is less able to inhibit insulin/AKT signalling. **(D)** Loss of SDC3 completely removes inhibition of insulin/AKT signalling and promotes differentiation as in (C). Key: IR = insulin receptor, RTK = receptor tyrosine kinase, P = phosphorylation of the same phosphorylated residue, leading to activation of downstream signalling.

Insulin is known to activate both the MAPK pathway and the PI3K/AKT pathway upon binding to the IR (Boucher *et al.*, 2014). Insulin treatment of both S3KD and Vector myoblasts activated AKT in both proliferating and differentiating cells. In contrast, ERK1/2 activation was not increased in response to insulin stimulation in either Vector or S3KD myoblasts. This was unexpected due to the increased proliferation observed in Vector myoblasts and ERK1/2's role in promotion of proliferation in myoblasts (Jones *et al.*, 2001).

Studies have shown that stimulation of myoblasts with IGFs, which share homology with insulin and can stimulate the insulin receptor, initially promote myoblast proliferation via increased ERK1/2 phosphorylation but then, later in time, promotes differentiation via downregulation of ERK1/2 activity, suggesting temporal regulation of IGF/ERK-1/2 signalling is important to promote proliferation followed by differentiation in myoblasts (Engert *et al.*, 1996, Wu *et al.*, 2000, Adi *et al.*, 2002). As no increase in ERK1/2 phosphorylation was observed when Vector and S3KD myoblasts were stimulated with insulin it is possible that insulin does not stimulate proliferation of C2C12 myoblasts via the ERK1/2 signalling pathway and that perhaps other pathways are involved in stimulating myoblast proliferation in response to insulin such as p38 MAPK which is required for proliferation and inhibition of differentiation (Jones *et al.*, 2005, Gillespie *et al.*, 2009). Alternatively, previous studies show that the loss of SDC3 hyperactivated the FGF2 signalling pathway (*Chapter 4*, Fig. 4.3 and (Cornelison *et al.*, 2004)) and results from the phosphoproteomics analysis shows that ERK1/2 was rapidly phosphorylated after 10 minutes of serum stimulation (*Chapter 5*, Table 5.3), suggesting ERK activation is a fast event and differences in ERK phosphorylation may not be found with chronic treatment of insulin.

Other factors that may influence insulin-mediated differentiation include cell adhesion as previous experiments have shown that integrins bind to IR and IRS1 upon insulin stimulation to mediate insulin signalling and promote proliferation (Vuori and Ruoslahti, 1994, Schneller *et al.*, 1997). Additionally insulin induces dephosphorylation of focal adhesion kinase (FAK) in adherent cells and FAK/IRS1 have been shown to interact, which strongly suggests co-operation of insulin and integrin signalling (El Annabi *et al.*, 2001). Loss of SDC3 perturbs satellite cell adhesion to myofibres (Pisconti *et al*., 2016) and S3KD cell adhesion to laminin-coated dishes (*Chapter 4*, Fig. 4.8), and increases differentiation (Pisconti *et al*., 2010, Chapter 4 Fig. 4.6). Thus, it is possible that SDC3 might regulate an insulin/integrin signalling cross-talk as the other syndecans can co-operate with integrins to mediate cell adhesion to the ECM (Conejo *et al.*, 2001, Hozumi *et al.*, 2006, Pisconti *et al.*, 2016). Moreover, it is known that SDC1 forms a ternary complex with IGFR and integrin αvβ3 in human mammary carcinoma cells (Beauvais and Rapraeger, 2010), which suggest that a similar ternary complex might involve the homologous SDC3, IR and an integrin dimer. Partially successful co-immunoprecipitation of SDC3 and IR supports this idea, however, further optimisation of the immunoprecipitation protocol is necessary to confirm an interaction between SDC3 and IR. A hypothetical model may include an integrin/IR/SDC3 interaction in myoblasts that promotes proliferation in response to insulin; when SDC3 is lost this interaction is impaired and differentiation is promoted via AKT. SDC3/IR in complex may prevent differentiation by inhibiting IRS1/AKT signalling as I

previously observed significant changes in the phosphorylation and total levels of IRS1 (*Chapter 5*).

As this part of the project progressed it became apparent that there were some experimental limitations. Firstly the AKT inhibitor used (AZD5363) potently inhibits all three isoforms of AKT which is useful to prevent all AKT-mediated downstream signalling however previous studies have shown differences in biological function of Akt1 and Akt2 in skeletal muscle differentiation (Rotwein and Wilson, 2009). It is possible that SDC3 exerts its effect on one isoform or the other but this could not be distinguished with the pAkt antibody used or the AKT inhibitor. Additionally, AZD5363 can also produce off-target effects by inhibiting ROCK2, which is involved in several processes such as cell adhesion, focal adhesion formation and regulation of the ERK1/2 signalling pathway during myogenic differentiation (Pelosi *et al.*, 2007). Considering the adhesion phenotypes observed in S3KD myoblasts, this inhibitor may disrupt several other signalling pathways that are important for myoblast function. Although, the potency of ROCK2 inhibition is approximately 20 times lower than AKT inhibition (Davies *et al.*, 2012), it may still be prudent to corroborate existing data with the use of an alternative AKT inhibitor.

In conclusion, the results in this chapter show that insulin stimulates proliferation and differentiation of C2C12 myoblasts and primary satellite cell-derived myoblasts. However when SDC3 is lost, insulin fails to promote myoblast proliferation but rather enhances differentiation in an AKT-dependent manner, suggesting that SDC3 negatively regulates insulin signalling, prominently via inhibition of AKT.

Chapter 7

Concluding remarks

Syndecans are complex macromolecules involved in regulating several signalling pathways including: growth factors, hormones, cytokines, cell-cell and cell-matrix adhesion. Many of the molecular mechanisms, particularly those involving the syndecan core proteins, are still not fully understood (De Rossi and Whiteford, 2013) The structural complexity of heparan sulphate only adds to the difficulty in understanding syndecan-mediated signalling events as different cell types, or the same cell type in different physiological contexts, produce different heparan sulphate structures, which in turn affect ligand-binding specificity (Turnbull *et al.*, 2001, Ghadiali *et al.*, 2017)

This project set out to uncover how SDC3 regulates myoblast cell signalling. Using an unbiased phosphoproteomics approach several changes in the phosphoproteome of S3KD myoblasts were discovered. The work completed in this project gives an overview of the complexity of the SDC3 interactome but equally has opened the door for further investigation of SDC3-mediated signalling in the regulation of myogenesis. Particularly, the scale of the phosphoproteomic analysis has left much more of the SDC3 functional interactome to be uncovered in the future.

Throughout the chapters presented in this thesis several open-ended lines of investigation were identified. In *Chapter 4*, I observed an adhesion phenotype where S3KD myoblasts adhered more to uncoated culture plates compared to Vector myoblasts. However, adhesion of S3KD myoblasts to laminin was significantly reduced. Furthermore, in *Chapter 5* several phosphoproteins involved in 'cell adhesion', 'cadherin binding in cell-cell adhesion' and 'actin binding' were differentially phosphorylated in S3KD myoblasts compared to Vector myoblasts. Suggesting that SDC3 is involved in regulating cell-cell and cell-cytoskeleton adhesion. Phosphoproteins involved in activation of integrin signalling were significantly enriched in serum-starved S3KD myoblasts suggesting that SDC3 is directly involved in integrin signalling and therefore cell-matrix adhesion. Together these three pieces of information provide a strong case for investigating SDC3/integrin signalling and myoblast adhesion. Particularly it would be interesting to test for SDC3-mediated

differences in myoblast adhesion to other substrates found within the satellite cell niche, such as collagen type IV and fibronectin.

Further investigation revealed that SDC3 knockdown prominently affects the insulin signalling pathway and that SDC3 likely plays a role in inhibiting the insulin/AKT pathway. In the short-term a few experiments to confirm whether SDC3 and IR are in complex would be beneficial, as this would help determine the mechanism by which SDC3 inhibits insulin signalling; is this a direct interaction with IR or via IR-adaptor proteins? Optimisation of SDC3 immunoprecipitations would be the first step but alternative methods such as Proximity Ligation Assay (Fredriksson *et al.*, 2002) could be used instead, as these can be used on intact myoblasts to confirm if SDC3 and IR are in complex on the plasma membrane. In *Chapter 6* I showed that the insulin signalling pathway is regulated by SDC3 but how this affects the metabolism of myoblasts is unknown. Insulin stimulates transport of glucose receptors to the cell membrane and increases glucose uptake in the cells (Siddle 2011). Therefore, it is likely that if the insulin signalling pathway is hyperactivated in S3KD and *Sdc3*$^{-/-}$ myoblasts then consequently glucose uptake will also be increased. This might also provide a better method to measure the activity of the insulin signalling pathway than quantifying the changes in IRS1 and AKT phosphorylation or IRS1 protein abundance.

An outstanding question remains: How does insulin signalling regulate two mutually exclusive biological processes such as proliferation and differentiation? It has been previously shown that the downstream effects of insulin signalling undergo a temporal switch from supporting proliferation at early time points after plating myoblasts to supporting differentiation at later time points (Conejo*, et al.*, 2001, Grabiec*, et al.*, 2014). However, how this switch is regulated is not known. The data presented in this thesis suggest that SDC3 might regulate this switch since SDC3 inhibits AKT-induced differentiation in proliferating myoblasts but is then downregulated during differentiation and therefore is no longer able to inhibit AKT signalling, allowing the progression of differentiation. Additionally, during proliferation it is likely that SDC3 acts as a co-receptor for several receptors/signalling pathways that support proliferation, such as Notch (Pisconti et al., 2010), FGF2 (Fuentealba *et al.*, 1999, Cornelison *et al.*, 2004), HGF (Cornelison *et al.*, 2004) possibly also TGFβ and EGF signalling pathways, which were identified here in the phosphoproteomics analysis as significantly regulated by SDC3 knockdown. Since TGFβ signalling is a potent inhibitor of differentiation (Schabort *et al.*, 2009) and EGF signalling controls both proliferation and differentiation (Leroy *et al.*, 2013, Figeac *et al.*, 2014), it is likely that AKT inhibition mediated by SDC3 during proliferation is the result of SDC3 regulating several signalling pathways simultaneously.

Another important question that stems from this project is: how does myoblast metabolism regulation cross-talk with regulation of differentiation? Previous studies have shown that the presence of high glucose concentrations are required to promote insulin-mediated myoblast proliferation and differentiation, yet high glucose conditions are not required for IGF-mediated myoblast proliferation and differentiation (Grabiec *et al.*, 2014), suggesting the insulin signalling relies heavily on nutrient availability. Our data seem to suggest that this cross-talk might be regulated by the insulin/SDC3 axis and warrants further investigation to address the questions that remain open. Previous studies have suggested a role for SDC3 in energy balance, food intake and obesity in mice (Reizes *et al.*, 2003). Therefore, how myoblast function is affected by nutrient availability and metabolic changes in combination with loss of SDC3 could be an interesting path to follow in the future.

References

Abmayr, S.M. & Pavlath, G.K. (2012) Myoblast fusion: lessons from flies and mice *Development* **139**, 641-56

Adi, S., Bin-Abbas, B., Wu, N.Y. & Rosenthal, S.M. (2002) Early stimulation and late inhibition of extracellular signal-regulated kinase 1/2 phosphorylation by IGF-I: a potential mechanism mediating the switch in IGF-I action on skeletal muscle cell differentiation *Endocrinology* **143**, 511-6

Alema, S. & Salvatore, A.M. (2007) p120 catenin and phosphorylation: Mechanisms and traits of an unresolved issue *Biochimica et biophysica acta* **1773**, 47-58

Alessi, D.R., James, S.R., Downes, C.P., Holmes, A.B., Gaffney, P.R., Reese, C.B. & Cohen, P. (1997) Characterization of a 3-phosphoinositide-dependent protein kinase which phosphorylates and activates protein kinase Balpha *Current biology : CB* **7**, 261-9

Allouh, M.Z., Yablonka-Reuveni, Z. & Rosser, B.W. (2008) PAX7 reveals a greater frequency and concentration of satellite cells at the ends of growing skeletal muscle fibers *The journal of histochemistry and cytochemistry : official journal of the Histochemistry Society* **56**, 77-87

Allsopp, R.C., Vaziri, H., Patterson, C., Goldstein, S., Younglai, E.V., Futcher, A.B., Greider, C.W. & Harley, C.B. (1992) Telomere length predicts replicative capacity of human fibroblasts *Proceedings of the National Academy of Sciences of the United States of America* **89**, 10114-8

Amanchy, R., Periaswamy, B., Mathivanan, S., Reddy, R., Tattikota, S.G. & Pandey, A. (2007) A curated compendium of phosphorylation motifs *Nature biotechnology* **25**, 285-6

Arecco, N., Clarke, C.J., Jones, F.K., Simpson, D.M., Mason, D., Beynon, R.J. & Pisconti, A. (2016) Elastase levels and activity are increased in dystrophic muscle and impair myoblast cell survival, proliferation and differentiation *Scientific reports* **6**, 24708

Aricescu, A.R., McKinnell, I.W., Halfter, W. & Stoker, A.W. (2002) Heparan sulfate proteoglycans are ligands for receptor protein tyrosine phosphatase sigma *Molecular and cellular biology* **22**, 1881-92

Arnold, L., Henry, A., Poron, F., Baba-Amer, Y., van Rooijen, N., Plonquet, A., Gherardi, R.K. & Chazaud, B. (2007) Inflammatory monocytes recruited after skeletal muscle injury switch into antiinflammatory macrophages to support myogenesis *The Journal of experimental medicine* **204**, 1057-69

Asakura, A., Komaki, M. & Rudnicki, M. (2001) Muscle satellite cells are multipotential stem cells that exhibit myogenic, osteogenic, and adipogenic differentiation *Differentiation; research in biological diversity* **68**, 245-53

Asp, P., Blum, R., Vethantham, V., Parisi, F., Micsinai, M., Cheng, J., Bowman, C., Kluger, Y. & Dynlacht, B.D. (2011) Genome-wide remodeling of the epigenetic landscape during myogenic differentiation *Proceedings of the National Academy of Sciences of the United States of America* **108**, E149-58

Astudillo, P., Carrasco, H. & Larraín, J. (2014) Syndecan-4 inhibits Wnt/β-catenin signaling through regulation of low-density-lipoprotein receptor-related protein (LRP6) and R-spondin 3. *The International Journal of Biochemistry & Cell Biology* **46**,103-112

Asundi, V.K. & Carey, D.J. (1995) Self-association of N-syndecan (syndecan-3) core protein is mediated by a novel structural motif in the transmembrane domain and ectodomain flanking region *The Journal of biological chemistry* **270**, 26404-10

Bailyes, E.M., Nave, B.T., Soos, M.A., Orr, S.R., Hayward, A.C. & Siddle, K. (1997) Insulin receptor/IGF-I receptor hybrids are widely distributed in mammalian tissues: quantification of individual receptor species by selective immunoprecipitation and immunoblotting *The Biochemical journal* **327 (Pt 1)**, 209-15

Bass, M.D., Morgan, M.R., Roach, K.A., Settleman, J., Goryachev, A.B. & Humphries, M.J. (2008) p190RhoGAP is the convergence point of adhesion signals from alpha 5 beta 1 integrin and syndecan-4 *J Cell Biol* **181**, 1013-26

Bass, M.D., Roach, K.A., Morgan, M.R., Mostafavi-Pour, Z., Schoen, T., Muramatsu, T., Mayer, U., Ballestrem, C., Spatz, J.P. & Humphries, M.J. (2007) Syndecan-4-dependent Rac1 regulation determines directional migration in response to the extracellular matrix *J Cell Biol* **177**, 527-38

Beausoleil, S.A., Villen, J., Gerber, S.A., Rush, J. & Gygi, S.P. (2006) A probability-based approach for high-throughput protein phosphorylation analysis and site localization *Nature biotechnology* **24**, 1285-92

Beauvais, D.M., Burbach, B.J. & Rapraeger, A.C. (2004) The syndecan-1 ectodomain regulates alphavbeta3 integrin activity in human mammary carcinoma cells *J Cell Biol* **167**, 171-81

Beauvais, D.M. & Rapraeger, A.C. (2003) Syndecan-1-mediated cell spreading requires signaling by alphavbeta3 integrins in human breast carcinoma cells *Experimental cell research* **286**, 219-32

Beauvais, D.M. & Rapraeger, A.C. (2010) Syndecan-1 couples the insulin-like growth factor-1 receptor to inside-out integrin activation *Journal of cell science* **123**, 3796-807

Belfiore, A., Frasca, F., Pandini, G., Sciacca, L. & Vigneri, R. (2009) Insulin receptor isoforms and insulin receptor/insulin-like growth factor receptor hybrids in physiology and disease *Endocrine reviews* **30**, 586-623

Bentzinger, C.F., Wang, Y.X., Dumont, N.A. & Rudnicki, M.A. (2013) Cellular dynamics in the muscle satellite cell niche *EMBO reports* **14**, 1062-72

Berggard, T., Linse, S. & James, P. (2007) Methods for the detection and analysis of protein-protein interactions *Proteomics* **7**, 2833-42

Bernfield, M., Gotte, M., Park, P.W., Reizes, O., Fitzgerald, M.L., Lincecum, J. & Zako, M. (1999) Functions of cell surface heparan sulfate proteoglycans *Annual review of biochemistry* **68**, 729-77

Biever, A., Valjent, E. & Puighermanal, E. (2015) Ribosomal Protein S6 Phosphorylation in the Nervous System: From Regulation to Function *Frontiers in molecular neuroscience* **8**, 75

Bjornson, C.R., Cheung, T.H., Liu, L., Tripathi, P.V., Steeper, K.M. & Rando, T.A. (2012) Notch signaling is necessary to maintain quiescence in adult muscle stem cells *Stem cells* **30**, 232-42

Blais, A., Tsikitis, M., Acosta-Alvear, D., Sharan, R., Kluger, Y. & Dynlacht, B.D. (2005) An initial blueprint for myogenic differentiation *Genes & development* **19**, 553-69

Blau, H.M., Webster, C., Chiu, C.P., Guttman, S. & Chandler, F. (1983) Differentiation properties of pure populations of human dystrophic muscle cells *Experimental cell research* **144**, 495-503

Boldrin, L., Muntoni, F. & Morgan, J.E. (2010) Are human and mouse satellite cells really the same? *The journal of histochemistry and cytochemistry : official journal of the Histochemistry Society* **58**, 941-55

Boonsanay, V., Zhang, T., Georgieva, A., Kostin, S., Qi, H., Yuan, X., Zhou, Y. & Braun, T. (2016) Regulation of Skeletal Muscle Stem Cell Quiescence by Suv4-20h1-Dependent Facultative Heterochromatin Formation *Cell stem cell* **18**, 229-42

Boucher, J., Kleinridders, A. & Kahn, C.R. (2014) Insulin receptor signaling in normal and insulin-resistant states *Cold Spring Harbor perspectives in biology* **6**,

Brack, A.S., Conboy, I.M., Conboy, M.J., Shen, J. & Rando, T.A. (2008) A temporal switch from notch to Wnt signaling in muscle stem cells is necessary for normal adult myogenesis *Cell stem cell* **2**, 50-9

Brandan, E. & Gutierrez, J. (2013) Role of skeletal muscle proteoglycans during myogenesis *Matrix biology : journal of the International Society for Matrix Biology* **32**, 289-97

Brunetti, A., Maddux, B.A., Wong, K.Y. & Goldfine, I.D. (1989) Muscle cell differentiation is associated with increased insulin receptor biosynthesis and messenger RNA levels *The Journal of clinical investigation* **83**, 192-8

Buckingham, M. (2007) Skeletal muscle progenitor cells and the role of Pax genes *Comptes rendus biologies* **330**, 530-3

Burattini, S., Ferri, P., Battistelli, M., Curci, R., Luchetti, F. & Falcieri, E. (2004) C2C12 murine myoblasts as a model of skeletal muscle development: morpho-functional characterization *European journal of histochemistry : EJH* **48**, 223-33

Bustos, F., de la Vega, E., Cabezas, F., Thompson, J., Cornelison, D.D., Olwin, B.B., Yates, J.R., 3rd & Olguin, H.C. (2015) NEDD4 Regulates PAX7 Levels Promoting Activation of the Differentiation Program in Skeletal Muscle Precursors *Stem cells* **33**, 3138-51

Carey, D.J., Evans, D.M., Stahl, R.C., Asundi, V.K., Conner, K.J., Garbes, P. & Cizmeci-Smith, G. (1992) Molecular cloning and characterization of N-syndecan, a novel transmembrane heparan sulfate proteoglycan *J Cell Biol* **117**, 191-201

Casar, J.C., Cabello-Verrugio, C., Olguin, H., Aldunate, R., Inestrosa, N.C. & Brandan, E. (2004) Heparan sulfate proteoglycans are increased during skeletal muscle regeneration: requirement of syndecan-3 for successful fiber formation *Journal of cell science* **117**, 73-84

Cavalheiro, R.P., Lima, M.A., Jarrouge-Boucas, T.R., Viana, G.M., Lopes, C.C., Coulson-Thomas, V.J., Dreyfuss, J.L., Yates, E.A., Tersariol, I.L.S. & Nader, H.B. (2017) Coupling of vinculin to F-actin demands Syndecan-4 proteoglycan *Matrix biology : journal of the International Society for Matrix Biology* **63**, 23-37

Chakravarthy, M.V., Abraha, T.W., Schwartz, R.J., Fiorotto, M.L. & Booth, F.W. (2000) Insulin-like growth factor-I extends in vitro replicative life span of skeletal muscle satellite cells by enhancing G1/S cell cycle progression via the activation of phosphatidylinositol 3'-kinase/AKT signaling pathway *The Journal of biological chemistry* **275**, 35942-52

Chang, H.Y., Chi, J.T., Dudoit, S., Bondre, C., van de Rijn, M., Botstein, D. & Brown, P.O. (2002) Diversity, topographic differentiation, and positional memory in human fibroblasts *Proceedings of the National Academy of Sciences of the United States of America* **99**, 12877-82

Chazaud, B., Sonnet, C., Lafuste, P., Bassez, G., Rimaniol, A.C., Poron, F., Authier, F.J., Dreyfus, P.A. & Gherardi, R.K. (2003) Satellite cells attract monocytes and use macrophages as a support to escape apoptosis and enhance muscle growth *J Cell Biol* **163**, 1133-43

Chen, E., Hermanson, S. & Ekker, S.C. (2004) Syndecan-2 is essential for angiogenic sprouting during zebrafish development *Blood* **103**, 1710-9

Chen, K. & Williams, K.J. (2013) Molecular mediators for raft-dependent endocytosis of syndecan-1, a highly conserved, multifunctional receptor *The Journal of biological chemistry* **288**, 13988-99

Chernousov, M.A. & Carey, D.J. (1993) N-syndecan (syndecan 3) from neonatal rat brain binds basic fibroblast growth factor *The Journal of biological chemistry* **268**, 16810-4

Chevallet, M., Luche, S. & Rabilloud, T. (2006) Silver staining of proteins in polyacrylamide gels *Nature protocols* **1**, 1852-8

Choi, S., Kim, Y., Park, H., Han, I.O., Chung, E., Lee, S.Y., Kim, Y.B., Lee, J.W., Oh, E.S. & Yi, J.Y. (2009) Syndecan-2 overexpression regulates adhesion and migration through cooperation with integrin alpha2 *Biochemical and biophysical research communications* **384**, 231-5

Choi, S., Lee, E., Kwon, S., Park, H., Yi, J.Y., Kim, S., Han, I.O., Yun, Y. & Oh, E.S. (2005) Transmembrane domain-induced oligomerization is crucial for the functions of syndecan-2 and syndecan-4 *The Journal of biological chemistry* **280**, 42573-9

Choi, Y., Chung, H., Jung, H., Couchman, J.R. & Oh, E.S. (2011) Syndecans as cell surface receptors: Unique structure equates with functional diversity *Matrix biology : journal of the International Society for Matrix Biology* **30**, 93-9

Choi, Y., Kwon, M.J., Lim, Y., Yun, J.H., Lee, W. & Oh, E.S. (2015) Trans-regulation of Syndecan Functions by Hetero-oligomerization *The Journal of biological chemistry* **290**, 16943-53

Choi, Y., Yun, J.H., Yoo, J., Lee, I., Kim, H., Son, H.N., Kim, I.S., Yoon, H.S., Zimmermann, P., Couchman, J.R.*, et al.* (2016) New structural insight of C-terminal region of Syntenin-1, enhancing the molecular dimerization and inhibitory function related on Syndecan-4 signaling *Scientific reports* **6**, 36818

Chou, M.F. & Schwartz, D. (2011) Biological sequence motif discovery using motif-x *Current protocols in bioinformatics* **Chapter 13**, Unit 13 15-24

Christ, B. & Ordahl, C.P. (1995) Early stages of chick somite development *Anatomy and embryology* **191**, 381-96

Christov, C., Chretien, F., Abou-Khalil, R., Bassez, G., Vallet, G., Authier, F.J., Bassaglia, Y., Shinin, V., Tajbakhsh, S., Chazaud, B.*, et al.* (2007) Muscle satellite cells and endothelial cells: close neighbors and privileged partners *Molecular biology of the cell* **18**, 1397-409

Chu, C.L., Buczek-Thomas, J.A. & Nugent, M.A. (2004) Heparan sulphate proteoglycans modulate fibroblast growth factor-2 binding through a lipid raft-mediated mechanism *The Biochemical journal* **379**, 331-41

Clayton, A., Thomas, J., Thomas, G.J., Davies, M. & Steadman, R. (2001) Cell surface heparan sulfate proteoglycans control the response of renal interstitial fibroblasts to fibroblast growth factor-2 *Kidney international* **59**, 2084-94

Clegg, C.H., Linkhart, T.A., Olwin, B.B. & Hauschka, S.D. (1987) Growth factor control of skeletal muscle differentiation: commitment to terminal differentiation occurs in G1 phase and is repressed by fibroblast growth factor *J Cell Biol* **105**, 949-56

Coleman, M.E., DeMayo, F., Yin, K.C., Lee, H.M., Geske, R., Montgomery, C. & Schwartz, R.J. (1995) Myogenic vector expression of insulin-like growth factor I stimulates muscle cell differentiation and myofiber hypertrophy in transgenic mice *The Journal of biological chemistry* **270**, 12109-16

Collins, C.A., Olsen, I., Zammit, P.S., Heslop, L., Petrie, A., Partridge, T.A. & Morgan, J.E. (2005) Stem cell function, self-renewal, and behavioral heterogeneity of cells from the adult muscle satellite cell niche *Cell* **122**, 289-301

Conboy, I.M. & Rando, T.A. (2002) The regulation of Notch signaling controls satellite cell activation and cell fate determination in postnatal myogenesis *Developmental cell* **3**, 397-409

Conejo, R., Valverde, A.M., Benito, M. & Lorenzo, M. (2001) Insulin produces myogenesis in C2C12 myoblasts by induction of NF-kappaB and downregulation of AP-1 activities *Journal of cellular physiology* **186**, 82-94

Coolican, S.A., Samuel, D.S., Ewton, D.Z., McWade, F.J. & Florini, J.R. (1997) The mitogenic and myogenic actions of insulin-like growth factors utilize distinct signaling pathways *The Journal of biological chemistry* **272**, 6653-62

Cooper, R.N., Tajbakhsh, S., Mouly, V., Cossu, G., Buckingham, M. & Butler-Browne, G.S. (1999) In vivo satellite cell activation via Myf5 and MyoD1 in regenerating mouse skeletal muscle *Journal of cell science* **112 (Pt 17)**, 2895-901

Copps, K.D. & White, M.F. (2012) Regulation of insulin sensitivity by serine/threonine phosphorylation of insulin receptor substrate proteins IRS1 and IRS2 *Diabetologia* **55**, 2565-2582

Cornelison, D.D. (2008) Context matters: in vivo and in vitro influences on muscle satellite cell activity *Journal of cellular biochemistry* **105**, 663-9

Cornelison, D.D., Filla, M.S., Stanley, H.M., Rapraeger, A.C. & Olwin, B.B. (2001) Syndecan-3 and syndecan-4 specifically mark skeletal muscle satellite cells and are implicated in satellite cell maintenance and muscle regeneration *Developmental biology* **239**, 79-94

Cornelison, D.D., Wilcox-Adelman, S.A., Goetinck, P.F., Rauvala, H., Rapraeger, A.C. & Olwin, B.B. (2004) Essential and separable roles for Syndecan-3 and Syndecan-4 in skeletal muscle development and regeneration *Genes & development* **18**, 2231-6

Cornelison, D.D.W. (1998) Gene expression in wild-type and MyoD1-null satellite cells: regulation of activation, proliferation, and myogenesis *Dissertation (Ph.D.), California Institute of Technology*

Couchman, J.R. (2003) Syndecans: proteoglycan regulators of cell-surface microdomains? *Nature reviews. Molecular cell biology* **4**, 926-37

Couchman, J.R., Gopal, S., Lim, H.C., Norgaard, S. & Multhaupt, H.A. (2015) Fell-Muir Lecture: Syndecans: from peripheral coreceptors to mainstream regulators of cell behaviour *International journal of experimental pathology* **96**, 1-10

Cousins, J.C., Woodward, K.J., Gross, J.G., Partridge, T.A. & Morgan, J.E. (2004) Regeneration of skeletal muscle from transplanted immortalised myoblasts is oligoclonal *Journal of cell science* **117**, 3259-69

Culp, L.A., Laterra, J., Lark, M.W., Beyth, R.J. & Tobey, S.L. (1986) Heparan sulphate proteoglycan as mediator of some adhesive responses and cytoskeletal reorganization of cells on fibronectin matrices: independent versus cooperative functions *Ciba Foundation symposium* **124**, 158-83

Dalpe, G., Mathieu, M., Comtois, A., Zhu, E., Wasiak, S., De Repentigny, Y., Leclerc, N. & Kothary, R. (1999) Dystonin-deficient mice exhibit an intrinsic muscle weakness and an instability of skeletal muscle cytoarchitecture *Developmental biology* **210**, 367-80

David, G., Bai, X.M., Van der Schueren, B., Marynen, P., Cassiman, J.J. & Van den Berghe, H. (1993) Spatial and temporal changes in the expression of fibroglycan (syndecan-2) during mouse embryonic development *Development* **119**, 841-54

David, G., van der Schueren, B., Marynen, P., Cassiman, J.J. & van den Berghe, H. (1992) Molecular cloning of amphiglycan, a novel integral membrane heparan sulfate proteoglycan expressed by epithelial and fibroblastic cells *J Cell Biol* **118**, 961-9

Davies, B.R., Greenwood, H., Dudley, P., Crafter, C., Yu, D.H., Zhang, J., Li, J., Gao, B., Ji, Q., Maynard, J.*, et al.* (2012) Preclinical pharmacology of AZD5363, an inhibitor of AKT: pharmacodynamics, antitumor activity, and correlation of monotherapy activity with genetic background *Molecular cancer therapeutics* **11**, 873-87

Davis, M.A., Ireton, R.C. & Reynolds, A.B. (2003) A core function for p120-catenin in cadherin turnover *J Cell Biol* **163**, 525-34

De Rossi, G., Evans, A.R., Kay, E., Woodfin, A., McKay, T.R., Nourshargh, S. & Whiteford, J.R. (2014) Shed syndecan-2 inhibits angiogenesis *Journal of cell science* **127**, 4788-99

De Rossi, G. & Whiteford, J.R. (2013) A novel role for syndecan-3 in angiogenesis *F1000Research* **2**, 270

Deane, C.S., Hughes, D.C., Sculthorpe, N., Lewis, M.P., Stewart, C.E. & Sharples, A.P. (2013) Impaired hypertrophy in myoblasts is improved with testosterone administration *The Journal of steroid biochemistry and molecular biology* **138**, 152-61

Deepa, S.S., Yamada, S., Zako, M., Goldberger, O. & Sugahara, K. (2004) Chondroitin sulfate chains on syndecan-1 and syndecan-4 from normal murine mammary gland epithelial cells are structurally and functionally distinct and cooperate with heparan sulfate chains to bind growth factors. A novel function to control binding of midkine, pleiotrophin, and basic fibroblast growth factor *The Journal of biological chemistry* **279**, 37368-76

Deller, M.C., Kong, L. & Rupp, B. (2016) Protein stability: a crystallographer's perspective *Acta crystallographica. Section F, Structural biology communications* **72**, 72-95

Denhez, F., Wilcox-Adelman, S.A., Baciu, P.C., Saoncella, S., Lee, S., French, B., Neveu, W. & Goetinck, P.F. (2002) Syndesmos, a syndecan-4 cytoplasmic domain interactor, binds to the focal adhesion adaptor proteins paxillin and Hic-5 *The Journal of biological chemistry* **277**, 12270-4

DERKsen, P.W., Keehnen, R.M., Evers, L.M., van Oers, M.H., Spaargaren, M. & Pals, S.T. (2002) Cell surface proteoglycan syndecan-1 mediates hepatocyte growth factor binding and promotes Met signaling in multiple myeloma *Blood* **99**, 1405-10

Di Donna, S., Mamchaoui, K., Cooper, R.N., Seigneurin-Venin, S., Tremblay, J., Butler-Browne, G.S. & Mouly, V. (2003) Telomerase can extend the proliferative capacity of human myoblasts, but does not lead to their immortalization *Molecular cancer research : MCR* **1**, 643-53

Do, M.K., Shimizu, N., Suzuki, T., Ohtsubo, H., Mizunoya, W., Nakamura, M., Sawano, S., Furuse, M., Ikeuchi, Y., Anderson, J.E.*, et al.* (2015) Transmembrane proteoglycans syndecan-2, 4, receptor candidates for the impact of HGF and FGF2 on semaphorin 3A expression in early-differentiated myoblasts *Physiological reports* **3**,

Doody, K.M., Stanford, S.M., Sacchetti, C., Svensson, M.N., Coles, C.H., Mitakidis, N., Kiosses, W.B., Bartok, B., Fos, C., Cory, E.*, et al.* (2015) Targeting phosphatase-dependent proteoglycan switch for rheumatoid arthritis therapy *Science translational medicine* **7**, 288ra76

Duan, R. & Gallagher, P.J. (2009) Dependence of myoblast fusion on a cortical actin wall and nonmuscle myosin IIA *Developmental biology* **325**, 374-85

Edmondson, D.G. & Olson, E.N. (1990) A gene with homology to the myc similarity region of MyoD11 is expressed during myogenesis and is sufficient to activate the muscle differentiation program *Genes & development* **4**, 1450

El Annabi, S., Gautier, N. & Baron, V. (2001) Focal adhesion kinase and Src mediate integrin regulation of insulin receptor phosphorylation *FEBS letters* **507**, 247-52

Elfenbein, A., Lanahan, A., Zhou, T.X., Yamasaki, A., Tkachenko, E., Matsuda, M. & Simons, M. (2012) Syndecan 4 regulates FGFR1 signaling in endothelial cells by directing macropinocytosis *Science signaling* **5**, ra36

Emanuelli, B., Peraldi, P., Filloux, C., Sawka-Verhelle, D., Hilton, D. & Van Obberghen, E. (2000) SOCS-3 is an insulin-induced negative regulator of insulin signaling *The Journal of biological chemistry* **275**, 15985-91

Endo, K., Takino, T., Miyamori, H., Kinsen, H., Yoshizaki, T., Furukawa, M. & Sato, H. (2003) Cleavage of syndecan-1 by membrane type matrix metalloproteinase-1 stimulates cell migration *The Journal of biological chemistry* **278**, 40764-70

Engert, J.C., Berglund, E.B. & Rosenthal, N. (1996) Proliferation precedes differentiation in IGF-I-stimulated myogenesis *J Cell Biol* **135**, 431-40

Esko, J.D. & Selleck, S.B. (2002) Order out of chaos: assembly of ligand binding sites in heparan sulfate *Annual review of biochemistry* **71**, 435-71

Esposito, D.L., Li, Y., Cama, A. & Quon, M.J. (2001) Tyr(612) and Tyr(632) in human insulin receptor substrate-1 are important for full activation of insulin-stimulated phosphatidylinositol 3-kinase activity and translocation of GLUT4 in adipose cells *Endocrinology* **142**, 2833-40

Fabrini, R., De Luca, A., Stella, L., Mei, G., Orioni, B., Ciccone, S., Federici, G., Lo Bello, M. & Ricci, G. (2009) Monomer-dimer equilibrium in glutathione transferases: a critical re-examination *Biochemistry* **48**, 10473-82

Farina, N.H., Hausburg, M., Betta, N.D., Pulliam, C., Srivastava, D., Cornelison, D. & Olwin, B.B. (2012) A role for RNA post-transcriptional regulation in satellite cell activation *Skeletal muscle* **2**, 21

Fears, C.Y., Gladson, C.L. & Woods, A. (2006) Syndecan-2 is expressed in the microvasculature of gliomas and regulates angiogenic processes in microvascular endothelial cells *The Journal of biological chemistry* **281**, 14533-6

Ferries, S., PERKins, S., Brownridge, P.J., Campbell, A., Eyers, P.A., Jones, A.R. & Eyers, C.E. (2017) Evaluation of Parameters for Confident Phosphorylation Site Localization Using an Orbitrap Fusion Tribrid Mass Spectrometer *Journal of proteome research* **16**, 3448-3459

Figeac, N., Serralbo, O., Marcelle, C. & Zammit, P.S. (2014) ErbB3 binding protein-1 (Ebp1) controls proliferation and myogenic differentiation of muscle stem cells *Developmental biology* **386**, 135-51

Figueiredo, V.C., Markworth, J.F. & Cameron-Smith, D. (2017) Considerations on mTOR regulation at serine 2448: implications for muscle metabolism studies *Cellular and molecular life sciences : CMLS* **74**, 2537-2545

Florini, J.R., Ewton, D.Z. & Coolican, S.A. (1996) Growth hormone and the insulin-like growth factor system in myogenesis *Endocrine reviews* **17**, 481-517

Florini, J.R., Magri, K.A., Ewton, D.Z., James, P.L., Grindstaff, K. & Rotwein, P.S. (1991) "Spontaneous" differentiation of skeletal myoblasts is dependent upon autocrine secretion of insulin-like growth factor-II *The Journal of biological chemistry* **266**, 15917-23

Fortini, P., Ferretti, C., Iorio, E., Cagnin, M., Garribba, L., Pietraforte, D., Falchi, M., Pascucci, B., Baccarini, S., Morani, F.*, et al.* (2016) The fine tuning of metabolism, autophagy and differentiation during in vitro myogenesis *Cell death & disease* **7**, e2168

Fredriksson, S., Gullberg, M., Jarvius, J., Olsson, C., Pietras, K., Gustafsdottir, S.M., Ostman, A. & Landegren, U. (2002) Protein detection using proximity-dependent DNA ligation assays *Nature biotechnology* **20**, 473-7

Fuentealba, L., Carey, D.J. & Brandan, E. (1999) Antisense inhibition of syndecan-3 expression during skeletal muscle differentiation accelerates myogenesis through a basic fibroblast growth factor-dependent mechanism *The Journal of biological chemistry* **274**, 37876-84

Fukada, S., Ma, Y., Ohtani, T., Watanabe, Y., Murakami, S. & Yamaguchi, M. (2013) Isolation, characterization, and molecular regulation of muscle stem cells *Frontiers in physiology* **4**, 317

Fukada, S., Uezumi, A., Ikemoto, M., Masuda, S., Segawa, M., Tanimura, N., Yamamoto, H., Miyagoe-Suzuki, Y. & Takeda, S. (2007) Molecular signature of quiescent satellite cells in adult skeletal muscle *Stem cells* **25**, 2448-59

Fukada, S., Yamaguchi, M., Kokubo, H., Ogawa, R., Uezumi, A., Yoneda, T., Matev, M.M., Motohashi, N., Ito, T., Zolkiewska, A.*, et al.* (2011) Hesr1 and Hesr3 are essential to generate undifferentiated quiescent satellite cells and to maintain satellite cell numbers *Development* **138**, 4609-19

Fukushima, T., Yoshihara, H., Furuta, H., Kamei, H., Hakuno, F., Luan, J., Duan, C., Saeki, Y., Tanaka, K., Iemura, S.*, et al.* (2015) NEDD4-induced monoubiquitination of IRS-2 enhances IGF signalling and mitogenic activity *Nature communications* **6**, 6780

Gao, Q., Chen, C.Y., Zong, C., Wang, S., Ramiah, A., Prabhakar, P., Morris, L.C., Boons, G.J., Moremen, K.W. & Prestegard, J.H. (2016) Structural Aspects of Heparan Sulfate Binding to Robo1-Ig1-2 *ACS chemical biology* **11**, 3106-3113

Gao, Y., Li, M., Chen, W. & Simons, M. (2000) Synectin, syndecan-4 cytoplasmic domain binding PDZ protein, inhibits cell migration *Journal of cellular physiology* **184**, 373-9

Gayraud-Morel, B., Chretien, F., Jory, A., Sambasivan, R., Negroni, E., Flamant, P., Soubigou, G., Coppee, J.Y., Di Santo, J., Cumano, A.*, et al.* (2012) Myf5 haploinsufficiency reveals distinct cell fate potentials for adult skeletal muscle stem cells *Journal of cell science* **125**, 1738-49

Ge, Y., Yoon, M.S. & Chen, J. (2011) Raptor and Rheb negatively regulate skeletal myogenesis through suppression of insulin receptor substrate 1 (IRS1) *The Journal of biological chemistry* **286**, 35675-82

Ghadiali, R.S., Guimond, S.E., Turnbull, J.E. & Pisconti, A. (2017) Dynamic changes in heparan sulfate during muscle differentiation and ageing regulate myoblast cell fate and FGF2 signalling *Matrix biology : journal of the International Society for Matrix Biology* **59**, 54-68

Gibson, M.C. & Schultz, E. (1982) The distribution of satellite cells and their relationship to specific fiber types in soleus and extensor digitorum longus muscles *The Anatomical record* **202**, 329-37

Gillespie, M.A., Le Grand, F., Scime, A., Kuang, S., von Maltzahn, J., Seale, V., Cuenda, A., Ranish, J.A. & Rudnicki, M.A. (2009) p38-{gamma}-dependent gene silencing restricts entry into the myogenic differentiation program *J Cell Biol* **187**, 991-1005

Gilson, H., Schakman, O., Kalista, S., Lause, P., Tsuchida, K. & Thissen, J.P. (2009) Follistatin induces muscle hypertrophy through satellite cell proliferation and inhibition of both myostatin and activin *American journal of physiology. Endocrinology and metabolism* **297**, E157-64

Giraud, J., Haas, M., Feener, E.P., Copps, K.D., Dong, X., Dunn, S.L. & White, M.F. (2007) Phosphorylation of IRS1 at SER-522 inhibits insulin signaling *Molecular endocrinology* **21**, 2294-302

Gonzalez, I., Tripathi, G., Carter, E.J., Cobb, L.J., Salih, D.A., Lovett, F.A., Holding, C. & Pell, J.M. (2004) Akt2, a novel functional link between p38 mitogen-activated protein kinase and phosphatidylinositol 3-kinase pathways in myogenesis *Molecular and cellular biology* **24**, 3607-22

Goulding, M., Lumsden, A. & Paquette, A.J. (1994) Regulation of Pax-3 expression in the dermomyotome and its role in muscle development *Development* **120**, 957-71

Grabiec, K., Gajewska, M., Milewska, M., Blaszczyk, M. & Grzelkowska-Kowalczyk, K. (2014) The influence of high glucose and high insulin on mechanisms controlling cell cycle progression and arrest in mouse C2C12 myoblasts: the comparison with IGF-I effect *Journal of endocrinological investigation* **37**, 233-45

Grabowska, I., Szeliga, A., Moraczewski, J., Czaplicka, I. & Brzoska, E. (2011) Comparison of satellite cell-derived myoblasts and C2C12 differentiation in two- and three-dimensional cultures: changes in adhesion protein expression *Cell biology international* **35**, 125-33
Granes, F., Berndt, C., Roy, C., Mangeat, P., Reina, M. & Vilaro, S. (2003) Identification of a novel Ezrin-binding site in syndecan-2 cytoplasmic domain *FEBS letters* **547**, 212-6
Granes, F., Urena, J.M., Rocamora, N. & Vilaro, S. (2000) Ezrin links syndecan-2 to the cytoskeleton *Journal of cell science* **113 (Pt 7)**, 1267-76
Grimes, M.L., Lee, W.J., van der Maaten, L. & Shannon, P. (2013) Wrangling phosphoproteomic data to elucidate cancer signaling pathways *PloS one* **8**, e52884
Grootjans, J.J., Zimmermann, P., Reekmans, G., Smets, A., Degeest, G., Durr, J. & David, G. (1997) Syntenin, a PDZ protein that binds syndecan cytoplasmic domains *Proceedings of the National Academy of Sciences of the United States of America* **94**, 13683-8
Gu, F., Wang, L., He, J., Liu, X., Zhang, H., Li, W., Fu, L. & Ma, Y. (2014) Girdin, an actin-binding protein, is critical for migration, adhesion, and invasion of human glioblastoma cells *Journal of neurochemistry* **131**, 457-69
Gual, P., Gremeaux, T., Gonzalez, T., Le Marchand-Brustel, Y. & Tanti, J.F. (2003) MAP kinases and mTOR mediate insulin-induced phosphorylation of insulin receptor substrate-1 on serine residues 307, 612 and 632 *Diabetologia* **46**, 1532-42
Gual, P., Le Marchand-Brustel, Y. & Tanti, J.F. (2005) Positive and negative regulation of insulin signaling through IRS-1 phosphorylation *Biochimie* **87**, 99-109
Guasconi, V. & Puri, P.L. (2009) Chromatin: the interface between extrinsic cues and the epigenetic regulation of muscle regeneration *Trends in cell biology* **19**, 286-94
Guimond, S., Turner, K., Kita, M., Ford-Perriss, M. & Turnbull, J. (2001) Dynamic biosynthesis of heparan sulphate sequences in developing mouse brain: a potential regulatory mechanism during development *Biochemical Society transactions* **29**, 177-81
Guimond, S.E. & Turnbull, J.E. (1999) Fibroblast growth factor receptor signalling is dictated by specific heparan sulphate saccharides *Current biology : CB* **9**, 1343-6
Gunes, C. & Rudolph, K.L. (2013) The role of telomeres in stem cells and cancer *Cell* **152**, 390-3
Gunther, S., Kim, J., Kostin, S., Lepper, C., Fan, C.M. & Braun, T. (2013) Myf5-positive satellite cells contribute to PAX7-dependent long-term maintenance of adult muscle stem cells *Cell stem cell* **13**, 590-601
Hall, J.K., Banks, G.B., Chamberlain, J.S. & Olwin, B.B. (2010) Prevention of muscle aging by myofiber-associated satellite cell transplantation *Science translational medicine* **2**, 57ra83
Hammond, E., Khurana, A., Shridhar, V. & Dredge, K. (2014) The Role of Heparanase and Sulfatases in the Modification of Heparan Sulfate Proteoglycans within the Tumor Microenvironment and Opportunities for Novel Cancer Therapeutics *Frontiers in oncology* **4**, 195
Handel, T.M., Johnson, Z., Crown, S.E., Lau, E.K. & Proudfoot, A.E. (2005) Regulation of protein function by glycosaminoglycans--as exemplified by chemokines *Annual review of biochemistry* **74**, 385-410
Harel, I., Nathan, E., Tirosh-Finkel, L., Zigdon, H., Guimaraes-Camboa, N., Evans, S.M. & Tzahor, E. (2009) Distinct origins and genetic programs of head muscle satellite cells *Developmental cell* **16**, 822-32
Hawke, T.J. & Garry, D.J. (2001) Myogenic satellite cells: physiology to molecular biology *Journal of applied physiology* **91**, 534-51
Hayashida, K., Stahl, P.D. & Park, P.W. (2008) Syndecan-1 ectodomain shedding is regulated by the small GTPase Rab5 *The Journal of biological chemistry* **283**, 35435-44
Hedo, J.A., Kahn, C.R., Hayashi, M., Yamada, K.M. & Kasuga, M. (1983) Biosynthesis and glycosylation of the insulin receptor. Evidence for a single polypeptide precursor of the two major subunits *The Journal of biological chemistry* **258**, 10020-6
Hemmati-Brivanlou, A., Kelly, O.G. & Melton, D.A. (1994) Follistatin, an antagonist of activin, is expressed in the Spemann organizer and displays direct neuralizing activity *Cell* **77**, 283-95
Herndon, M.E., Stipp, C.S. & Lander, A.D. (1999) Interactions of neural glycosaminoglycans and proteoglycans with protein ligands: assessment of selectivity, heterogeneity and the participation of core proteins in binding *Glycobiology* **9**, 143-55
Heron-Milhavet, L., Franckhauser, C., Rana, V., Berthenet, C., Fisher, D., Hemmings, B.A., Fernandez, A. & Lamb, N.J. (2006) Only Akt1 is required for proliferation, while Akt2 promotes cell cycle exit through p21 binding *Molecular and cellular biology* **26**, 8267-80
Hooper, N.M., Karran, E.H. & Turner, A.J. (1997) Membrane protein secretases *The Biochemical journal* **321 (Pt 2)**, 265-79

Hozumi, K., Suzuki, N., Nielsen, P.K., Nomizu, M. & Yamada, Y. (2006) Laminin alpha1 chain LG4 module promotes cell attachment through syndecans and cell spreading through integrin alpha2beta1 *The Journal of biological chemistry* **281**, 32929-40

Huang da, W., Sherman, B.T. & Lempicki, R.A. (2009) Bioinformatics enrichment tools: paths toward the comprehensive functional analysis of large gene lists *Nucleic acids research* **37**, 1-13

Huang da, W., Sherman, B.T. & Lempicki, R.A. (2009) Systematic and integrative analysis of large gene lists using DAVID bioinformatics resources *Nature protocols* **4**, 44-57

Ishikawa, T. and Kramer, H.R. (2011) SDC1 Negatively Modulates Carcinoma Cell Motility and Invasion. *Experimental Cell Research* **6,** 951-965

Jiang, B.H., Aoki, M., Zheng, J.Z., Li, J. & Vogt, P.K. (1999) Myogenic signaling of phosphatidylinositol 3-kinase requires the serine-threonine kinase AKT/protein kinase B *Proceedings of the National Academy of Sciences of the United States of America* **96**, 2077-81

Joe, A.W., Yi, L., Natarajan, A., Le Grand, F., So, L., Wang, J., Rudnicki, M.A. & Rossi, F.M. (2010) Muscle injury activates resident fibro/adipogenic progenitors that facilitate myogenesis *Nature cell biology* **12**, 153-63

Jones, N.C., Fedorov, Y.V., Rosenthal, R.S. & Olwin, B.B. (2001) ERK1/2 is required for myoblast proliferation but is dispensable for muscle gene expression and cell fusion *Journal of cellular physiology* **186**, 104-15

Jones, N.C., Tyner, K.J., Nibarger, L., Stanley, H.M., Cornelison, D.D., Fedorov, Y.V. & Olwin, B.B. (2005) The p38alpha/beta MAPK functions as a molecular switch to activate the quiescent satellite cell *J Cell Biol* **169**, 105-16

Judson, R.N., Zhang, R.H. & Rossi, F.M. (2013) Tissue-resident mesenchymal stem/progenitor cells in skeletal muscle: collaborators or saboteurs? *The FEBS journal* **280**, 4100-8

Jue, T., Rothman, D.L., Shulman, G.I., Tavitian, B.A., DeFronzo, R.A. & Shulman, R.G. (1989) Direct observation of glycogen synthesis in human muscle with 13C NMR *Proceedings of the National Academy of Sciences of the United States of America* **86**, 4489-91

Jung, C.H., Ro, S.H., Cao, J., Otto, N.M. & Kim, D.H. (2010) mTOR regulation of autophagy *FEBS letters* **584**, 1287-95

Kahlert, S., Grohe, C., Karas, R.H., Lobbert, K., Neyses, L. & Vetter, H. (1997) Effects of estrogen on skeletal myoblast growth *Biochemical and biophysical research communications* **232**, 373-8

Kalia, M., Chandra, V., Rahman, S.A., Sehgal, D. & Jameel, S. (2009) Heparan sulfate proteoglycans are required for cellular binding of the hepatitis E virus ORF2 capsid protein and for viral infection *Journal of virology* **83**, 12714-24

Karpievitch, Y.V., Dabney, A.R. & Smith, R.D. (2012) Normalization and missing value imputation for label-free LC-MS analysis *BMC bioinformatics* **13 Suppl 16**, S5

Kato, M., Wang, H., Bernfield, M., Gallagher, J.T. & Turnbull, J.E. (1994) Cell surface syndecan-1 on distinct cell types differs in fine structure and ligand binding of its heparan sulfate chains *The Journal of biological chemistry* **269**, 18881-90

Katz, M., Shtiegman, K., Tal-Or, P., Yakir, L., Mosesson, Y., Harari, D., Machluf, Y., Asao, H., Jovin, T., Sugamura, K.*, et al.* (2002) Ligand-independent degradation of epidermal growth factor receptor involves receptor ubiquitylation and Hgs, an adaptor whose ubiquitin-interacting motif targets ubiquitylation by NEDD4 *Traffic* **3**, 740-51

Kawesa, S., Vanstone, J. & Tsilfidis, C. (2015) A differential response to newt regeneration extract by C2C12 and primary mammalian muscle cells *Skeletal muscle* **5**, 19

Kherif, S., Lafuma, C., Dehaupas, M., Lachkar, S., Fournier, J.G., Verdiere-Sahuque, M., Fardeau, M. & Alameddine, H.S. (1999) Expression of matrix metalloproteinases 2 and 9 in regenerating skeletal muscle: a study in experimentally injured and mdx muscles *Developmental biology* **205**, 158-70

Kim, J., Kundu, M., Viollet, B. & Guan, K.L. (2011) AMPK and mTOR regulate autophagy through direct phosphorylation of ULK1 *Nature cell biology* **13**, 132-41

Kimple, M.E., Brill, A.L. & Pasker, R.L. (2013) Overview of affinity tags for protein purification *Current protocols in protein science* **73**, Unit 9 9

Kinnunen, T., Kaksonen, M., Saarinen, J., Kalkkinen, N., Peng, H.B. & Rauvala, H. (1998) Cortactin-Src kinase signaling pathway is involved in N-syndecan-dependent neurite outgrowth *The Journal of biological chemistry* **273**, 10702-8

Kitzmann, M., Bonnieu, A., Duret, C., Vernus, B., Barro, M., Laoudj-Chenivesse, D., Verdi, J.M. & Carnac, G. (2006) Inhibition of Notch signaling induces myotube hypertrophy by recruiting a subpopulation of reserve cells *Journal of cellular physiology* **208**, 538-48

Knelson, E.H., Nee, J.C. & Blobe, G.C. (2014) Heparan sulfate signaling in cancer *Trends in biochemical sciences* **39**, 277-88

Koncarevic, A., Jackman, R.W. & Kandarian, S.C. (2007) The ubiquitin-protein ligase NEDD4 targets NOTCH1 in skeletal muscle and distinguishes the subset of atrophies caused by reduced muscle tension *FASEB journal : official publication of the Federation of American Societies for Experimental Biology* **21**, 427-37

Kopan, R., Nye, J.S. & Weintraub, H. (1994) The intracellular domain of mouse Notch: a constitutively activated repressor of myogenesis directed at the basic helix-loop-helix region of MyoD1 *Development* **120**, 2385-96

Kouzi-Koliakos, K., Koliakos, G.G., Tsilibary, E.C., Furcht, L.T. & Charonis, A.S. (1989) Mapping of three major heparin-binding sites on laminin and identification of a novel heparin-binding site on the B1 chain *The Journal of biological chemistry* **264**, 17971-8

Kuang, S., Charge, S.B., Seale, P., Huh, M. & Rudnicki, M.A. (2006) Distinct roles for PAX7 and PAX3 in adult regenerative myogenesis *J Cell Biol* **172**, 103-13

Kuang, S., Gillespie, M.A. & Rudnicki, M.A. (2008) Niche regulation of muscle satellite cell self-renewal and differentiation *Cell stem cell* **2**, 22-31

Kuang, S., Kuroda, K., Le Grand, F. & Rudnicki, M.A. (2007) Asymmetric self-renewal and commitment of satellite stem cells in muscle *Cell* **129**, 999-1010

Kumar, C. & Mann, M. (2009) Bioinformatics analysis of mass spectrometry-based proteomics data sets *FEBS letters* **583**, 1703-12

Kuroda, K., Tani, S., Tamura, K., Minoguchi, S., Kurooka, H. & Honjo, T. (1999) Delta-induced Notch signaling mediated by RBP-J inhibits MyoD1 expression and myogenesis *The Journal of biological chemistry* **274**, 7238-44

Kusano, Y., Oguri, K., Nagayasu, Y., Munesue, S., Ishihara, M., Saiki, I., Yonekura, H., Yamamoto, H. & Okayama, M. (2000) Participation of syndecan 2 in the induction of stress fiber formation in cooperation with integrin alpha5beta1: structural characteristics of heparan sulfate chains with avidity to COOH-terminal heparin-binding domain of fibronectin *Experimental cell research* **256**, 434-44

Kwon, M.J., Park, J., Jang, S., Eom, C.Y. & Oh, E.S. (2016) The Conserved Phenylalanine in the Transmembrane Domain Enhances Heteromeric Interactions of Syndecans *The Journal of biological chemistry* **291**, 872-81

Lamanna, W.C., Kalus, I., Padva, M., Baldwin, R.J., Merry, C.L. & Dierks, T. (2007) The heparanome--the enigma of encoding and decoding heparan sulfate sulfation *Journal of biotechnology* **129**, 290-307

Lambaerts, K., Wilcox-Adelman, S.A. & Zimmermann, P. (2009) The signaling mechanisms of syndecan heparan sulfate proteoglycans *Current opinion in cell biology* **21**, 662-9

Lamon, S., Zacharewicz, E., Stephens, A.N. & Russell, A.P. (2014) EPO-receptor is present in mouse C2C12 and human primary skeletal muscle cells but EPO does not influence myogenesis *Physiological reports* **2**, e00256

Langlais, P., Yi, Z., Finlayson, J., Luo, M., Mapes, R., De Filippis, E., Meyer, C., Plummer, E., Tongchinsub, P., Mattern, M.*, et al.* (2011) Global IRS-1 phosphorylation analysis in insulin resistance *Diabetologia* **54**, 2878-89

Langley, B., Thomas, M., Bishop, A., Sharma, M., Gilmour, S. & Kambadur, R. (2002) Myostatin inhibits myoblast differentiation by down-regulating MyoD1 expression *The Journal of biological chemistry* **277**, 49831-40

Langsdorf, A., Do, A.T., Kusche-Gullberg, M., Emerson, C.P., Jr. & Ai, X. (2007) Sulfs are regulators of growth factor signaling for satellite cell differentiation and muscle regeneration *Developmental biology* **311**, 464-77

Larrain, J., Cizmeci-Smith, G., Troncoso, V., Stahl, R.C., Carey, D.J. & Brandan, E. (1997) Syndecan-1 expression is down-regulated during myoblast terminal differentiation. Modulation by growth factors and retinoic acid *The Journal of biological chemistry* **272**, 18418-24

Le Grand, F., Jones, A.E., Seale, V., Scime, A. & Rudnicki, M.A. (2009) Wnt7a activates the planar cell polarity pathway to drive the symmetric expansion of satellite stem cells *Cell stem cell* **4**, 535-47

Lee, S.J. (2004) Regulation of muscle mass by myostatin *Annual review of cell and developmental biology* **20**, 61-86

Lee, S.J. (2007) Quadrupling muscle mass in mice by targeting TGF-beta signaling pathways *PloS one* **2**, e789

Lee, S.J. & McPherron, A.C. (2001) Regulation of myostatin activity and muscle growth *Proceedings of the National Academy of Sciences of the United States of America* **98**, 9306-11

Lee, T.Y., Bo-Kai Hsu, J., Chang, W.C. & Huang, H.D. (2011) RegPhos: a system to explore the protein kinase-substrate phosphorylation network in humans *Nucleic acids research* **39**, D777-87

Leonova, E.I. & Galzitskaya, O.V. (2015) Cell communication using intrinsically disordered proteins: what can syndecans say? *Journal of biomolecular structure & dynamics* **33**, 1037-50
Leroy, M.C., Perroud, J., Darbellay, B., Bernheim, L. & Konig, S. (2013) Epidermal growth factor receptor down-regulation triggers human myoblast differentiation *PloS one* **8**, e71770
Lexell, J. (1995) Human aging, muscle mass, and fiber type composition *The journals of gerontology. Series A, Biological sciences and medical sciences* **50 Spec No**, 11-6
Li, J.J., Ferry, R.J., Jr., Diao, S., Xue, B., Bahouth, S.W. & Liao, F.F. (2015) NEDD4 haploinsufficient mice display moderate insulin resistance, enhanced lipolysis, and protection against high-fat diet-induced obesity *Endocrinology* **156**, 1283-91
Li, Q., Park, P.W., Wilson, C.L. & Parks, W.C. (2002) Matrilysin shedding of syndecan-1 regulates chemokine mobilization and transepithelial efflux of neutrophils in acute lung injury *Cell* **111**, 635-46
Lilja, K.C., Zhang, N., Magli, A., Gunduz, V., Bowman, C.J., Arpke, R.W., Darabi, R., Kyba, M., Perlingeiro, R. & Dynlacht, B.D. (2017) PAX7 remodels the chromatin landscape in skeletal muscle stem cells *PloS one* **12**, e0176190
Lim, S.T., Longley, R.L., Couchman, J.R. & Woods, A. (2003) Direct binding of syndecan-4 cytoplasmic domain to the catalytic domain of protein kinase C alpha (PKC alpha) increases focal adhesion localization of PKC alpha *The Journal of biological chemistry* **278**, 13795-802
Lin, H., Lal, R. & Clegg, D.O. (2000) Imaging and mapping heparin-binding sites on single fibronectin molecules with atomic force microscopy *Biochemistry* **39**, 3192-6
Lin, W., Zhang, J., Lin, H., Li, Z., Sun, X., Xin, D., Yang, M., Sun, L., Li, 1., Wang, H., Chen, D. & Sun, Q. (2016) Syndecan-4 negatively regulates antiviral signalling by mediating RIG-I deubiquitination via CYLD. *Nature communications* **7**
Linkhart, T.A., Clegg, C.H. & Hauschka, S.D. (1980) Control of mouse myoblast commitment to terminal differentiation by mitogens *Journal of supramolecular structure* **14**, 483-98
Litchfield, D.W. (2003) Protein kinase CK2: structure, regulation and role in cellular decisions of life and death *The Biochemical journal* **369**, 1-15
Liu, D., Black, B.L. & Derynck, R. (2001) TGF-beta inhibits muscle differentiation through functional repression of myogenic transcription factors by Smad3 *Genes & development* **15**, 2950-66
Liu, D., Kang, J.S. & Derynck, R. (2004) TGF-beta-activated Smad3 represses MEF2-dependent transcription in myogenic differentiation *The EMBO journal* **23**, 1557-66
Longley, R.L., Woods, A., Fleetwood, A., Cowling, G.J., Gallagher, J.T. & Couchman, J.R. (1999) Control of morphology, cytoskeleton and migration by syndecan-4 *Journal of cell science* **112 (Pt 20)**, 3421-31
Lorenz, U. (2011) Protein tyrosine phosphatase assays *Current protocols in immunology* **Chapter 11**, Unit 11 7
Lukjanenko, L., Jung, M.J., Hegde, N., Perruisseau-Carrier, C., Migliavacca, E., Rozo, M., Karaz, S., Jacot, G., Schmidt, M., Li, L.*, et al.* (2016) Loss of fibronectin from the aged stem cell niche affects the regenerative capacity of skeletal muscle in mice *Nature medicine* **22**, 897-905
Luque, E., Pena, J., Martin, P., Jimena, I. & Vaamonde, R. (1995) Capillary supply during development of individual regenerating muscle fibers *Anatomia, histologia, embryologia* **24**, 87-9
Luyten, A., Mortier, E., Van Campenhout, C., Taelman, V., Degeest, G., Wuytens, G., Lambaerts, K., David, G., Bellefroid, E.J. & Zimmermann, P. (2008) The postsynaptic density 95/disc-large/zona occludens protein syntenin directly interacts with frizzled 7 and supports noncanonical Wnt signaling *Molecular biology of the cell* **19**, 1594-604
Ma, X.M. & Blenis, J. (2009) Molecular mechanisms of mTOR-mediated translational control *Nature reviews. Molecular cell biology* **10**, 307-18
Mahoney, C.M., Morgan, M.R., Harrison, A., Humphries, M.J. & Bass, M.D. (2009) Therapeutic ultrasound bypasses canonical syndecan-4 signaling to activate rac1 *The Journal of biological chemistry* **284**, 8898-909
Mahtouk, K., Cremer, F.W., Reme, T., Jourdan, M., Baudard, M., Moreaux, J., Requirand, G., Fiol, G., De Vos, J., Moos, M.*, et al.* (2006) Heparan sulphate proteoglycans are essential for the myeloma cell growth activity of EGF-family ligands in multiple myeloma *Oncogene* **25**, 7180-91
Malarkey, K., Belham, C.M., Paul, A., Graham, A., McLees, A., Scott, P.H. & Plevin, R. (1995) The regulation of tyrosine kinase signalling pathways by growth factor and G-protein-coupled receptors *The Biochemical journal* **309 (Pt 2)**, 361-75
Mann, M., Ong, S.E., Gronborg, M., Steen, H., Jensen, O.N. & Pandey, A. (2002) Analysis of protein phosphorylation using mass spectrometry: deciphering the phosphoproteome *Trends in biotechnology* **20**, 261-8

Manon-Jensen, T., Itoh, Y. & Couchman, J.R. (2010) Proteoglycans in health and disease: the multiple roles of syndecan shedding *The FEBS journal* **277**, 3876-89

Manon-Jensen, T., Multhaupt, H.A. & Couchman, J.R. (2013) Mapping of matrix metalloproteinase cleavage sites on syndecan-1 and syndecan-4 ectodomains *The FEBS journal* **280**, 2320-31

Marmor, M.D. & Yarden, Y. (2004) Role of protein ubiquitylation in regulating endocytosis of receptor tyrosine kinases *Oncogene* **23**, 2057-70

Martin, J.F., Li, L. & Olson, E.N. (1992) Repression of myogenin function by TGF-beta 1 is targeted at the basic helix-loop-helix motif and is independent of E2A products *The Journal of biological chemistry* **267**, 10956-60

Marynen, P., Zhang, J., Cassiman, J.J., Van den Berghe, H. & David, G. (1989) Partial primary structure of the 48- and 90-kilodalton core proteins of cell surface-associated heparan sulfate proteoglycans of lung fibroblasts. Prediction of an integral membrane domain and evidence for multiple distinct core proteins at the cell surface of human lung fibroblasts *The Journal of biological chemistry* **264**, 7017-24

Mauro, A. (1961) Satellite cell of skeletal muscle fibers *The Journal of biophysical and biochemical cytology* **9**, 493-5

McAvoy, T. & Nairn, A.C. (2010) Serine/threonine protein phosphatase assays *Current protocols in molecular biology* **Chapter 18**, Unit18 18

McFall, A.J. & Rapraeger, A.C. (1997) Identification of an adhesion site within the syndecan-4 extracellular protein domain *The Journal of biological chemistry* **272**, 12901-4

McPherron, A.C., Lawler, A.M. & Lee, S.J. (1997) Regulation of skeletal muscle mass in mice by a new TGF-beta superfamily member *Nature* **387**, 83-90

Michel, U., Farnworth, P. & Findlay, J.K. (1993) Follistatins: more than follicle-stimulating hormone suppressing proteins *Molecular and cellular endocrinology* **91**, 1-11

Moller, D.E., Yokota, A., Caro, J.F. & Flier, J.S. (1989) Tissue-specific expression of two alternatively spliced insulin receptor mRNAs in man *Molecular endocrinology* **3**, 1263-9

Montarras, D., Aurade, F., Johnson, T., J, I.I., Gros, F. & Pinset, C. (1996) Autonomous differentiation in the mouse myogenic cell line, C2, involves a mutual positive control between insulin-like growth factor II and MyoD1, operating as early as at the myoblast stage *Journal of cell science* **109 (Pt 3)**, 551-60

Moran, J.L., Li, Y., Hill, A.A., Mounts, W.M. & Miller, C.P. (2002) Gene expression changes during mouse skeletal myoblast differentiation revealed by transcriptional profiling *Physiological genomics* **10**, 103-11

Morgan, J.E. (1988) Myogenicity in vitro and in vivo of mouse muscle cells separated on discontinuous Percoll gradients *Journal of the neurological sciences* **85**, 197-207

Morgan, M.R., Hamidi, H., Bass, M.D., Warwood, S., Ballestrem, C. & Humphries, M.J. (2013) Syndecan-4 phosphorylation is a control point for integrin recycling *Developmental cell* **24**, 472-85

Morgan, M.R., Humphries, M.J. & Bass, M.D. (2007) Synergistic control of cell adhesion by integrins and syndecans *Nature reviews. Molecular cell biology* **8**, 957-69

Morrione, A., Plant, P., Valentinis, B., Staub, O., Kumar, S., Rotin, D. & Baserga, R. (1999) mGrb10 interacts with NEDD4 *The Journal of biological chemistry* **274**, 24094-9

Mourikis, P., Sambasivan, R., Castel, D., Rocheteau, P., Bizzarro, V. & Tajbakhsh, S. (2012) A critical requirement for notch signaling in maintenance of the quiescent skeletal muscle stem cell state *Stem cells* **30**, 243-52

Muramatsu, T., Muramatsu, H. & Kojima, T. (2006) Identification of proteoglycan-binding proteins *Methods in enzymology* **416**, 263-78

Murphy, M.M., Lawson, J.A., Mathew, S.J., Hutcheson, D.A. & Kardon, G. (2011) Satellite cells, connective tissue fibroblasts and their interactions are crucial for muscle regeneration *Development* **138**, 3625-37

Nakae, J., Kido, Y. & Accili, D. (2001) Distinct and overlapping functions of insulin and IGF-I receptors *Endocrine reviews* **22**, 818-35

Nedachi, T., Kadotani, A., Ariga, M., Katagiri, H. & Kanzaki, M. (2008) Ambient glucose levels qualify the potency of insulin myogenic actions by regulating SIRT1 and FoxO3a in C2C12 myocytes *American journal of physiology. Endocrinology and metabolism* **294**, E668-78

Nilsson, C.L. (2012) Advances in quantitative phosphoproteomics *Analytical chemistry* **84**, 735-46

Nishi, H., Hashimoto, K. & Panchenko, A.R. (2011) Phosphorylation in protein-protein binding: effect on stability and function *Structure* **19**, 1807-15

Nothaft, H. & Szymanski, C.M. (2010) Protein glycosylation in bacteria: sweeter than ever *Nature reviews. Microbiology* **8**, 765-78

Noujaim, J., Payne, L.S., Judson, I., Jones, R.L. & Huang, P.H. (2016) Phosphoproteomics in translational research: a sarcoma perspective *Annals of oncology : official journal of the European Society for Medical Oncology* **27**, 787-94

Nusse, R. (2008) Wnt signaling and stem cell control *Cell research* **18**, 523-7

O'Connell, M.P., Billings, P.C., Fiori, J.L., Deirmengian, G., Roach, H.I., Shore, E.M. & Kaplan, F.S. (2007) HSPG modulation of BMP signaling in fibrodysplasia ossificans progressiva cells *Journal of cellular biochemistry* **102**, 1493-503

O'Connor, M.S., Carlson, M.E. & Conboy, I.M. (2009) Differentiation rather than aging of muscle stem cells abolishes their telomerase activity *Biotechnology progress* **25**, 1130-7

Oh, E.S., Woods, A. & Couchman, J.R. (1997) Syndecan-4 proteoglycan regulates the distribution and activity of protein kinase C *The Journal of biological chemistry* **272**, 8133-6

Oh, E.S., Woods, A., Lim, S.T., Theibert, A.W. & Couchman, J.R. (1998) Syndecan-4 proteoglycan cytoplasmic domain and phosphatidylinositol 4,5-bisphosphate coordinately regulate protein kinase C activity *The Journal of biological chemistry* **273**, 10624-9

Okina, E., Grossi, A., Gopal, S., Multhaupt, H.A. & Couchman, J.R. (2012) Alpha-actinin interactions with syndecan-4 are integral to fibroblast-matrix adhesion and regulate cytoskeletal architecture *The international journal of biochemistry & cell biology* **44**, 2161-74

Olguin, H. & Brandan, E. (2001) Expression and localization of proteoglycans during limb myogenic activation *Developmental dynamics : an official publication of the American Association of Anatomists* **221**, 106-15

Olguin, H.C. & Olwin, B.B. (2004) Pax-7 up-regulation inhibits myogenesis and cell cycle progression in satellite cells: a potential mechanism for self-renewal *Developmental biology* **275**, 375-88

Olguin, H.C. & Pisconti, A. (2012) Marking the tempo for myogenesis: PAX7 and the regulation of muscle stem cell fate decisions *Journal of cellular and molecular medicine* **16**, 1013-25

Olguin, H.C., Yang, Z., Tapscott, S.J. & Olwin, B.B. (2007) Reciprocal inhibition between PAX7 and muscle regulatory factors modulates myogenic cell fate determination *J Cell Biol* **177**, 769-79

Olwin, B.B. & Rapraeger, A. (1992) Repression of myogenic differentiation by aFGF, bFGF, and K-FGF is dependent on cellular heparan sulfate *J Cell Biol* **118**, 631-9

Ono, Y., Boldrin, L., Knopp, P., Morgan, J.E. & Zammit, P.S. (2010) Muscle satellite cells are a functionally heterogeneous population in both somite-derived and branchiomeric muscles *Developmental biology* **337**, 29-41

Ono, Y., Masuda, S., Nam, H.S., Benezra, R., Miyagoe-Suzuki, Y. & Takeda, S. (2012) Slow-dividing satellite cells retain long-term self-renewal ability in adult muscle *Journal of cell science* **125**, 1309-17

Ori, A., Wilkinson, M.C. & Fernig, D.G. (2011) A systems biology approach for the investigation of the heparin/heparan sulfate interactome *The Journal of biological chemistry* **286**, 19892-904

Otto, A., Schmidt, C., Luke, G., Allen, S., Valasek, P., Muntoni, F., Lawrence-Watt, D. & Patel, K. (2008) Canonical Wnt signalling induces satellite-cell proliferation during adult skeletal muscle regeneration *Journal of cell science* **121**, 2939-50

Oulion, S., Bertrand, S. & Escriva, H. (2012) Evolution of the FGF Gene Family *International journal of evolutionary biology* **2012**, 298147

Park, H., Kim, Y., Lim, Y., Han, I. & Oh, E.S. (2002) Syndecan-2 mediates adhesion and proliferation of colon carcinoma cells *The Journal of biological chemistry* **277**, 29730-6

Park, I.H., Erbay, E., Nuzzi, P. & Chen, J. (2005) Skeletal myocyte hypertrophy requires mTOR kinase activity and S6K1 *Experimental cell research* **309**, 211-9

Park, P.W., Reizes, O. & Bernfield, M. (2000) Cell surface heparan sulfate proteoglycans: selective regulators of ligand-receptor encounters *The Journal of biological chemistry* **275**, 29923-6

Pataki, C.A., Couchman, J.R. & Brabek, J. (2015) Wnt Signaling Cascades and the Roles of Syndecan Proteoglycans *The journal of histochemistry and cytochemistry : official journal of the Histochemistry Society* **63**, 465-80

Patel, V.N., Knox, S.M., Likar, K.M., Lathrop, C.A., Hossain, R., Eftekhari, S., Whitelock, J.M., Elkin, M., Vlodavsky, I. & Hoffman, M.P. (2007) Heparanase cleavage of perlecan heparan sulfate modulates FGF10 activity during ex vivo submandibular gland branching morphogenesis *Development* **134**, 4177-86

Pearson, R.B. & Kemp, B.E. (1991) Protein kinase phosphorylation site sequences and consensus specificity motifs: tabulations *Methods in enzymology* **200**, 62-81

Pellegrini, L., Burke, D.F., von Delft, F., Mulloy, B. & Blundell, T.L. (2000) Crystal structure of fibroblast growth factor receptor ectodomain bound to ligand and heparin *Nature* **407**, 1029-34

Pelosi, M., Marampon, F., Zani, B.M., Prudente, S., Perlas, E., Caputo, V., Cianetti, L., Berno, V., Narumiya, S., Kang, S.W.*, et al.* (2007) ROCK2 and its alternatively spliced isoform ROCK2m positively control the maturation of the myogenic program *Molecular and cellular biology* **27**, 6163-76

Penn, B.H., Bergstrom, D.A., Dilworth, F.J., Bengal, E. & Tapscott, S.J. (2004) A MyoD1-generated feed-forward circuit temporally patterns gene expression during skeletal muscle differentiation *Genes & development* **18**, 2348-53

Pessin, J. E. & Saltiel, A. R. (2000) Signaling pathways in insulin action: molecular targets of insulin resistance. *J Clin Invest* **106**, 165-9.

Pette, D. & Staron, R.S. (2000) Myosin isoforms, muscle fiber types, and transitions *Microscopy research and technique* **50**, 500-9

Pisconti, A., Banks, G.B., Babaeijandaghi, F., Betta, N.D., Rossi, F.M., Chamberlain, J.S. & Olwin, B.B. (2016) Loss of niche-satellite cell interactions in syndecan-3 null mice alters muscle progenitor cell homeostasis improving muscle regeneration *Skeletal muscle* **6**, 34

Pisconti, A., Bernet, J.D. & Olwin, B.B. (2012) Syndecans in skeletal muscle development, regeneration and homeostasis *Muscles, ligaments and tendons journal* **2**, 1-9

Pisconti, A., Cornelison, D.D., Olguin, H.C., Antwine, T.L. & Olwin, B.B. (2010) Syndecan-3 and Notch cooperate in regulating adult myogenesis *J Cell Biol* **190**, 427-41

Pruessmeyer, J., Martin, C., Hess, F.M., Schwarz, N., Schmidt, S., Kogel, T., Hoettecke, N., Schmidt, B., Sechi, A., Uhlig, S.*, et al.* (2010) A disintegrin and metalloproteinase 17 (ADAM17) mediates inflammation-induced shedding of syndecan-1 and -4 by lung epithelial cells *The Journal of biological chemistry* **285**, 555-64

Pye, D.A., Vives, R.R., Turnbull, J.E., Hyde, P. & Gallagher, J.T. (1998) Heparan sulfate oligosaccharides require 6-O-sulfation for promotion of basic fibroblast growth factor mitogenic activity *The Journal of biological chemistry* **273**, 22936-42

Quarta, M., Brett, J.O., DiMarco, R., De Morree, A., Boutet, S.C., Chacon, R., Gibbons, M.C., Garcia, V.A., Su, J., Shrager, J.B.*, et al.* (2016) An artificial niche preserves the quiescence of muscle stem cells and enhances their therapeutic efficacy *Nature biotechnology* **34**, 752-9

Raggiaschi, R., Gotta, S. & Terstappen, G.C. (2005) Phosphoproteome analysis *Bioscience reports* **25**, 33-44

Ramalingam, M. & Kim, S.J. (2016) Insulin on activation of autophagy with integrins and syndecans against MPP+-induced alpha-synuclein neurotoxicity *Neuroscience letters* **633**, 94-100

Rando, T.A. & Blau, H.M. (1994) Primary mouse myoblast purification, characterization, and transplantation for cell-mediated gene therapy *J Cell Biol* **125**, 1275-87

Rapraeger, A.C. (2000) Syndecan-regulated receptor signaling *J Cell Biol* **149**, 995-8

Rapraeger, A.C., Krufka, A. & Olwin, B.B. (1991) Requirement of heparan sulfate for bFGF-mediated fibroblast growth and myoblast differentiation *Science* **252**, 1705-8

Raulo, E., Chernousov, M.A., Carey, D.J., Nolo, R. & Rauvala, H. (1994) Isolation of a neuronal cell surface receptor of heparin binding growth-associated molecule (HB-GAM). Identification as N-syndecan (syndecan-3) *The Journal of biological chemistry* **269**, 12999-3004

Reiland, J., Ott, V.L., Lebakken, C.S., Yeaman, C., McCarthy, J. & Rapraeger, A.C. (1996) Pervanadate activation of intracellular kinases leads to tyrosine phosphorylation and shedding of syndecan-1 *The Biochemical journal* **319 (Pt 1)**, 39-47

Reizes, O., Benoit, S.C., Strader, A.D., Clegg, D.J., Akunuru, S. & Seeley, R.J. (2003) Syndecan-3 modulates food intake by interacting with the melanocortin/AgRP pathway *Annals of the New York Academy of Sciences* **994**, 66-73

Relaix, F., Rocancourt, D., Mansouri, A. & Buckingham, M. (2005) A PAX3/PAX7-dependent population of skeletal muscle progenitor cells *Nature* **435**, 948-53

Relaix, F. & Zammit, P.S. (2012) Satellite cells are essential for skeletal muscle regeneration: the cell on the edge returns centre stage *Development* **139**, 2845-56

Richler, C. & Yaffe, D. (1970) The in vitro cultivation and differentiation capacities of myogenic cell lines *Developmental biology* **23**, 1-22

Rigbolt, K.T., Zarei, M., Sprenger, A., Becker, A.C., Diedrich, B., Huang, X., Eiselein, S., Kristensen, A.R., Gretzmeier, C., Andersen, J.S.*, et al.* (2014) Characterization of early autophagy signaling by quantitative phosphoproteomics *Autophagy* **10**, 356-71

Rocheteau, P., Gayraud-Morel, B., Siegl-Cachedenier, I., Blasco, M.A. & Tajbakhsh, S. (2012) A subpopulation of adult skeletal muscle stem cells retains all template DNA strands after cell division *Cell* **148**, 112-25

Rodgers, J.T., King, K.Y., Brett, J.O., Cromie, M.J., Charville, G.W., Maguire, K.K., Brunson, C., Mastey, N., Liu, L., Tsai, C.R.*, et al.* (2014) mTORC1 controls the adaptive transition of quiescent stem cells from G0 to G(Alert) *Nature* **510**, 393-6

Rotwein, P. & Wilson, E.M. (2009) Distinct actions of Akt1 and Akt2 in skeletal muscle differentiation *Journal of cellular physiology* **219**, 503-11

Ruvinsky, I., Sharon, N., Lerer, T., Cohen, H., Stolovich-Rain, M., Nir, T., Dor, Y., Zisman, P. & Meyuhas, O. (2005) Ribosomal protein S6 phosphorylation is a determinant of cell size and glucose homeostasis *Genes & development* **19**, 2199-211

Sacco, A., Doyonnas, R., Kraft, P., Vitorovic, S. & Blau, H.M. (2008) Self-renewal and expansion of single transplanted muscle stem cells *Nature* **456**, 502-6

Saclier, M., Yacoub-Youssef, H., Mackey, A.L., Arnold, L., Ardjoune, H., Magnan, M., Sailhan, F., Chelly, J., Pavlath, G.K., Mounier, R.*, et al.* (2013) Differentially activated macrophages orchestrate myogenic precursor cell fate during human skeletal muscle regeneration *Stem cells* **31**, 384-96

San Antonio, J.D., Lander, A.D., Karnovsky, M.J. & Slayter, H.S. (1994) Mapping the heparin-binding sites on type I collagen monomers and fibrils *J Cell Biol* **125**, 1179-88

Sarbassov, D.D., Guertin, D.A., Ali, S.M. & Sabatini, D.M. (2005) Phosphorylation and regulation of AKT/PKB by the rictor-mTOR complex *Science* **307**, 1098-101

Sarhan, A.R., Szyroka, J., Begum, S., Tomlinson, M.G., Hotchin, N.A., Heath, J.K. & Cunningham, D.L. (2017) Quantitative Phosphoproteomics Reveals a Role for Collapsin Response Mediator Protein 2 in PDGF-Induced Cell Migration *Scientific reports* **7**, 3970

Sarrazin, S., Lamanna, W.C. & Esko, J.D. (2011) Heparan sulfate proteoglycans *Cold Spring Harbor perspectives in biology* **3**,

Sarrazin, S., Lyon, M., Deakin, J.A., Guerrini, M., Lassalle, P., Delehedde, M. & Lortat-Jacob, H. (2010) Characterization and binding activity of the chondroitin/dermatan sulfate chain from Endocan, a soluble endothelial proteoglycan *Glycobiology* **20**, 1380-8

Saunders, S., Jalkanen, M., O'Farrell, S. & Bernfield, M. (1989) Molecular cloning of syndecan, an integral membrane proteoglycan *J Cell Biol* **108**, 1547-56

Scadden, D.T. (2006) The stem-cell niche as an entity of action *Nature* **441**, 1075-9

Schabort, E.J., van der Merwe, M., Loos, B., Moore, F.P. & Niesler, C.U. (2009) TGF-beta's delay skeletal muscle progenitor cell differentiation in an isoform-independent manner *Experimental cell research* **315**, 373-84

Schmutz, C., Ahrne, E., Kasper, C.A., Tschon, T., Sorg, I., Dreier, R.F., Schmidt, A. & Arrieumerlou, C. (2013) Systems-level overview of host protein phosphorylation during Shigella flexneri infection revealed by phosphoproteomics *Molecular & cellular proteomics : MCP* **12**, 2952-68

Schneller, M., Vuori, K. & Ruoslahti, E. (1997) Alphavbeta3 integrin associates with activated insulin and PDGFbeta receptors and potentiates the biological activity of PDGF *The EMBO journal* **16**, 5600-7

Schultz, E. (1974) A quantitative study of the satellite cell population in postnatal mouse lumbrical muscle *The Anatomical record* **180**, 589-95

Schwartz, D. & Gygi, S.P. (2005) An iterative statistical approach to the identification of protein phosphorylation motifs from large-scale data sets *Nature biotechnology* **23**, 1391-8

Seale, P., Sabourin, L.A., Girgis-Gabardo, A., Mansouri, A., Gruss, P. & Rudnicki, M.A. (2000) PAX7 is required for the specification of myogenic satellite cells *Cell* **102**, 777-86

Seidel, C., Ringden, O. & Remberger, M. (2003) Increased levels of syndecan-1 in serum during acute graft-versus-host disease *Transplantation* **76**, 423-6

Semsarian, C., Sutrave, P., Richmond, D.R. & Graham, R.M. (1999) Insulin-like growth factor (IGF-I) induces myotube hypertrophy associated with an increase in anaerobic glycolysis in a clonal skeletal-muscle cell model *The Biochemical journal* **339 (Pt 2)**, 443-51

Shah, O.J. & Hunter, T. (2006) Turnover of the active fraction of IRS1 involves raptor-mTOR- and S6K1-dependent serine phosphorylation in cell culture models of tuberous sclerosis *Molecular and cellular biology* **26**, 6425-34

Shea, K.L., Xiang, W., LaPorta, V.S., Licht, J.D., Keller, C., Basson, M.A. & Brack, A.S. (2010) Sprouty1 regulates reversible quiescence of a self-renewing adult muscle stem cell pool during regeneration *Cell stem cell* **6**, 117-29

Shefer, G., Wleklinski-Lee, M. & Yablonka-Reuveni, Z. (2004) Skeletal muscle satellite cells can spontaneously enter an alternative mesenchymal pathway *Journal of cell science* **117**, 5393-404

Shen, Y., Tenney, A.P., Busch, S.A., Horn, K.P., Cuascut, F.X., Liu, K., He, Z., Silver, J. & Flanagan, J.G. (2009) PTPsigma is a receptor for chondroitin sulfate proteoglycan, an inhibitor of neural regeneration *Science* **326**, 592-6

Sherwood, R.I., Christensen, J.L., Conboy, I.M., Conboy, M.J., Rando, T.A., Weissman, I.L. & Wagers, A.J. (2004) Isolation of adult mouse myogenic progenitors: functional heterogeneity of cells within and engrafting skeletal muscle *Cell* **119**, 543-54

Shi, Y., Wang, J., Chandarlapaty, S., Cross, J., Thompson, C., Rosen, N. & Jiang, X. (2014) PTEN is a protein tyrosine phosphatase for IRS1 *Nature structural & molecular biology* **21**, 522-7

Shin, J., Lee, W., Lee, D., Koo, B.K., Han, I., Lim, Y., Woods, A., Couchman, J.R. & Oh, E.S. (2001) Solution structure of the dimeric cytoplasmic domain of syndecan-4 *Biochemistry* **40**, 8471-8

Shworak, N.W., Shirakawa, M., Mulligan, R.C. & Rosenberg, R.D. (1994) Characterization of ryudocan glycosaminoglycan acceptor sites *The Journal of biological chemistry* **269**, 21204-14

Sickmann, A. & Meyer, H.E. (2001) Phosphoamino acid analysis *Proteomics* **1**, 200-6

Siddle, K. (2011) Signalling by insulin and IGF receptors: supporting acts and new players *Journal of molecular endocrinology* **47**, R1-10

Siegel, A.L., Atchison, K., Fisher, K.E., Davis, G.E. & Cornelison, D.D. (2009) 3D timelapse analysis of muscle satellite cell motility *Stem cells* **27**, 2527-38

Simons, M. & Horowitz, A. (2001) Syndecan-4-mediated signalling *Cellular signalling* **13**, 855-62

Sin, J., Andres, A.M., Taylor, D.J., Weston, T., Hiraumi, Y., Stotland, A., Kim, B.J., Huang, C., Doran, K.S. & Gottlieb, R.A. (2016) Mitophagy is required for mitochondrial biogenesis and myogenic differentiation of C2C12 myoblasts *Autophagy* **12**, 369-80

Smith, D.B. (2000) Generating fusions to glutathione S-transferase for protein studies *Methods in enzymology* **326**, 254-70

Smith, F.M., Holt, L.J., Garfield, A.S., Charalambous, M., Koumanov, F., Perry, M., Bazzani, R., Sheardown, S.A., Hegarty, B.D., Lyons, R.J.*, et al.* (2007) Mice with a disruption of the imprinted Grb10 gene exhibit altered body composition, glucose homeostasis, and insulin signaling during postnatal life *Molecular and cellular biology* **27**, 5871-86

Solari, F.A., Dell'Aica, M., Sickmann, A. & Zahedi, R.P. (2015) Why phosphoproteomics is still a challenge *Molecular bioSystems* **11**, 1487-93

Stead, D.A., Paton, N.W., Missier, P., Embury, S.M., Hedeler, C., Jin, B., Brown, A.J. & Preece, A. (2008) Information quality in proteomics *Briefings in bioinformatics* **9**, 174-88

Steinfeld, R., Van Den Berghe, H. & David, G. (1996) Stimulation of fibroblast growth factor receptor-1 occupancy and signaling by cell surface-associated syndecans and glypican *J Cell Biol* **133**, 405-16

Stewart, C.E., James, P.L., Fant, M.E. & Rotwein, P. (1996) Overexpression of insulin-like growth factor-II induces accelerated myoblast differentiation *Journal of cellular physiology* **169**, 23-32

Strader, A.D., Reizes, O., Woods, S.C., Benoit, S.C. & Seeley, R.J. (2004) Mice lacking the syndecan-3 gene are resistant to diet-induced obesity *The Journal of clinical investigation* **114**, 1354-60

Su, G., Blaine, S.A., Qiao, D. & Friedl, A. (2007) Shedding of syndecan-1 by stromal fibroblasts stimulates human breast cancer cell proliferation via FGF2 activation *The Journal of biological chemistry* **282**, 14906-15

Suarez, E., Bach, D., Cadefau, J., Palacin, M., Zorzano, A. & Guma, A. (2001) A novel role of neuregulin in skeletal muscle. Neuregulin stimulates glucose uptake, glucose transporter translocation, and transporter expression in muscle cells *The Journal of biological chemistry* **276**, 18257-64

Subramanian, S.V., Fitzgerald, M.L. & Bernfield, M. (1997) Regulated shedding of syndecan-1 and -4 ectodomains by thrombin and growth factor receptor activation *The Journal of biological chemistry* **272**, 14713-20

Sun, A., Wei, J., Childress, C., Shaw, J.H.t., Peng, K., Shao, G., Yang, W. & Lin, Q. (2017) The E3 ubiquitin ligase NEDD4 is an LC3-interactive protein and regulates autophagy *Autophagy* **13**, 522-537

Sun, X.J., Goldberg, J.L., Qiao, L.Y. & Mitchell, J.J. (1999) Insulin-induced insulin receptor substrate-1 degradation is mediated by the proteasome degradation pathway *Diabetes* **48**, 1359-64

Sun, X.J., Rothenberg, P., Kahn, C.R., Backer, J.M., Araki, E., Wilden, P.A., Cahill, D.A., Goldstein, B.J. & White, M.F. (1991) Structure of the insulin receptor substrate IRS-1 defines a unique signal transduction protein *Nature* **352**, 73-7

Tanaka, K.K., Hall, J.K., Troy, A.A., Cornelison, D.D., Majka, S.M. & Olwin, B.B. (2009) Syndecan-4-expressing muscle progenitor cells in the SP engraft as satellite cells during muscle regeneration *Cell stem cell* **4**, 217-25

Tang, A.H. & Rando, T.A. (2014) Induction of autophagy supports the bioenergetic demands of quiescent muscle stem cell activation *The EMBO journal* **33**, 2782-97

Tapscott, S.J. (2005) The circuitry of a master switch: MyoD1 and the regulation of skeletal muscle gene transcription *Development* **132**, 2685-95

Tatsumi, R., Sheehan, S.M., Iwasaki, H., Hattori, A. & Allen, R.E. (2001) Mechanical stretch induces activation of skeletal muscle satellite cells in vitro *Experimental cell research* **267**, 107-14

Taylor, W.E., Bhasin, S., Artaza, J., Byhower, F., Azam, M., Willard, D.H., Jr., Kull, F.C., Jr. & Gonzalez-Cadavid, N. (2001) Myostatin inhibits cell proliferation and protein synthesis in C2C12 muscle cells *American journal of physiology. Endocrinology and metabolism* **280**, E221-8

Thomas, K., Engler, A.J. & Meyer, G.A. (2015) Extracellular matrix regulation in the muscle satellite cell niche *Connective tissue research* **56**, 1-8

Thoreson, M.A. & Reynolds, A.B. (2002) Altered expression of the catenin p120 in human cancer: implications for tumor progression *Differentiation; research in biological diversity* **70**, 583-9

Tidball, J.G. (2017) Regulation of muscle growth and regeneration by the immune system *Nature reviews. Immunology* **17**, 165-178

Tkachenko, E., Lutgens, E., Stan, R.V. & Simons, M. (2004) Fibroblast growth factor 2 endocytosis in endothelial cells proceed via syndecan-4-dependent activation of Rac1 and a Cdc42-dependent macropinocytic pathway *Journal of cell science* **117**, 3189-99

Tkachenko, E., Rhodes, J.M. & Simons, M. (2005) Syndecans: new kids on the signaling block *Circulation research* **96**, 488-500

Tobe, B.T., Hou, J., Crain, A.M., Singec, I., Snyder, E.Y. & Brill, L.M. (2012) Phosphoproteomic analysis: an emerging role in deciphering cellular signaling in human embryonic stem cells and their differentiated derivatives *Stem cell reviews* **8**, 16-31

Trentini, D.B., Suskiewicz, M.J., Heuck, A., Kurzbauer, R., Deszcz, L., Mechtler, K. & Clausen, T. (2016) Arginine phosphorylation marks proteins for degradation by a Clp protease *Nature* **539**, 48-53

Troy, A., Cadwallader, A.B., Fedorov, Y., Tyner, K., Tanaka, K.K. & Olwin, B.B. (2012) Coordination of satellite cell activation and self-renewal by Par-complex-dependent asymmetric activation of p38alpha/beta MAPK *Cell stem cell* **11**, 541-53

Tumova, S., Woods, A. & Couchman, J.R. (2000) Heparan sulfate chains from glypican and syndecans bind the Hep II domain of fibronectin similarly despite minor structural differences *The Journal of biological chemistry* **275**, 9410-7

Turnbull, J., Powell, A. & Guimond, S. (2001) Heparan sulfate: decoding a dynamic multifunctional cell regulator *Trends in cell biology* **11**, 75-82

Turnbull, J.E., Miller, R.L., Ahmed, Y., Puvirajesinghe, T.M. & Guimond, S.E. (2010) Glycomics profiling of heparan sulfate structure and activity *Methods in enzymology* **480**, 65-85

Urciuolo, A., Quarta, M., Morbidoni, V., Gattazzo, F., Molon, S., Grumati, P., Montemurro, F., Tedesco, F.S., Blaauw, B., Cossu, G.*, et al.* (2013) Collagen VI regulates satellite cell self-renewal and muscle regeneration *Nature communications* **4**, 1964

Vandromme, M., Rochat, A., Meier, R., Carnac, G., Besser, D., Hemmings, B.A., Fernandez, A. & Lamb, N.J. (2001) Protein kinase B beta/Akt2 plays a specific role in muscle differentiation *The Journal of biological chemistry* **276**, 8173-9

von Maltzahn, J., Bentzinger, C.F. & Rudnicki, M.A. (2011) Wnt7a-Fzd7 signalling directly activates the AKT/mTOR anabolic growth pathway in skeletal muscle *Nature cell biology* **14**, 186-91

von Maltzahn, J., Chang, N.C., Bentzinger, C.F. & Rudnicki, M.A. (2012) Wnt signaling in myogenesis *Trends in cell biology* **22**, 602-9

von Maltzahn, J., Jones, A.E., Parks, R.J. & Rudnicki, M.A. (2013) PAX7 is critical for the normal function of satellite cells in adult skeletal muscle *Proceedings of the National Academy of Sciences of the United States of America* **110**, 16474-9

Vuori, K. & Ruoslahti, E. (1994) Association of insulin receptor substrate-1 with integrins *Science* **266**, 1576-8

Vuori, K. & Ruoslahti, E. (1995) Tyrosine phosphorylation of p130Cas and cortactin accompanies integrin-mediated cell adhesion to extracellular matrix *The Journal of biological chemistry* **270**, 22259-62

Vyse, S., Desmond, H. & Huang, P.H. (2017) Advances in mass spectrometry based strategies to study receptor tyrosine kinases *IUCrJ* **4**, 119-130

Wang, H., Leavitt, L., Ramaswamy, R. & Rapraeger, A.C. (2010) Interaction of syndecan and alpha6beta4 integrin cytoplasmic domains: regulation of ErbB2-mediated integrin activation *The Journal of biological chemistry* **285**, 13569-79

Weigert, C., Kron, M., Kalbacher, H., Pohl, A.K., Runge, H., Haring, H.U., Schleicher, E. & Lehmann, R. (2008) Interplay and effects of temporal changes in the phosphorylation state of serine-302, -307, and -318 of insulin receptor substrate-1 on insulin action in skeletal muscle cells *Molecular endocrinology* **22**, 2729-40

Weintraub, H., Tapscott, S.J., Davis, R.L., Thayer, M.J., Adam, M.A., Lassar, A.B. & Miller, A.D. (1989) Activation of muscle-specific genes in pigment, nerve, fat, liver, and fibroblast cell lines by forced expression of MyoD1 *Proceedings of the National Academy of Sciences of the United States of America* **86**, 5434-8

Wen, Y., Bi, P., Liu, W., Asakura, A., Keller, C. & Kuang, S. (2012) Constitutive Notch activation upregulates PAX7 and promotes the self-renewal of skeletal muscle satellite cells *Molecular and cellular biology* **32**, 2300-11

Werner, H., Weinstein, D. & Bentov, I. (2008). Similarities and differences between insulin and IGF-I: structures, receptors, and signalling pathways. *Arch Physiol Biochem* **114**, 17-22.

White, M.F. & Kahn, C.R. (1994) The insulin signaling system *The Journal of biological chemistry* **269**, 1-4

Whiteford, J.R., Behrends, V., Kirby, H., Kusche-Gullberg, M., Muramatsu, T. & Couchman, J.R. (2007) Syndecans promote integrin-mediated adhesion of mesenchymal cells in two distinct pathways *Experimental cell research* **313**, 3902-13

Whiteford, J.R. & Couchman, J.R. (2006) A conserved NXIP motif is required for cell adhesion properties of the syndecan-4 ectodomain *The Journal of biological chemistry* **281**, 32156-63

Whitelock, J.M. & Iozzo, R.V. (2005) Heparan sulfate: a complex polymer charged with biological activity *Chemical reviews* **105**, 2745-64

Wilcox, G. (2005) Insulin and insulin resistance *The Clinical biochemist. Reviews* **26**, 19-39

Wozniak, A.C. & Anderson, J.E. (2007) Nitric oxide-dependence of satellite stem cell activation and quiescence on normal skeletal muscle fibers *Developmental dynamics : an official publication of the American Association of Anatomists* **236**, 240-50

Wright, P.E. & Dyson, H.J. (2015) Intrinsically disordered proteins in cellular signalling and regulation *Nature reviews. Molecular cell biology* **16**, 18-29

Wu, Z., Woodring, P.J., Bhakta, K.S., Tamura, K., Wen, F., Feramisco, J.R., Karin, M., Wang, J.Y. & Puri, P.L. (2000) p38 and extracellular signal-regulated kinases regulate the myogenic program at multiple steps *Molecular and cellular biology* **20**, 3951-64

Xian, X., Gopal, S. & Couchman, J.R. (2010) Syndecans as receptors and organizers of the extracellular matrix *Cell and tissue research* **339**, 31-46

Xu, Q. & Wu, Z. (2000) The insulin-like growth factor-phosphatidylinositol 3-kinase-AKT signaling pathway regulates myogenin expression in normal myogenic cells but not in rhabdomyosarcoma-derived RD cells *The Journal of biological chemistry* **275**, 36750-7

Yablonka-Reuveni, Z. (1988) Discrimination of myogenic and nonmyogenic cells from embryonic skeletal muscle by 90 degrees light scattering *Cytometry* **9**, 121-5

Yaffe, D. & Saxel, O. (1977) Serial passaging and differentiation of myogenic cells isolated from dystrophic mouse muscle *Nature* **270**, 725-7

Yamada, M., Tatsumi, R., Kikuiri, T., Okamoto, S., Nonoshita, S., Mizunoya, W., Ikeuchi, Y., Shimokawa, H., Sunagawa, K. & Allen, R.E. (2006) Matrix metalloproteinases are involved in mechanical stretch-induced activation of skeletal muscle satellite cells *Muscle & nerve* **34**, 313-9

Yamaguchi, M., Watanabe, Y., Ohtani, T., Uezumi, A., Mikami, N., Nakamura, M., Sato, T., Ikawa, M., Hoshino, M., Tsuchida, K.*, et al.* (2015) Calcitonin Receptor Signaling Inhibits Muscle Stem Cells from Escaping the Quiescent State and the Niche *Cell reports* **13**, 302-14

Yamashita, H., Goto, A., Kadowaki, T. & Kitagawa, Y. (2004) Mammalian and Drosophila cells adhere to the laminin alpha4 LG4 domain through syndecans, but not glypicans *The Biochemical journal* **382**, 933-43

Yanagishita, M. & Hascall, V.C. (1984) Metabolism of proteoglycans in rat ovarian granulosa cell culture. Multiple intracellular degradative pathways and the effect of chloroquine *The Journal of biological chemistry* **259**, 10270-83

Yang, N. & Friedl, A. (2016) Syndecan-1-Induced ECM Fiber Alignment Requires Integrin alphavbeta3 and Syndecan-1 Ectodomain and Heparan Sulfate Chains *PloS one* **11**, e0150132

Yin, H., Price, F. & Rudnicki, M.A. (2013) Satellite cells and the muscle stem cell niche *Physiological reviews* **93**, 23-67

Yoo, J., Jeong, M.J., Cho, H.J., Oh, E.S. & Han, M.Y. (2005) Dynamin II interacts with syndecan-4, a regulator of focal adhesion and stress-fiber formation *Biochemical and biophysical research communications* **328**, 424-31

Yoon, S.H., Ramalingam, M. & Kim, S.J. (2015) Insulin stimulates integrin-linked kinase in UMR-106 cells: potential role of heparan sulfate on syndecan-1 *Journal of receptor and signal transduction research* **35**, 613-7

Yu, M., Wang, H., Xu, Y., Yu, D., Li, D., Liu, X. & Du, W. (2015) Insulin-like growth factor-1 (IGF-1) promotes myoblast proliferation and skeletal muscle growth of embryonic chickens via the PI3K/AKT signalling pathway *Cell biology international* **39**, 910-22

Zammit, P.S., Golding, J.P., Nagata, Y., Hudon, V., Partridge, T.A. & Beauchamp, J.R. (2004) Muscle satellite cells adopt divergent fates: a mechanism for self-renewal? *J Cell Biol* **166**, 347-57

Zammit, P.S., Partridge, T.A. & Yablonka-Reuveni, Z. (2006) The skeletal muscle satellite cell: the stem cell that came in from the cold *The journal of histochemistry and cytochemistry : official journal of the Histochemistry Society* **54**, 1177-91

Zhou, M. & Wu, H. (2009) Glycosylation and biogenesis of a family of serine-rich bacterial adhesins *Microbiology* **155**, 317-27

Zimmermann, P., Zhang, Z., Degeest, G., Mortier, E., Leenaerts, I., Coomans, C., Schulz, J., N'Kuli, F., Courtoy, P.J. & David, G. (2005) Syndecan recycling [corrected] is controlled by syntenin-PIP2 interaction and Arf6 *Developmental cell* **9**, 377-88

Appendix

Appendix 1: Screenshots of chromatogram alignment conducted by Progenesis QI™

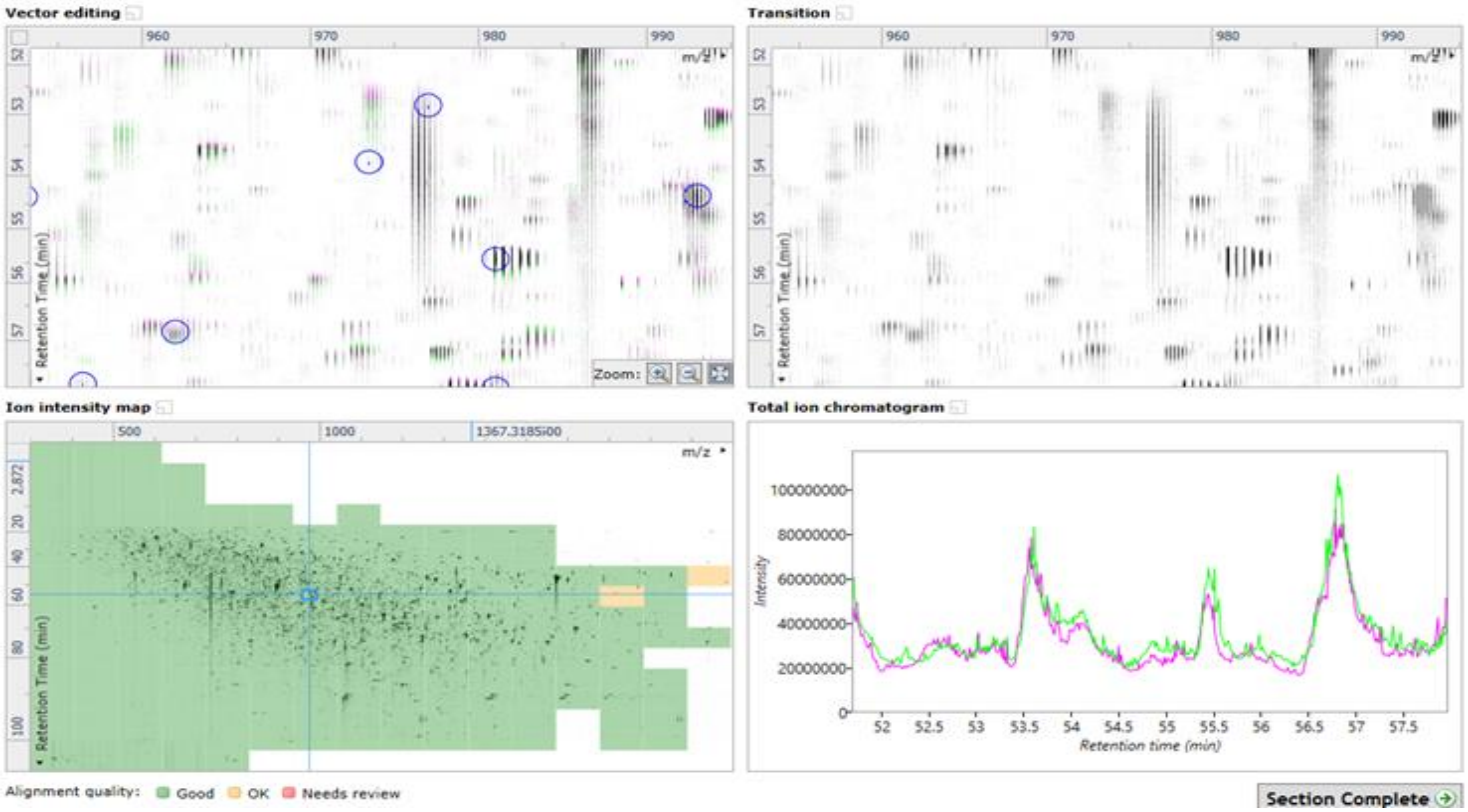

Appendix 1.1: An example of an alignment score of 94.5% compared with the reference run. Pink lines represent the reference sample run and green lines represent the run being aligned to the reference.

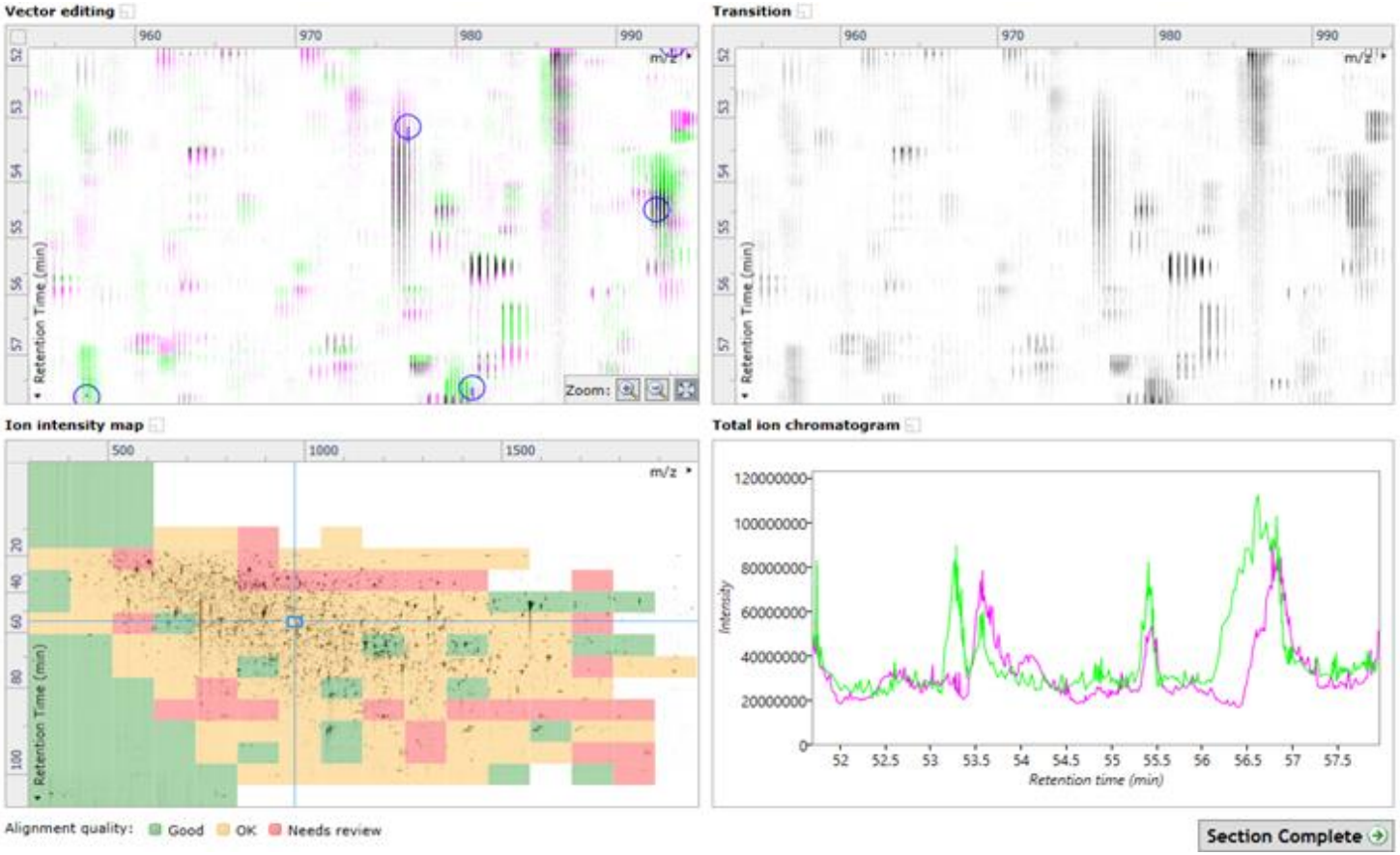

Appendix 1.2: An example of an alignment score of 53.9% compared with the reference run. Pink lines represent the reference sample run and green lines represent the run being aligned to the reference.

Appendix 2: Differentially abundant phosphopeptides

See attached CD-ROM

Appendix 2.1: Differentially abundant phosphopeptides at Time 0 between Vector and S3KD myoblasts. Red indicates increasing phosphopeptide abundance, Red indicates decreasing phosphopeptide abundance

Appendix 2.1.1: Proteins mapped to Gene Ontology terms at Time 0

Multiple Microsoft Excel tabs separate Biological Process, Molecular Function and Cellular component.

Appendix 2.2: Differentially abundant phosphopeptides at Time 10 between Vector and S3KD myoblasts. Red indicates increasing phosphopeptide abundance, Red indicates decreasing phosphopeptide abundance

Appendix 2.2.1: Proteins mapped to Gene Ontology terms at Time 10

Multiple Microsoft Excel tabs separate Biological Process, Molecular Function and Cellular component.

Appendix 3: Pathway and functional enrichment

Appendix 3.1: Enriched biological processes and molecular functions in all phosphoproteins identified in the phosphoproteomics. All the phosphopeptides identified in the study were converted to their corresponding Uniprot Accession protein identifier and submitted to DAVID for analysis using the whole mouse genome as background dataset. **(A)** Enrichment of Biological Processes. **(B)** Enrichment of Molecular Function.

Bioloigcal process	p-value
protein phosphorylation	0.000
regulation of transcription, DNA-templated	0.000
transcription, DNA-templated	0.000
phosphorylation	0.000
positive regulation of transcription from RNA polymerase II promoter	0.000
cell cycle	0.000
intracellular signal transduction	0.000
signal transduction	0.000
covalent chromatin modification	0.000
negative regulation of transcription from RNA polymerase II promoter	0.001
cell differentiation	0.002
negative regulation of transcription, DNA-templated	0.002
peptidyl-serine phosphorylation	0.003
protein autophosphorylation	0.006
positive regulation of transcription, DNA-templated	0.008
mitotic nuclear division	0.008
heart development	0.008
regulation of Rho protein signal transduction	0.010
microtubule-based movement	0.010
cell division	0.011
negative regulation of cell proliferation	0.012
actin cytoskeleton organization	0.018
insulin receptor signaling pathway	0.019
hematopoietic progenitor cell differentiation	0.022
cellular response to DNA damage stimulus	0.032
nucleosome assembly	0.035
mRNA processing	0.038
MAPK cascade	0.045
defense response to virus	0.045
positive regulation of NF-kappaB transcription factor activity	0.045

Molecular Function	p-value
protein kinase activity	0.000
protein serine/threonine kinase activity	0.000
DNA binding	0.000
kinase activity	0.000
chromatin binding	0.000
transcription factor activity, sequence-specific DNA binding	0.000
transcription factor binding	0.001
sequence-specific DNA binding	0.001
GTPase activator activity	0.002
guanyl-nucleotide exchange factor activity	0.002
protein binding	0.003
core promoter binding	0.003
transcriptional activator activity	0.005
Rho guanyl-nucleotide exchange factor activity	0.005
protein kinase binding	0.007
receptor signaling protein serine/threonine kinase activity	0.007
nucleic acid binding	0.011
SH3 domain binding	0.015
p53 binding	0.019
zinc ion binding	0.024
microtubule motor activity	0.026
RNA polymerase II core promoter proximal region sequence-specific DNA binding	0.028
transferase activity	0.043
histone binding	0.043
RNA polymerase II regulatory region sequence-specific DNA binding	0.046

Appendix 3.2: List of proteins mapped to significantly enriched IPA pathways.

Phosphopeptides that were differentially abundant between Vector myoblasts and S3KD myoblasts, at **(A)** Time 0 and at **(B)** Time 10, were converted to their corresponding Uniprot Accession protein identifier then analysed using IPA to enrich for canonical pathways.

Time 0:

Ingenuity Canonical Pathways	-log(p-value)	Ratio	z-score	Molecules
mTOR Signaling	2	0.044	1	ULK1,MAPK1,IRS1,EIF3B,EIF3J,EIF4EBP1,EIF4G1
ERK/MAPK Signaling	1.86	0.0412	0.378	TLN1,MAPK1,IRS1,PAK4,MAP2K1,EIF4EBP1,PRKAR1A
Insulin Receptor Signaling	1.5	0.0424	0	MAPK1,IRS1,MAP2K1,EIF4EBP1,PRKAR1A
Ephrin Receptor Signaling	1.47	0.0373	-0.447	DOK1,SORBS1,MAPK1,PAK4,MAP2K1,EPHA2

Time10

Ingenuity Canonical Pathways	-log(p-value)	Ratio	z-score	Molecules
EGF Signaling	3.71	0.0656	0	IRS2,PRKCA,IRS1,MAPK3
p70S6K Signaling	3.66	0.0431	-0.447	IRS2,PRKCA,IRS1,EEF2,MAPK3
ErbB4 Signaling	3.6	0.0615	0	IRS2,PRKCA,IRS1,MAPK3
JAK/Stat Signaling	3.39	0.0541	0	IRS2,IRS1,PTPN1,MAPK3
VEGF Family Ligand-Receptor Interactions	3.32	0.0519	0	IRS2,PRKCA,IRS1,MAPK3
PDGF Signaling	3.3	0.0513	0	IRS2,PRKCA,IRS1,MAPK3
FGF Signaling	3.26	0.05	0	IRS2,PRKCA,IRS1,MAPK3
VEGF Signaling	3.06	0.0444	1	IRS2,PRKCA,IRS1,MAPK3
mTOR Signaling	3.02	0.0312	0.447	IRS2,PRKCA,EIF4B,IRS1,MAPK3
HGF Signaling	2.85	0.0388	0	IRS2,PRKCA,IRS1,MAPK3
Insulin Receptor Signaling	2.63	0.0339	0	IRS2,IRS1,PTPN1,MAPK3
ERK/MAPK Signaling	2.07	0.0235	0	IRS2,PRKCA,IRS1,MAPK3

:

Appendix 3.2: All significantly enriched IPA pathways at Time 0. Phosphoproteins that had one or more differentially abundant phosphopeptides between S3KD and Vector myoblasts were submitted to IPA for pathway enrichment. No filter applied.

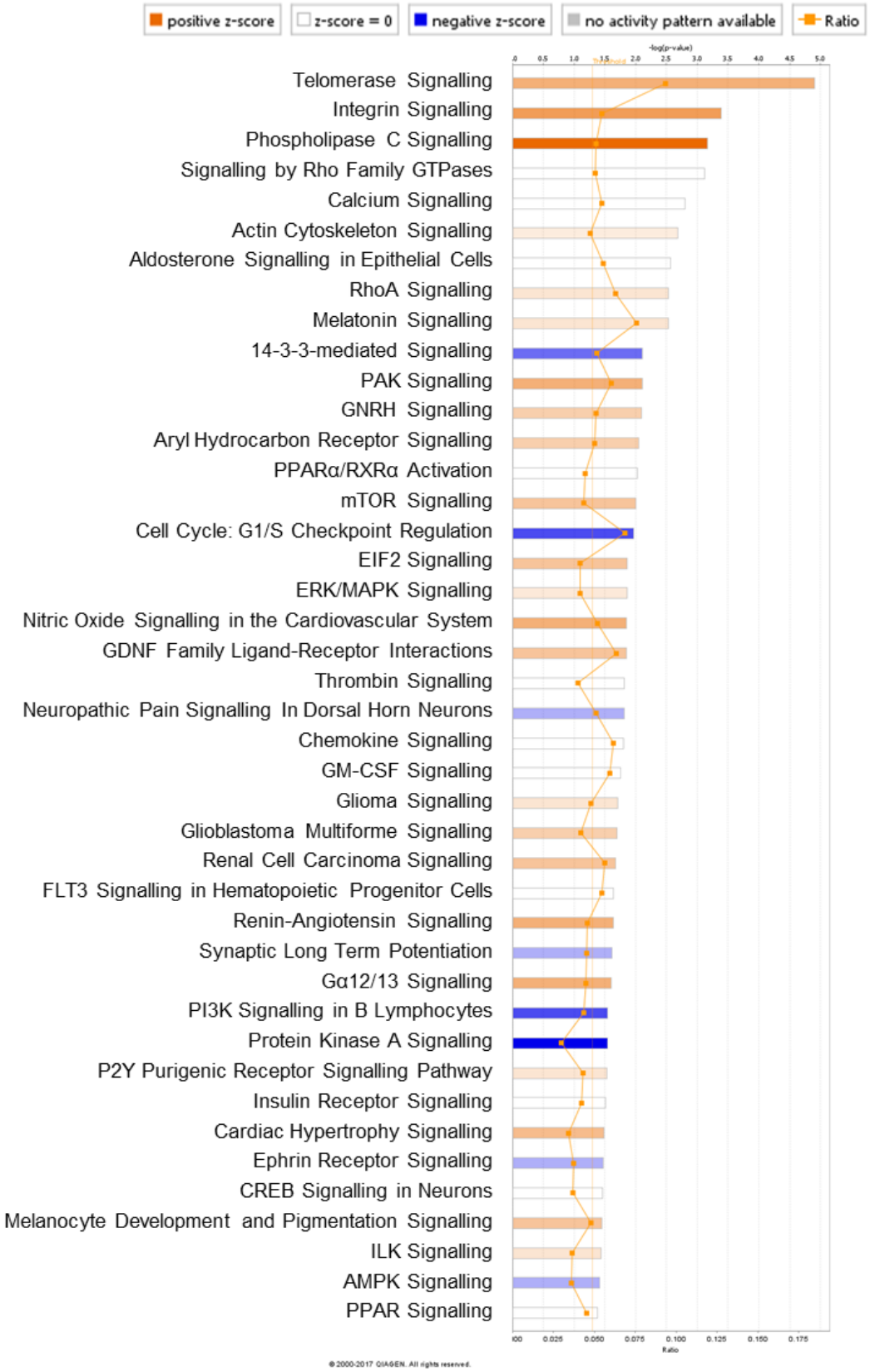

Appendix 4: Optimisation of phospho-insulin receptor antibody.

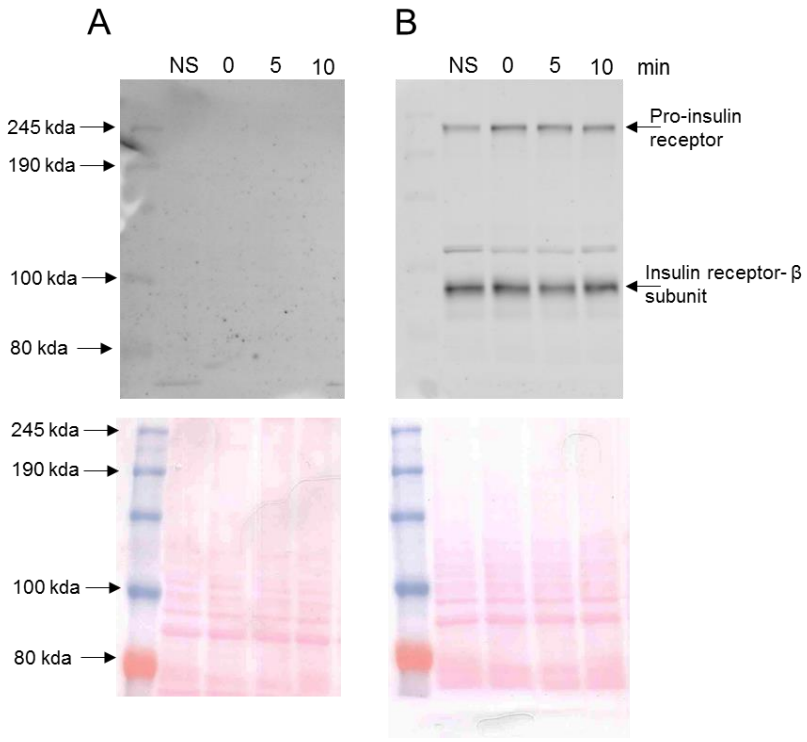

Appendix 4: Optimisation of phospho-insulin receptor antibody. Parental C2C12 myoblasts were cultured in growth medium then lysed (non starved, NS) or serum-starved (0) for 5 hours before treatment with insulin (concentration) for 5 or 10 minutes and then lysed. Proteins were separated by SDS-PAGE before western blotting with **(A)** phospho-insulin receptor antibody or **(B)** insulin receptor antibody. Poncaue stains of the membranes before antibody incubation are shown below to show that similar amount of total proteins were loaded.

Appendix 5: SDC3 is downregulated in C2C12 myoblasts during differentiation.

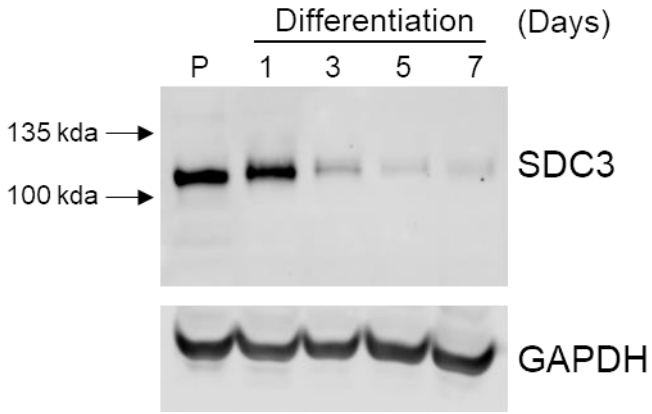

Appendix 5: SDC3 expression declines with myoblast differentiation. C2C12 myoblasts were cultured in proliferating conditions (P) or induced to differentiate via serum lowering for 1, 3, 5, or 7 days. Cells were lysed and treated with heparinase-III to removed heparan sulphate chains. Proteins were separated by SDS-PAGE and immunoblotted to detect SDC3 or GAPDH.